


2000

Experimental and analytical study of integral-abutment bridges

Brad Harold Sayers
Iowa State University

Follow this and additional works at: <https://lib.dr.iastate.edu/rtd>

 Part of the [Civil Engineering Commons](#), and the [Structural Engineering Commons](#)

Recommended Citation

Sayers, Brad Harold, "Experimental and analytical study of integral-abutment bridges" (2000). *Retrospective Theses and Dissertations*. 17274.

<https://lib.dr.iastate.edu/rtd/17274>

This Thesis is brought to you for free and open access by the Iowa State University Capstones, Theses and Dissertations at Iowa State University Digital Repository. It has been accepted for inclusion in Retrospective Theses and Dissertations by an authorized administrator of Iowa State University Digital Repository. For more information, please contact digirep@iastate.edu.

Experimental and analytical study of integral-abutment bridges

by

Brad Harold Sayers

A thesis submitted to the graduate faculty
in partial fulfillment of the requirements for the degree of
MASTER OF SCIENCE

Major: Civil Engineering (Structural Engineering)

Major Professors: Lowell F. Greimann and Robert E. Abendroth

Iowa State University

Ames, Iowa

2000

Graduate College
Iowa State University

This is to certify that the Master's thesis of
Brad Harold Sayers
has met the thesis requirements of Iowa State University

Co-major Professor

Co-major Professor

For the Major Program

For the Graduate College

TABLE OF CONTENTS

ABSTRACT	vi
1. INTRODUCTION.....	1
1.1. Background.....	1
1.2. Objective and scope	2
2. LITERATURE REVIEW.....	4
2.1. Current practice in the United States and Canada.....	4
2.2. Bridge field studies and instrumentation	6
2.3. Analytical studies	8
2.4. Integral-abutment design models.....	13
2.4.1. Coefficient of thermal expansion and contraction of concrete	13
2.4.2. Bridge displacement	14
2.4.3. Abutment backfill	15
3. EXPERIMENTAL MONITORING PROGRAM.....	17
3.1. Overview.....	17
3.1.1. Bridge descriptions	17
3.1.2. Instrumentation packages.....	19
3.2. Instrument temperature corrections	21
3.2.1. Corrections for displacement transducers	22
3.2.2. Corrections for compensated resistance strain gages.....	23
3.2.3. Corrections for uncompensated resistance strain gages.....	26
3.2.4. Corrections for vibrating wire strain gages.....	27
3.2.5. Corrections for tiltmeters.....	28
4. EXPERIMENTAL RESULTS.....	29
4.1. Experimental data filtering	29
4.1.1. Thermocouples.....	29
4.1.2. Displacement transducers	30
4.1.3. Pile strain gages	37
4.1.4. Girder strain gages	53
4.2. Bridge temperatures	58
4.2.1. Average bridge temperatures	58
4.2.2. Vertical temperature gradients.....	63
4.2.3. Transverse temperature gradients.....	74
4.2.4. Longitudinal temperature gradients	77
4.2.5. Pile temperatures	77
4.3. Bridge displacements.....	79
4.3.1. Longitudinal abutment displacements and change in bridge length	79
4.3.2. Abutment rotation in a horizontal plane	84

4.3.3. Abutment rotation in a vertical plane	86
4.3.4. Transverse abutment displacements	86
4.3.5. Relative displacements	89
4.4. Bridge member strains	95
4.4.1. Pile strains	95
4.4.2. Girder strains	101
5. DEVELOPMENT OF FINITE ELEMENT BRIDGE MODELS	106
5.1. Structural model	106
5.2. Pile-soil model	113
5.3. Abutment backfill model	117
5.4. Applied temperature distribution	125
5.4.1. Spatial distribution	125
5.4.2. Time variations	127
6. ANALYTICAL STUDY AND INTERPRETATION OF EXPERIMENTAL RESULTS FOR THE GUTHRIE COUNTY BRIDGE	129
6.1. Bridge displacement	129
6.1.1. Longitudinal abutment displacements and change in bridge length ..	131
6.1.2. Transverse abutment displacement	134
6.1.3. Abutment rotation in a vertical plane	136
6.1.4. Relative displacements at the piers	141
6.1.5. Relative displacements at the abutments	142
6.2. Pile strains	144
6.2.1. Pile flexural-bending strains	144
6.2.2. Pile axial strains	155
6.3. Girder strains	155
7. ANALYTICAL STUDY AND INTERPRETATION OF EXPERIMENTAL RESULTS FOR THE STORY COUNTY BRIDGE	163
7.1. Bridge displacement	163
7.1.1. Longitudinal abutment displacements and change in bridge length ..	163
7.1.2. Transverse abutment displacement	167
7.1.3. Abutment rotation in a vertical plane	168
7.1.4. Relative displacements at the piers	169
7.1.5. Relative displacements at the abutments	170
7.2. Pile strains	171
7.2.1. Pile flexural-bending strains	171
7.2.2. Pile axial strains	181
7.3. Girder strains	182
8. SUMMARY, CONCLUSIONS, AND RECOMMENDATIONS	187
8.1. Summary	187
8.2. Conclusions	188
8.3. Recommendations	191

APPENDIX A – EXPERIMENTAL MONITORING PROGRAM 193

APPENDIX B – ADDITIONAL ANALYSIS OF THE EXPERIMENTAL RESULTS.. 232

APPENDIX C – PILE-TO-SOIL INTERACTION 244

REFERENCES..... 254

ACKNOWLEDGMENTS..... 259

ABSTRACT

Integral-abutment bridges eliminate the expansion joints that are generally used to accommodate bridge length changes due to daily and annual temperature variations. Additional stresses and displacements due to the thermal loading are induced in these indeterminate structures that are not typically associated with bridge structures supported on pins and rollers. The goal of this research was to determine the effects of the thermal loading on two integral-abutment bridges.

Extensive field monitoring was conducted on two, in-service, skewed, integral-abutment bridges located in central Iowa. The experimental program included long-term monitoring of longitudinal and transverse abutment displacements, relative displacements of the superstructure over the pier caps, strains in selected steel HP-shaped piles supporting the abutments, strains in several PC girders, bridge member temperatures, and end fixity of selected piles and girders in the abutments. The experimental temperature and displacement data was used to calibrate an ANSYS, finite-element model for each of the two monitored bridge structures. Experimental strains were verified and maximum strains due to the thermal loading were predicted for various members using the finite-element models.

1 INTRODUCTION

1.1 Background

Traditional bridge structures use expansion joint systems to accommodate bridge length changes due to annual temperature variations. Maintenance of the expansion joints incurs additional costs over the life of highway bridges. Water runoff from the bridge deck, often containing corrosive de-icing agents, permeates through the joint seals leading to corrosion and deterioration of the expansion joints. Integral-abutment bridges eliminate the expansion joints by casting the superstructure together with the abutment wall. Eliminating the expansion joint reduces the initial cost, maintenance cost, and also the cost of future modification such as widening [1,2].

Many states are currently designing integral-abutment bridges. A recent survey by the New York Department of Transportation indicated that more than thirty state transportation agencies in the United States and a few provincial agencies in Canada have experience with integral-abutment bridges. Most agencies indicate that the structures are performing well. Transportation agencies typically impose limits on bridge lengths and skew angles, which are often based on the agency's previous experience rather than a rational analysis. Bridge length limitations vary from 200 ft to 800 ft for bridges with precast-concrete (PC) girders [3].

Improved knowledge of the behavior of integral-abutment bridges is desired to develop a rational method for design. A primary concern of designers and researchers are the forces induced in the abutment and abutment piles due to the

expansion and contraction of the bridge. Previous studies have focused on, amongst other issues, the capacity of the piles, soil pressures acting on integral-abutments, bridge temperatures, thermal expansion properties of the construction materials, and creep and shrinkage effects [4-8].

Integral construction introduces additional structural stresses as a result of the restrained displacement of the bridge superstructure. Bridge displacements are caused by the thermal expansion and contraction of the bridge and by the creep and shrinkage of the concrete. The increased stresses must be considered when designing an integral-abutment bridge. The displacement of the abutments into the abutment backfill creates pressures on the wall and introduces forces into the supporting piles. The restraining forces of the abutment backfill and piles create additional forces in the bridge superstructure.

There are other benefits of integral construction other than reducing the cost of the structure. Reduced forming requirements and fewer parts results in more rapid construction. Integral construction of the girder and abutment provides additional capacity for seismic events. Tolerance problems associated with expansion bearings and joints are eliminated [2].

1.2 Objective and scope

Two, prestressed-concrete (PC) girder, integral-abutment bridges were instrumented to measure temperature, strain, and displacements at various locations on the bridges over a period of about two years. A finite-element, analytical model

was developed for each of the two monitored bridges to aid in the understanding of the responses of integral-abutment bridges to temperature changes.

The experimental investigation consisted of determining longitudinal and transverse abutment movements, strains in H-shaped steel piles, strains in prestressed concrete girders, temperature distributions, and the rotational fixity at the top of the piles and the ends of the girders in an abutment. Data were collected to measure effects of daily and seasonal temperature variations.

The experimental data were used to calibrate and refine finite element bridge models. The recorded temperature data was used as the input into the finite-element models. The analytical strain and displacement responses were compared to the experimental measurements. Maximum bridge member strains were predicted by the finite-element models.

Experimental results for entire duration of the monitoring period between December 17, 1997 and April 1, 2000 for the Guthrie County Bridge is included in this thesis. For the Story County Bridge, experimental results presented in this thesis are for the time period between July 8, 1998 and July 12, 1999. Experimental results for the Story County Bridge for the time period between July 12, 1999 and April 1, 2000 will be published in the final report for the Iowa Department of Transportation, which is scheduled for submittal in December of 2000.

2 LITERATURE REVIEW

2.1 Current practice in the United States and Canada

A survey of current practices for the design of integral-abutment bridges was performed by Kunin and Alampalli [9] for the New York State Department of Transportation. The questionnaire covered various aspects of the design and performance of integral-abutment bridges such as length and skew-angle limits, design assumptions, design procedures, and analysis procedures.

A total of 39 state and provincial transportation agencies in the United States and Canada responded to the survey. Thirty-one of these agencies indicated they had experience with integral-abutment bridges. For the most part, only minor problems with this type of a bridge had been encountered, including minor cracking in the deck near the piers, concrete cracking and spalling in the girder bearing areas, drainage problems for the abutment backfill, and the settlement of the bridge approach slabs. Only the State of Arizona did not recommend the use of integral-abutment bridges based on their experience with expensive repairs of the approach slabs [9].

Usually, passive-soil pressure is applied in the design of integral-abutment bridges. A few agencies neglect the effect of earth pressure on the abutments during longitudinal expansion of the bridge. The States of Alaska and North Dakota assume a specific soil pressure regardless of the actual design conditions. About one-third of the responding agencies apply special construction details to reduce backfill pressures on the abutment walls. These details include the use of a granular

embankment with an underdrain, foam backing on the abutment wall, and providing a gap between the abutment wall and a geotextile-reinforced backfill. Most of the agencies neglect the effects of the bridge skew on soil pressure [9].

Most agencies use steel HP-shaped piles to support integral-abutment bridges. However, some agencies use PC pipe and concrete-filled, steel-shell piles. More than half of the agencies design these piles for axial load and bending moment effects. Depending on the pile-to-abutment connection detail, fixed, pinned, or free pile-head conditions are used in the bridge analysis. Only twelve of the agencies require the use of prebored holes for pile driving. These prebored holes are filled with a bentonite slurry or sands, or are left unfilled [9].

A similar survey was performed by Wolde-Tinsae, Greimann, and Johnson [10] in the early 1980's. Twenty-nine of the fifty-two responses indicated that integral-abutment bridges were used at the time of that survey. The length limit on PC girder, integral-abutment bridges did not change significantly during the time between the two surveys. More than half of the agencies oriented piles for strong axis bending in the early 1980's. The recent survey indicated that states are more frequently orienting piles for weak-axis bending that is induced by longitudinal bridge movements. Only four of the twenty-nine agencies indicated the use of prebored holes before pile driving in the early 1980's, compared to twelve of the thirty agencies in the more recent study.

2.2 Bridge field studies and instrumentation

Hoppe and Gomez [11] monitored strain, temperature, and earth pressures for a two-span, composite, steel-girder bridge with integral backwalls during its construction and for two-and-a-half years after the completion of its construction. Earth pressures were monitored behind both abutments near the base of the abutment backwalls. Earth pressure was also measured near the bottom of the pile cap at one of the abutments, directly below the gage installed on the abutment backwall. Earth pressure within the backfill soil behind the pile cap was found to be nearly constant and close to the predicted at-rest soil pressure. Earth pressures directly behind the abutment backwall indicated the development of passive pressures at each end of the bridge. In the first two years after construction of the bridge, repeated resurfacing of the approach slabs was necessary due to excessive settlement of these slabs. The rate of settlement decreased in the second year after construction of the bridge.

Hoppe and Gomez measured the combined effects of axial and bending strains longitudinal stress in the bottom flange of the steel girders. As the air temperature increased, the compressive strain in the steel girder near the abutment increased simultaneously with the soil pressure behind the backwall. Compressive strains in the girder near the abutment were also observed during the winter when the measured soil pressures were negligible. The authors attributed this to the thermal gradient through the superstructure. They noted that the stresses in the girders caused by the daily temperature fluctuations might be more critical than the compressive forces caused by the restraining forces of the abutment backfill.

Field tests of a steel-girder, integral-abutment bridge were performed by Construction Technologies Laboratories (CTL) [8] to determine the temperature gradients in a bridge superstructure. CTL determined that the positive temperature gradient recommended by the AASHTO Specifications [12] was conservative, and that the AASHTO temperature gradient followed the general shape of the experimentally-measured, temperature gradients within the cross section. The maximum, experimentally-measured temperature differential was approximately 60% of the recommended maximum AASHTO temperature differential within a cross section.

Long-term monitoring of an unskewed, PC girder, integral-abutment bridge in Minnesota was performed by Lawver, French, and Shield [13]. The abutment piles were oriented for weak-axis bending with respect to abutment displacements in the longitudinal direction of the bridge. Longitudinal abutment movement was primarily a translational movement that induced double curvature bending of the piles. Tensile strains, which were recorded in a reinforcing bar in the approach slab near the connection of the slab to the deck of the bridge, were measured in the winter as the superstructure pulled the abutment away from the backfill.

Since these researchers applied strain gages to the abutment piles during the construction of the bridge, measurements were made of the induced axial strains in specific piles due to the weight of the bridge superstructure. For the combined dead load and thermal movements of the bridge, the maximum, axial, compressive strain in a monitored abutment pile was 390 microstrains. As the temperature of the bridge deck increased, the axial strains increased on an interior abutment pile and

decreased on an exterior abutment pile. The maximum longitudinal strains on an abutment pile that were induced by combined axial forces and bending moments corresponded to a compressive strain that was larger than the yield strain of the steel. The maximum combined strain was measured near the pile cap at the pile flange tips on the approach slab side of a monitored exterior pile.

Static live-load tests of the bridge involved the use of dump trucks loaded with sand. The results from the live-load test indicated that the three bridge spans acted independent from each other. Although the spans acted independently, the end spans did not behave as simple spans. The experimental midspan moments for the exterior spans were approximately 30% smaller than those for a pinned-end span model, and 20% greater than the moments predicted from a pinned/fixed-end span model. The center span behaved as a simple span.

2.3 Analytical studies

Previous analytical studies have investigated many aspects of integral bridges. Research has included the reaction of the soil backfill behind a translating abutment, the pile-to-soil interaction, bridge displacements, stresses induced in bridge members, and concrete creep and shrinkage effects.

CTL [8] performed a nonlinear, finite-element analysis involving the interaction between an abutment wall and the soil backfill. The CTL researchers determined that the Rankine, passive, soil-pressure model provided an adequate estimation of the soil pressures against the back of a bridge abutment when large abutment movements were caused by expansion of the bridge superstructure. The

Clough and Duncan [14] design curve for soil pressure that is based on wall movement provided a reasonable upper-bound for the soil pressure against an abutment experiencing large movements. A concentration of soil pressure occurs near the base of the abutment. This base pressure decreases with an increase in the abutment rotation. The CTL researchers determined that a decrease in compaction of the soil backfill from 90% to 80% will decrease the resultant passive-pressure soil force by a factor of 2.5. The researchers also determined that a decrease in the slope of the in-situ, backfill soil from 45° to 30° will decrease the resultant passive-pressure soil force by a factor of 2.

Lehane, Keogh, and O'Brein [15] developed a simplified, elastic model to predict the axial forces and bending moments induced in the superstructure of a frame-type, integral bridge due to the thermal expansion of the bridge. An expression for the equivalent, linear-stiffness modulus for a cohesionless-soil backfill was developed for various dry-soil densities, effective soil stresses, and average, shear-strain levels. A simplified, plane-frame model that incorporated an equivalent abutment height and a translational, linear spring at the deck level was developed to represent the abutment and soil backfill system. The results from the simplified analytical model correlated well with the results predicted by a more detailed finite-element model.

Ting and Faraji [16] performed a three-dimensional, finite-element analysis of a three-span, unskewed, steel-girder, integral-abutment bridge using GT-STRUDL [17]. The bridge deck and abutments were modeled using plate elements, and the girders, piles, piers, and pier caps are modeled as beam elements. Two conditions

were considered to represent the interaction between the girders and the deck: with and without considering eccentricity between the centers of gravity of the girders and deck. The soil backfill behind the abutments and against the piles were modeled as uncoupled, non-linear springs that were located at the abutment wall and pile nodes. The non-linear soil properties for the soil against the back of the abutment backfill and against the pile were based on design curves by Clough and Duncan [14] and the American Petroleum Institute [18], respectively. A soil-parameter study was conducted by varying the stiffness of the soil behind the abutment and against the piles: loose and loose, loose and dense, dense and dense, and dense and loose, respectively.

Ting and Faraji determined that the eccentricity between the centers of gravity of the deck and girders must be considered to properly predict bridge behavior. Modeling the deck and girders without the proper eccentricity greatly decreases the flexural rigidity of the superstructure. For the models incorporating eccentricity of the deck and girder system, the abutment backfill stiffness controlled the displacement of the abutments. Longitudinal displacement of the base of the abutment ranged from 0.36 to 0.38 in. (9.1 to 9.7 mm) for a loose abutment backfill and 0.26 to 0.28 in. (6.6 to 7.1 mm) for a dense abutment backfill. The abutment rotation was approximately 0.060° (1050 microradians) for a loose abutment backfill and about 0.100° (1750 microradians) for a dense abutment backfill. The maximum moments in the piles, which occurred at the abutment-to-pile connection, ranged from 55 to 80 k-ft (75 to 110 kN-m) for a loose abutment backfill and 20 to 35 k-ft (27 to 47 kN-m) for a dense abutment backfill. The abutment backfill nearly reached a full-passive-

soil stress condition. The distribution of backfill pressures with depth was slightly nonlinear, with lower soil pressures near the bottom of the abutment.

Ting and Faraji developed two-dimensional, finite-element models for the same bridge. One-seventh of the bridge cross section was modeled since the bridge contained seven piles per abutment and seven girders. Pier support conditions were varied using pins, rollers, or a pier model incorporating nonlinear-soil springs. For non-skew bridges, the abutment and pile displacements, the pile moments, and the girder moments from a two-dimensional model with the bridge piers modeled as roller supports had good correlation with those from a three-dimensional model.

A two-dimensional model was developed by Girton [7] to predict the longitudinal movement of an abutment in an integral-abutment bridge. A frame model, which incorporated the flexural stiffness of the piles and the axial and flexural stiffness of the bridge superstructure, was developed that is used to determine the longitudinal displacement of the bridge. Girton neglected the abutment displacement restraint of the soil backfill, since the magnitude was small relative to the bridge movement. A bi-linear, temperature distribution through the depth of the superstructure was applied to the model. Girton also used the two-dimensional frame model for the prediction of pile strains due to longitudinal thermal movement of an abutment.

A lateral-frame model was developed by Girton to predict the pile strains induced by the lateral movement of a skewed abutment. Equivalent cantilevers were used to model the piles. An axial spring at the bottom of the equivalent

cantilever length to represent the axial shortening of the pile. Transverse abutment movements were calculated for an applied lateral force that corresponded to the transverse component of a passive normal and frictional soil backfill forces acting on the abutment.

Small-scale-model tests on steel H-shaped piles subject to lateral and vertical loads were performed by Amde, Chini, and Mafi [19]. The piles were tested in a tank that contained compacted sand with a uniform density throughout the depth. The first test involved measuring the vertical displacement response of a pile due to an applied axial load. A second test measured the flexural bending strains induced in the pile due to an applied lateral load at the top of a pile. Finally, the researchers performed a combined axial and lateral load test on the piles.

Amde, Chini, and Mafi compared the experimental results for lateral pile displacements, bending moments due to lateral displacements of the pile head, and vertical load capacities with those results that were predicted by a nonlinear, finite-element program developed by Wolde-Tinsae, Greimann, and Yang [20] for soil-to-pile interaction. The soil force versus displacement curves were approximated using the Ramberg-Osgood model [21]. The finite-element predictions for the lateral displacement at the top of the pile were conservative for the lateral loading condition, i.e. the analytical displacement was greater than the experimental displacement for the same applied lateral load. The finite-element model underestimated the vertical-load capacity of a friction pile. For the case with a combined axial and lateral load on the piles, the vertical soil resistance was exceeded before a plastic hinge was

developed in the steel piles. This behavior was observed in both the experimental testing and the analytical models.

Kamel, et.al. [22] investigated the use of PC piles in integral-abutment bridges. These researchers investigated the lateral load versus lateral deflection responses for PC piles and steel HP-shaped piles. Steel piles experienced greater lateral displacements than that for the PC piles before the pile cross section reached the allowable moment strength. The laboratory pile tests revealed that loose sand, which is typically used to fill prebored holes, had a significant effect on the lateral displacement of both types of piles. Maximum lateral displacements for a given pile were dependent on the lateral stiffness of the soil against the piles in the upper 10 ft. of the pile length. Soil stiffness below this depth had a negligible effect on the lateral pile displacement at the pile head. This behavior was observed for both PC and steel HP-shaped piles.

2.4 Integral-abutment design models

2.4.1 Coefficient of thermal expansion and contraction of concrete (α -coefficient)

The American Concrete Institute (ACI) publication ACI 209R [23] provides a lower and upper-bound value for the coefficient of thermal expansion and contraction (α -coefficient) of 4.7×10^{-6} in./in./°F (8.5×10^{-6} mm/mm/°C) and 6.5×10^{-6} in./in./°F (11.7×10^{-6} mm/mm/°C), respectively. These α -coefficients can be used to estimate a range of longitudinal thermal movement for highways and bridges. Also, ACI 209R provides an empirical equation to determine an α -coefficient that is based on the

environmental conditions for exposed concrete and for the characteristics of the total aggregate.

Researchers at CTL [8] recommended design values for the α -coefficient of concrete equal to 6.0×10^{-6} in./in./°F (10.8 mm/mm/°C) in the absence of more precise information. This magnitude for the α -coefficient was conservative. The researchers at CTL experimentally determined an average α -coefficient for concrete equal to 4.9×10^{-6} in./in./°F (8.8 mm/mm/°C).

Methods developed by Emanuel and Hulseley [24] may be used to determine an accurate value for the α -coefficient of concrete when the concrete mixture information is available. Their approach incorporates the characteristics of the aggregates, the concrete-mix proportions, moisture content, temperature, and age of the cured concrete.

2.4.2 Bridge displacement

Researchers at CTL determined that free expansion of a bridge superstructure provides a reasonable estimation of the thermal expansion for a bridge. Abutment and pier restraints against longitudinal displacement of a bridge superstructure have a negligible effect on the change in bridge length due to thermal expansion. The PC-girder, integral-abutment bridge monitored by Lawver [13] had a thermal expansion equal to about 96% of the theoretical elongation of an unrestrained structure.

Abutment movements that are transverse to the bridge length need to be considered in the design of integral-abutment bridges. The skew angle of a bridge, abutment wingwalls, and length-to-width ratio of the bridge affect the magnitudes of

transverse movements of the abutments. Based on the typical soil-friction angles of a granular backfill, researchers at CTL noted that special transverse movement provisions for an abutment could be neglected when the bridge skew angle does not exceed 20° . Transverse movement of an abutment can occur when the friction angle for the abutment backfill is exceeded. CTL presented a design chart for determining the magnitude of transverse movement of an abutment that is based on the skew angle for a bridge, length of the bridge, and bridge length-to-width ratio. Thermal expansion of the abutment was included by CTL after using the design chart to determine the transverse abutment movement. This expansion induces displacements along the width of an abutment with respect to the longitudinal centerline of the bridge [8].

2.4.3 Abutment backfill

Springman, Norrish, and Ng [25] provided recommendations for the design of integral-abutments. These researchers recommended that a medium-dense to dense, granular backfill be used behind the abutments. A lower stiffness backfill was not recommended, since the cyclical movements of the abutment over time will compact the backfill material. If a loose backfill was used, settlement problems would occur for the approach slab. The grain size of the granular material should be in the sand-to-gravel range. A backfill containing silt may cause capillary action for the water in the backfill, which would increase the effective stresses in the soil and increase the ultimate passive force on the abutment. The length of the soil settlement region behind an abutment was expected to be about 60% of the abutment wall height.

CTL [8] stated that high compaction of the backfill soil behind the abutment does not seem to be advantageous, since voids will still occur in the soil. CTL noted that the passive-soil pressure is lower for a loose backfill compared to that for a dense backfill. CTL recommended the use of a well-graded, granular soil with approximately 90% relative compaction, which approximately represents the medium-dense condition as defined by Clough and Duncan [14].

3 EXPERIMENTAL MONITORING PROGRAM

3.1 Overview

This section provides a brief overview of the experimental monitoring program used in this project. A more detailed discussion of the characteristics of the instrumented bridges and the experimental monitoring program is provided in Appendix A.

3.1.1 Bridge descriptions

Two, in-service, integral-abutment bridges that have steel, HP-shaped piles and PC girders were experimentally monitored in this project. The first bridge, referred to in this thesis as the Guthrie County Bridge, is on Route P28 where the highway crosses the Middle Raccoon River in Guthrie County near the town of Panora, Iowa. The installation of the instrumentation at the Guthrie County Bridge was completed in December of 1997. The second bridge, referred to in this thesis as the Story County Bridge, is on Route E26 where this highway crosses over Squaw Creek in Story County, just northwest of the City of Ames, Iowa. The installation of the instrumentation was completed at the Story County Bridge in August of 1998.

The Guthrie County Bridge is a three-span, integral-abutment bridge with a skew angle of 30° . A summary of the geometric characteristics of the Guthrie County Bridge is provided in Table 3.1. The abutments are supported on piles in a U-shaped arrangement, with a single row of ten, HP10x42, steel piles under the backwall and an HP10x42 pile under each wingwall. In the abutment backwall, the

Table 3.1. Characteristics of the instrumented bridges [26]

	GUTHRIE COUNTY BRIDGE	STORY COUNTY BRIDGE
Total bridge length	318 ft. - 0 in. (96.9 m)	201 ft. - 4 in. (61.4 m)
Spans	105.75, 106.5, 105.75 ft. (32.2, 32.5, 32.2 m)	64.08, 73.17, 64.08 ft (19.5, 22.3, 19.5 m)
Skew	30°	15°
Abutment pile arrangement	U-shaped	Single row
# of piles per abutment	12	7
Bridge orientation	North-south	East-west
PC girders (number/type)	5 girders, Iowa D	5 girders, Iowa C
Pier type	Tee pier	Pedestal pier
Bridge width	30 ft. (9.1 m)	30 ft. (9.1 m)

piles are oriented with their webs parallel to the abutment face. The piles in the wingwalls are oriented with their webs perpendicular to the roadway. Prebored holes that were filled with a bentonite slurry were specified for the abutment piles at this bridge. The two, Tee-shaped piers are supported by a reinforced concrete (RC) footing keyed into shale bedrock. The bridge geometry is symmetrical, except for at the connection of the bridge superstructure to the piers. An expansion pier was specified at the south pier. At the expansion pier, the PC girders rest on 3.75 in. (95 mm)-thick, steel-reinforced, neoprene pads and the RC diaphragm cast between the girders does not extend down to the top of the pier cap. A fixed pier was specified at the north pier. The RC diaphragm at the fixed pier was cast into a keyway that was lined with expansion-joint filler. The PC girders are supported by thinner, 1 in. (25 mm)-thick, neoprene pads at this pier.

The Story County Bridge is a three-span, integral-abutment bridge with a skew angle of 15°. The characteristics of the Story County Bridge are provided in Table 3.1. Each abutment is supported on seven, HP10x42, steel piles, oriented with their webs parallel to the abutment face. The wingwalls are cantilevered straight back from the backwall, parallel to the roadway centerline. The wingwalls in this bridge are not supported on piles. The piers at this bridge are pedestal-type piers supported by twelve, HP10x42, steel piles. A fixed detail between the bridge superstructure and the pier cap was specified at both piers.

3.1.2 Instrumentation packages

Instrumentation packages were developed to measure the seasonal thermal effects on the selected integral-abutment bridges [26]. String-potentiometer, displacement transducers were used to measure abutment displacements in the longitudinal and transverse directions of the bridges, relative displacements of the bridge superstructure over the piers, relative rotations between an abutment pile cap and a pile, and the relative rotation between a PC girder and an abutment backwall. At one abutment for each of the monitored bridges, a tiltmeter was installed to measure the abutment rotation in the vertical plane parallel to the longitudinal axis of the bridge. Weldable, electrical-resistance, strain gages were applied to selected steel, HP-shaped, abutment piles at each bridge to measure longitudinal strains in these piles. Electrical-resistance, strain gages were used at the Guthrie County Bridge to measure the strain gradient through the depth of the PC girders. Vibrating-wire strain gages were installed at the Story County Bridge to measure these PC girder strains. Thermocouples were embedded in various bridge members to

establish temperature distributions in the monitored bridges. Thermocouples were also installed near the strain gages and displacement transducers to correct for the temperature induced errors in the gages. A data-acquisition system was installed at each bridge to record data for each instrumentation device at selected time intervals.

Table 3.2 provides a list of the measurements made during the experimental monitoring program at the Guthrie County Bridge and Story County Bridge. Table 3.3 shows the number of each type of instrumentation device that was used at the monitored bridges.

Table 3.2. Experimental measurements at the monitored bridges [26]

MEASUREMENT	GUTHRIE COUNTY BRIDGE	STORY COUNTY BRIDGE
Longitudinal abutment displacements	Each abutment	Each abutment
Transverse abutment displacements	One abutment	One abutment
Strains in steel piling	Five piles	Four piles
PC girder strains	Eight locations	Six locations
Displacements of a pile relative to RC pile cap	One pile location	One pile location
Vertical temperature gradient through superstructure	12 locations	14 locations
Relative displacements of bridge superstructure over piers	Each pier	Each pier
Concrete strains in pile cap	One abutment	One abutment

Table 3.3. Number of instrumentation devices installed for field monitoring [26]

INSTRUMENT TYPE	NUMBER OF INSTRUMENTS INSTALLED AT THE:	
	Guthrie County Bridge	Story County Bridge
Displacement transducers	16	11
Tiltmeters	1	1
Strain gages on piles	40	31
Strain gages on PC girders	16	12
Strain gages on pile cap	5	4
Thermocouples	43	46
Total	121	105

3.2 Instrument temperature corrections

Since the instrumentation devices were subjected to the same temperatures as the bridges, temperature corrections had to be made for some of the displacement and strain data. The strain measurements made with the electrical-resistance strain gages were more sensitive to temperature-induced errors than the other instrumentation devices. This section will describe the basic concepts involved in the corrections applied to the strain and displacement data.

Thermocouples were installed near the instrumentation devices to provide a temperature of the instrument at the time that measurements were made. The temperatures of the displacement transducer extension wires were measured with thermocouples placed near the mid-length of the wire in each of the wooden box enclosures. The temperature of the vibrating-wire strain gages was measured with a thermistor that was built into each strain gage. The temperatures of the electrical-resistance strain gages applied to the steel piles at both bridges were measured with

thermocouples mounted to each pile surface with adhesive. The temperatures of the electrical-resistance strain gages bonded to concrete at the Guthrie County Bridge were measured by the thermocouples embedded in the PC girders near strain gage.

3.2.1 Corrections for displacement transducer

Laboratory tests [27] of a displacement transducer showed that these devices were insensitive to temperature changes. However, the extension wire that linked the displacement transducer wire to the bridge experienced a change in its length, L_{wire} , when the temperature changed. The length of some of these extension wires was large enough (108 to 120 in., or 2700 to 3000 mm) that the change in length of the wire due to temperature changes would affect the magnitude of the displacement measurements. The change in length, ΔL_{wire} , of an extension wire due to a change in temperature, ΔT_{wire} , of the wire is:

$$\Delta L_{\text{wire}} = \alpha_{\text{wire}} \Delta T_{\text{wire}} L_{\text{wire}} \quad (3.1)$$

The α -coefficient of the wire, α_{wire} , was 6.33×10^{-6} in./in./°F (11.4×10^{-6} mm/mm/°C), as specified by the manufacturer. This change in the wire length was added to the raw displacement transducer measurement to obtain the correct displacement magnitude.

3.2.2 Corrections for compensated resistance strain gages

The change in strain, $\Delta \varepsilon$, is defined as the change in length, ΔL , of a specimen divided by its original length, L . Changes in length are, amongst other factors, due to imposed stress, $\Delta \sigma$, and due to temperature change, ΔT . The resulting change in total strain, $\Delta \varepsilon_{total}$, is:

$$\Delta \varepsilon_{total} = \frac{\Delta L}{L} \quad (3.2)$$

$$\Delta \varepsilon_{total} = \Delta \varepsilon_{stress} + \Delta \varepsilon_{temp} \quad (3.3)$$

$$\Delta \varepsilon_{total} = \frac{\Delta \sigma}{E} + \alpha \Delta T \quad (3.4)$$

in which α is the α -coefficient and E is the modulus of elasticity of the specimen.

Strain is experimentally determined by measuring the change in resistance of the strain gage. To obtain the change in strain due to stress, $\Delta \varepsilon_{stress}$, from the electrical-resistance strain gages, two temperature corrections are involved: (1) adjusting for apparent strain as described in manufacturer project literature [28], and (2) adjusting the output for a thermally induced Wheatstone-bridge completion error.

The first correction is necessary because the change in temperature effects the gage-grid elongation, base-material elongation, and the resistivity of the gage material. The temperature-induced resistance change, $(\Delta R/R)_{\Delta T}$, due to these effects is:

$$\left(\frac{\Delta R}{R} \right)_{\Delta T} = (\alpha_s - \alpha_g) S_g \Delta T + \gamma \Delta T \quad (3.5)$$

where α_s and α_g are the coefficients of thermal expansion for the specimen and gage, respectively, S_g is the gage factor, and γ is the temperature coefficient of resistivity of the gage material [29].

Temperature-compensated electrical-resistance strain gages were used for measuring strain due to stress on the steel piles. Temperature-compensated gages were selected so that the temperature-induced resistance change in Equation 3.5 was minimized. Over a wide temperature range, the gages are not perfectly compensated because of the nonlinear responses of the resistivity coefficient and expansion coefficients [29]. This resulted in a temperature-induced strain that is not caused by stress in the specimen, called an apparent strain [28].

The apparent strain induced by the change in gage material properties over a wide range in temperatures was adjusted using a fourth-order polynomial correction provided by the manufacturer. The resulting strain, $\Delta\varepsilon'$, measured by the gage after compensation for the apparent strain is:

$$\Delta\varepsilon' = \Delta\varepsilon - \Delta\varepsilon_{app} \quad (3.6)$$

where $\Delta\varepsilon$ was the uncorrected reading of the gage and $\Delta\varepsilon_{app}$ was the polynomial correction for apparent strain.

The second correction occurs because the electrical-resistance strain gages for this project were multiplexed into a Wheatstone quarter-bridge circuit. The Wheatstone-bridge completion resistor within the data acquisition system created a temperature-induced source of error. The resistance of this resistor, which was opposite the strain gage in the quarter-bridge circuit, changed with changes in temperature. To correct this error, a dummy, electrical-resistance, strain gage was attached to an unrestrained steel bar located in the box containing the datalogger. After correcting for the nonlinear thermal response of the dummy gage using Equation 3.6, with $\Delta\varepsilon'$ equal to $\Delta\varepsilon'_{dummy}$, the strain reading for this unrestrained steel bar should be equal to zero, since the bar was free of stress. Since $\Delta\varepsilon'_{dummy}$ was not equal to zero, the corrected dummy gage reading represents the Wheatstone-bridge completion error.

In summary, the uncorrected strain gage output recorded by the data acquisition system, $\Delta\varepsilon_m$, was corrected for the Wheatstone-bridge completion error by:

$$\Delta\varepsilon'_m = \Delta\varepsilon_m - \Delta\varepsilon'_{dummy} \quad (3.7)$$

The gage was then compensated for its apparent strain by Equation 3.6 to obtain the final compensated change in strain due to stress, $\Delta\varepsilon_{stress}$:

$$\Delta\varepsilon''_m = \Delta\varepsilon_{stress} = \Delta\varepsilon'_m - \Delta\varepsilon_{app} \quad (3.8)$$

3.2.3 Corrections for uncompensated resistance strain gages

Temperature-compensated, resistance gages were not used for PC girders at the Guthrie County Bridge. The girder strain gages have an α -coefficient equal to that of mild steel (6.5×10^{-6} in./in./°F, or 11.7×10^{-6} mm/mm/°C).

To illustrate the strains obtained from the uncompensated gages, the simple example of an unrestrained bar is used. A temperature increase in the bar will result in a total strain equal to $\alpha_{\text{specimen}}\Delta T_{\text{specimen}}$. Strain due to stress, $\Delta\varepsilon_{\text{stress}}$, is zero for the unrestrained bar. However, because of the difference in expansion coefficients, the strain gage will have a non-zero strain reading:

$$\Delta\varepsilon_m'' = \Delta\varepsilon_{\text{stress}} - \Delta T_{\text{specimen}} (\alpha_{\text{gage}} - \alpha_{\text{specimen}}) \quad (3.9)$$

The temperature term in Equation 3.9 was eliminated in the temperature compensated gages since α_{gage} equaled α_{specimen} . It should be noted that the gage strain reading in Equation 3.9, $\Delta\varepsilon_m''$, is the corrected value after accounting for apparent strain and Wheatstone-bridge completion errors in Equation 3.8.

Rearranging Equation 3.9 to solve for strain in the specimen due to stress:

$$\Delta\varepsilon_{\text{stress}} = \Delta\varepsilon_m'' + \Delta T_{\text{specimen}} (\alpha_{\text{gage}} - \alpha_{\text{specimen}}) = 0 \quad (3.10)$$

Substituting Equation 3.10 into Equation 3.3, the total strain in the unrestrained bar is:

$$\Delta\varepsilon_{total} = \left[\Delta\varepsilon_m'' + \Delta T_{specimen} (\alpha_{gage} - \alpha_{specimen}) \right] + \alpha_{specimen} \Delta T_{specimen} \quad (3.11)$$

which simplifies to:

$$\Delta\varepsilon_{total} = \Delta\varepsilon_m'' + \alpha_{gage} \Delta T_{specimen} \quad (3.12)$$

The changes in the PC girder strains reported in Chapter 4 are in the form of this “total-strain”, which includes strains due to stress and the contraction or expansion of the girder due to temperature. The analytical model results in Chapters 6 and 7 will compute strains due to stress in the PC girders.

3.2.4 Corrections for vibrating-wire strain gages

The temperature correction for the vibrating-wire strain gages is similar to the temperature correction applied to the uncompensated, resistance strain gages. A vibrating-wire gage measures the change in strain in the specimen by measuring the change in the natural frequency of a vibrating wire that is stretched between two mounting blocks. If the vibrating-wire gage is subject to temperature changes, the wire length and, hence, the natural vibration frequency of the wire changes without, necessarily, an associated expansion or contraction between the gage mounting blocks. Similar to Equation 3.12, the total strain at the location of the vibrating-wire gage is:

$$\Delta\varepsilon_{\text{total}} = \Delta\varepsilon'_m + \alpha_{\text{vibr}} \Delta T_{\text{vibr}} \quad (3.13)$$

The expansion coefficient, α_{vibr} , for the vibrating wire in the gage was 7.2×10^{-6} in./in./°F (13.0×10^{-6} mm/mm/°C), as provided by the gage manufacturer. The gage strain reading in Equation 3.9, $\Delta\varepsilon'_m$, is the corrected value after accounting for Wheatstone-bridge completion error in Equation 3.7.

3.2.5 Corrections for tiltmeters

The temperature corrections for the tiltmeters installed on the abutment walls at the Guthrie County Bridge and the Story County Bridge were described by Thomas [26]:

“Temperature corrections for the tiltmeters were made according to literature provided by the tiltmeter manufacture, Applied Geomechanics, Inc. Temperature variations can affect the output of an electrolytic tiltmeter by affecting the zero value of the tiltmeter and the scale factor, which relates measured voltage to an angular rotation magnitude. The tiltmeters were, to some degree, temperature-compensated by their internal circuitry. However, increased accuracy was obtained by using the results of temperature tests that were conducted by the manufacturer. Two temperature coefficients were provided by the manufacturer for each tiltmeter and the corrections were made according to an article supplied by the tiltmeter supplier.”

4 EXPERIMENTAL RESULTS

This chapter contains a summary of the experimental results obtained from the Guthrie County Bridge and the Story County Bridge. Supplementary commentary for the results presented in this chapter is provided in Appendix B.

4.1 Experimental data filtering

The Guthrie County Bridge was monitored from December 17, 1997 until April 1, 2000. The Story County Bridge was monitored from July 12, 1998 to April 1, 2000, but the filtering process for this bridge had only been completed through July 12, 1999 at the completion of this report.

With the massive amount of data accumulated, gages were expected to occasionally produce outlying data points. The initial data reduction process, as discussed in Appendix A, eliminated many of these data points. Gages were also expected to exhibit unreliable data or completely fail over the monitoring period due to a variety of problems. Problems encountered include water infiltration damaging the gage connection to the bridge element, moisture accumulating in the wire splices, or gage failure. Erroneous data was identified and corrected or eliminated before final experimental results were presented in this report.

4.1.1 *Thermocouples*

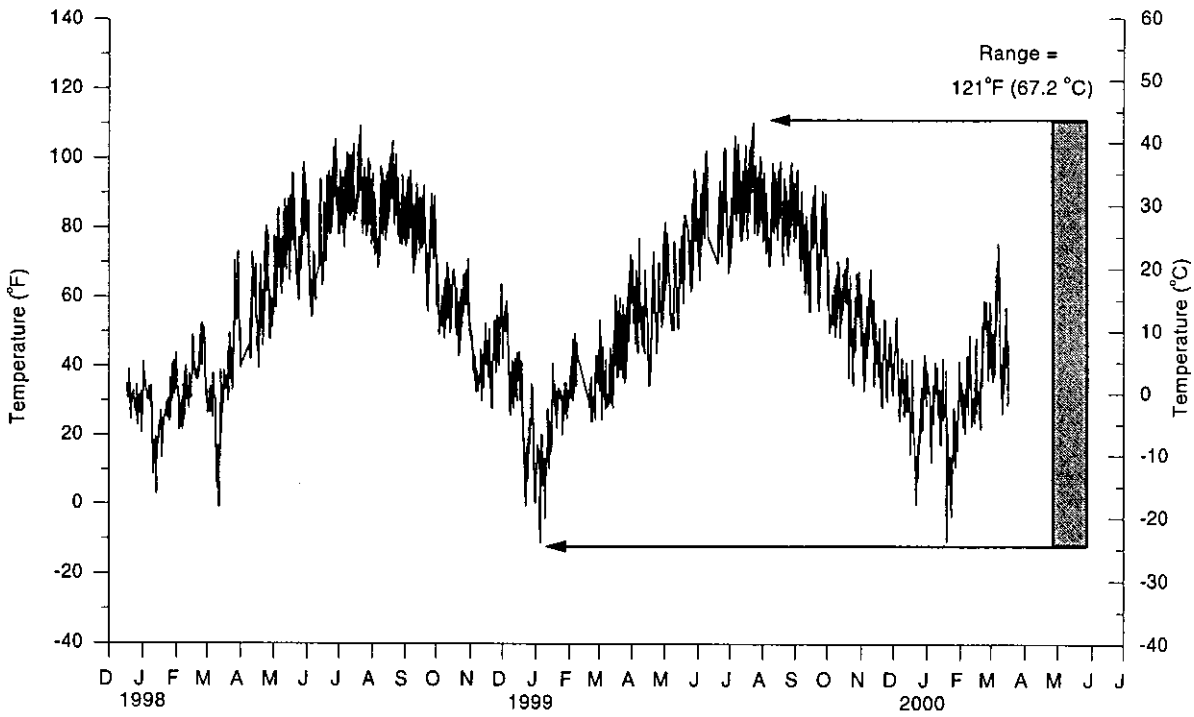
Since thermocouples measure absolute temperatures, the raw data was presented without modifications. Each thermocouple reading was plotted versus time to determine if it was functioning properly. Jumps and drifting of the thermocouple data were not encountered. Thermocouples were either working and

producing reliable temperatures, which followed an expected pattern of the concrete temperature over time, or were not working and producing temperature readings outside of the expected range. Temperatures that were obviously incorrect were discarded. A thermocouple (Guthrie TC-E-1SC-S) with reliable data over the entire monitoring period is shown in Figure 4.1(a). The maximum temperature range measured by the example thermocouple is shown to the right of the plot. In the case where the gage is considered reliable over the entire time period, the range is the difference between the maximum and minimum values of the gage. When a thermocouple failed during the monitoring period, the experimental temperature range was determined from the overall maximum and minimum reliable readings. Figure 4.1(b) shows a thermocouple (Guthrie TC-E-1SW-S) with time periods of unreliable data and the accepted temperature range for the gage.

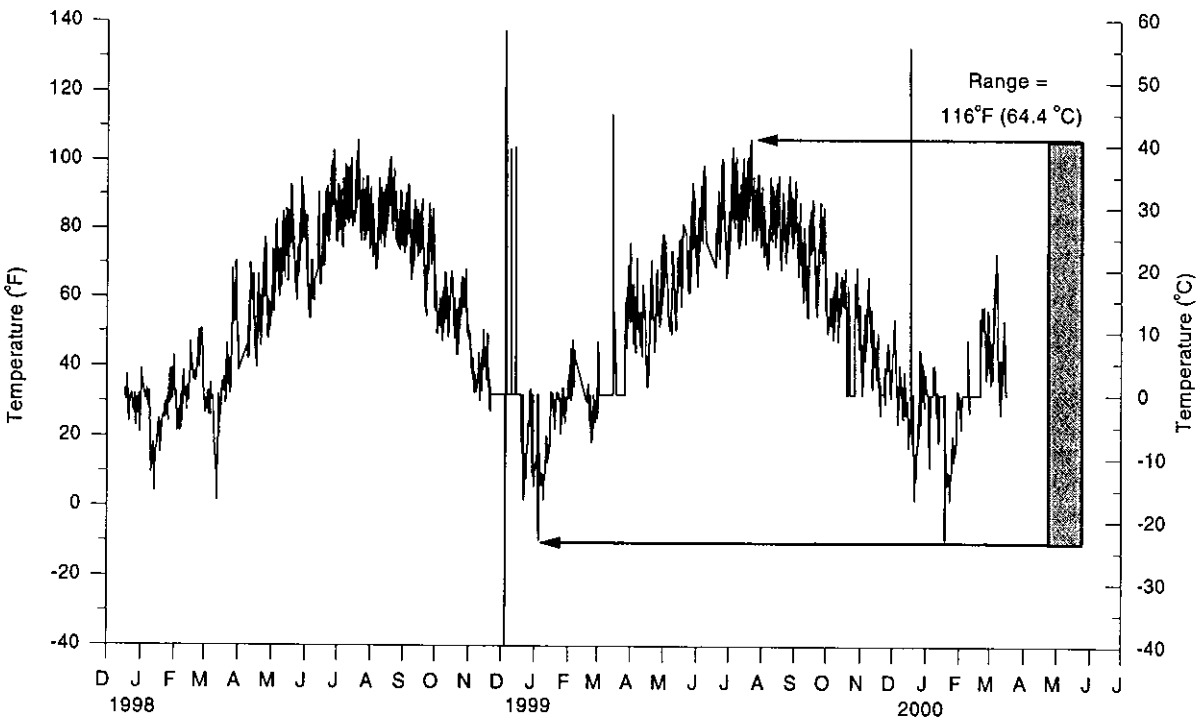
Tables 4.1 and 4.2 provide a summary of the times that each thermocouple was functioning properly for the Guthrie County Bridge and Story County Bridges, respectively.

4.1.2 Displacement transducers

Data from each of the displacement transducers were plotted versus time to determine if the gages were functioning properly. The displacement plots were compared with the average bridge temperature to verify that the recorded displacement correlated with temperature change. Faulty displacement measurements included sudden jumps in a displacement or the drifting of a displacement over time. Data was considered reliable after a displacement jump if the displacements regain correlation with temperature. However, a new temperature



(a) Reliable thermocouple (Guthrie TC-E-1SC-S)



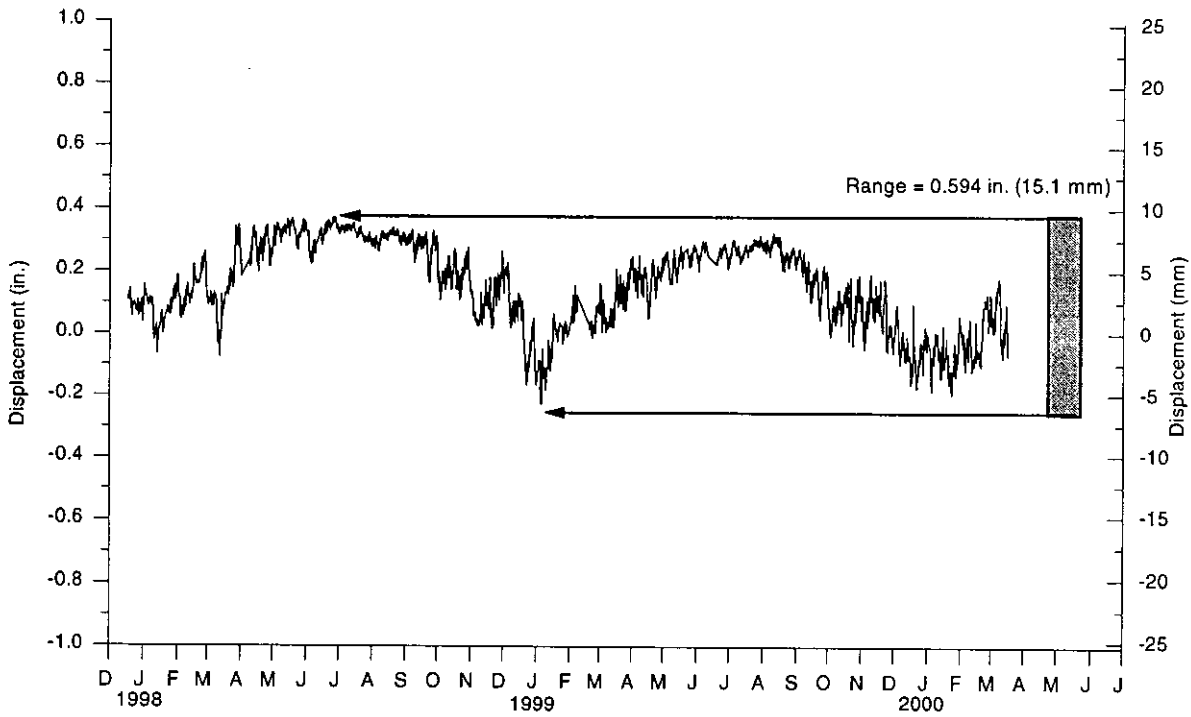
(b) Thermocouple with errors (Guthrie TC-E-1SW-S)

Figure 4.1. Typical thermocouple plots

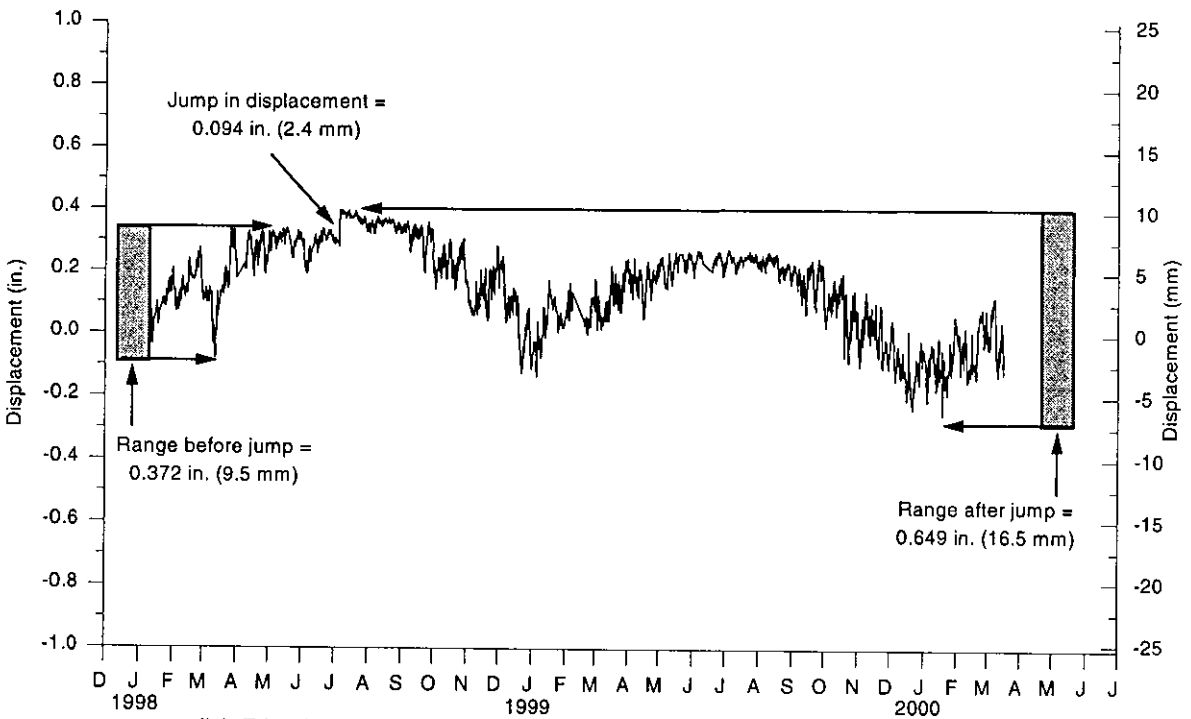
cycle for that displacement was started since the absolute displacement was not continuous across a displacement jump. Displacements continuously increasing or decreasing with time and not correlating with changes in temperature indicated a displacement drift. Drift may be a sign of a broken transducer or a moving benchmark post. Measurements from drifting displacement transducers are not considered reliable.

Figure 4.2(a) shows a plot of displacement versus temperature from a displacement transducer (Guthrie SP-SC-LB) with reliable data over the entire monitoring period. Figure 4.2(b) shows a plot of a displacement transducer (Guthrie SP-SE-LB) with an apparent jump in the displacement that occurred on July 5, 1999. The experimental displacement range was determined from a time period over which the gage was continuously producing reliable data. In the case of a distinct jump in a displacement, the range can be determined from the maximum and minimum displacement in the time period before the jump and after the jump, as shown by the bars in Figure 4.2(b). The displacement transducer (Guthrie SP-SE-LB) data shown in Figure 4.2(b) also indicated a possible drift, since the displacement in the second yearly cycle (1999) did not return to the level of the previous yearly cycle (1998). The displacement data is inconclusive whether there was drifting in the gage, or if the side of the abutment at the obtuse angle of the bridge deck is displacing over time towards the river.

Tables 4.3 and 4.4 provide a summary of the times that reliable data was obtained from each displacement transducer for the Guthrie County Bridge and Story County Bridge, respectively.



(a) Reliable displacement transducer (Guthrie SP-SC-LB)



(b) Displacement transducer with error (Guthrie SP-SE-LB)

Figure 4.2. Typical displacement transducer plots

4.1.3 Pile strain gages

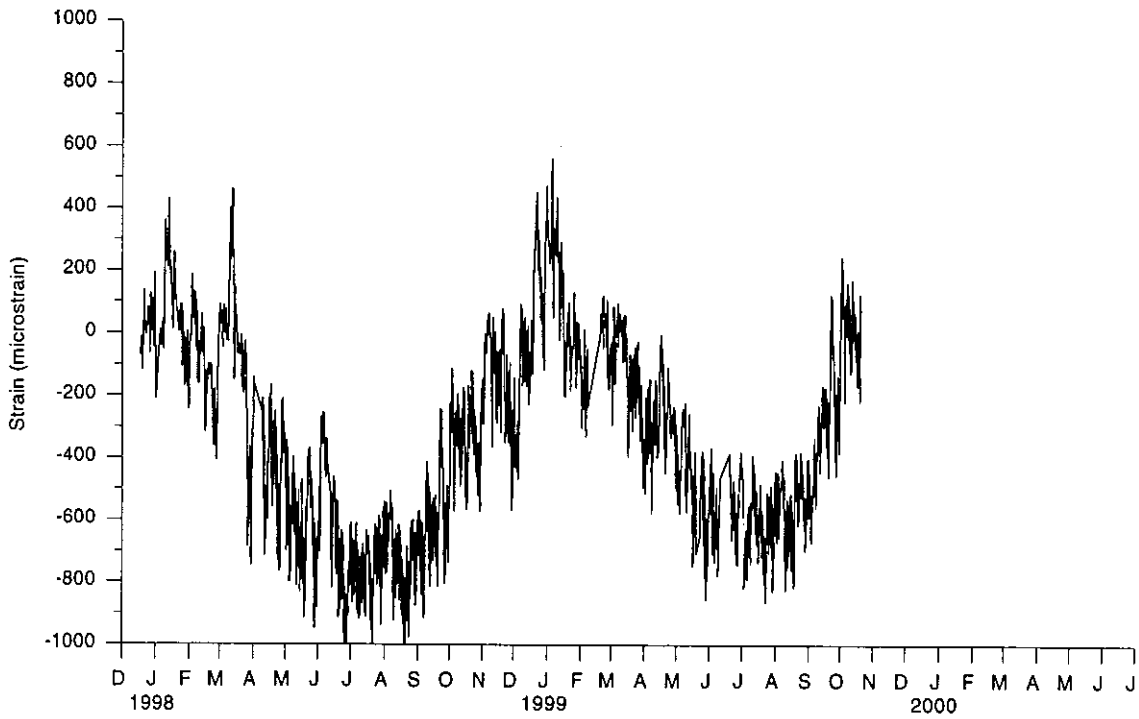
Pile strain gages required a more in-depth filtering process because the weldable, electrical-resistance strain gages had a higher rate of failure than the other instrumentation. The individual pile strain gage readings were plotted versus time and compared to the corresponding abutment displacement. Pile strain gage errors include strain jumps, drifting, and complete failure of the gages. Strain gage data was filtered by checking each gage individually and also by checking the bending, axial, and torsion strain components for each pile cross section.

A field investigation to determine the cause of the gage failure at the Guthrie County Bridge was described by Thomas [26]:

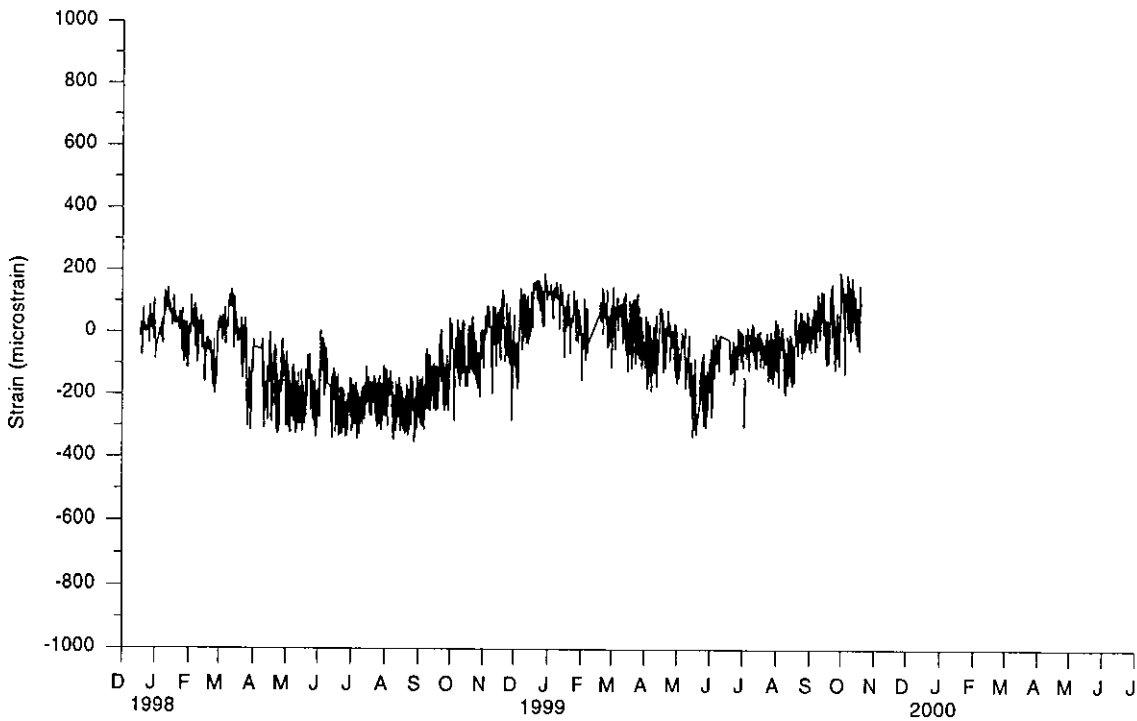
“A significant amount of reliable pile strain data was lost due to drifting of the strain gage readings. The drifting was most likely caused by moisture infiltration into the splice between a strain gage lead wire and the gage extension wire. These splices were protected with shrink-wrap tubing. Several of the lead-wire splices for the pile strain gages at the Guthrie County Bridge were examined on February 28, 1999. Several wire splices were disconnected to reveal that moisture had in fact infiltrated the wire splices. The inside surface of the outer layer of the shrink-wrap tubing was wet when it was cut away. Also, the shrink-wrap tubing that was originally placed around each of the three strain gage conductors did not appear to have closed tightly around the conductor insulation. Several splices were rehabilitated by applying heat to dry the splice and by coating the splice with a waterproof caulk to prevent any future moisture infiltration.”

The measured strains from the gages in the top cross section of the pile near the mid-width of the north abutment at the Guthrie County Bridge (Guthrie SG-NCP-SWT, SG-NCP-NWT, SG-NCP-SET, SG-NCP-NET) are shown in Figure 4.3. Initial data reduction had been completed to eliminate data points outside of the limits as described in Appendix A. Figure 4.4 shows the same set of strain gages after the apparent strain and the Wheatstone-bridge completion errors were corrected, as described in Section 3.2.2. The dummy gage used to correct the Wheatstone-bridge completion error was installed in March 1998; therefore, individual strain gage results could not be obtained before this date. The Wheatstone-bridge error is most noticeable for gages with small strain ranges, such as the gage (Guthrie SG-NCP-NWT) shown in Figure 4.4(b). Strain data obtained from the individual strain gages were visually checked for jumps and drifting.

Smaller individual gage errors are difficult to isolate when plotted over long time periods. Investigating each gage over daily or weekly time periods is a time consuming process and is impractical when large amounts of data exist, so other methods were investigated to assess the reliability of the strain gage readings. The method used to detect less visible errors in individual strain gage readings was to plot average strain components (bending, axial, and torsion) over time. The strain components should correlate with the abutment displacement over seasonal cycles. At each pile cross section with applied strain gages, as shown in Figure 4.5, the longitudinal strain, ϵ_i , due to stress in the pile is a superposition of the axial strain, ϵ_a , x-axis bending strain, ϵ_x , y-axis bending strain, ϵ_y , and normal warpage torsional

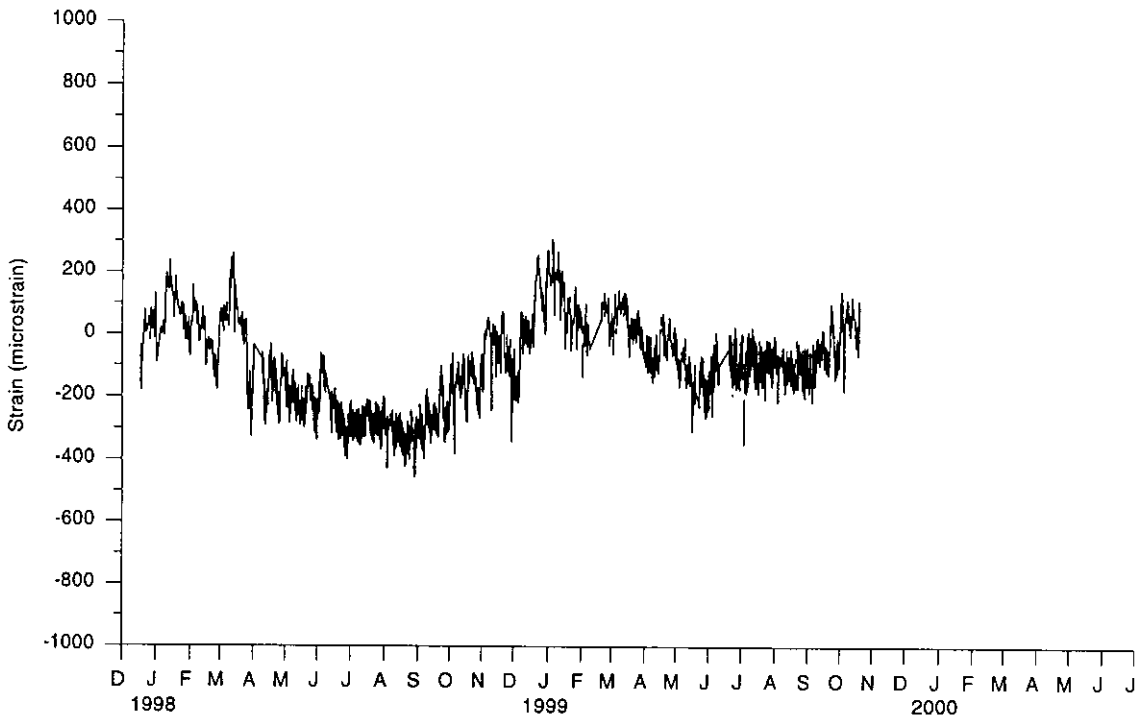


(a) Strain gage (SG-NCP-SWT) near the southwest flange tip

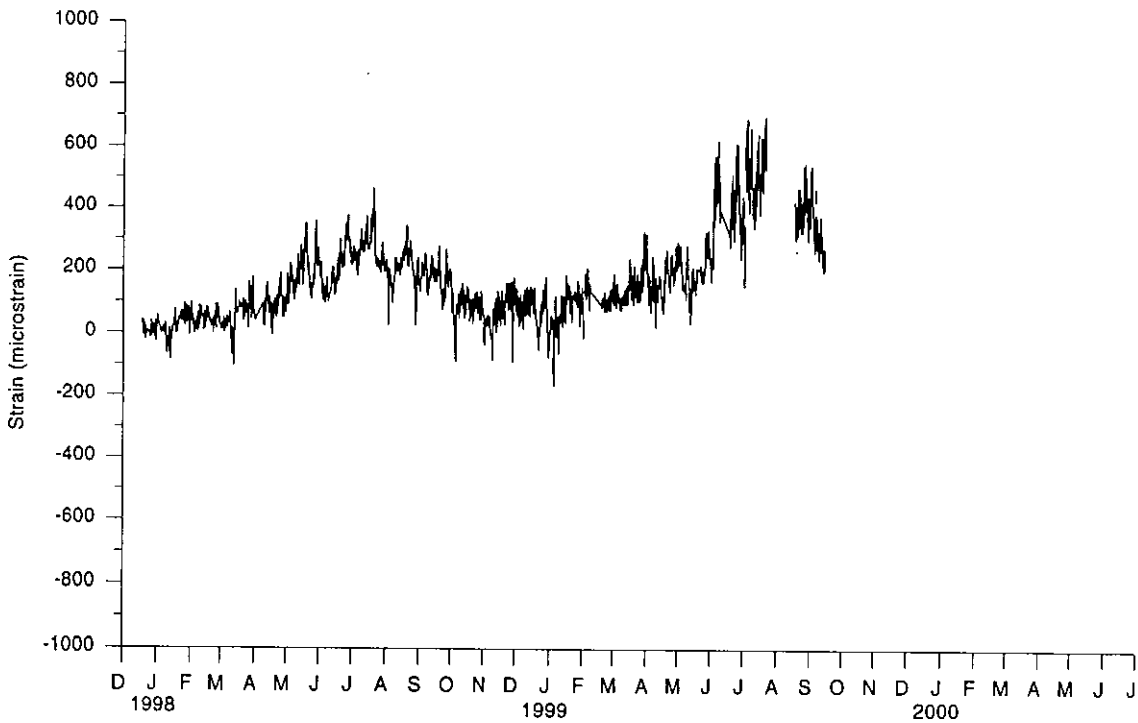


(b) Strain gage (SG-NCP-NWT) near the northwest flange tip

Figure 4.3. Raw individual strain gage data for the top cross section of the pile near the mid-width of the north abutment at the Guthrie County Bridge

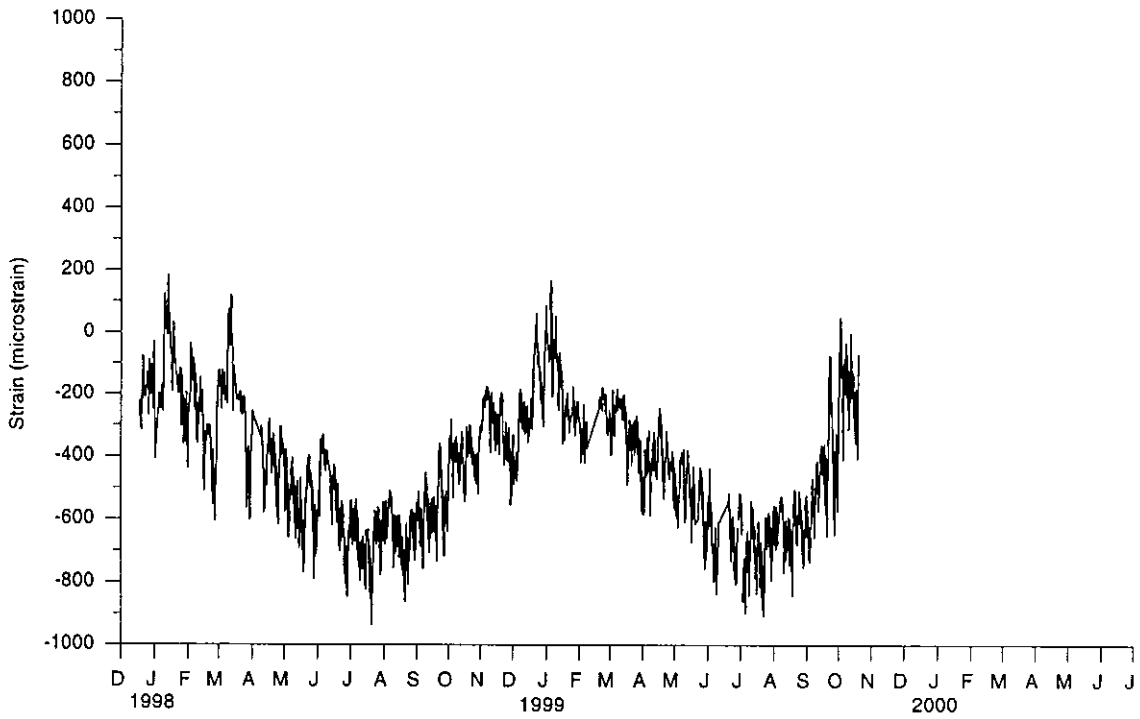


(c) Strain gage (SG-NCP-SET) near the southeast flange tip

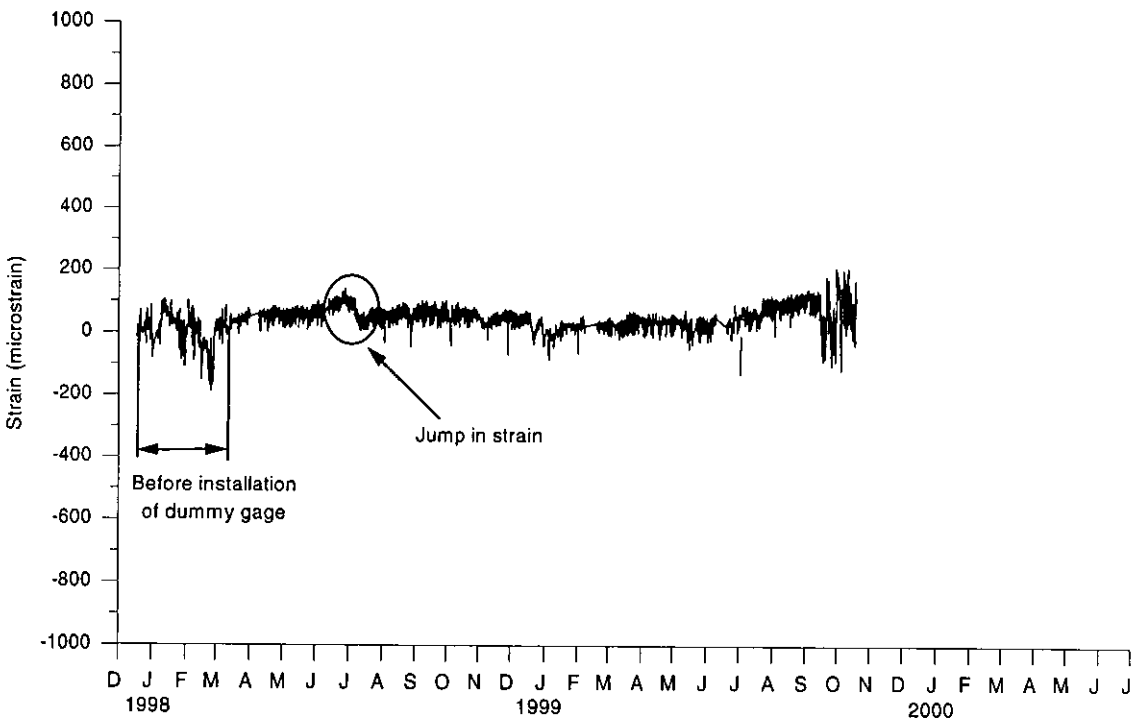


(d) Strain gage (SG-NCP-NET) near the northeast flange tip

Figure 4.3. (continued)

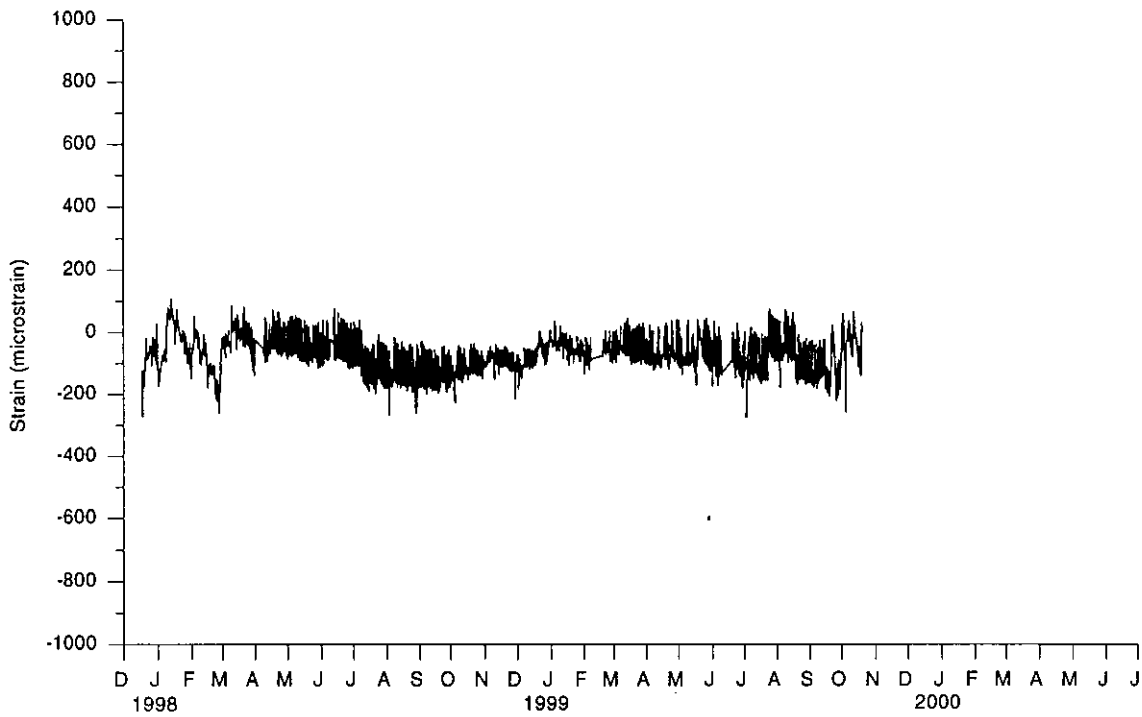


(a) Strain gage (SG-NCP-SWT) near the southwest flange tip

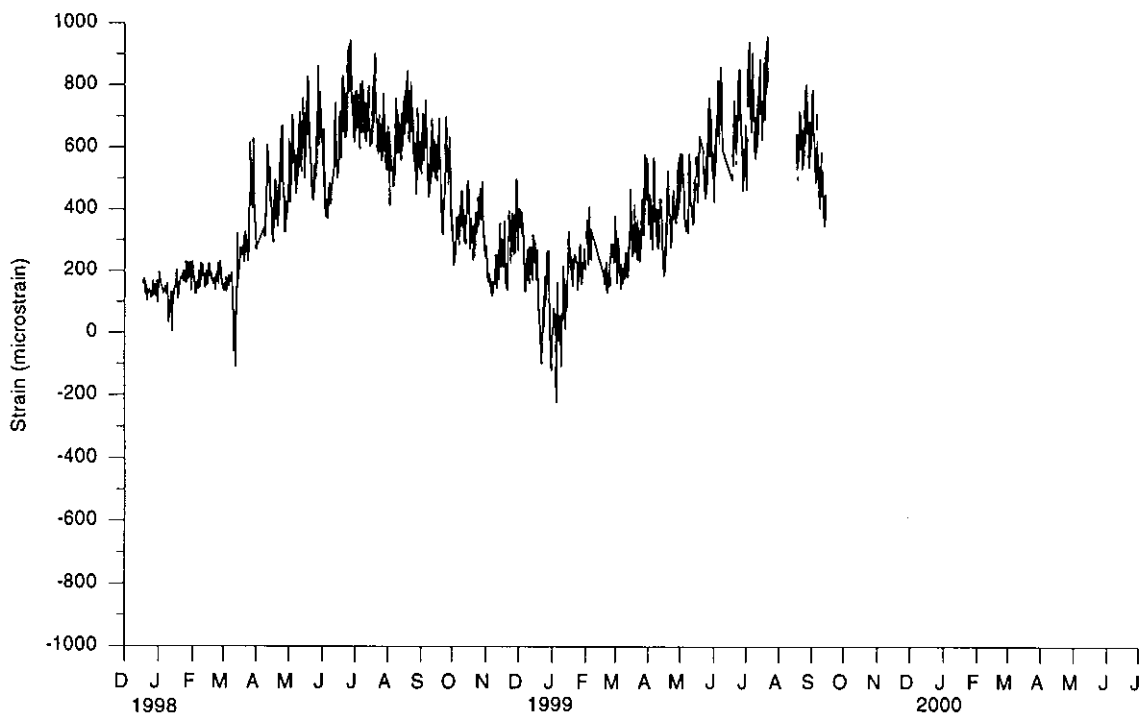


(b) Strain gage (SG-NCP-NWT) near the northwest flange tip

Figure 4.4. Individual pile strain gage results for the top cross section of the pile near the mid-width of the north abutment at the Guthrie County Bridge

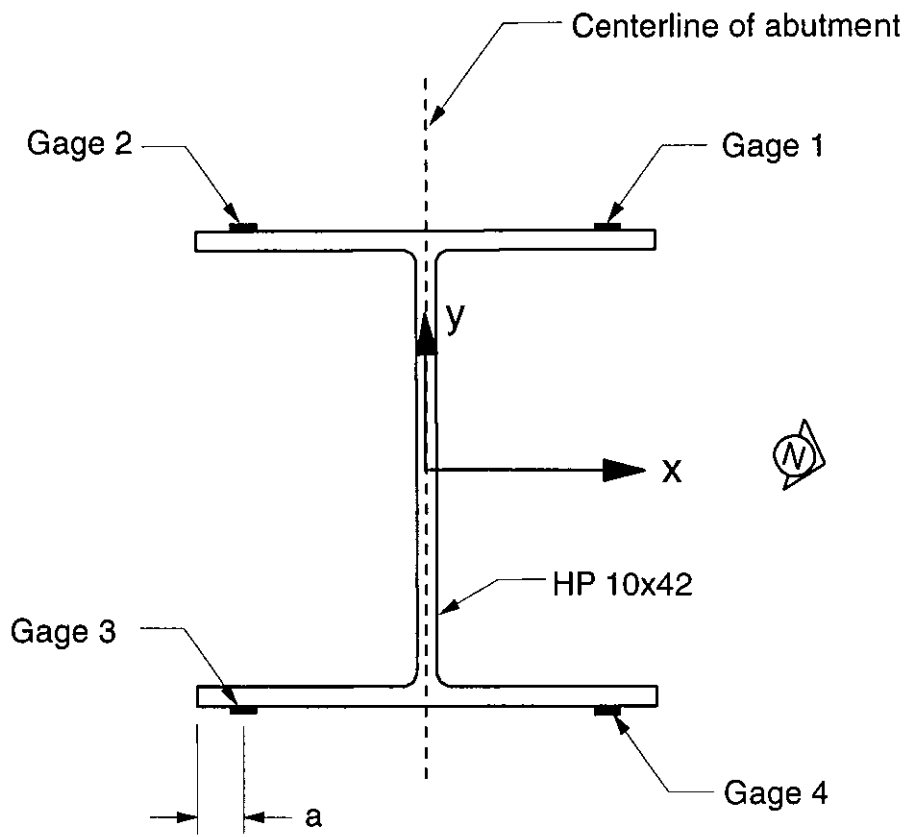


(c) Strain gage (SG-NCP-SWT) near the southeast flange tip



(d) Strain gage (SG-NCP-NWT) near the northeast flange tip

Figure 4.4. (continued)



$a = 1$ in. typical (all monitored piles at both bridges), except
1/2 in. at NW pile at the Guthrie County Bridge

Figure 4.5. Typical strain gage locations on a HP10x42 steel pile cross section

strains(ε_i). The strain relationships are given by Equation 4.1. The subscripts 1, 2, 3, and 4 correspond to the strain gages 1, 2, 3, and 4, respectively, shown in Figure 4.5.

$$\varepsilon_1 = \varepsilon_a + \varepsilon_x - \varepsilon_y + \varepsilon_t \quad (4.1)$$

$$\varepsilon_2 = \varepsilon_a + \varepsilon_x + \varepsilon_y - \varepsilon_t$$

$$\varepsilon_3 = \varepsilon_a - \varepsilon_x + \varepsilon_y + \varepsilon_t$$

$$\varepsilon_4 = \varepsilon_a - \varepsilon_x - \varepsilon_y - \varepsilon_t$$

With a properly functioning strain gage near each flange tip on an HP-shaped pile cross section, the range in pile strain components induced by axial force, x-axis bending, y-axis bending, and torsion can be determined from the following equations [30]:

$$\Delta\varepsilon_a = (\Delta\varepsilon_1 + \Delta\varepsilon_2 + \Delta\varepsilon_3 + \Delta\varepsilon_4)/4 \quad (4.2)$$

$$\Delta\varepsilon_t = (\Delta\varepsilon_1 - \Delta\varepsilon_2 + \Delta\varepsilon_3 - \Delta\varepsilon_4)/4$$

$$\Delta\varepsilon_x = (\Delta\varepsilon_1 + \Delta\varepsilon_2 - \Delta\varepsilon_3 - \Delta\varepsilon_4)/4$$

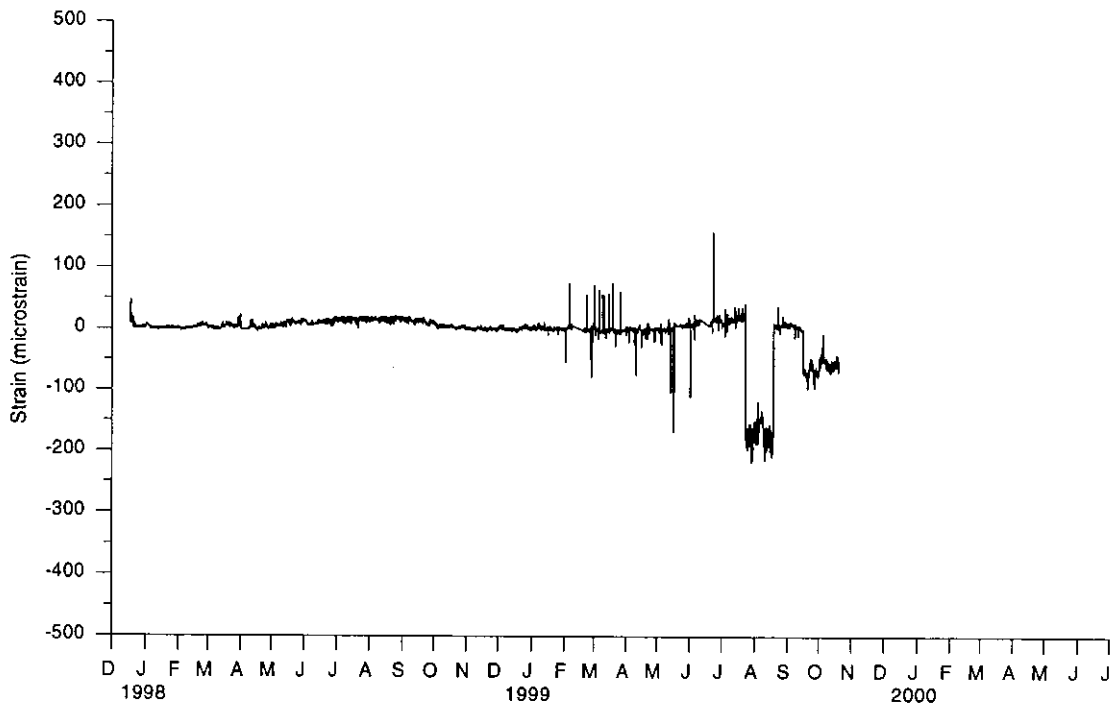
$$\Delta\varepsilon_y = (-\Delta\varepsilon_1 + \Delta\varepsilon_2 + \Delta\varepsilon_3 - \Delta\varepsilon_4)/4$$

in which $\Delta\varepsilon_1$, $\Delta\varepsilon_2$, $\Delta\varepsilon_3$, $\Delta\varepsilon_4$ are the range in temperature corrected strains from Equation 3.8 for the four gages at a particular cross section.

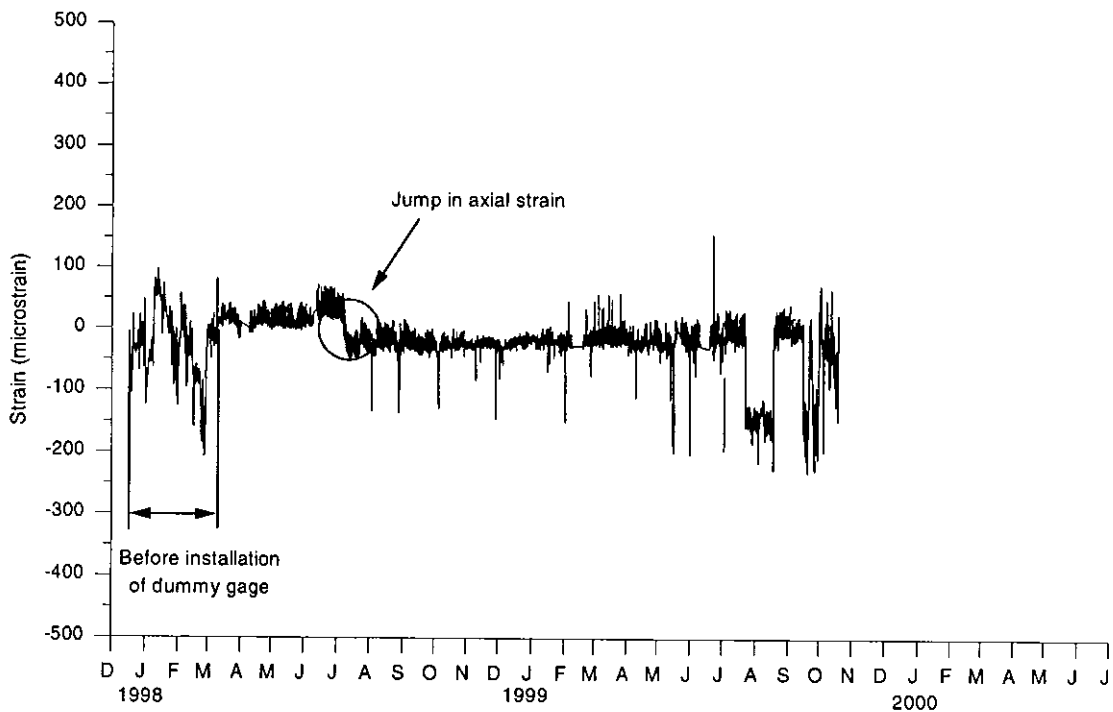
As described in Section 3.2.2, the dummy gage correction was required for the calculation of axial strains since the Wheatstone-bridge completion error is additive. Hence, axial strain could not be computed for the Guthrie County Bridge piles before the dummy gage installation in March 1998 and after July 1999 when the dummy gage readings became unreliable. For the other three strain components, the Wheatstone-bridge completion error is eliminated when taking the difference in gages. These strain components could be computed at times when reliable individual strain gage data was available.

Normal warpage torsional strains can be assumed to be near zero, as shown in Figure 4.6(a) for a cross section with four reliable strain gages. The ANSYS, finite-element models also verified that these torsional strains are negligible. With a near zero daily and seasonal variation in the normal warpage torsional strains, strain jumps for individual gages could easily be identified. Axial strains also had low daily and seasonal variations, and were used as a second check for the reliability of the gages in the cross section. Examination of Figure 4.6(b) shows a jump in an axial strain at the Guthrie County Bridge in July of 1998. A similar jump in axial strain occurred for every set of pile strain gages at the Guthrie County Bridge. Individual strain gage and axial strain components were considered unreliable for the time period containing the jump in strain. The strain jump error was eliminated when computing the bending and torsional strains in Equation 4.2 since the error equally affected each gage.

When other jumps or drifting of the strain component plots were noticed, individual strain gages were investigated more thoroughly. Using the assumption

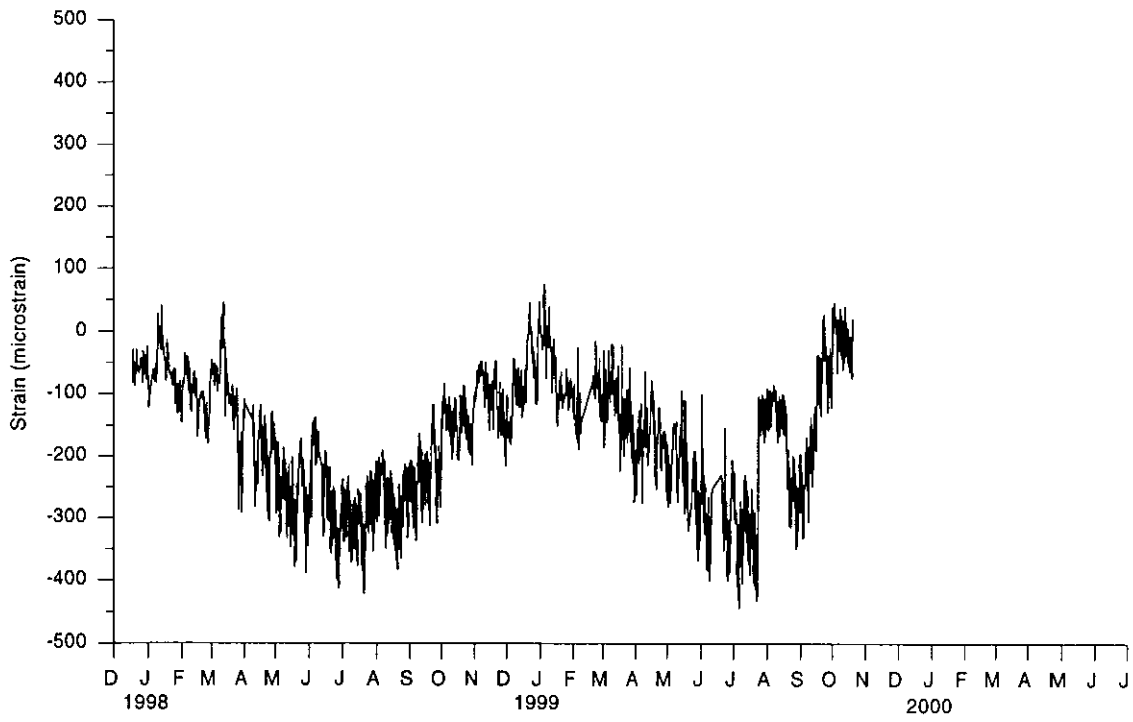


(a) Normal warpage torsional strain

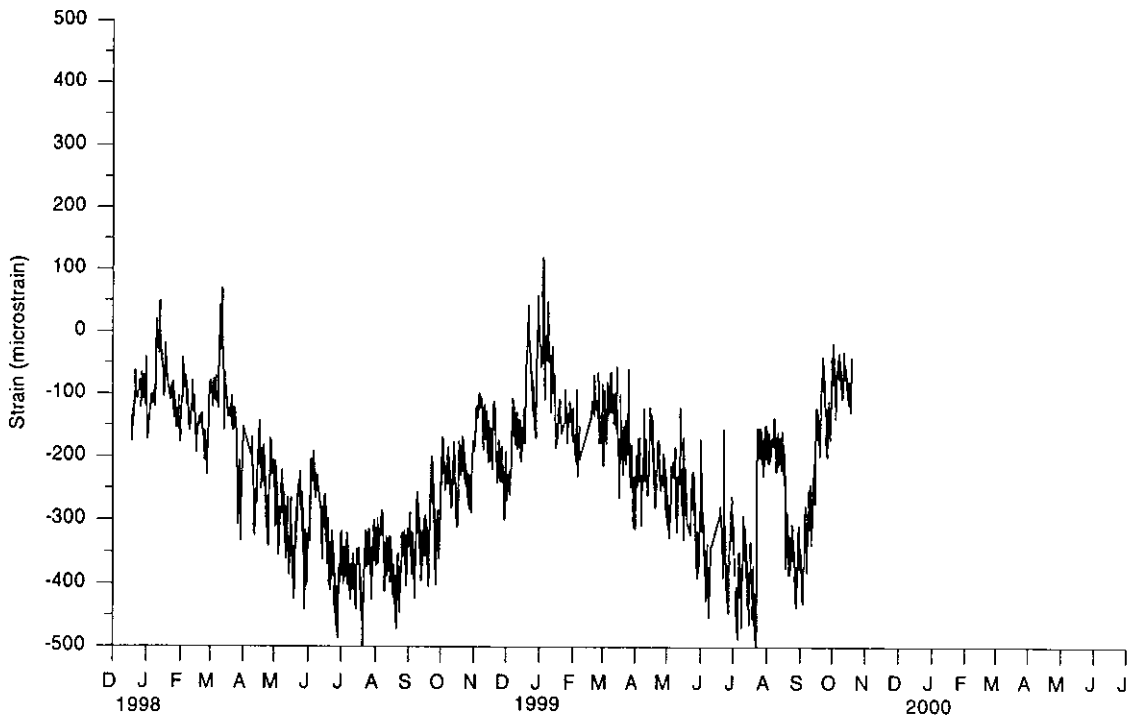


(b) Axial strain

Figure 4.6. Pile strain components calculated using all four strain gages at the top cross section of the pile near the mid-width of the north abutment at the Guthrie County Bridge



(c) X-axis bending strain



(d) Y-axis bending strain

Figure 4.6. (continued)

that the torsional strains were negligible, a specific combination of two gages in a cross section could be used to determine axial, x-axis, or y-axis bending. When only two or three gages function properly, strain component ranges can be calculated as follows:

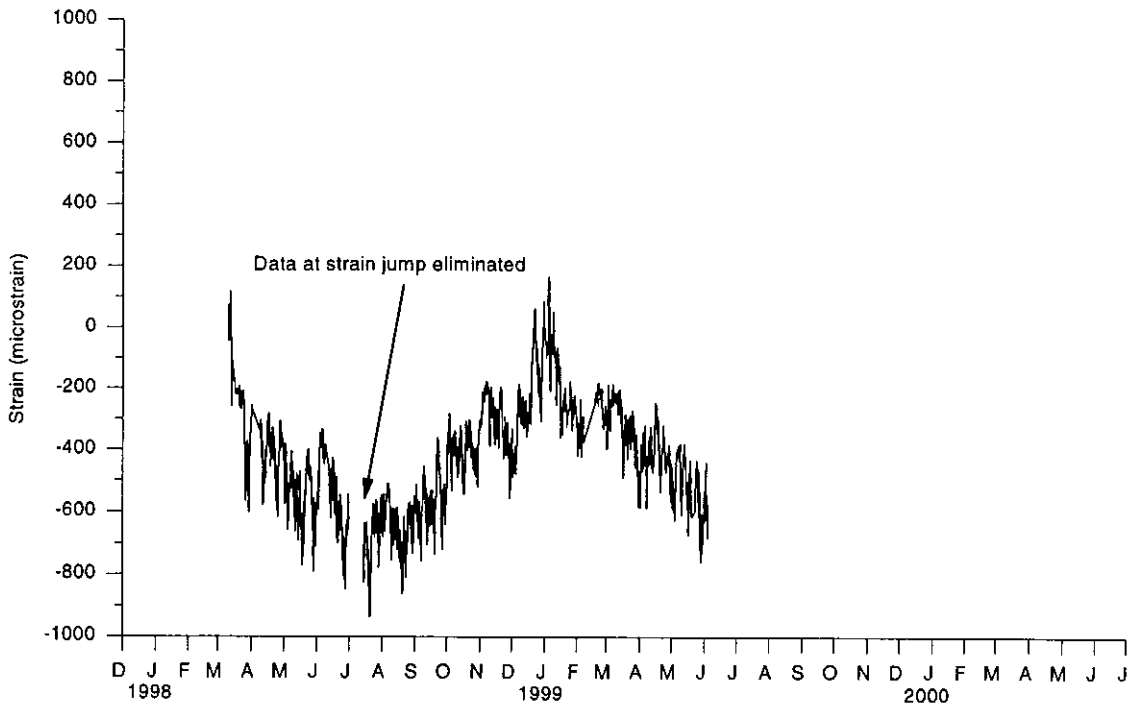
$$\Delta\varepsilon_a = (\Delta\varepsilon_1 + \Delta\varepsilon_3)/2 \text{ or } (\Delta\varepsilon_2 + \Delta\varepsilon_4)/2 \quad (4.3)$$

$$\Delta\varepsilon_x = (\Delta\varepsilon_1 - \Delta\varepsilon_4)/2 \text{ or } (\Delta\varepsilon_2 - \Delta\varepsilon_3)/2$$

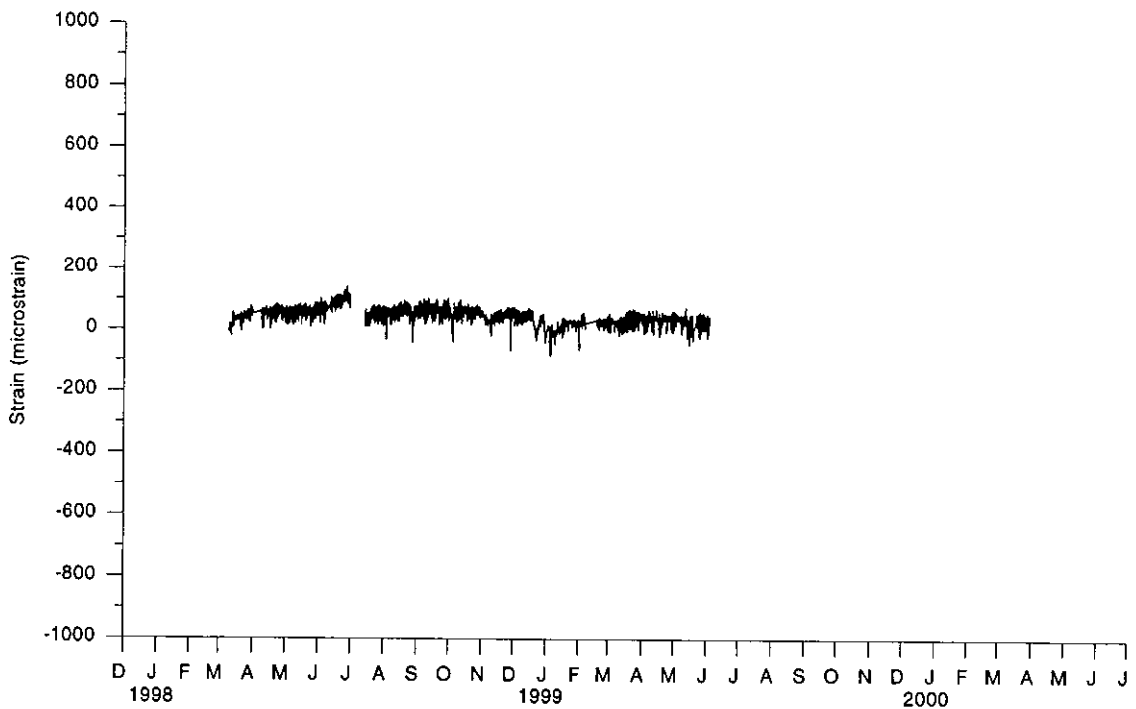
$$\Delta\varepsilon_y = (\Delta\varepsilon_2 - \Delta\varepsilon_1)/2 \text{ or } (\Delta\varepsilon_3 - \Delta\varepsilon_4)/2$$

The strain components evaluated by Equation 4.3 were compared with the plots of longitudinal abutment displacement versus time. If the strain component correlated well with the abutment displacement nearest to the gages, the gages were considered reliable. If the strain component did not correlate well with displacement, at least one of the two gages contained an error. The two-gage combinations were used to determine which gage or gages were causing errors in the strain component calculations at the particular cross section. Each of the corresponding strain components was computed using two or four reliable strain gages in the cross section, whichever was available.

Individual strain gage plots and corresponding strain component plots after the filtering process for the same pile cross section, as discussed above, are shown in Figures 4.7 and 4.8, respectively. The reported range for each of the strain components was determined from the time period with the largest strain range in an

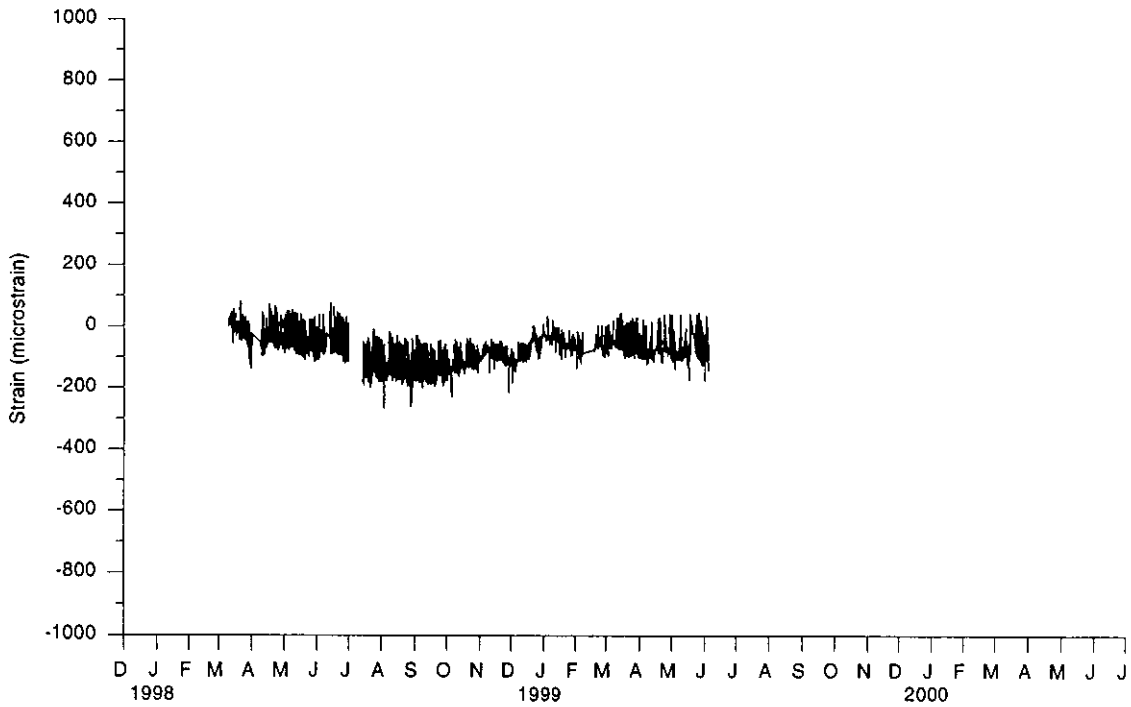


(a) Strain gage (SG-NCP-SWT) near the southwest flange tip

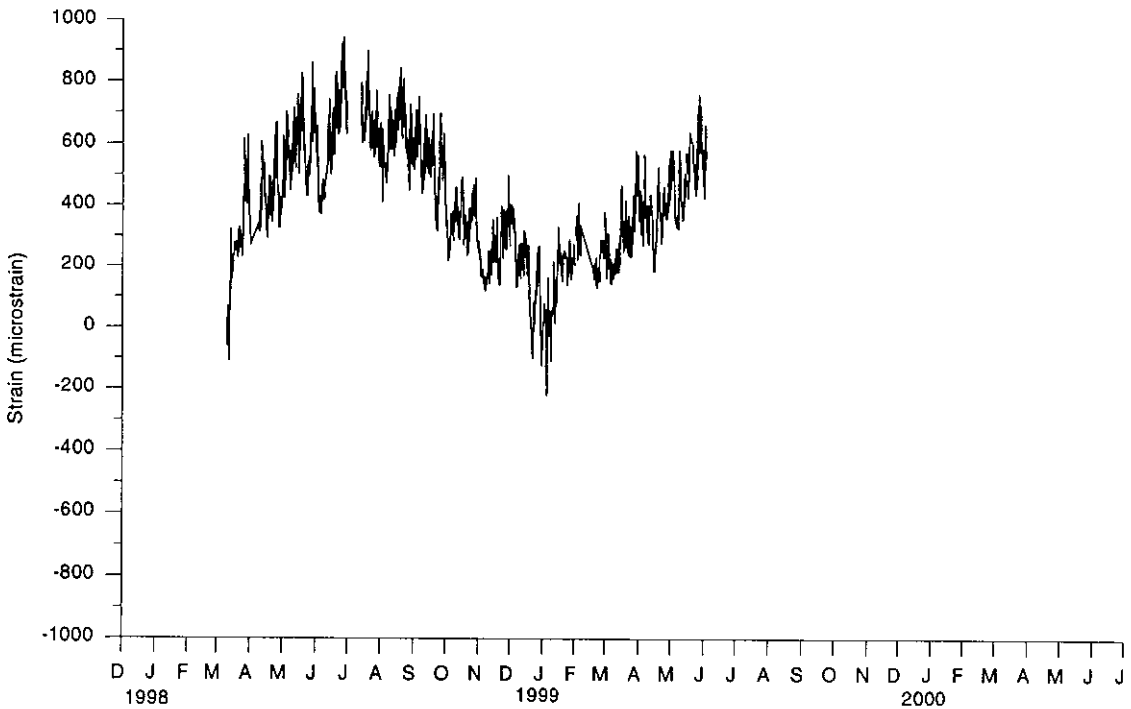


(b) Strain gage (SG-NCP-NWT) near the northwest flange

Figure 4.7. Final results for the strain gages on the top cross section of the pile near the mid-width of the north abutment at the Guthrie County Bridge after completion of the filtering process

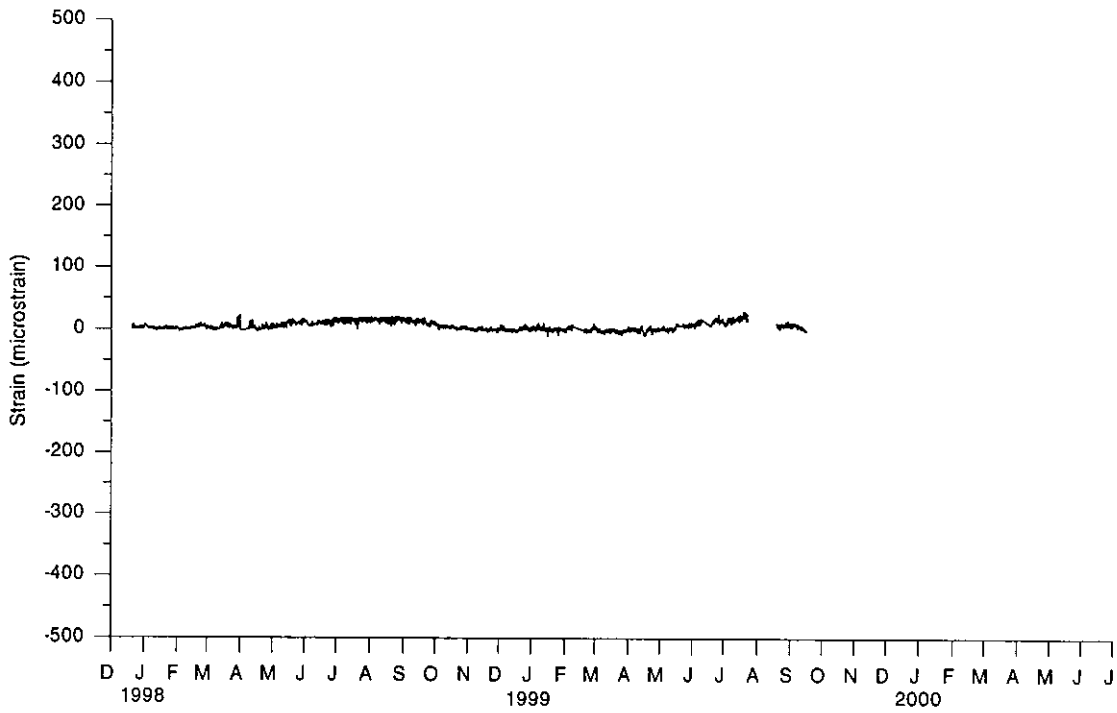


(c) Strain gage (SG-NCP-SET) near the southeast flange tip

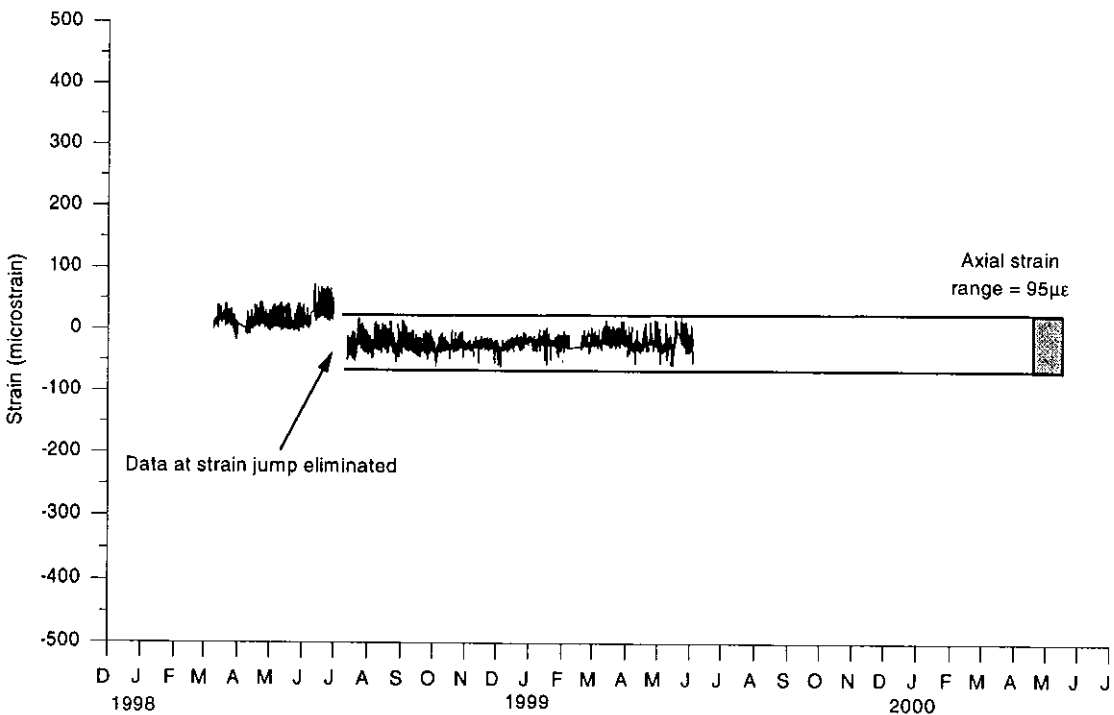


(d) Strain gage (SG-NCP-NET) near the northeast flange tip

Figure 4.7. (continued)

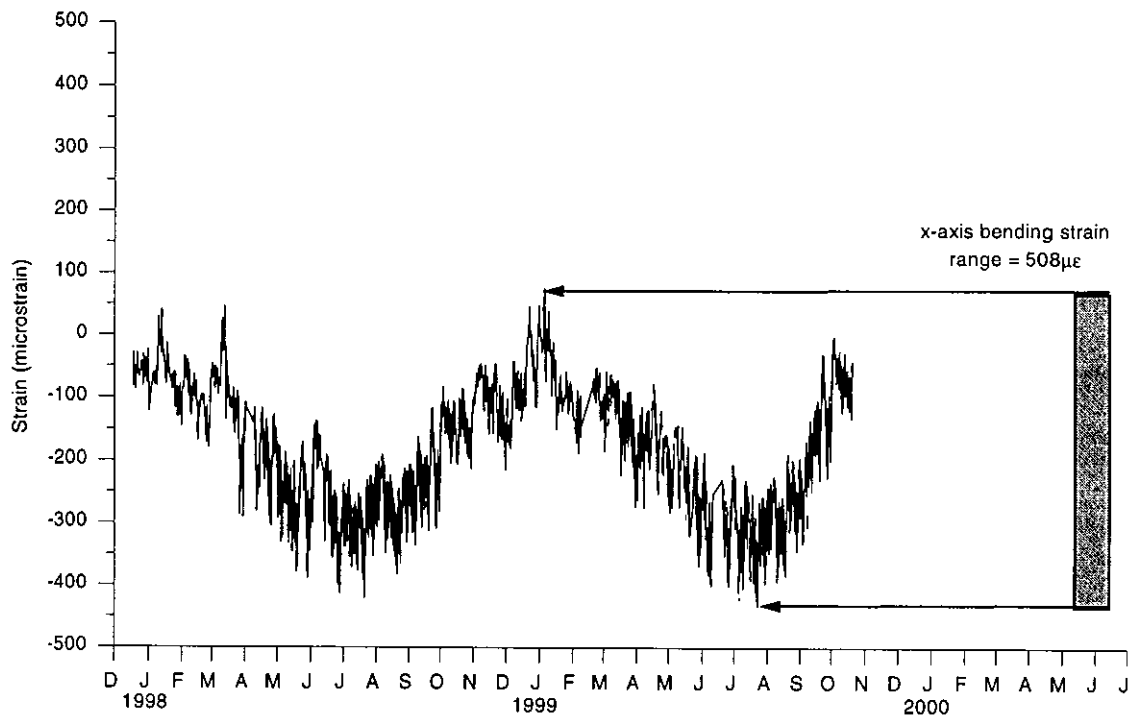


(a) Normal warpage torsional strain

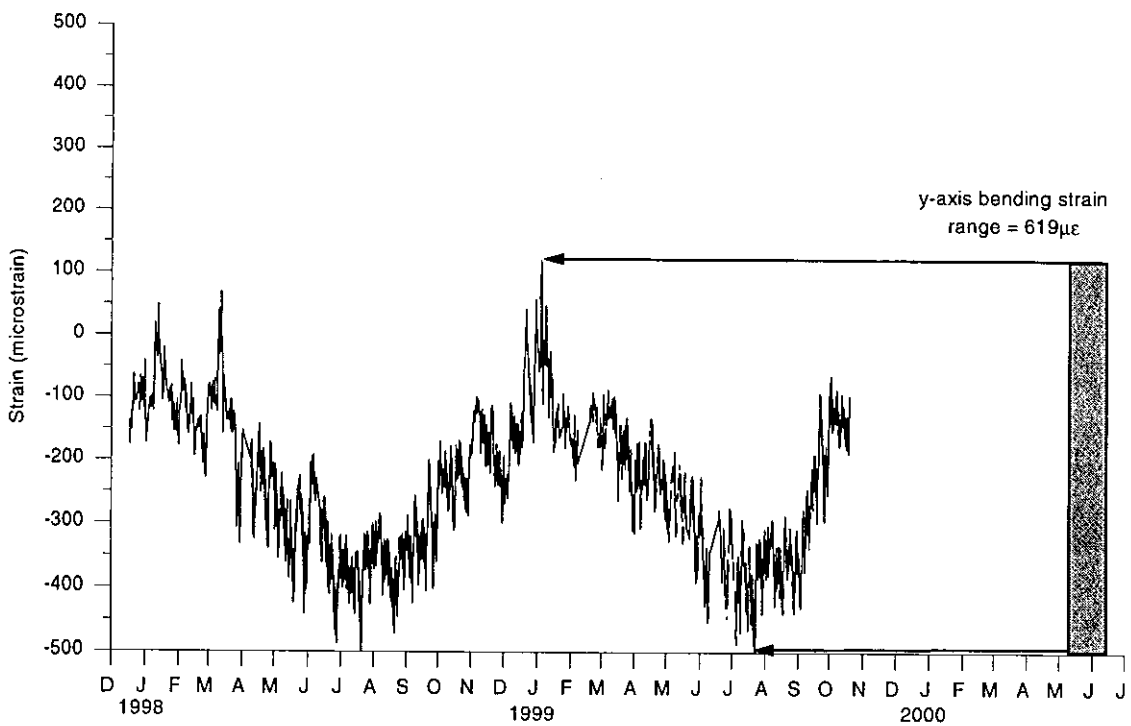


(b) Axial strain

Figure 4.8. Final strain components after the filtering process for the top cross section of the pile near the mid-width of the north abutment at the Guthrie County Bridge



(c) X-axis bending strain



(d) Y-axis bending strain

Figure 4.8. (continued)

uninterrupted data set. The reported ranges for the strain components are shown as a bar on the plots in Figure 4.8. The maximum range of the normal warpage torsional strain was considered negligible and was not shown in Figure 4.8(a).

Tables 4.5 and 4.6 provide a summary of reliable pile strain gages for the Guthrie County Bridge and Story County Bridge, respectively. The dummy gage at the Guthrie County Bridge failed in June 1999, making the individual strain gage readings incorrect after the failure. As discussed before, the bending and torsion pile strains can still be evaluated after the dummy gage failure since the bridge completion error is eliminated using Equation 4.2. Summaries of reliable strain component data available at each pile cross section are shown in Tables 4.7 and 4.8 for the Guthrie County Bridge and Story County Bridge, respectively.

4.1.4 Girder strain gages

The same process as that used to filter pile strain data was used for the girder strain gages. Only two gages were installed at each girder cross section. Assuming torsion was negligible, the change in x-axis, total-strain (strain in the girder due to stress and temperature) gradient measured between the two strain gages on the girder flanges is determined by:

$$\Delta\epsilon_x = \Delta\epsilon_{top} - \Delta\epsilon_{bottom} \quad (4.4)$$

If one of the gages fails, the change in the x-axis, total-strain (strain in the girder due to stress and temperature) gradient can not be computed.

The time periods containing reliable girder strain gage data and the

corresponding reliable x-axis, total-strain gradients are shown in Table 4.9 and 4.10. The strain jump detected in the pile strain gages at the Guthrie County Bridge in July 1998 also occurred in the girder strain gages. The strain jump equally affected all girder strain gages; therefore, the error was eliminated in Equation 4.4.

4.2 Bridge temperatures

Temperatures measured at the various locations on the bridge structures were used to compute an average bridge temperature and the thermal gradients in the bridge at specific times during the study period. This section describes the experimental results obtained for each bridge.

4.2.1 Average bridge temperatures

Average temperatures of the bridge superstructures, which will be referred to as the “average bridge temperature” in this report, were computed at each time interval during the monitoring period. The average bridge temperature was the weighted average of the temperature values indicated by all of the thermocouples embedded in the bridge superstructure. Each thermocouple was assumed to provide a uniform temperature for a region in the cross section of the superstructure, as shown by the shaded areas in Figure 4.9. The cross section was divided into four regions: slab, top flange, web, and bottom flange. The average bridge temperature, T_{ave} , was determined as:

$$T_{ave} = \frac{\sum_{j=1}^n T_j A_j}{\sum_{j=1}^n A_j} \quad (4.5)$$

Table 4.10. Summary of reliable concrete strain gage data for the Story County Bridge

(a) Individual girder strain gages

GIRDER	INSTRUMENT CODE	1998												1999												2000		
		J	F	M	A	M	J	J	A	S	O	N	D	J	F	M	A	M	J	J	A	S	O	N	D	J	F	M
North	1EN-T																											
	1EN-B																											
Center	1EC-T																											
	1EC-B																											
	1WC-T																											
	1WC-B																											
	3EC-T																											
	3EC-B																											
	3WC-T																											
	3WC-B																											
South	1ES-T																											
	1ES-B																											

LEGEND: Shaded areas indicate the girder strain gage data were reliable for the month

(b) X-axis girder total-strain gradient

GIRDER	SUPPORT LOCATION	1998												1999												2000		
		J	F	M	A	M	J	J	A	S	O	N	D	J	F	M	A	M	J	J	A	S	O	N	D	J	F	M
North	East abutment																											
Center	East abutment																											
	East pier																											
	West pier																											
	West abutment																											
South	East abutment																											

LEGEND: Shaded areas indicate the girder strain gage data were reliable for the month

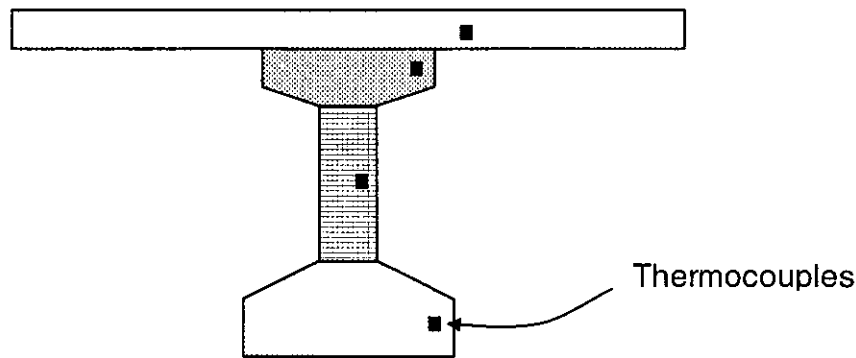
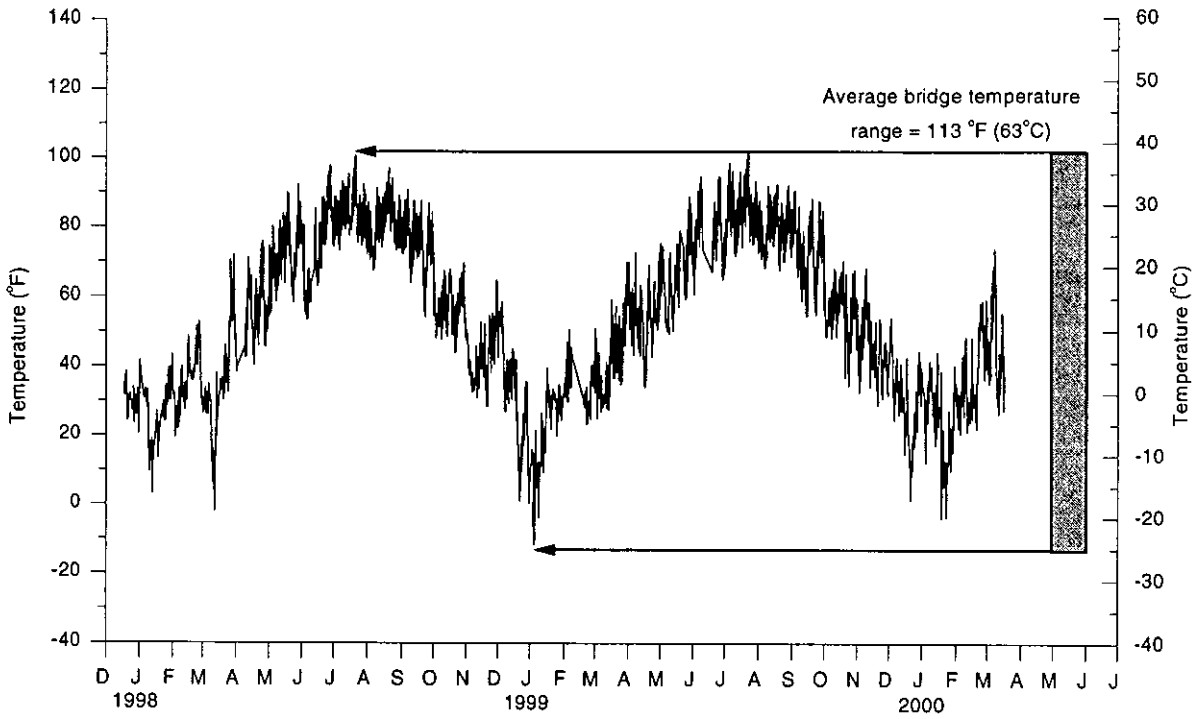


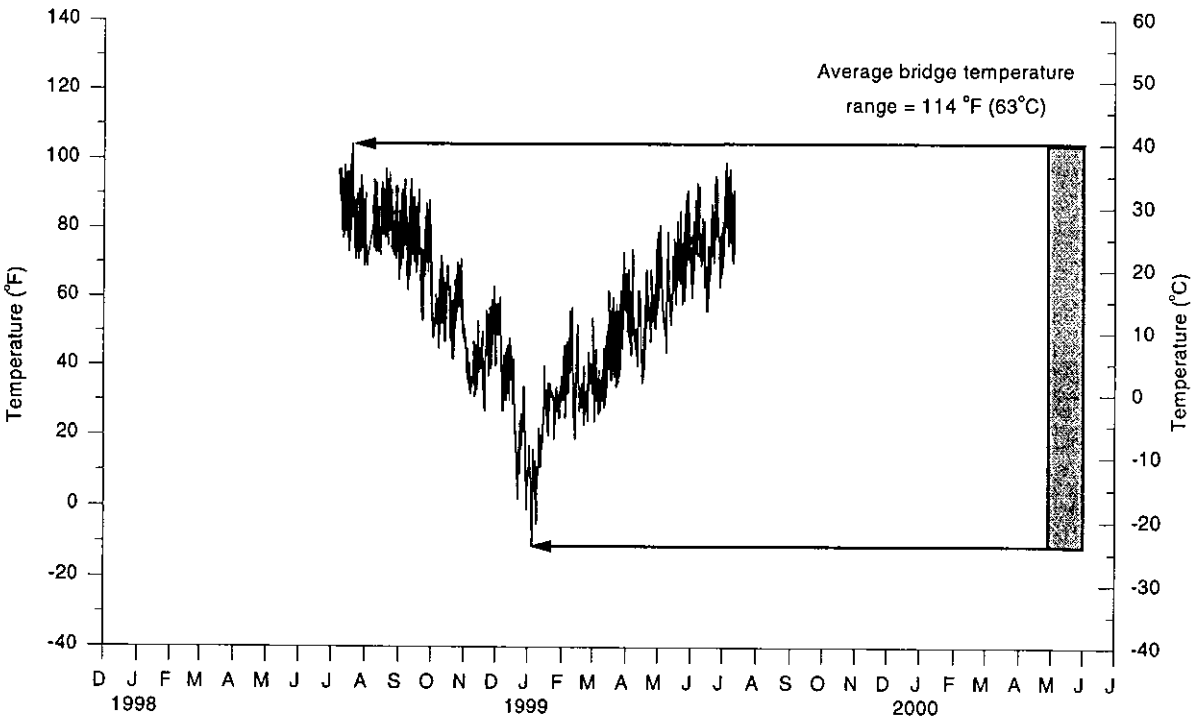
Figure 4.9. Typical temperature regions (not to scale)

where T_j was the temperature measured by a thermocouple in the selected region and A_j was area of that region. The average bridge temperatures versus time for the Guthrie County Bridge and the Story County Bridge are shown in Figure 4.10.

At the Guthrie County Bridge, the maximum average bridge temperature of 101°F (38°C) occurred in the early evening hours of July 20, 1998 and July 22, 1999. The minimum, average, bridge temperature measured at the Guthrie County Bridge was -12°F (-24°C), which occurred before the sunrise on January 5, 1999. At the Story County Bridge, a maximum, average, bridge temperature of 104°F (40°C) occurred in the early evening hours of July 20, 1998. The minimum, average, bridge temperature of -10°F (-23°C) was measured before sunrise on January 5, 1999 at the Story County Bridge. The maximum ranges in average bridge temperatures for each monitored bridge are shown in Figure 4.10. The range in average bridge temperatures was 113°F (63°C) and 114°F (63°C) for the Guthrie County Bridge and Story County Bridge, respectively.



(a) Guthrie County Bridge



(b) Story County Bridge

Figure 4.10. Average bridge temperature of the monitored bridges

The maximum, average, bridge temperatures exceeded the air temperatures measured at each bridge site. Figure 4.11 shows that for the Guthrie County Bridge, the average bridge temperature lagged behind and exceeded the measured air temperature.

4.2.2 Vertical temperature gradients

Significant temperature gradients were measured through the depth of each bridge superstructure. The largest positive thermal gradients occurred at the times of the maximum, average, bridge temperatures. Girton, et al. [7] determined that the vertical temperature distributions are bi-linear through the depth of a PC-girder bridge superstructure. The experimental temperature measurements at the Guthrie

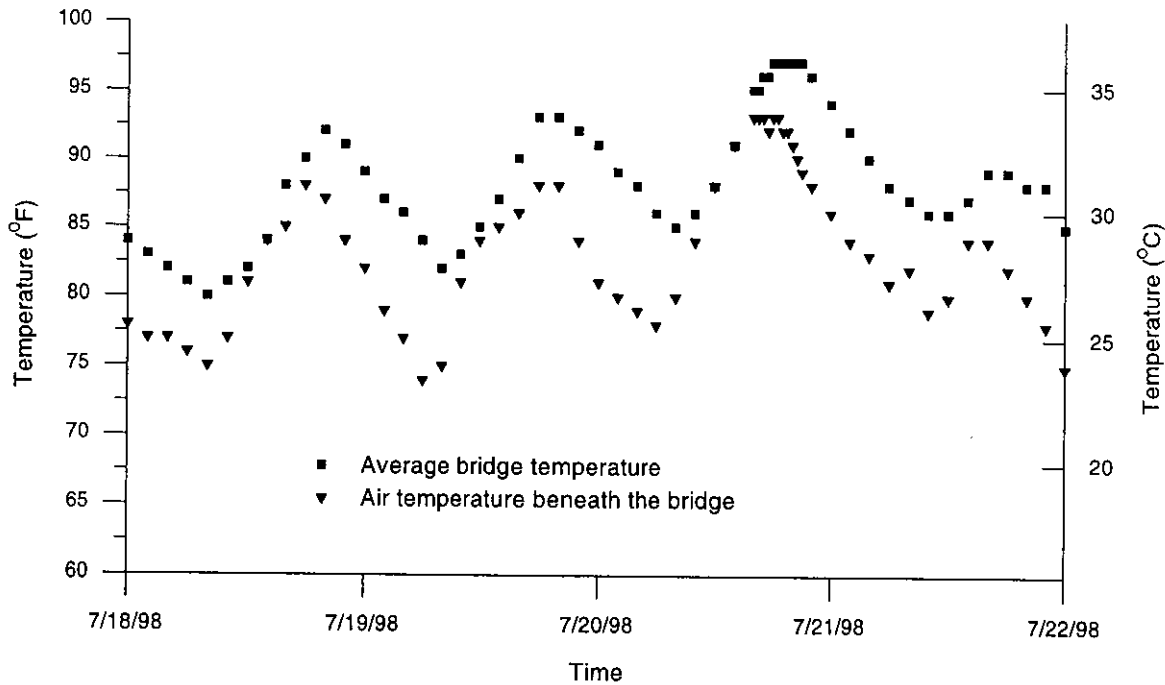


Figure 4.11. Average superstructure and air temperatures at the Guthrie County Bridge between July 18, 1998 and July 22, 1998 [26]

and Story County Bridges were used to compute bi-linear temperature gradients through the depth of the superstructure at each monitored cross section. These bi-linear gradients were extrapolated to compute the temperatures to the top of the slab, top of the PC girder, and bottom of the PC girder.

Tables 4.11 and 4.12 list the measured temperatures in the bridge superstructures at the time of the maximum and minimum average bridge temperatures, respectively, at the Guthrie County Bridge. In these tables, locations for thermocouples that did not provide reliable data or locations where a thermocouple was not installed are left blank. Tables 4.13 and 4.14 list the same temperature information for the Story County Bridge. Figure 4.12 shows the measured temperatures at all thermocouple locations in the superstructure of the Guthrie County Bridge and the Story County Bridge, respectively, at the time of the maximum and minimum, average, bridge temperatures. This figure also shows as solid lines the average, bi-linear temperature gradient for the respective bridge. Based on extrapolation of the average thermocouple values, the average, extrapolated temperature at the top of the concrete slab was 126°F (52°C) for the Guthrie County Bridge and 132°F (56°C) for the Story County Bridge.

Figures 4.13(a), 4.13(b), and 4.13(c) show the extrapolated top-of-slab, top-of-girder, and bottom-of-girder temperatures, respectively, for the Guthrie and Story County Bridges at the time of the maximum and minimum, average, bridge temperatures. Figures 4.14(a), 4.14(b), and 4.14(c) show the same temperature information for the Story County Bridge.

Table 4.11. Temperature values at the Guthrie County Bridge at the time of the maximum average bridge temperature (July 20, 1998, 8:00 p.m.)

GAGE	MEASURED TEMPERATURES (°F)				EXTRAPOLATED BILINEAR TEMPERATURES (°F)		
	SLAB	TOP FLANGE	WEB	BOTTOM FLANGE	TOP OF SLAB	TOP OF GIRDER	BOT. OF GIRDER
Average	109.8	96.7	93.4	91.8	126.3	96.5	91.1
1MSE	109.1	97.0	96.1	93.6	123.7	97.4	93.4
1MSW	108.7	98.2	96.5	93.3	121.2	98.7	93.0
1SC	109.4	97.1	91.4	89.7	125.4	96.6	88.4
1SE	105.3	93.3	90.5	87.9	120.2	93.4	87.3
1SW	105.8	95.6	95.5	89.0	116.7	97.1	89.2
3NC	110.6	96.4	91.5	89.6	128.8	96.1	88.5
2MSC	113.9	99.7	92.7	92.2	132.9	98.7	90.5
1MSC	115.3		93.3	92.8	138.4	96.8	90.2
3SC		97.3		97.8		97.3	97.9
1NW		95.3					
1NC		96.7		91.6		97.0	91.2
1NE				92.6			

Table 4.12. Temperature values at the Guthrie County Bridge at the time of the minimum average bridge temperature (January 5, 1999, 4:00 a.m.)

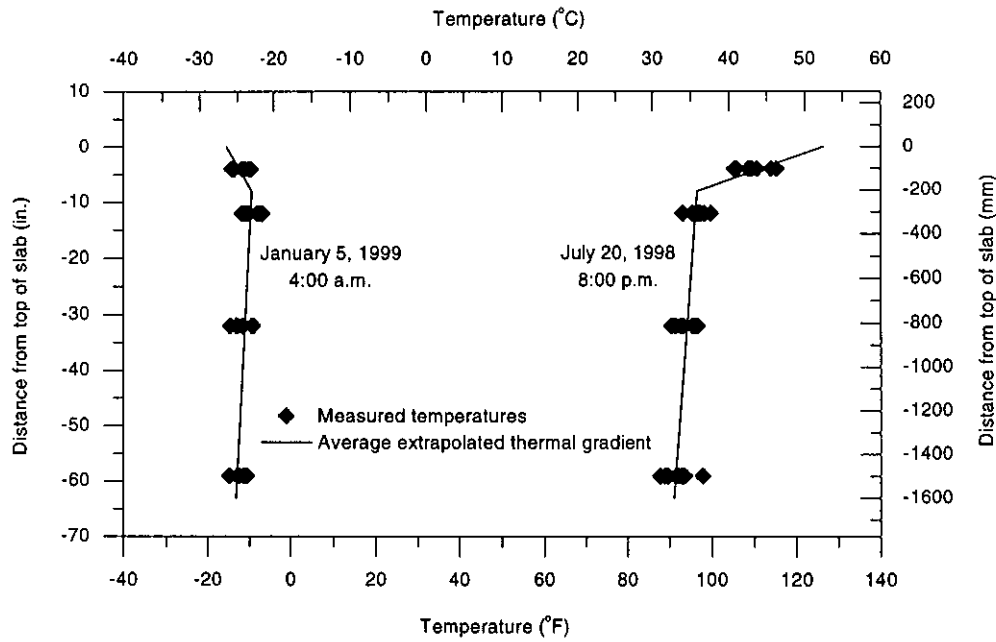
GAGE	MEASURED TEMPERATURES (°F)				EXTRAPOLATED BILINEAR TEMPERATURES (°F)		
	SLAB	TOP FLANGE	WEB	BOTTOM FLANGE	TOP OF SLAB	TOP OF GIRDER	BOT. OF GIRDER
Average	-12.2	-9.2	-11.8	-12.7	-15.6	-9.4	-13.3
1MSE	-14.3	-10.8	-14.8	-14.9	-18.0	-11.4	-15.8
1MSW	-13.7	-10.2	-13.2	-13.0	-17.5	-10.7	-13.8
1SC	-11.2	-8.1		-11.6	-15.3	-7.9	-11.8
1SE	-10.2	-7.0	-13.0	-13.0	-13.0	-7.9	-14.4
1SW	-9.6	-6.8	-11.8	-11.1	-11.9	-7.8	-12.3
3NC	-11.8	-7.7	-9.1	-10.6	-17.1	-7.6	-10.9
2MSC	-14.2	-10.9	-11.6	-12.6	-18.5	-10.8	-12.7
1MSC							
3SC		-11.8		-14.8		-11.7	-15.1
1NW							
1NC							
1NE							

Table 4.13. Temperature values at the Story County Bridge at the time of the maximum average bridge temperature (June 20, 1998, 6:00 p.m.)

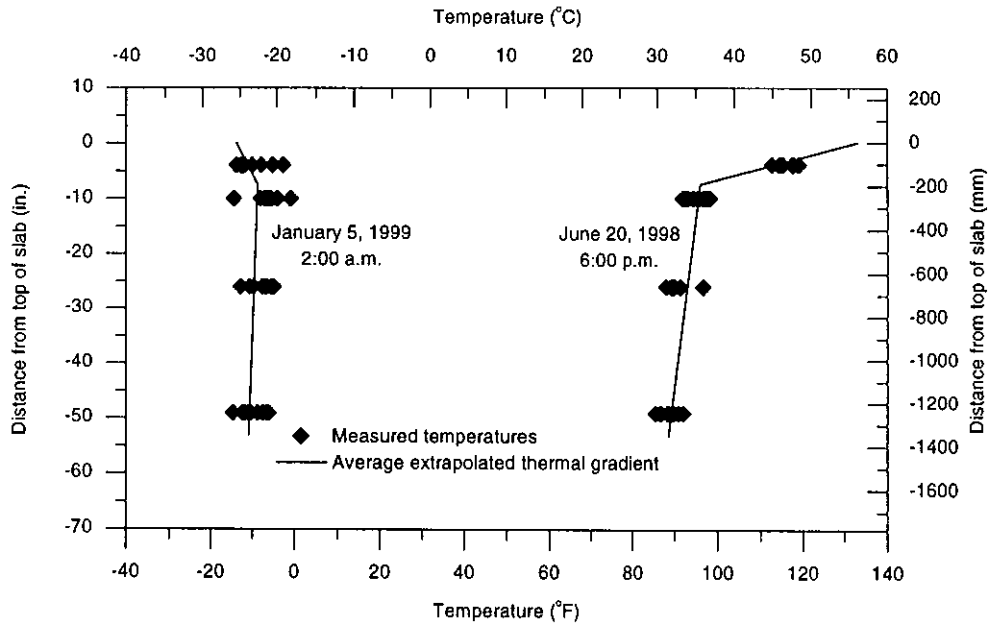
GAGE	MEASURED TEMPERATURES (°F)				EXTRAPOLATED BILINEAR TEMPERATURES (°F)		
	SLAB	TOP FLANGE	WEB	BOTTOM FLANGE	TOP OF SLAB	TOP OF GIRDER	BOT. OF GIRDER
Average	114.1	97.0	91.6	90.4	132.9	95.9	88.6
1EN							
1EC	117.5	96.6	89.4		137.5	97.5	
1ES		94.3		85.5		94.7	85.5
1MSNX			89.1	88.3		89.7	88.3
1MSNI	115.4	95.3	88.0	86.6	136.5	94.3	86.6
1MSC	112.8		89.6	88.6	135.2	90.4	88.6
1MSSI	114.5	92.7	89.8	89.8	136.8	92.2	89.8
1MSSX	95.7		91.2	92.0	100.8	90.6	92.0
1WS		93.1		90.9		93.2	90.9
1WC	119.0	97.6	91.3	89.4	141.1	96.9	89.4
1WN		95.6		89.3		95.9	89.3
2MSC	114.9	92.0	90.0	89.5	138.0	91.7	89.5
3WC	117.8	98.2	96.6	86.9	135.6	100.0	86.9
3EC		97.2					

Table 4.14. Temperature values at the Story County Bridge at the time of the minimum average bridge temperature (January 5, 1999, 2:00 a.m.)

GAGE	MEASURED TEMPERATURES (°F)				EXTRAPOLATED BILINEAR TEMPERATURES (°F)		
	SLAB	TOP FLANGE	WEB	BOTTOM FLANGE	TOP OF SLAB	TOP OF GIRDER	BOT. OF GIRDER
Average	-11.3	-8.9	-9.4	-10.7	-13.9	-8.7	-10.9
1EN		-4.1					
1EC	-12.8	-7.0	-5.5	-7.6	-19.3	-6.3	-7.2
1ES		-0.8		-6.1		-0.6	-6.8
1MSNX	-7.8		-12.9	-14.7		-11.5	-15.1
1MSNI	-2.6	-5.4	-10.7	-11.1	1.0	-6.3	-12.6
1MSC	-13.9		-6.9	-8.8	-22.5	-5.4	-9.2
1MSSI	-10.0	-14.5	-7.6	-8.0	-6.8	-13.2	-4.7
1MSSX	-5.1		-9.7	-12.5	-2.6	-7.5	-13.1
1WS				-6.6		-19.5	-2.2
1WC	-12.4	-6.1	-4.8	-7.6	-19.6	-5.3	-7.3
1WN		-3.9		-11.9		-3.4	-14.8
2MSC	-12.0		-6.5	-10.4	-4.5	-19.4	-3.1
3WC	-11.9	-6.3		-7.4	-17.6	-6.2	-7.8
3EC		-8.0					

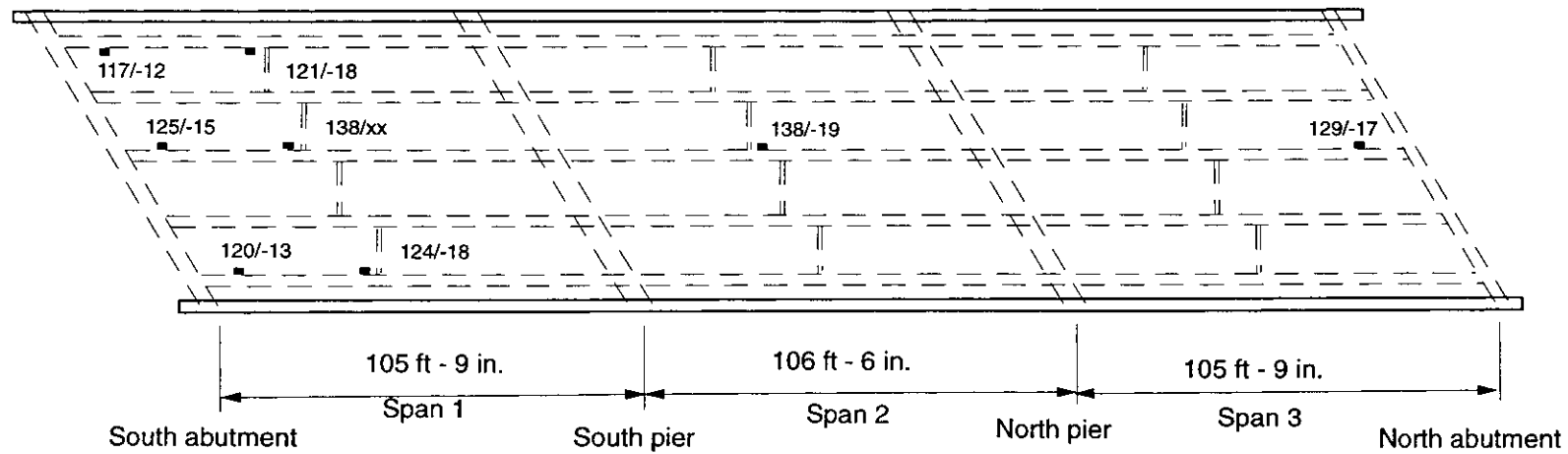


(a) Guthrie County Bridge



(b) Story County Bridge

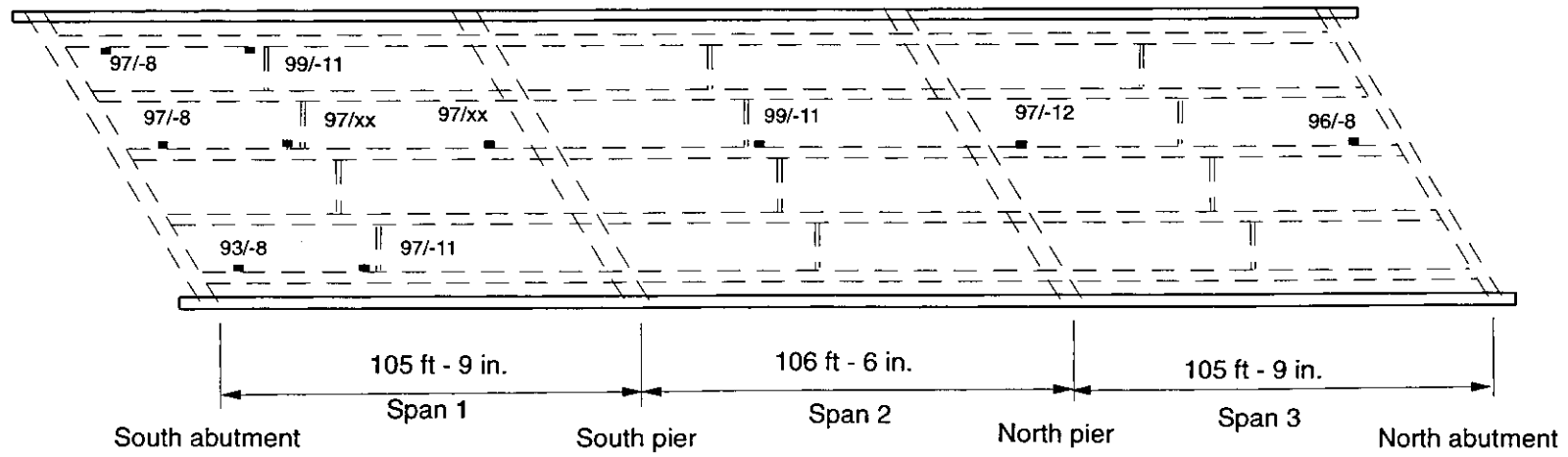
Figure 4.12. Vertical temperature distributions through the depth of the superstructure at the times of minimum and maximum average bridge temperature



(a) Top of slab



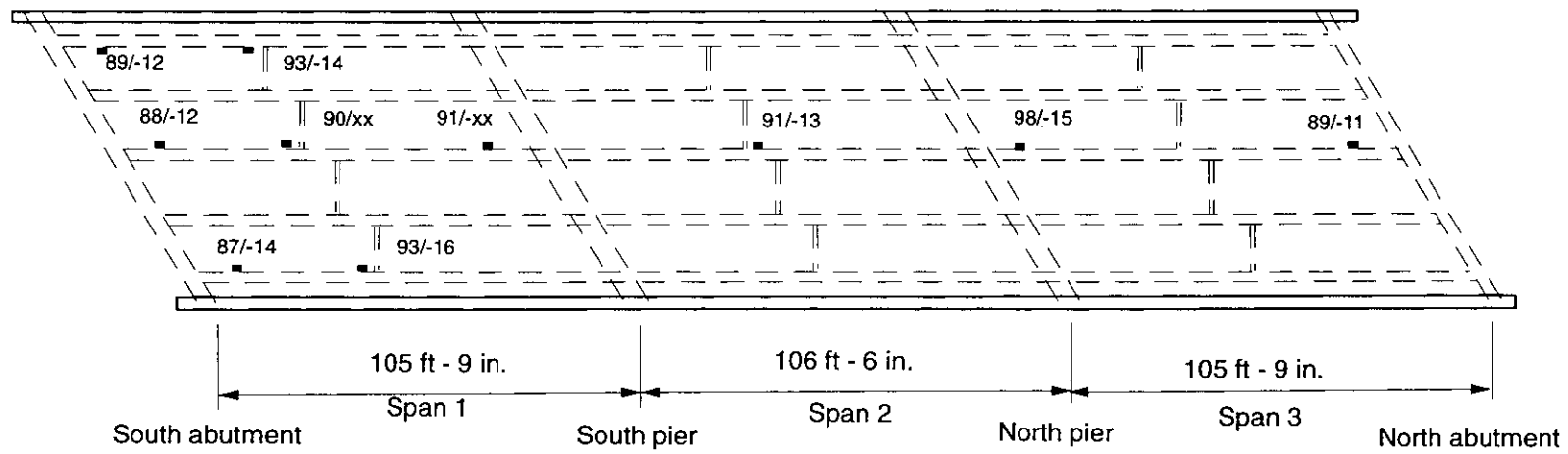
Figure 4.13. Extrapolated temperatures (in degrees Fahrenheit) at the Guthrie County Bridge at the time of the maximum and minimum average bridge temperatures



(b) Top of girder



Figure 4.13. (continued)

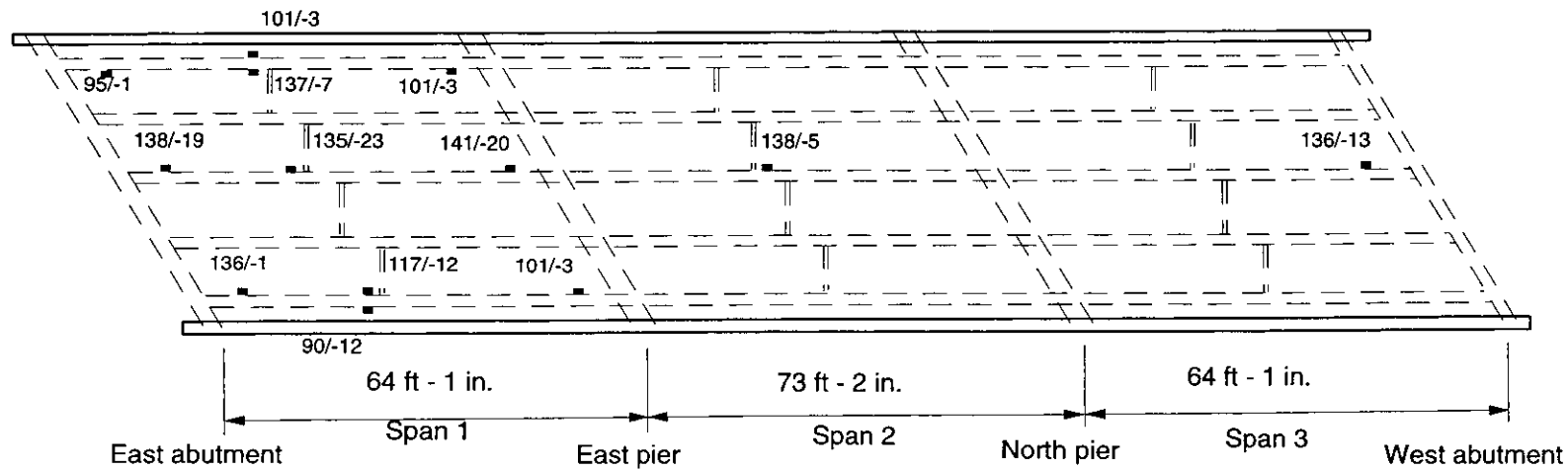


70

(c) Bottom of girder



Figure 4.13. (continued)

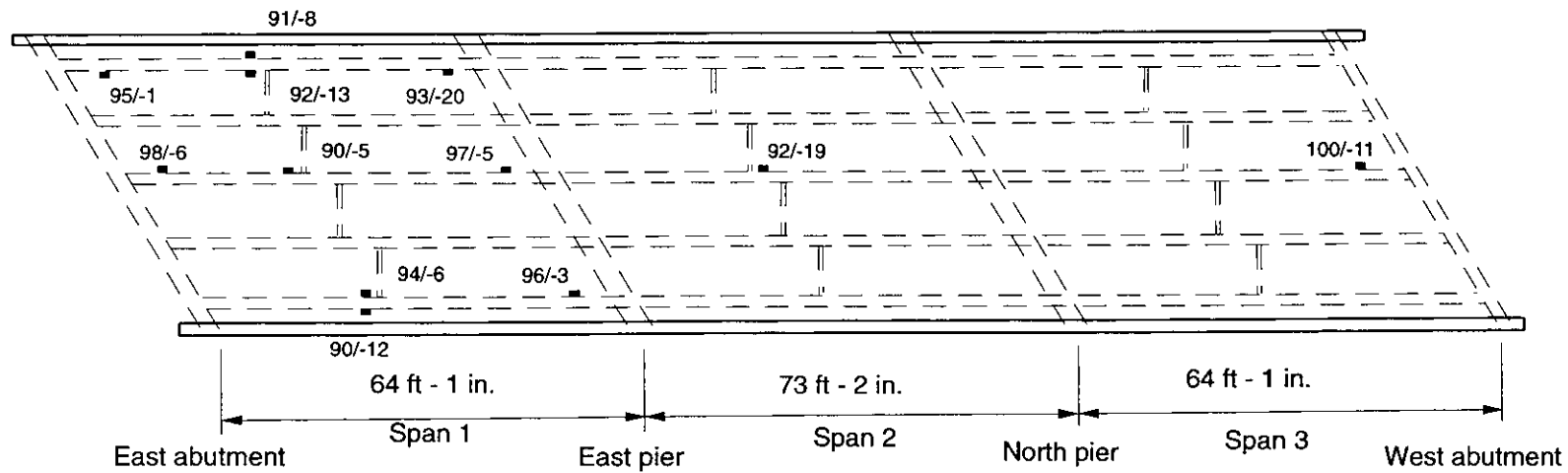


71

(a) Top of slab



Figure 4.14. Extrapolated temperatures (in degrees Fahrenheit) at the Story County Bridge at the time of the maximum and minimum average bridge temperatures

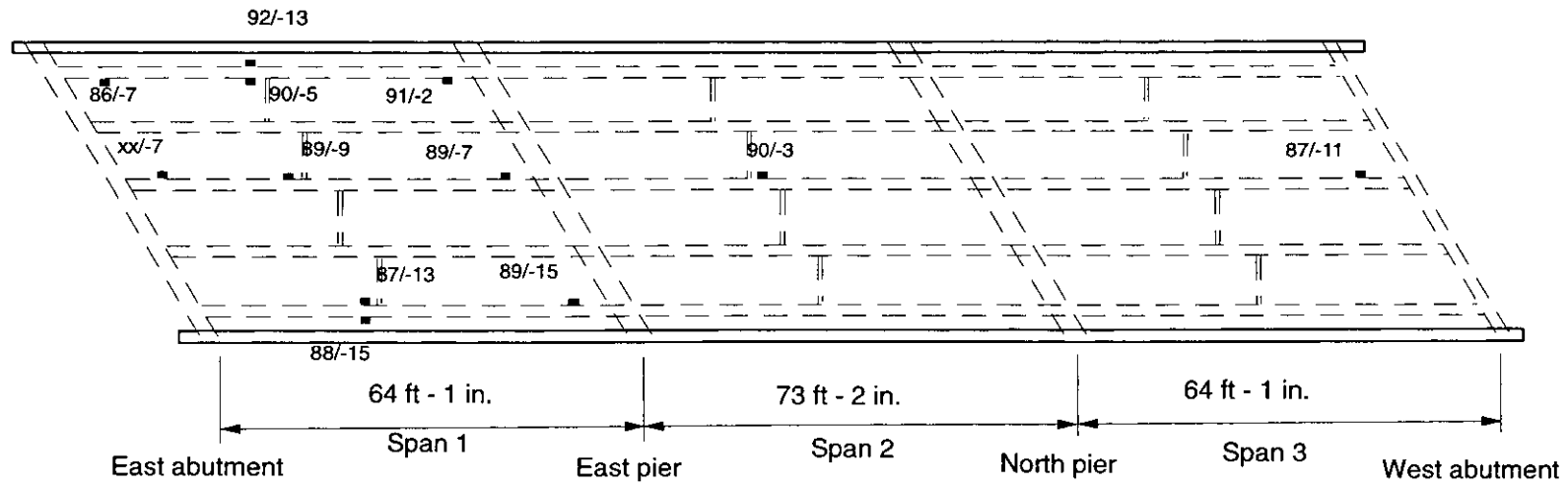


72

(b) Top of girder



Figure 4.14. (continued)



73

(c) Bottom of girder



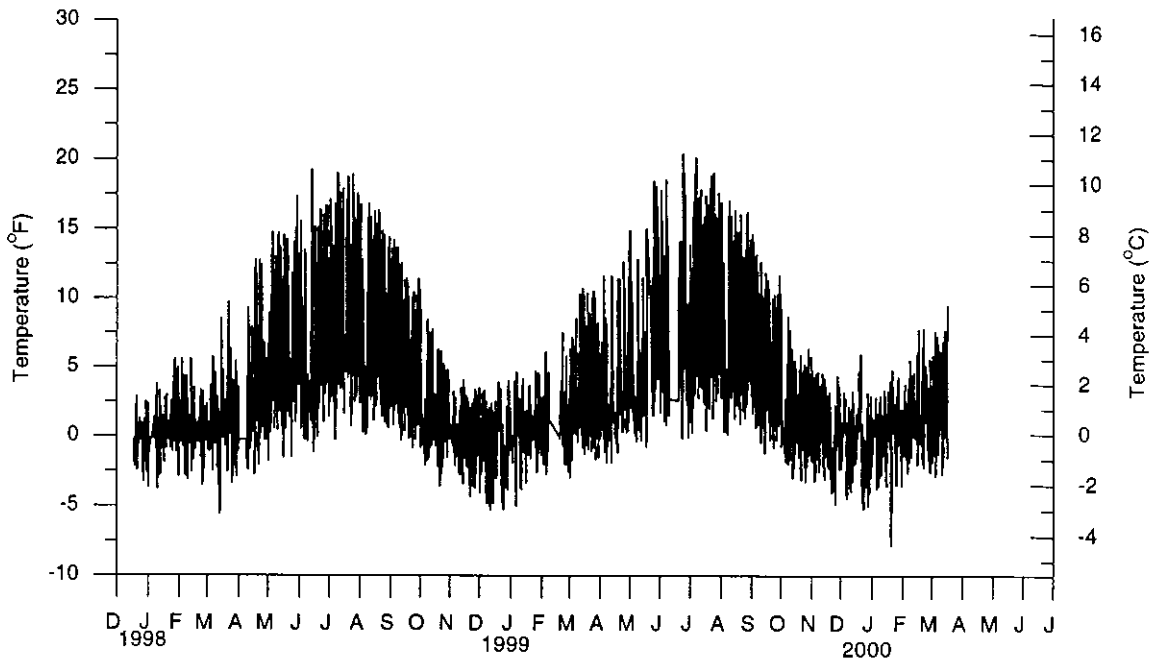
Figure 4.14. (continued)

Figure 4.15(a) shows the difference between the average slab temperature and the average, PC-girder, bottom-flange temperature at the Guthrie County Bridge. Figure 4.15(b) shows the same temperature difference measured at the Story County Bridge. The magnitude of the vertical temperature gradient is much larger in the summer due to increased exposure of the bridge deck to solar radiation.

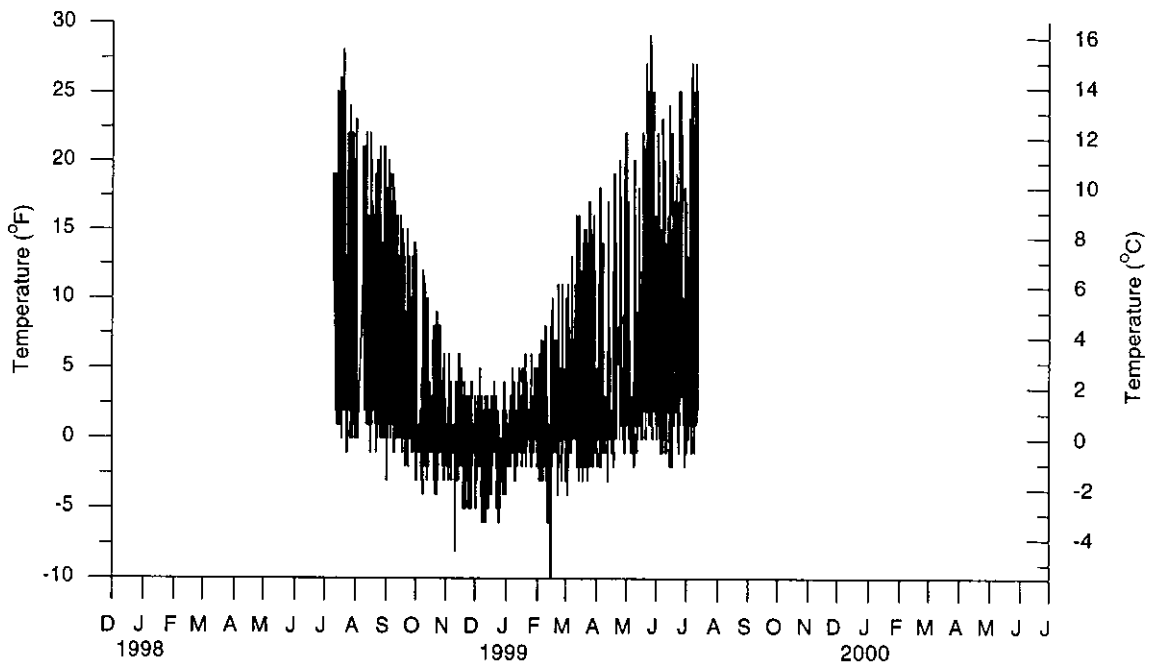
4.2.3 Transverse temperature gradients

Figure 4.16(a) shows the temperature variations across the width of the Story County Bridge for two hot days and two cold days. In Figure 4.16(a), positive distances from the bridge centerline are towards the north and negative distances are towards the south. Except for the slab temperatures near the edges of the bridge, the variation in the slab temperature across the width of the bridge was negligible. Near the edges of the bridge, the slab temperatures were measured beneath the continuous, Jersey-type, concrete barriers. These slab temperatures were significantly cooler than the rest of the slab at the time of the maximum, average, bridge temperature. The concrete barriers shade the slab surface beneath them and provide a large thermal mass at these locations.

A limited number of thermocouples were installed across the width of the Guthrie County Bridge. Figure 4.16(b) shows the temperature distribution across the width of the Guthrie County Bridge. Temperatures near the centerline of the bridge were slightly higher than those measured near the exterior girders, but the difference was not significant. Since an open-type of a reinforced-concrete guardrail was used at the Guthrie County Bridge, less thermal mass exists at the edges of this bridge. Since thermocouples were not placed in the slab directly beneath the open guardrail

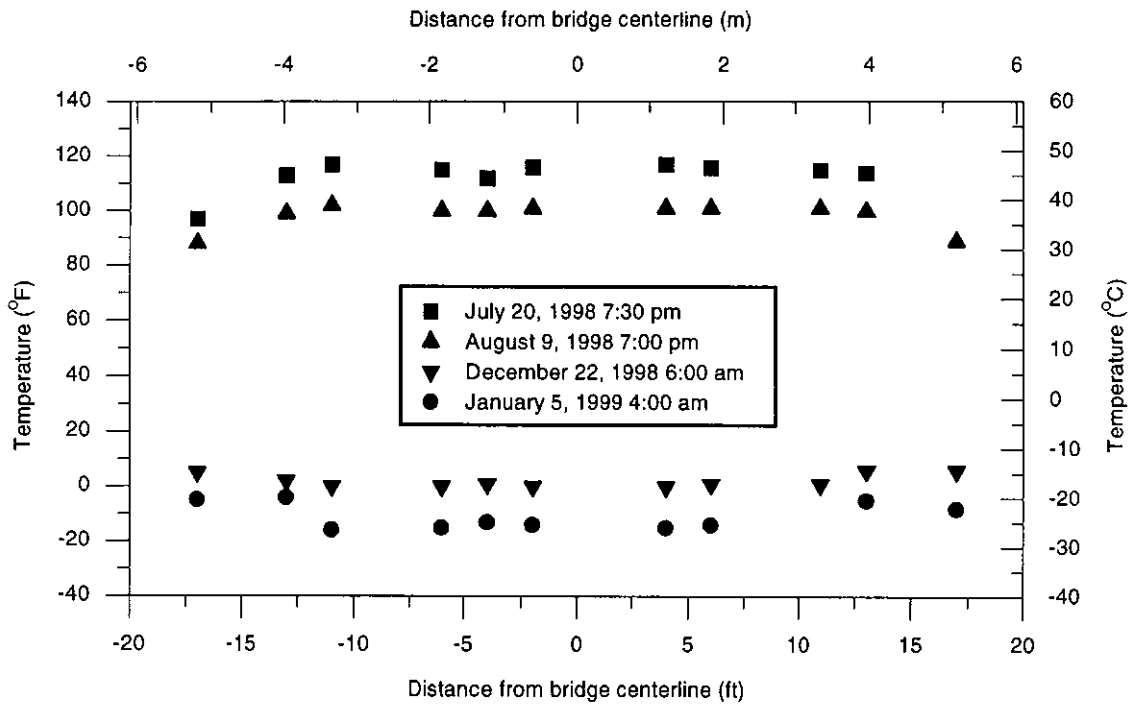


(a) Guthrie County Bridge

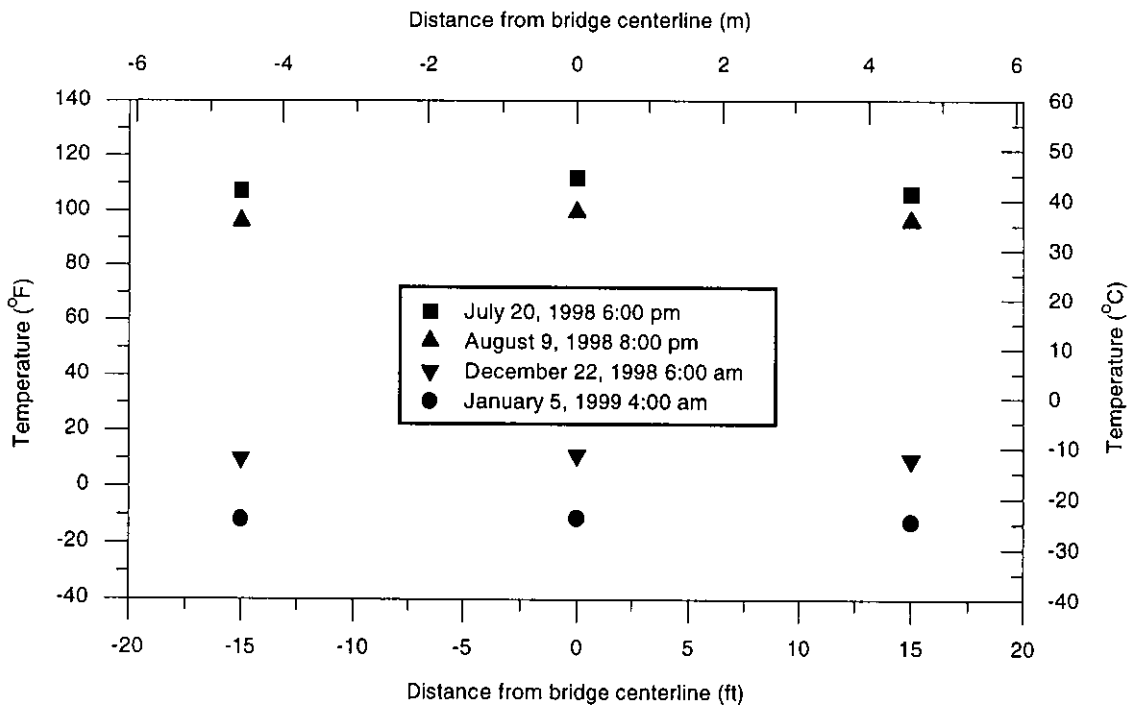


(b) Story County Bridge

Figure 4.15. Difference between the average slab temperature and the average bottom flange temperature



(a) Story County Bridge [26]



(b) Guthrie County Bridge

Figure 4.16. Transverse temperature distribution across the bridge width

and since the thermocouples were at about a 15-ft (4570-mm) transverse spacing, the researchers could not determine whether a temperature gradient existed across the width of the Guthrie County Bridge.

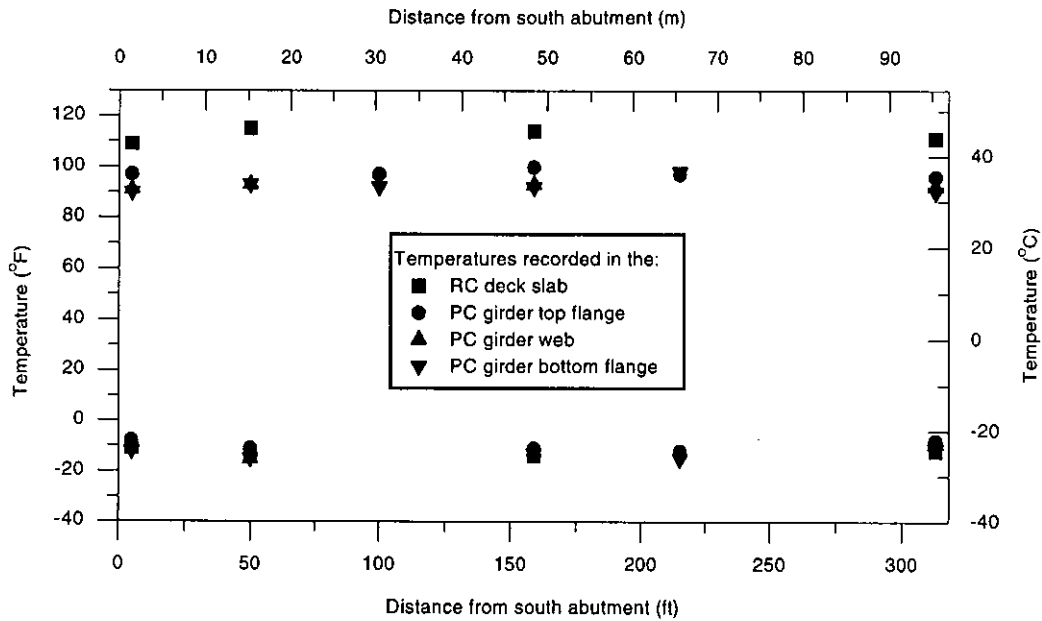
4.2.4 Longitudinal temperature gradients

Temperatures were measured at six locations along the longitudinal axis of each bridge. Figure 4.17 shows the temperatures measured through the depth of the superstructure at the selected cross sections along the length of the Guthrie County Bridge and Story County Bridge at the time of the maximum and minimum, average, bridge temperature. For a particular depth in the bridge superstructure, the differences in the measured temperatures along the bridge length are not significant.

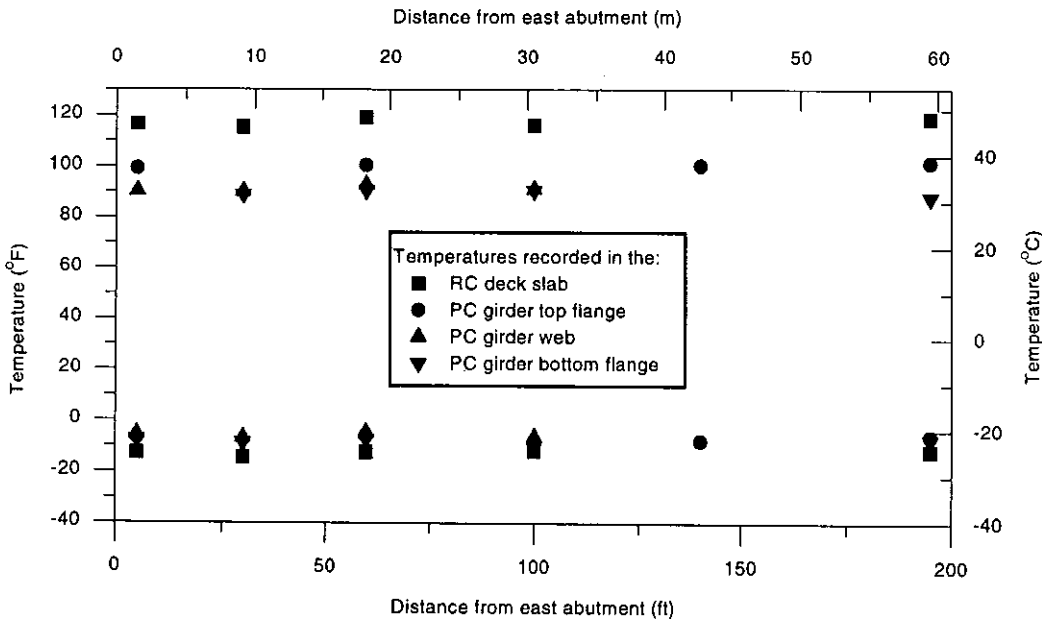
4.2.5 Pile temperatures

The temperatures of several piles were measured near the bottom of an abutment pile cap at each bridge. At the time of the maximum, average, bridge temperature of 101°F (37°C), the average pile temperature was approximately 80°F (27°C) at the Guthrie County Bridge. At the time of the coldest average bridge temperature of -12°F (-24°C), the piles at this bridge had a temperature of about 10°F (-12°C). Therefore, the pile temperature range was 70°F (39°C) at the Guthrie County Bridge.

At the Story County Bridge, the pile temperatures were approximately 75°F (24°C) and 15°F (-9°C) at the time of the maximum and minimum, average, concrete temperatures of 104°F (40°C) and -10°F (-23°C), respectively. Only the top several inches of the piles were exposed to open air. For the Story County Bridge, the range in the pile temperature was 60°F (33°C).



(a) Guthrie County Bridge (July 20, 1998 and January 5, 1999)



(b) Story County Bridge (July 20, 1998 and January 5, 1999)

Figure 4.17. Measured bridge temperatures along the bridge length at the time of the maximum and minimum average bridge temperatures [26]

4.3 Bridge displacements

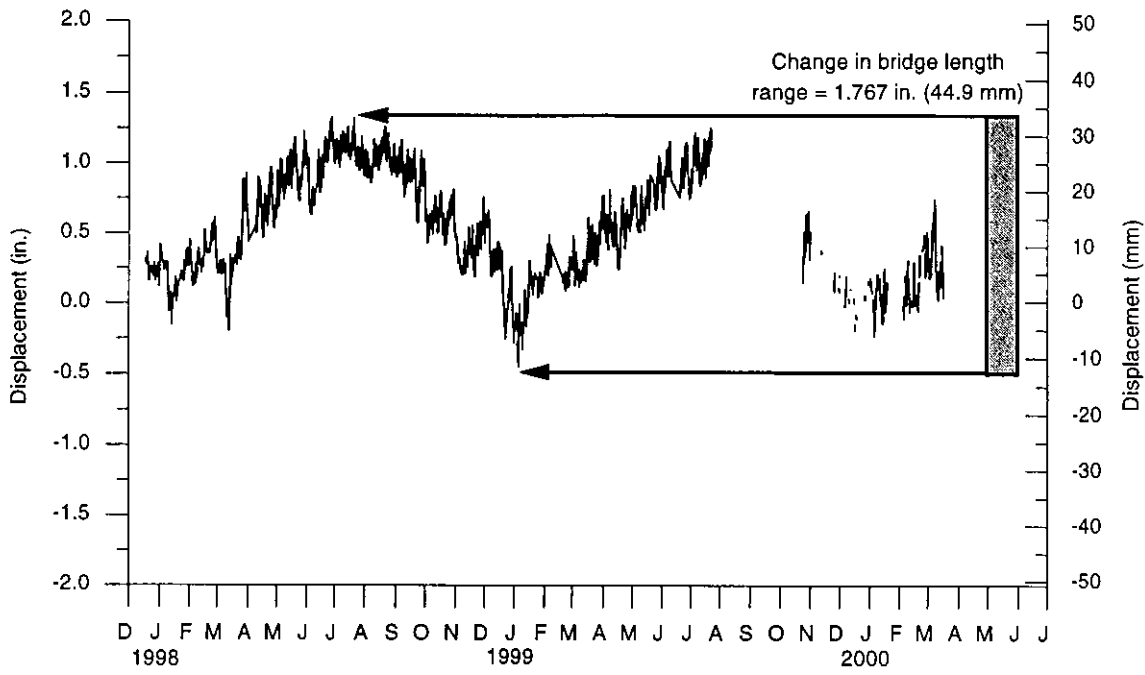
This section describes the longitudinal abutment displacements, transverse abutment displacements, abutment rotations in a vertical plane that is parallel to the longitudinal axis of the bridge, and abutment rotations in a horizontal plane.

Differential displacements between several bridge elements are also discussed.

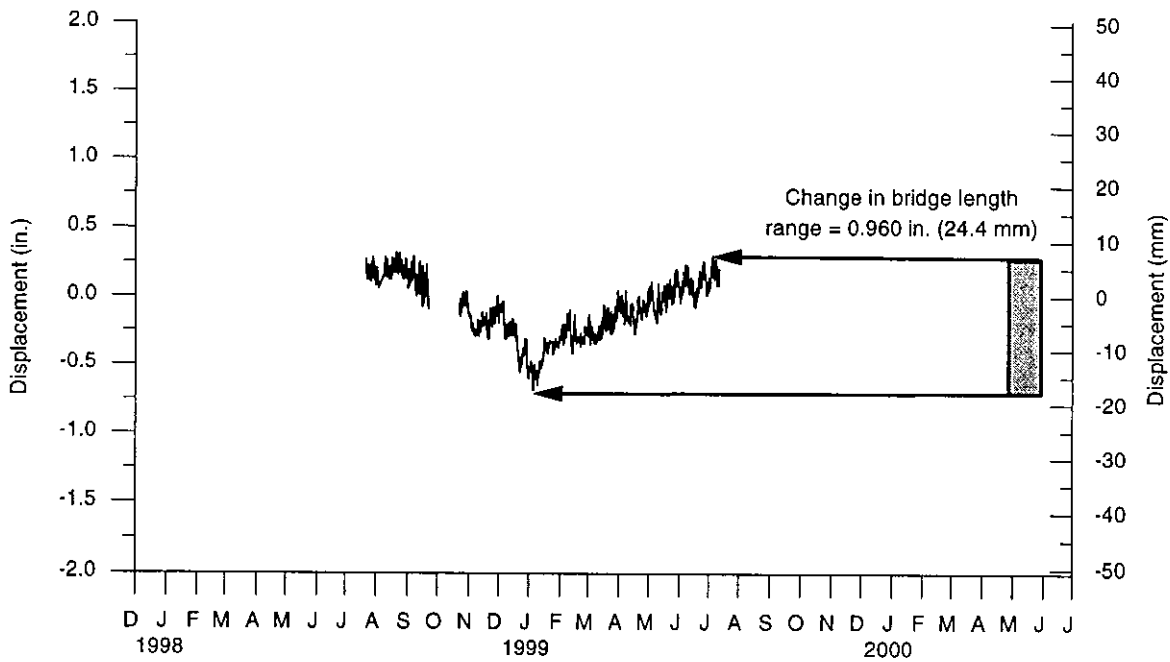
4.3.1 Longitudinal abutment displacements and change in bridge length

Figure 4.18 shows the change in bridge length between December 17, 1997 and April 1, 2000 at the Guthrie County Bridge and between October 17, 1998 and July 12, 1999 at the Story County Bridge. The change in the bridge length was determined by summing the longitudinal abutment displacements measured at the mid-width of the abutment pile cap at each end of the bridge. Positive values for the change in Guthrie County bridge length indicate expansion of the bridge relative to the bridge length at 11:20 p.m. on March 9, 1998, which coincided with the time of the first, dummy, strain-gage reading. The reference time for the Story County Bridge displacements was at 1:30 a.m. on October 1, 1998. Positive values indicate expansion of the bridge superstructure with respect to this reference time.

The recorded range for the change in Guthrie County Bridge length was 1.767 in. (44.9 mm). The maximum change in average bridge temperature, and thus the maximum change in bridge length, occurred in the time period between July 20, 1998 and January 5, 1999. The displacement transducer (SP-NC-LB) produced unreliable data in August of 1999 through October of 1999, but resumed producing some reliable data after November of 1999. At the Story County Bridge, the maximum



(a) Guthrie County Bridge



(b) Story County Bridge

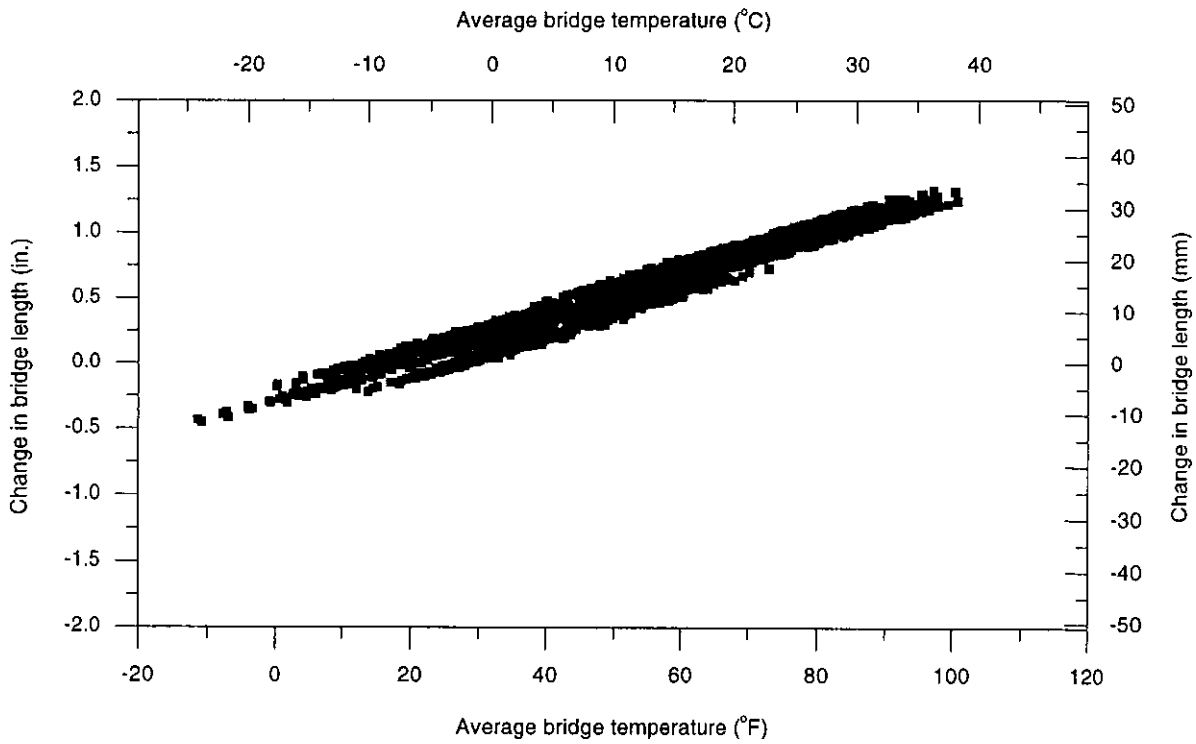
Figure 4.18. Change in the bridge length

change in bridge length was 0.960 in. (24.4 mm), over the time period between January 5, 1999 and July 5, 1999. Each of the displacement transducers that were used to determine the change in the length of the Story County Bridge produced unreliable data in October of 1998.

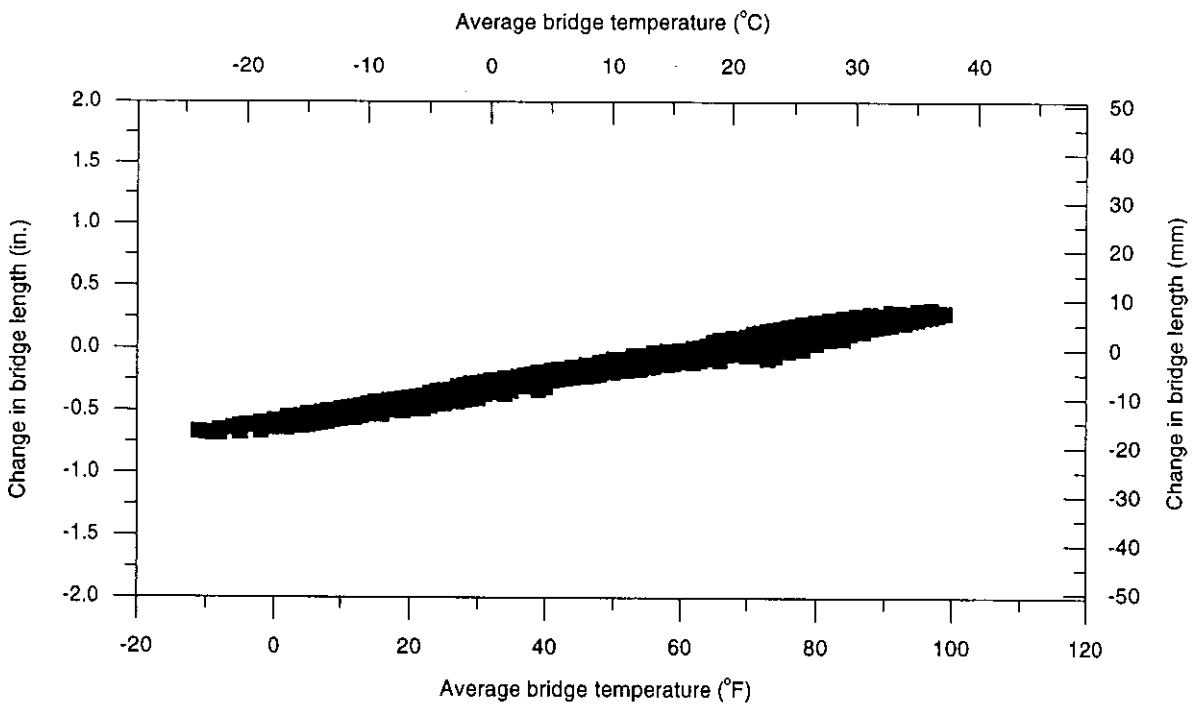
Figure 4.19 shows the change in bridge length versus average bridge temperature for the Guthrie County Bridge and Story County Bridge, respectively. The longitudinal displacement data correlated well with the recorded change in the average bridge temperature.

The magnitudes of the longitudinal abutment displacements measured at each end of the Guthrie County Bridge were not equal. The longitudinal displacements measured at the north abutment were approximately twice as large as those measured at the south abutment. Except for the pier details, the bridge geometry is symmetric. (The pier details are discussed in detail in Section 5.1 and the relative movements of the bridge superstructure over the piers are discussed in Section 4.3.5.) The south pier is an expansion pier; therefore, the researchers assumed that the south abutment would displace further longitudinally than the north pier. The experimental longitudinal abutment displacements proved otherwise. Other factors, such as abutment backfill stiffness, may have caused the difference in abutment displacement. Factors affecting backfill stiffness include backfill slope, backfill compaction, and moisture content of the backfill [8].

The relationship between the longitudinal abutment displacements and the average concrete temperature at the Guthrie County Bridge is shown in Figure 4.20.



(a) Guthrie County Bridge



(b) Story County Bridge

Figure 4.19. Change in the bridge length versus the average bridge temperature

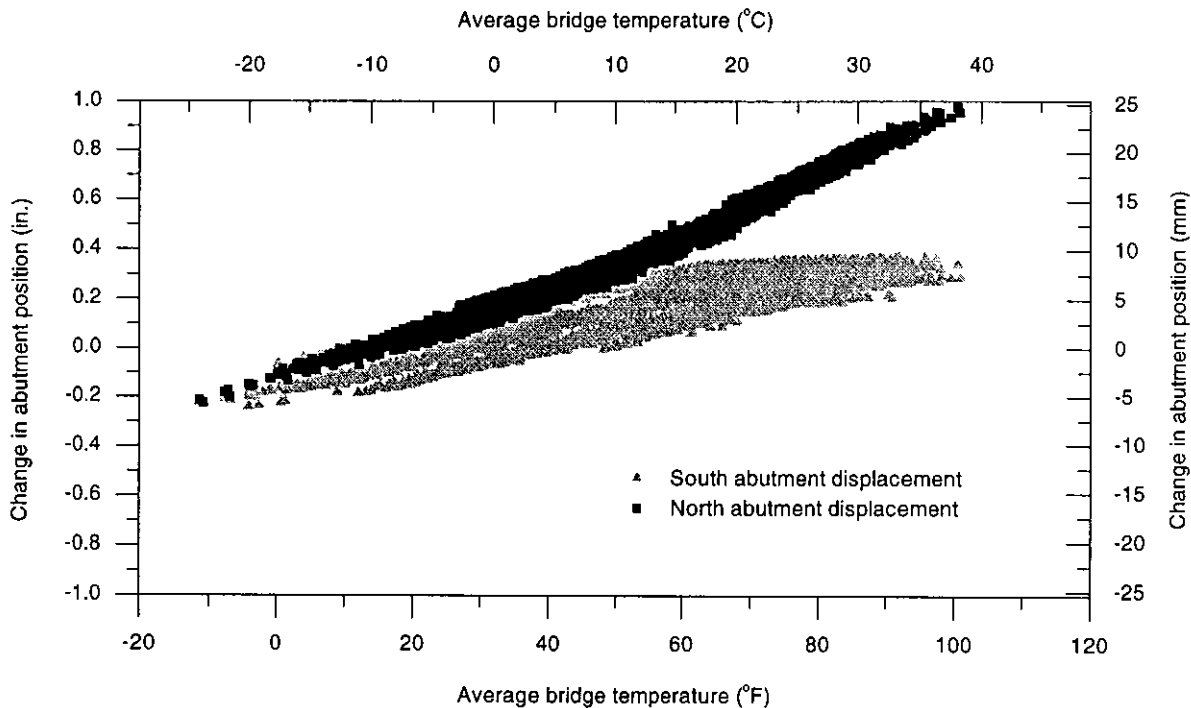


Figure 4.20. Change in the north and south abutment positions at the Guthrie County Bridge versus average bridge temperature

Nonlinear, longitudinal, abutment displacements were observed at the Guthrie County Bridge. The south abutment experienced a decrease in the rate of displacement in the longitudinal direction of the bridge for an average bridge temperature greater than 60°F (16°C). The north abutment experienced an increase in the rate of longitudinal displacement when the average bridge temperature exceeded 60°F (16°C).

At the Story County Bridge, the abutment displacements are more symmetric. The geometry of this bridge is symmetric, with both piers having a fixed pier detail. For this bridge, the west abutment displacements accounted for approximately 55% of the change in bridge length. The longitudinal abutment displacements measured

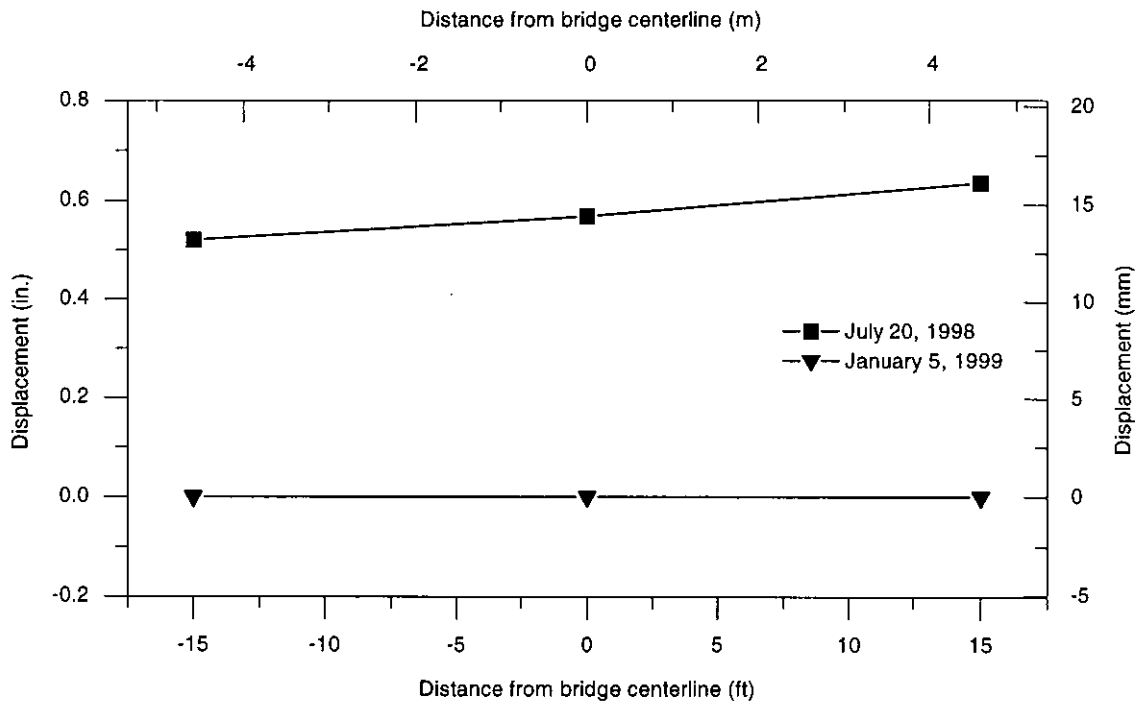
at the Story County Bridge remained linear over the entire range of the average bridge temperature.

4.3.2 Abutment rotation in a horizontal plane

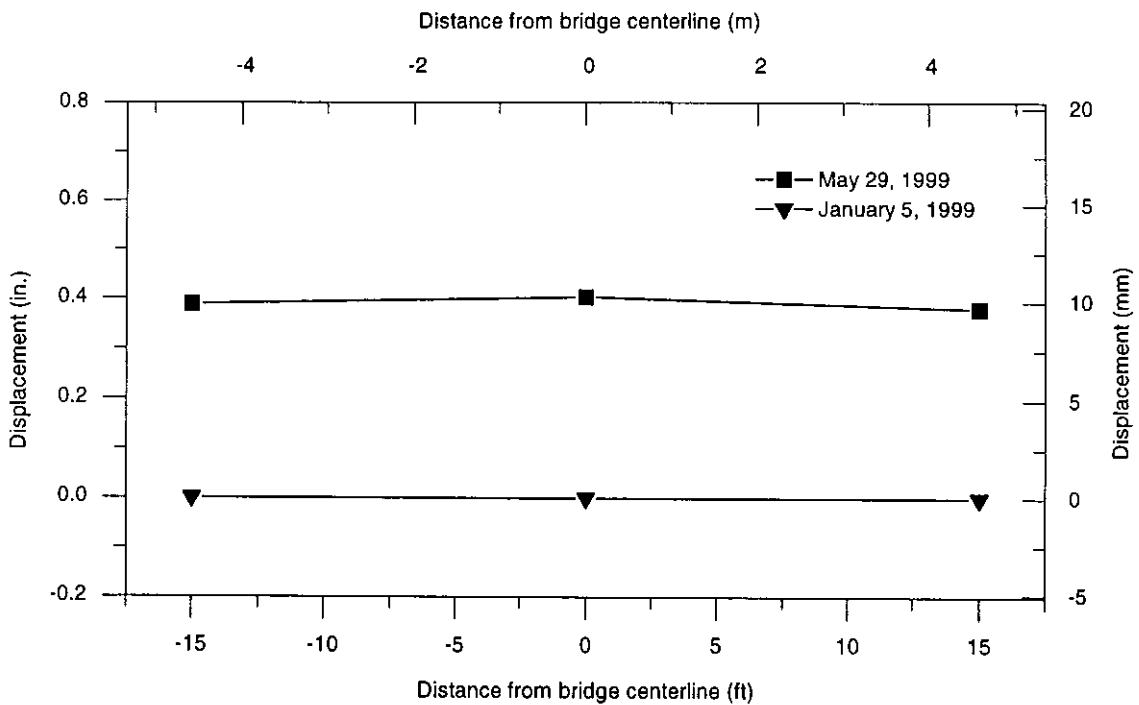
Longitudinal abutment displacements were measured at three positions across the width of one abutment at each bridge to determine the plan view rotation of the abutment. Any difference in the longitudinal displacements at these points on an abutment may be due to rigid-body rotation of the abutment pile cap about a vertical axis and to horizontal curvature of the pile cap.

The change in longitudinal positions for the three points along the width of the south abutment pile cap of the Guthrie County Bridge are shown in Figure 4.21(a). Positive distances for the abscissa scale in the graph are measured normal to the longitudinal axis of the acute-angle corner in the bridge deck. Figure 4.21(a) shows the south abutment displacements relative to the displacements measured on January 5, 1999. At this bridge, the south abutment appears to have rotated in a counterclockwise direction in a horizontal plane, i.e. the longitudinal abutment displacement of this abutment near the acute-angle corner of the bridge deck was greater than that for the obtuse-angle corner of the bridge deck.

The longitudinal displacements of three points across the width of the east abutment of the Story County Bridge are shown in Figure 4.21(b). A jump in the displacement reading at the south corner of the east abutment occurred on June 2, 1999; therefore, the three, longitudinal, abutment displacements could not be compared between the times of the largest range in average bridge temperatures. Figure 4.21(b) shows the east abutment displacement between January 5, 1999 and



(a) South abutment at the Guthrie County Bridge



(b) East abutment at the Story County Bridge

Figure 4.21. Range in longitudinal displacement at three positions across the width of the abutments

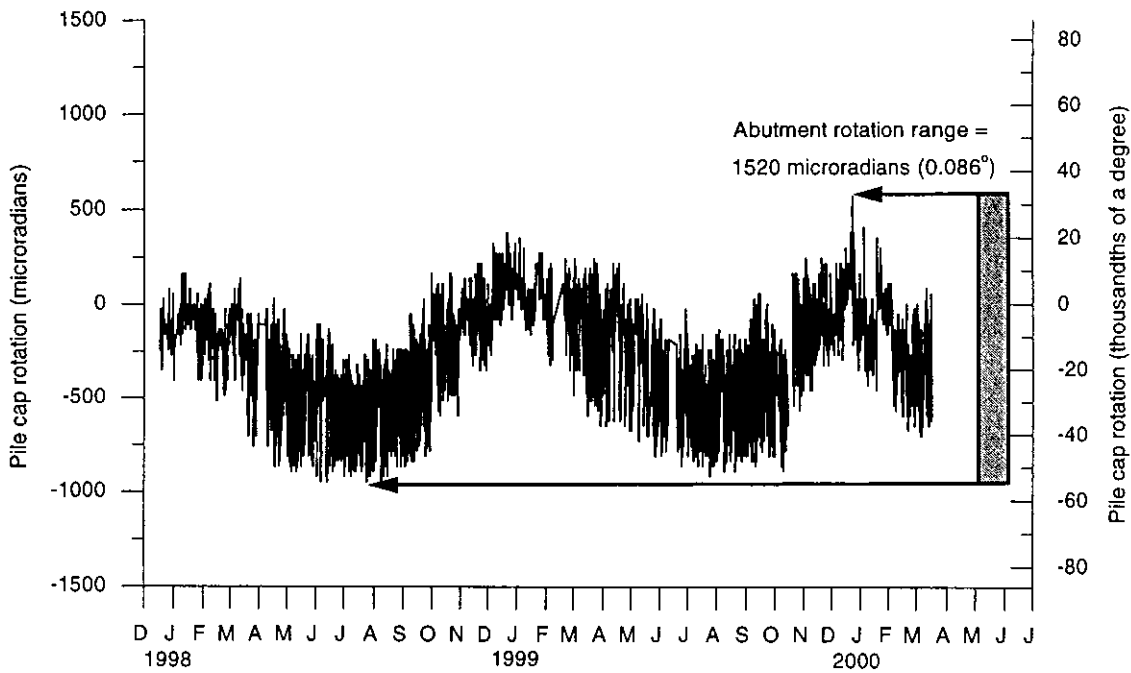
May 29, 1999. Over this time period the change in the average bridge temperature was 95°F (53°C). The east abutment displacements were relative to the displacements that were measured on January 5, 1999. The east abutment at the Story County Bridge does not appear as though it has undergone a rotation about a vertical axis. However, the magnitude of the longitudinal displacement measured at the mid-width of the abutment is slightly larger than the longitudinal displacement measurements at the ends. The difference in these displacements indicate that the abutment was subject to flexural bending in a horizontal plane.

4.3.3 Abutment rotation in a vertical plane

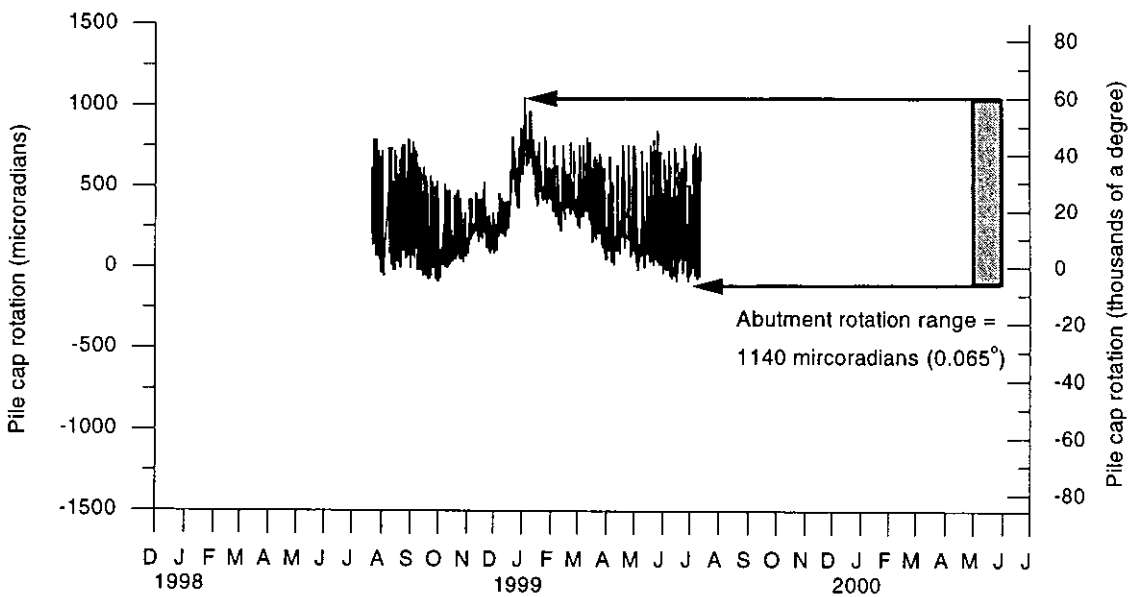
Figure 4.22(a) shows the rotation of the pile cap at the mid-width of the south abutment at the Guthrie County Bridge. Figure 4.22(b) shows the rotation of the pile cap at the mid-width of the east abutment at the Story County Bridge. The magnitudes for the ranges in the measured rotations are similar at both bridges. The pile cap at the Guthrie County Bridge has rotated through a range of about 1520 microradians (0.087°). The pile cap at the Story County Bridge has experienced a rotation of about 1140 microradians (0.065°). The range in the pile cap rotations at each bridge varied in some instances by as much as 700 microradians (0.040°). The daily variation of the pile cap rotation was greater during the summer months than during the winter months.

4.3.4 Transverse abutment displacements

Figure 4.23 shows the measured transverse displacement of the center of mass for the pile cap at the south abutment of the Guthrie County Bridge. Positive displacements indicate that the abutment translated towards the acute-angle corner



(a) South abutment pile cap at the Guthrie County Bridge



(b) East abutment pile cap at the Story County Bridge

Figure 4.22. Abutment rotation in a vertical plane parallel to the longitudinal axis of the bridge

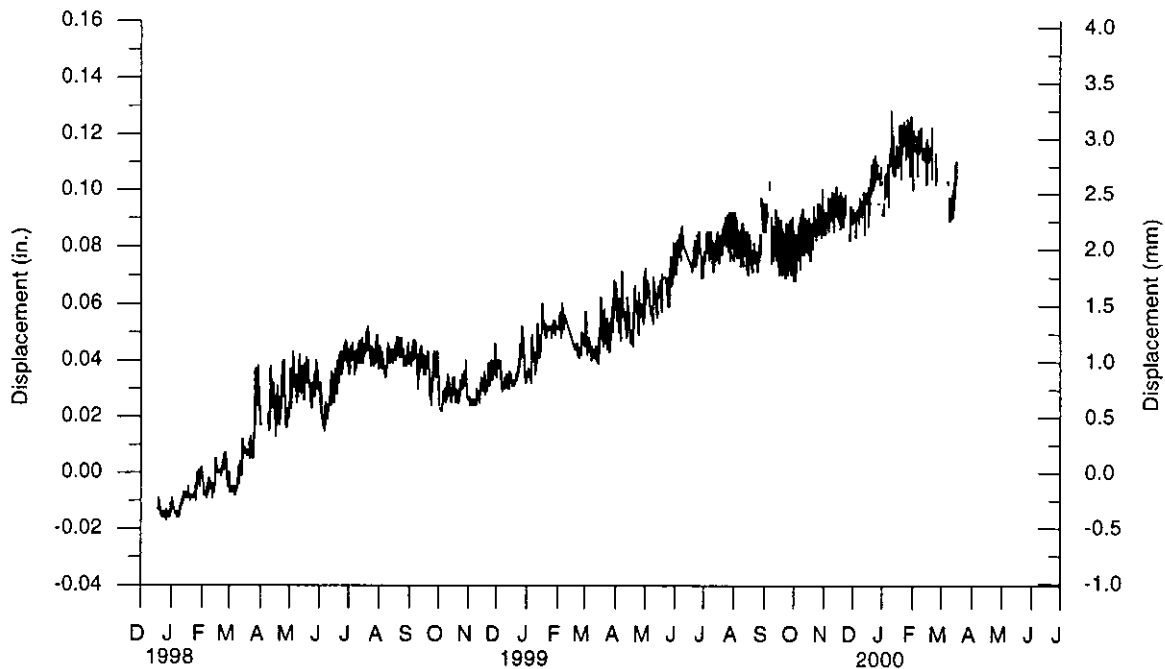


Figure 4.23. Change in transverse position of the south abutment of the Guthrie County Bridge

of the bridge deck. Expansion of an integral-abutment bridge activates soil pressures behind the abutments. For a skew, integral-abutment bridge, a component of this passive-soil force is directed towards the acute-angle corner of the bridge deck. The south abutment in the Guthrie County Bridge did not return to the same lateral position after each yearly cycle of temperature changes. Over the monitored time period shown in Figure 4.23, the south abutment of this bridge experienced a residual displacement towards the acute-corner of the bridge deck.

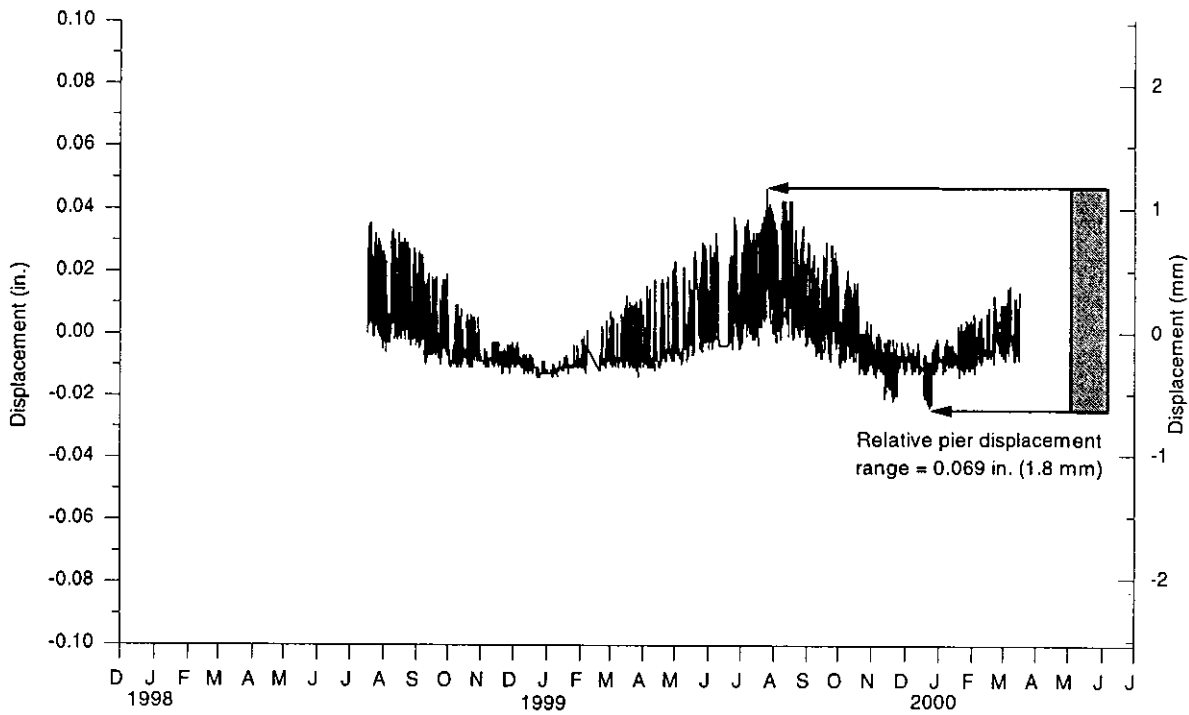
The transverse displacements of the east abutment for the Story County Bridge measured at the northeast corner did not appear to be realistic since these displacements did not correlate well with the average bridge temperature. These displacements were much higher than the comparable displacements that were

measured at the Guthrie County Bridge, whose skew angle is larger than that for the Story County Bridge. The average abutment expansion and transverse displacement of the mid-width of the east abutment of the Story County Bridge could not be computed using the measured transverse displacements.

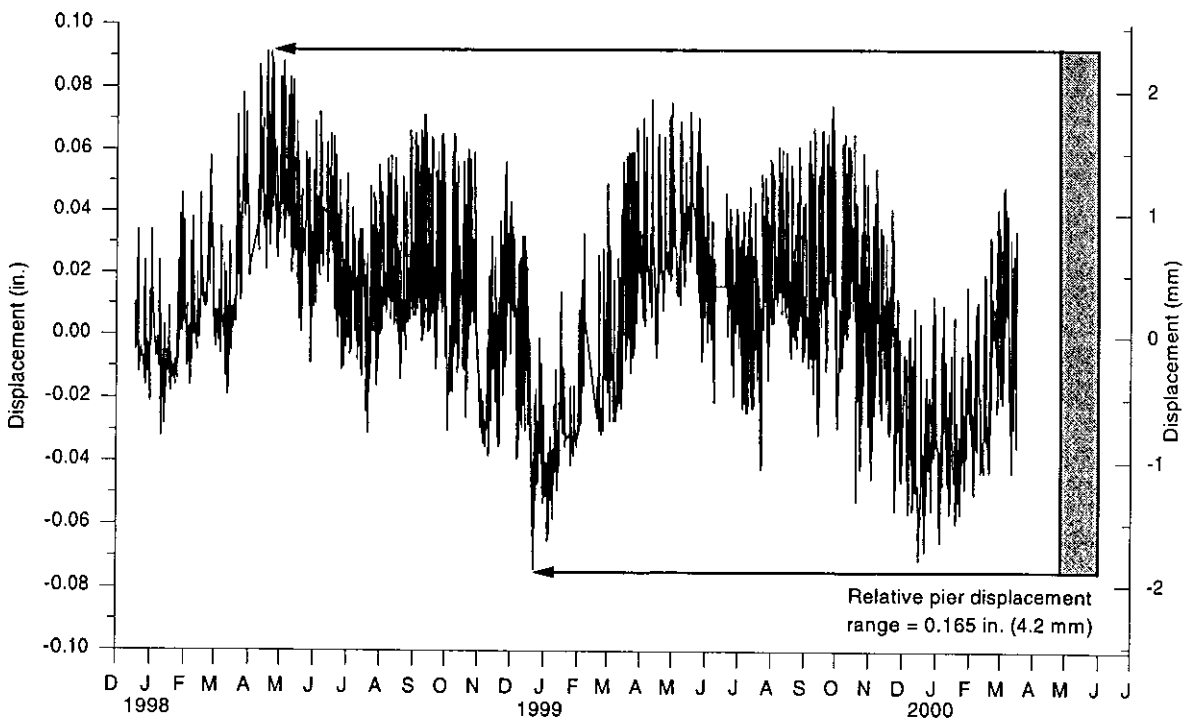
4.3.5 Relative displacements

Relative longitudinal movements of the bridge superstructure over the pier caps were measured at each pier at both bridge sites. These relative displacements at the Guthrie County Bridge and Story County Bridge are shown in Figures 4.24 and 4.25, respectively. The range of the superstructure relative displacement at the south and north piers of the Guthrie County Bridge were approximately 0.165 in. (4.2 mm) and 0.069 in. (1.8 mm), respectively. The pier details for the Guthrie County Bridge indicate that less longitudinal restraint to the superstructure should occur at the south pier than that at the north pier. At the south pier, the superstructure sits on 3.75-in. (95-mm) thick, steel-reinforced, neoprene pads. The north pier detail shows a full-depth, RC diaphragm cast into a beveled keyway in the pier cap that is lined with expansion joint filler. The daily range of relative displacements over the north pier decreased in the winter months, while the daily variation in the relative displacements of the bridge superstructure over the south pier had a nearly constant magnitude over the entire monitoring period.

The construction details for both of the pier diaphragms at the Story County Bridge are similar to the pier details for the fixed pier at the Guthrie County Bridge. The relative displacements of the Story County Bridge superstructure over the piers were smaller than the displacements measured over the north pier at the Guthrie

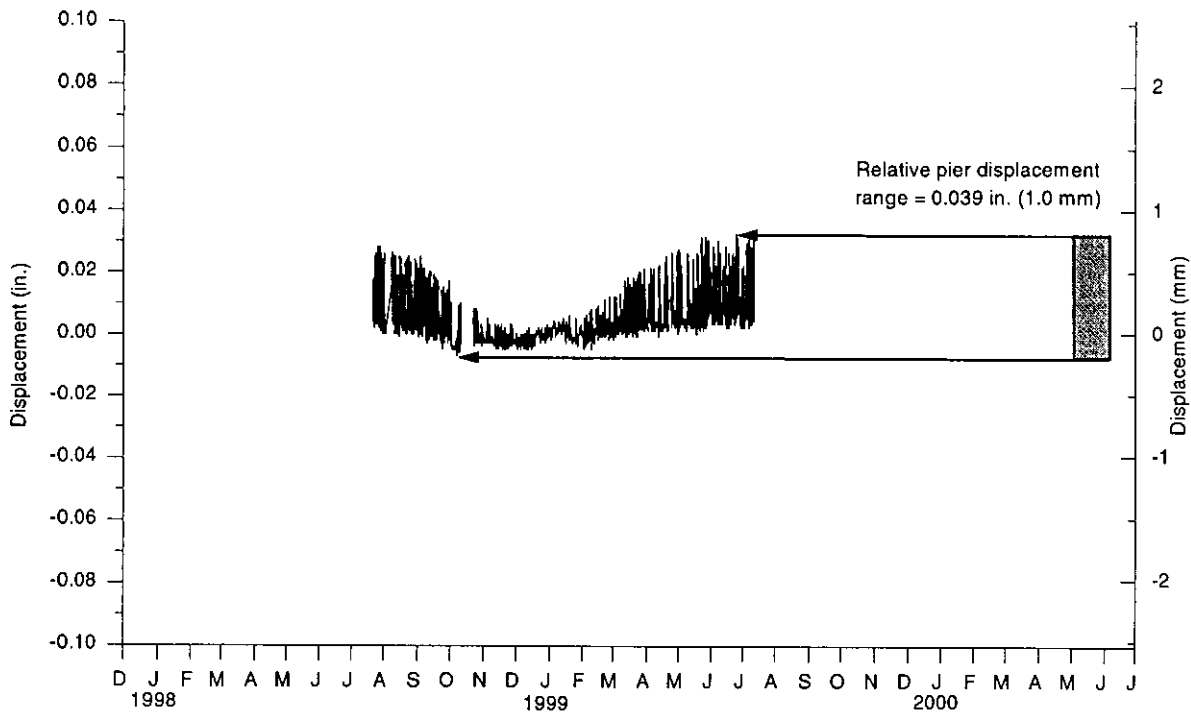


(a) North pier

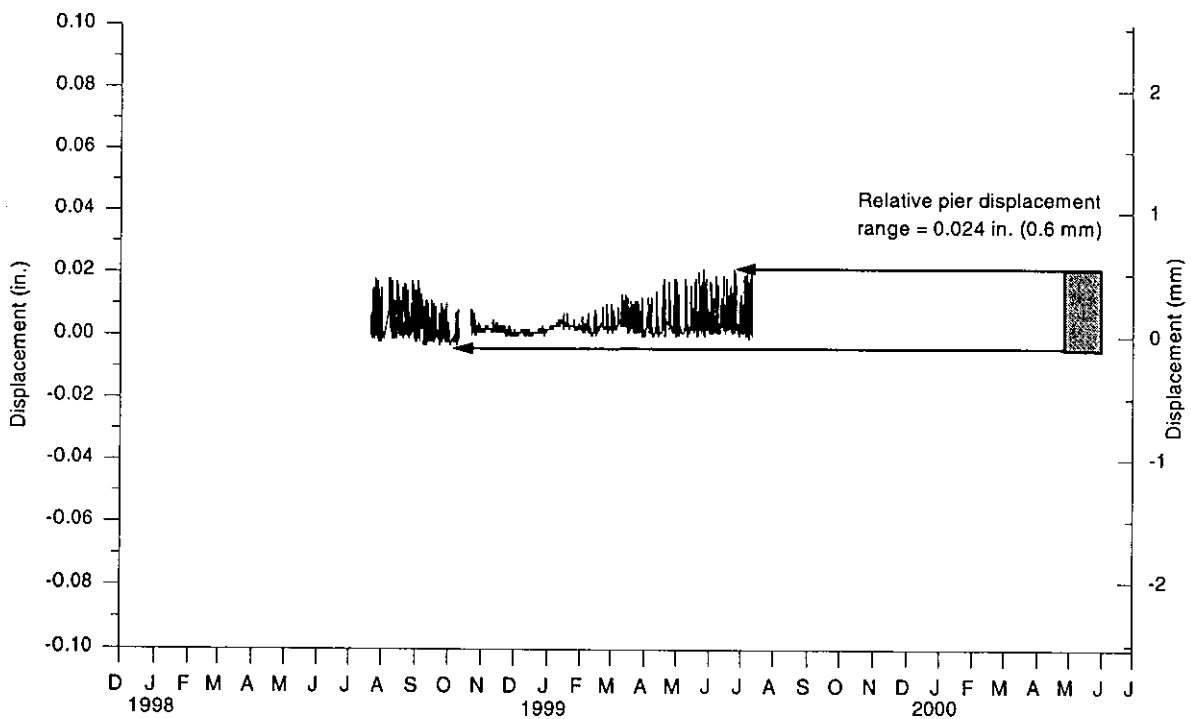


(b) South pier

Figure 4.24. Relative displacements of the Guthrie County Bridge superstructure over the piers



(a) West pier



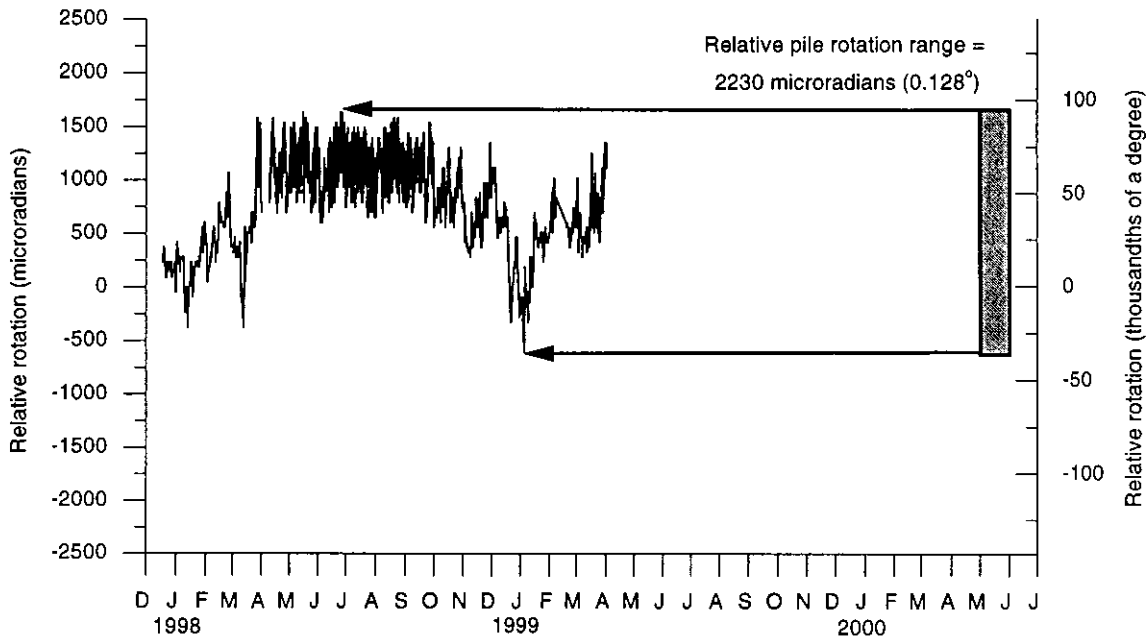
(b) East pier

Figure 4.25. Relative displacements of the Story County Bridge superstructure over the piers

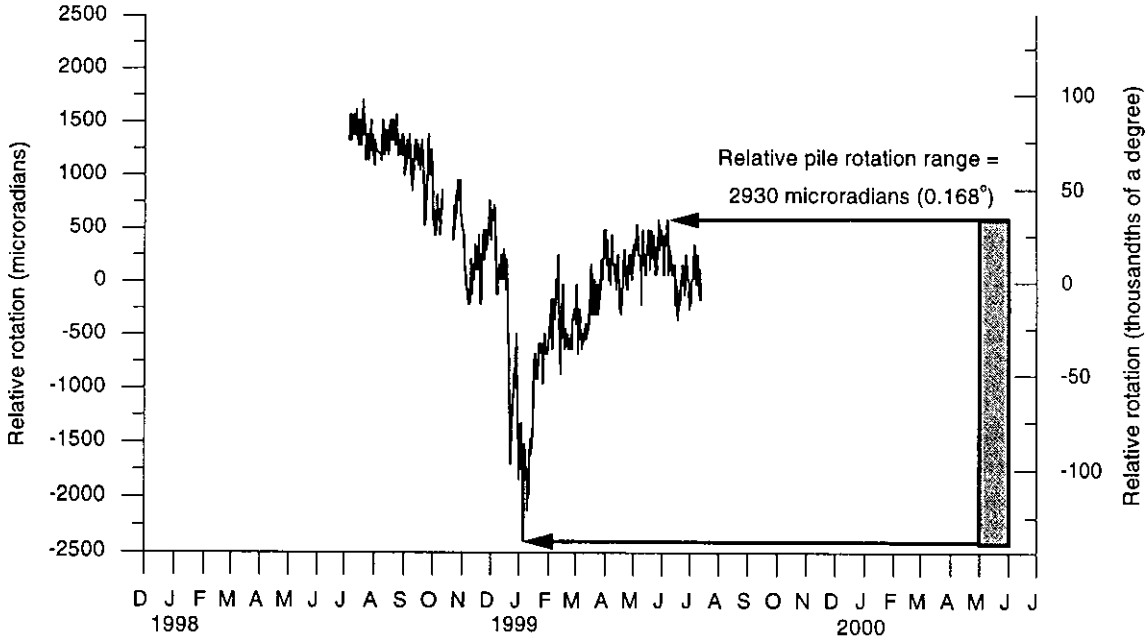
County Bridge. The ranges of relative pier displacements measured at the Story County Bridge were 0.039 in. (1.0 mm) and 0.024 in. (0.6 mm) for the east and west piers, respectively. The range of motion of the superstructure over the piers at the Story County Bridge decreased in the winter months.

Figure 4.26 shows the relative rotations measured between a monitored pile cross section and a pile cap at the Guthrie County Bridge and Story County Bridge, respectively. This relative rotation measurement was the relative rotation between the bottom of the pile cap and a point on a pile 18 in. (460 mm) below the pile cap. In the summer of 1999, the relative pile rotations at a pile in the Story County Bridge did not return to same measurements as those recorded in the summer of 1998. Also, the relative rotation measured on July 5, 1999 was nearly 0.030° (500 microradians) less than that which was recorded a month earlier. The bar shown in Figure 4.26(b) shows the change in relative pile rotations measured for one temperature cycle in 1999.

Relative displacements measured between the top and bottom flanges of the center PC girder and the south abutment backwall at the Guthrie County Bridge are shown in Figure 4.27. The displacements measured at the top flange location changed significantly in the spring of 1998 compared to the measurements over the remaining monitoring period. The initial data from this gage was not considered reliable. Since that time, the readings of both transducers are similar and small. No evidence of cracking in the RC backwall or the PC girder near the abutments was observed at either bridge.

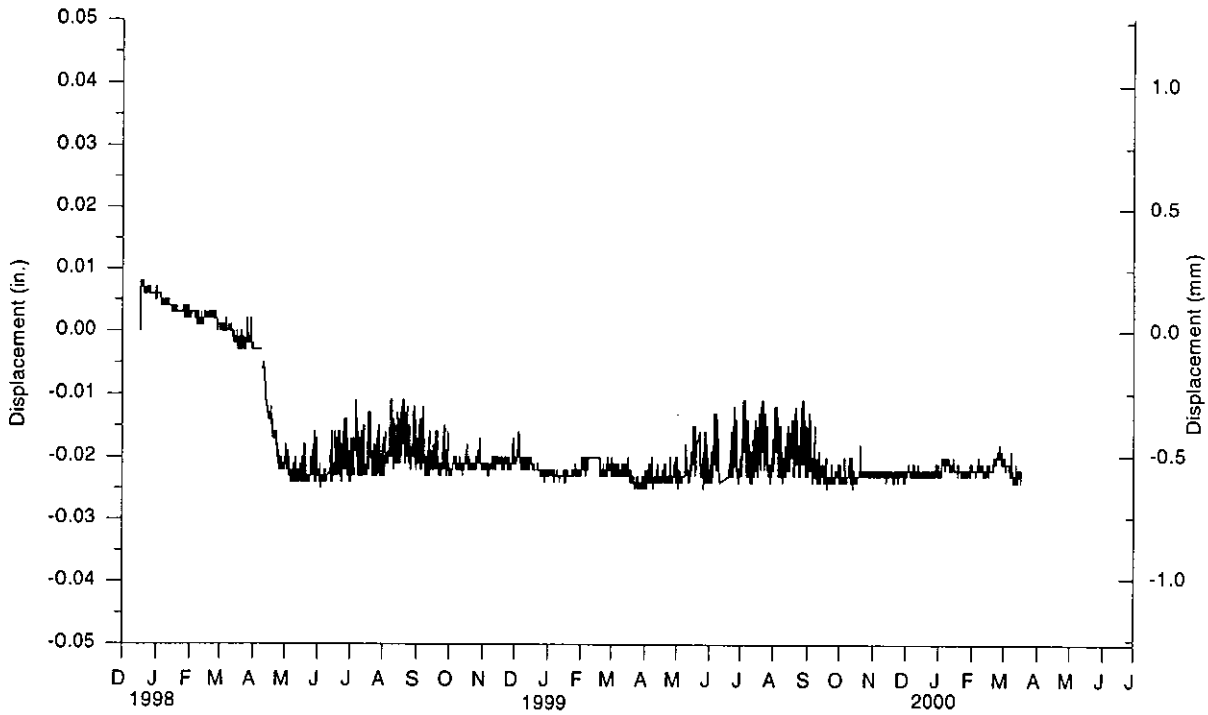


(a) Guthrie County Bridge

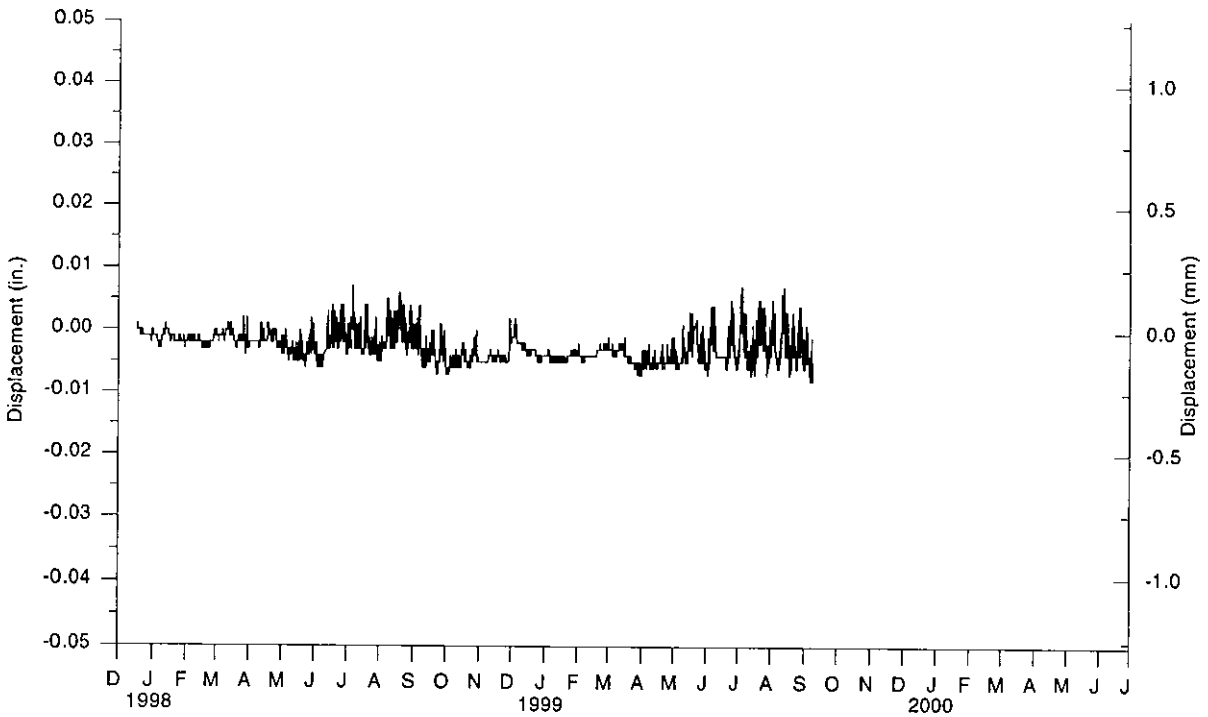


(b) Story County Bridge

Figure 4.26. Relative rotation between a pile and a pile cap



(a) Displacement at the top flange



(b) Displacement at the bottom flange

Figure 4.27. Relative displacement between the center PC girder and the south abutment backwall at the Guthrie County Bridge

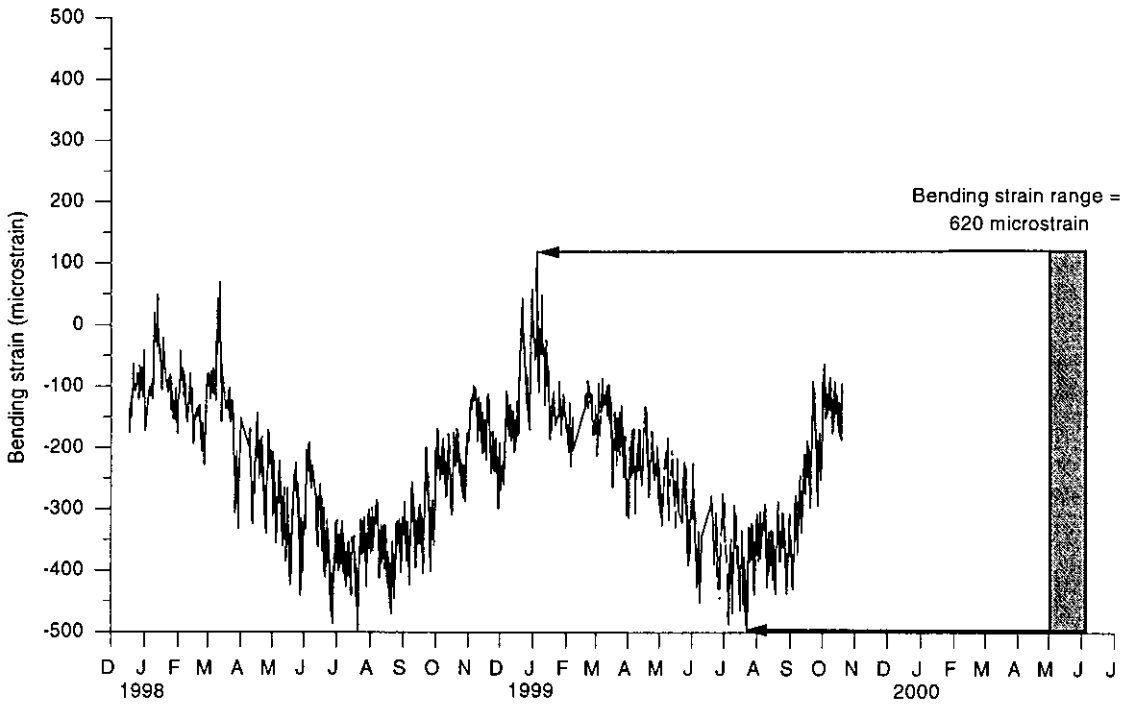
4.4 Bridge member strains

This section describes strains measured in the abutment piles and PC girders at the Guthrie County Bridge and Story County Bridge. The experimentally measured strains presented in this section represent the typical strains measured in the piles at both of the bridges.

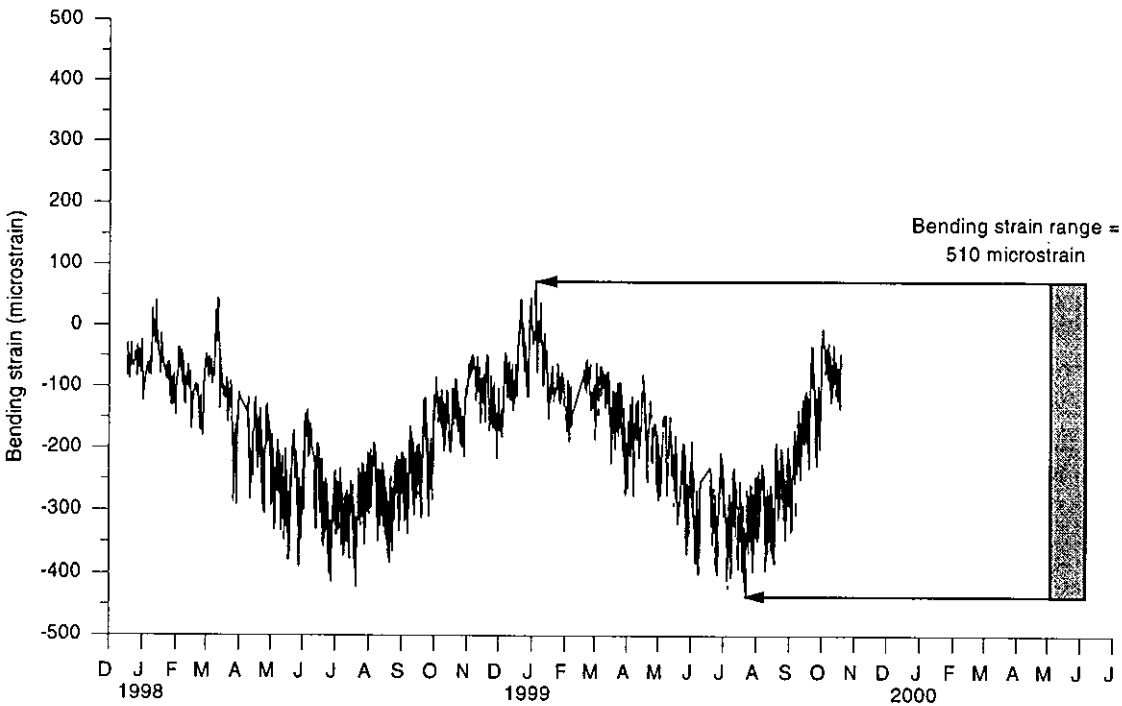
4.4.1 Pile strains

The orientation of the abutment piles for the Guthrie County Bridge is such that the webs of the piles are parallel to the abutment face. Since the bridge has a 30° skew angle, a component of the pile-head displacement along the longitudinal axis of the bridge will induce x- and y-axis, flexural-bending strains. Figure 4.28 shows the x- and y-axis, flexural-bending strains at the monitored, top cross section of the pile near the mid-width of the north abutment for the Guthrie County Bridge. The top cross section was located at 9 in. (230 mm) below the bottom of the pile cap. The range in the x- and y-axis, flexural-bending strains were approximately 510 and 620 microstrains, respectively. For a structural steel with a yield stress of 36 ksi (248 MPa), the yield strain is about 1240 microstrains. If the y-axis, flexural-bending strains, which were measured at about one inch from the flange tips, are linearly extrapolated to the extreme fibers of the cross section, the magnitude of the y-axis, flexural-bending strains becomes approximately 770 microstrains. At the extreme fiber location in the monitored top cross section of the pile, the ratio of the x-axis bending strains to the y-axis bending strains was about 0.66.

At two corners of the HP-shaped, steel piles, the x- and y-axis, flexural-bending strains will be additive. If the measured flexural bending strains in the pile



(a) Y-axis bending strain

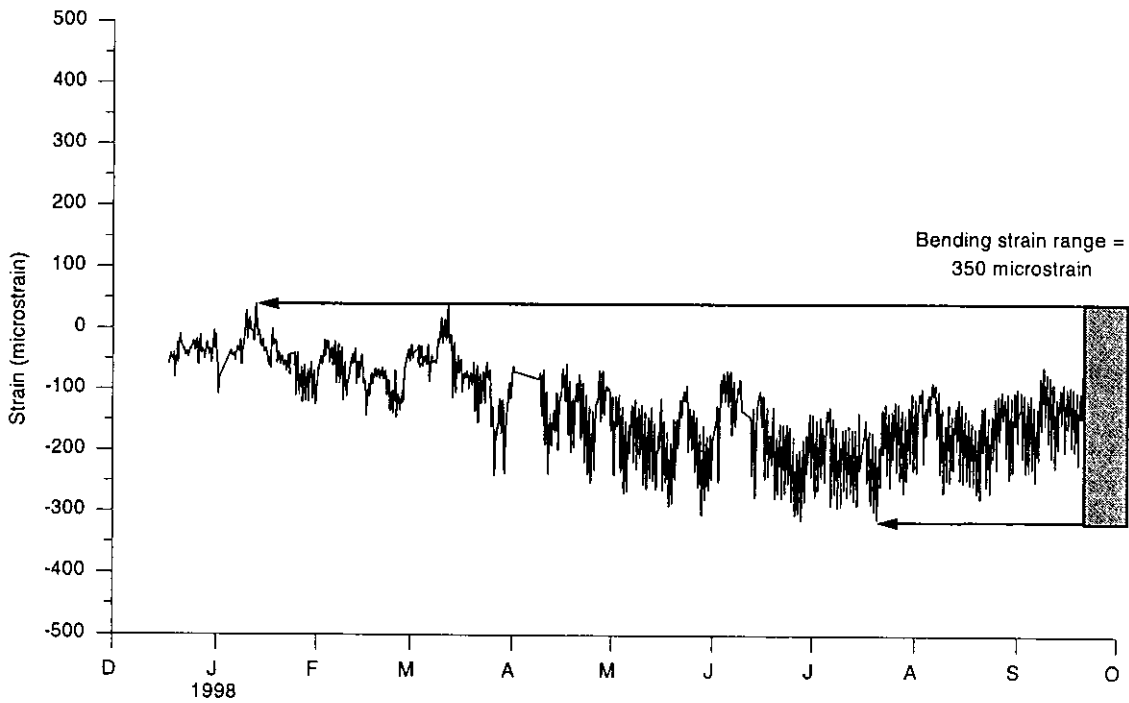


(b) X-axis bending strain

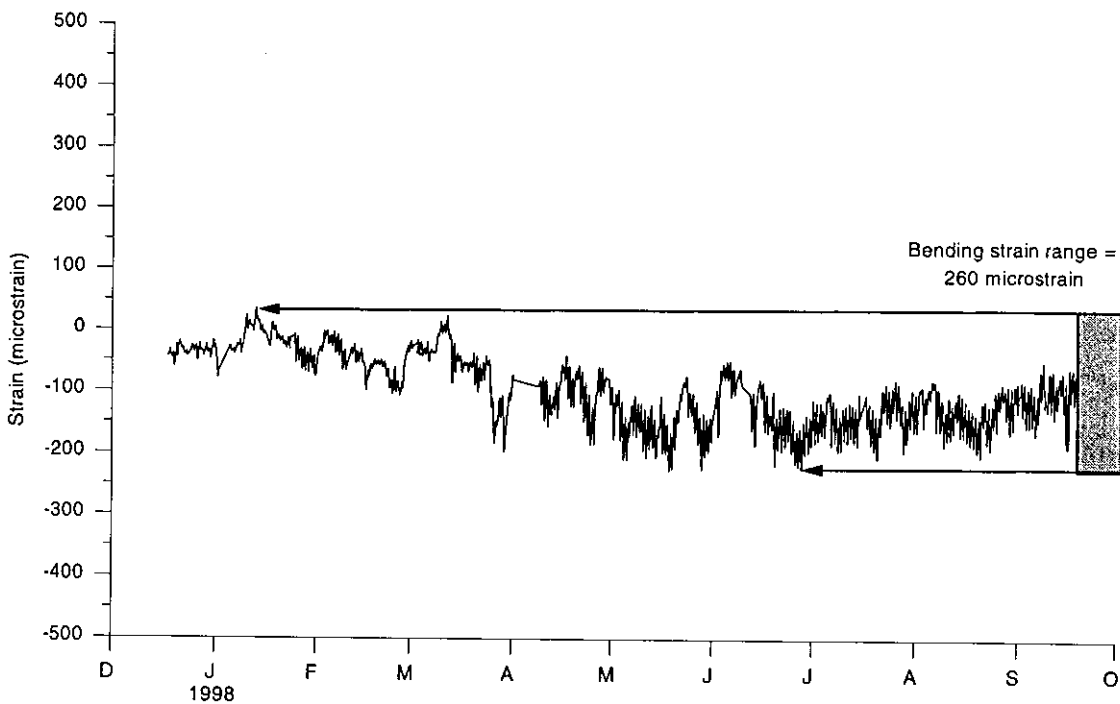
Figure 4.28. Biaxial pile bending strains at 9 in. below the bottom of the pile cap in the pile near the mid-width of the north abutment at the Guthrie County Bridge

near the mid-width of the north abutment of the Guthrie County Bridge are added, the flexural-strain range at the extreme fibers of these corners at 9 in. (230 mm) below the pile cap is approximately 1300 microstrains. This range in strain change is approximately equal to the yield strain of A36 steel. The combined, flexural-bending strain in the steel pile at a cross section that is located at the bottom of the pile cap would be even higher than 1300 microstrains. When this strain change is superimposed with the compressive axial strain in the steel piles due to the dead load of the bridge and with the residual compressive strains at the flange tips, a portion of one flange of the HP-shaped pile yielded in compression.

Larger magnitudes of bending strains in the abutment piles were measured at 9 in. (230 mm) than at 33 in. (840 mm) below the pile cap. Many of the strain gages on the lower cross sections of the piles at the Guthrie County Bridge failed early in the monitoring period. Due to the lack of reliable strain data for the lower pile cross sections, a vertical extrapolation of the y-axis, flexural-bending strain was not possible for any of the monitored piles at the Guthrie County Bridge. Figure 4.29 shows the x-axis, flexural-bending strains measured at the two instrumented cross sections along the length of the west pile for the north abutment of the Guthrie County Bridge. The bending strain measurements about the x-axis in the lower cross section were reliable until October of 1998. During times when the strain gages at both pile cross sections provided reliable data, the bending strains measured at the two cross sections had a similar trend versus time. The range in the x-axis, flexural-bending strains measured at the upper and lower cross sections



(a) Bending strain at 9 in. below the bottom of the pile cap

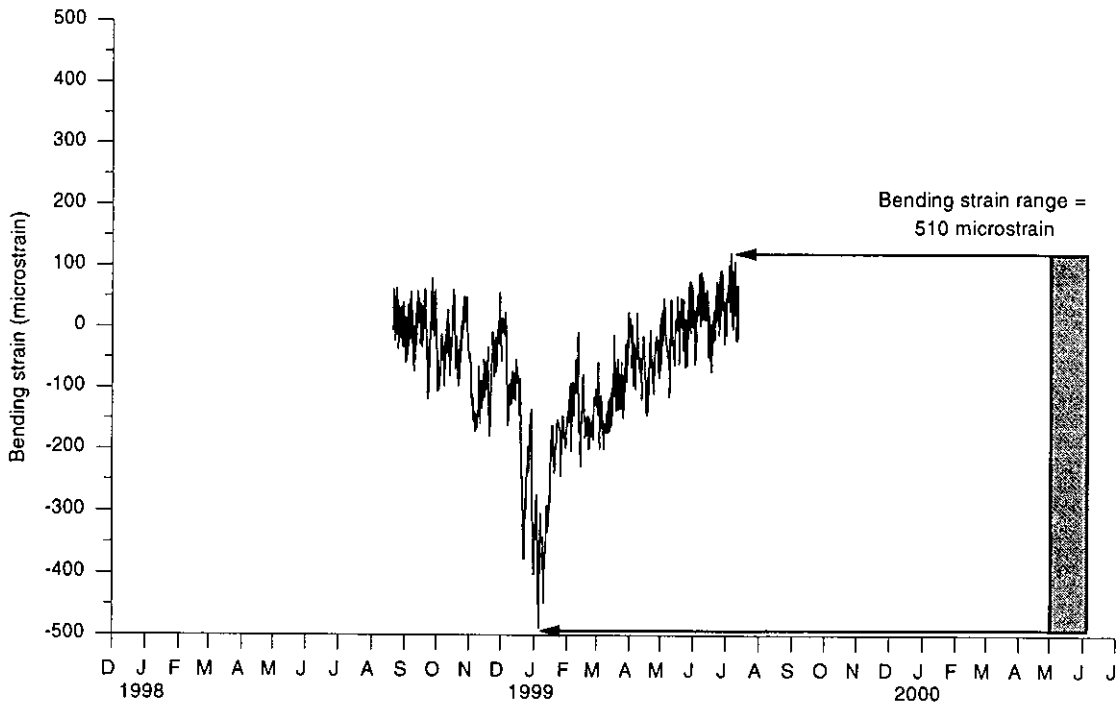


(b) Bending strain at 33 in. below the bottom of the pile cap

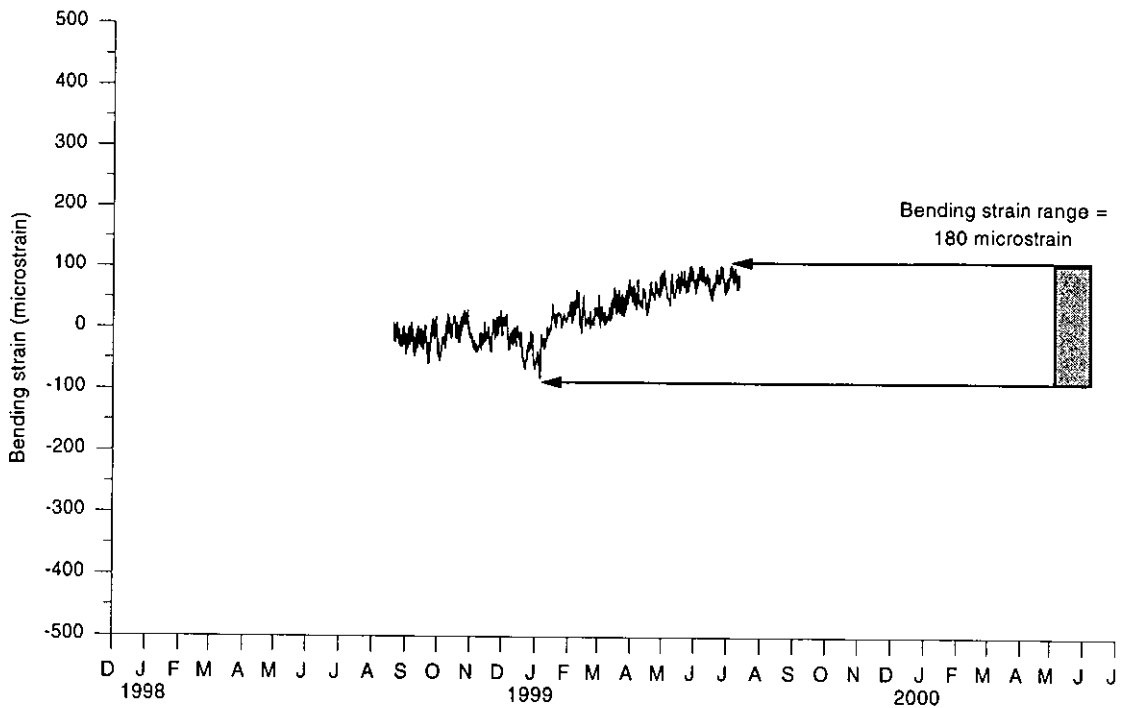
Figure 4.29. X-axis pile bending strains at two cross sections in the west pile of the north abutment at the Guthrie County Bridge

was approximately 350 and 260 microstrains, respectively. For the west pile of the north abutment of the Guthrie County Bridge, the extrapolated, x-axis, flexural-bending strain in the steel pile at the bottom of the pile cap was approximately 380 microstrains.

Figure 4.30 shows the x- and y-axis, flexural-bending strains for the center pile at 9 in. (230 mm) below the bottom of the pile cap of the east abutment for the Story County Bridge. Between the middle of August of 1998 and early July of 1999, the range in measured x- and y-axis, flexural-bending strains was approximately 180 and 510 microstrains, respectively. The extrapolated, y-axis, flexural-bending strain at the tips of the pile flanges for this cross section was about 640 microstrains. The ratio of the x-axis to the y-axis flexural-bending strains was about 0.28. This bending strains ratio for the abutment piles of the Story County Bridge was lower than that for the abutment piles of the Guthrie County Bridge. As was the case at the Guthrie County Bridge, the abutment piles at the Story County Bridge were oriented with their webs parallel to the abutment face. However, the 15° skew angle for this bridge was smaller than that for the Guthrie County Bridge. Therefore, the component of the abutment displacement that induced x-axis, pile bending was smaller than that for the abutment piles at the Guthrie County Bridge. The superposition of the flexural bending strains measured at the top cross section of the center pile of the east abutment at the Story County Bridge resulted in a combined-bending, flexural-strain range of approximately 820 microstrains. The combined, flexural-bending strain in the steel pile at a cross section that is located at the bottom of the pile cap would be even higher than 820 microstrains. When this strain change



(a) Y-axis bending strain



(b) X-axis bending strain

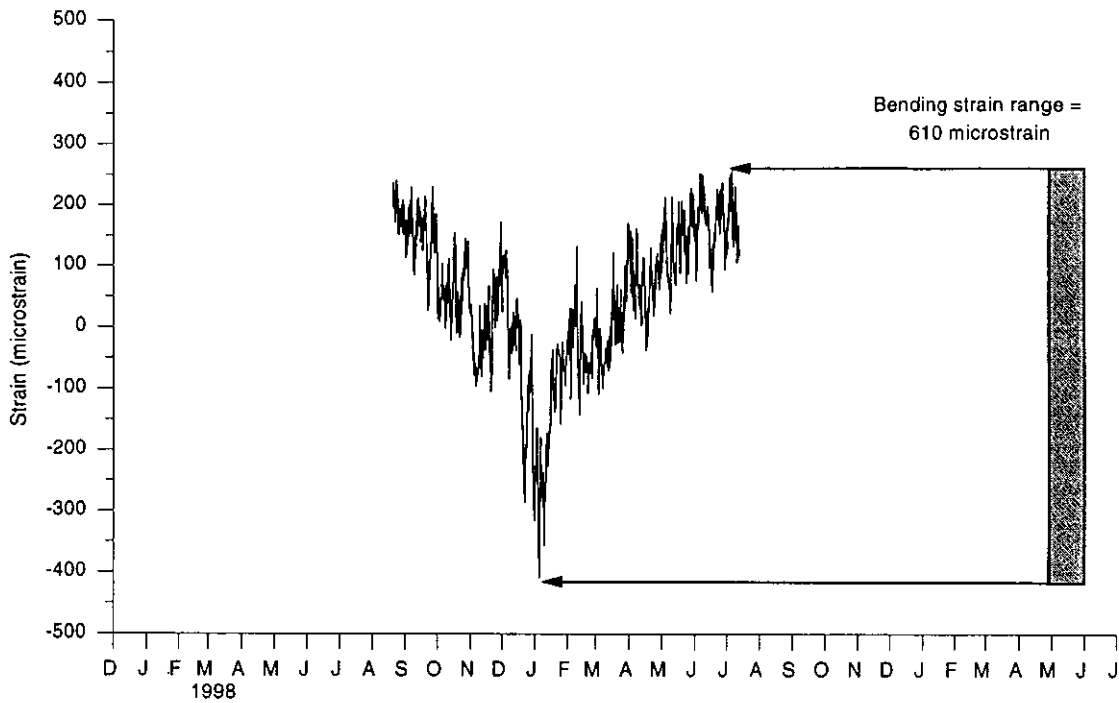
Figure 4.30. Biaxial pile bending strains at 9 in. below the bottom of the pile cap in the center pile at the east abutment at the Story County Bridge

is superimposed with the compressive axial strain in the steel piles due to the dead load of the bridge and with the residual compressive strains at the flange tips, a portion of one flange of the HP-shaped pile has probably yielded in compression.

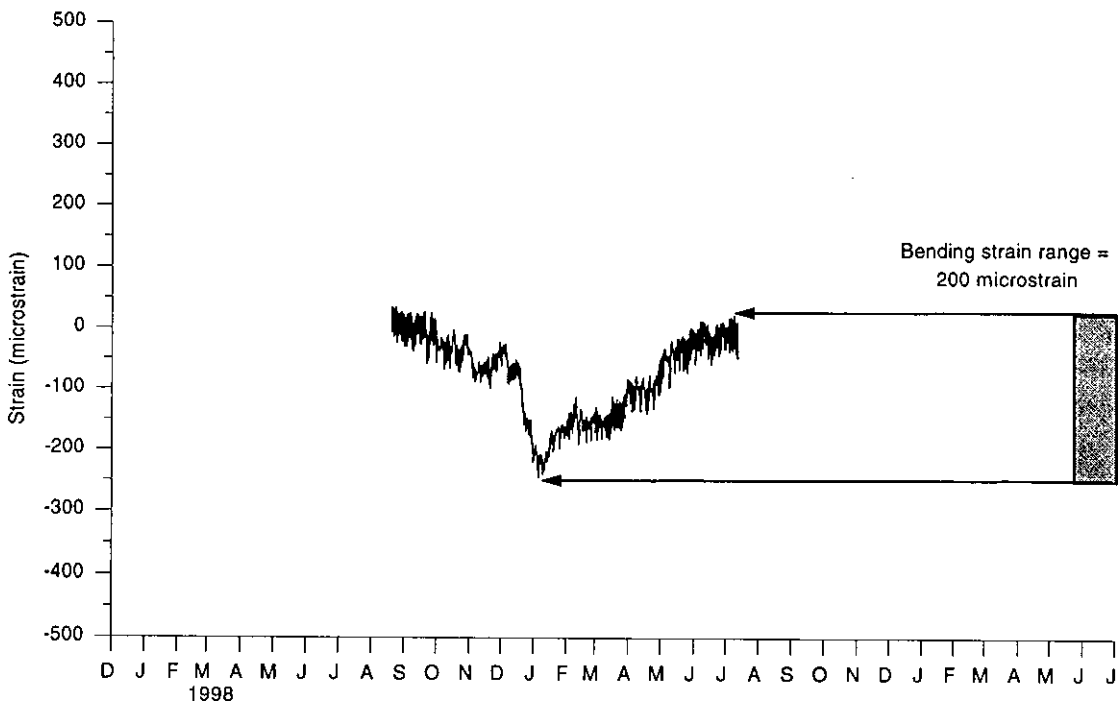
Figure 4.31 shows the y-axis, flexural-bending strains at the two, instrumented cross sections in the north pile of the east abutment for the Story County Bridge. The range in y-axis, flexural-bending strain in the top and bottom cross sections in this pile was approximately 610 and 200 microstrains, respectively. The difference between the y-axis, flexural-bending strains at the two cross sections in the piles was greater than the difference in y-axis pile bending strains recorded at the Guthrie County Bridge. At the flange tips, the extrapolated y-axis bending strain at the bottom of the pile cap in the north pile of the east abutment was approximately 950 microstrains, which is less than the theoretical yield strain of 1250 microstrains. When the x- and y-axis flexural-bending strains, the compressive axial strain due to the dead load of the bridge, and residual compressive strains at the flange tips are included in the total strain, a portion of one flange has probably yielded in compression.

4.4.2 Girder strains

The measured strains in the PC girders did not explicitly indicate strain due to stress in the girder, but rather indicated the deformation in the concrete at the gage locations. The total, bending-strain gradient included strains due to stress in the girder and the contraction or expansion of the girder due to temperature. Strains due to stress in the PC girders were determined using the finite-element models.



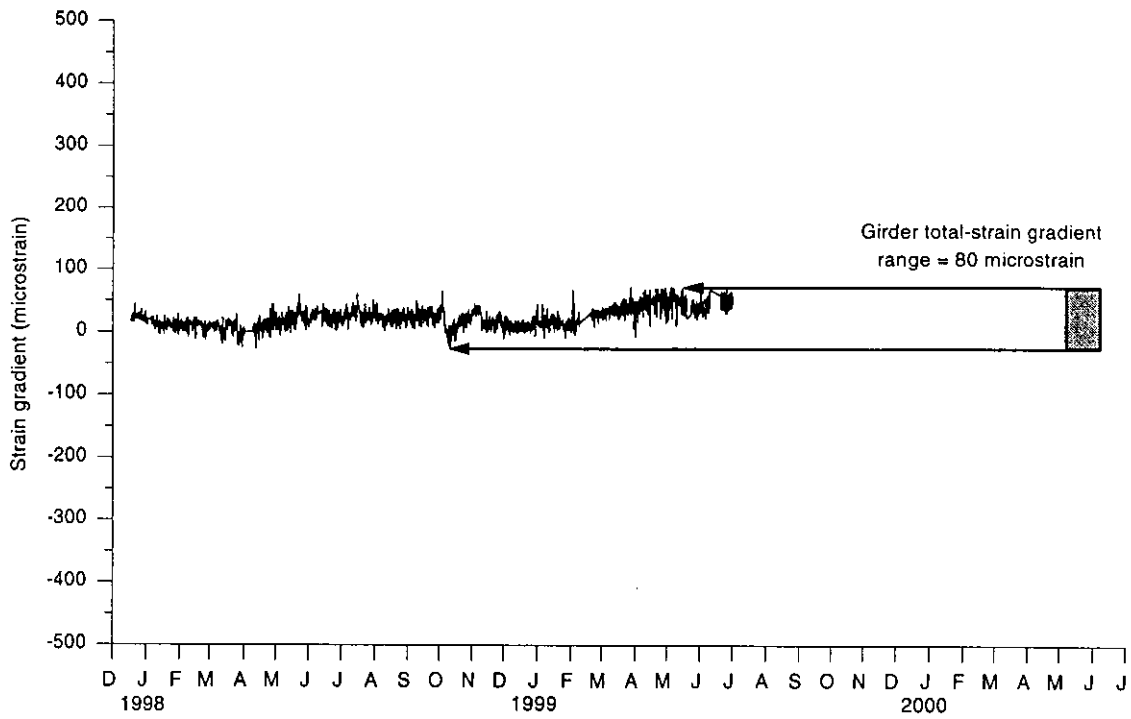
(a) Bending strain at 9 in. below the bottom of the pile cap



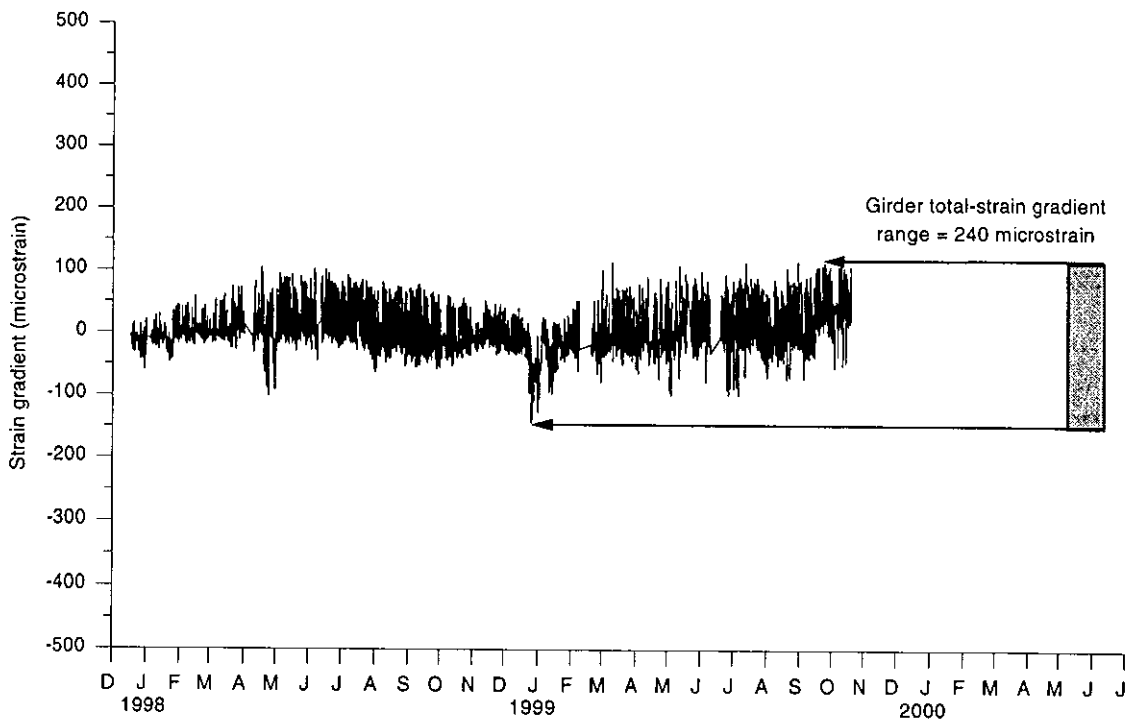
(b) Bending strain at 33 in. below the bottom of the pile cap

Figure 4.31. Y-axis bending strains at two cross sections in the north pile of the east abutment at the Story County Bridge

Figures 4.32 and 4.33 show the difference between the measured, total strain at the top and bottom flanges for a PC girder near an abutment location and near a pier location of the Guthrie County Bridge and Story County Bridge, respectively. The total strain gradient in the girder near an abutment was larger than that near a pier. This finding indicated that less curvature of the PC girders occurred near the piers than near the abutments.

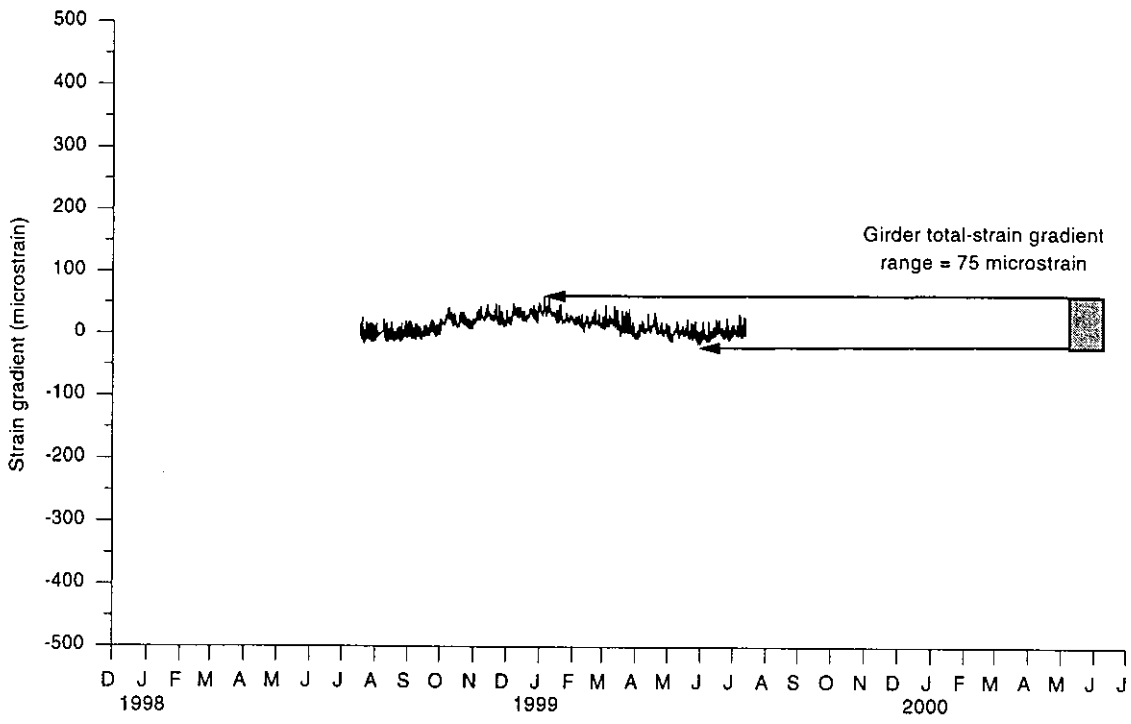


(a) Near the south pier

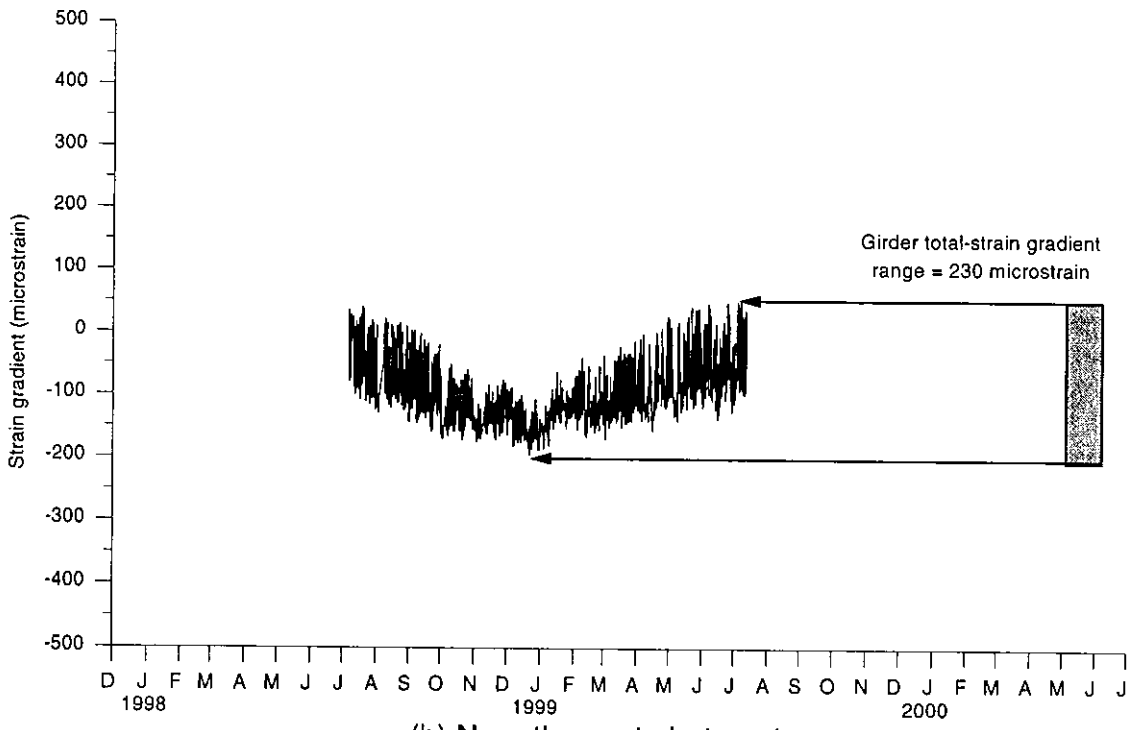


(b) Near the south abutment

Figure 4.32. X-axis total-strain gradient in the east exterior PC girder at the Guthrie County Bridge



(a) Near the east pier



(b) Near the east abutment

Figure 4.33. X-axis total-strain gradient in the north exterior PC girder at the Story County Bridge

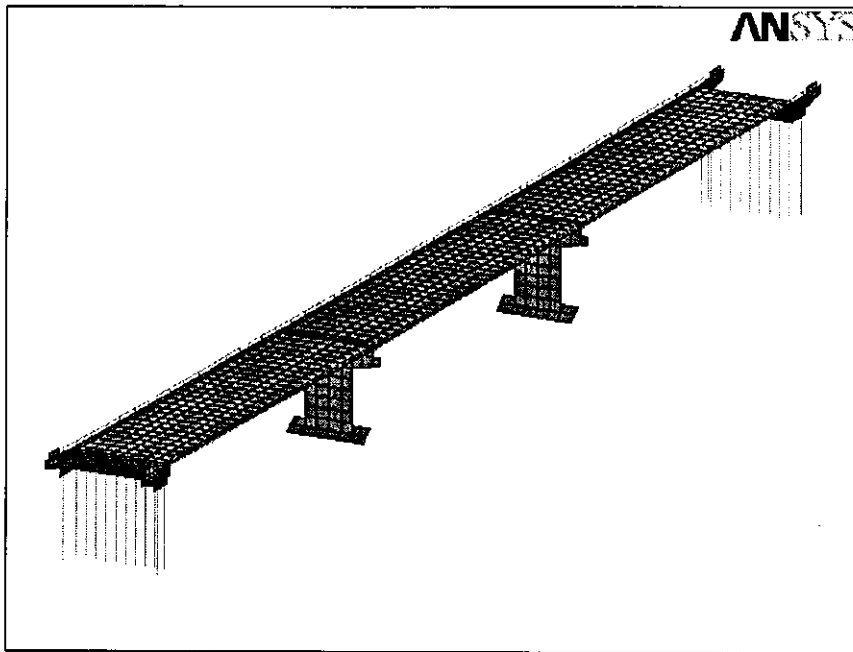
5 DEVELOPMENT OF FINITE ELEMENT BRIDGE MODELS

5.1 Structural model

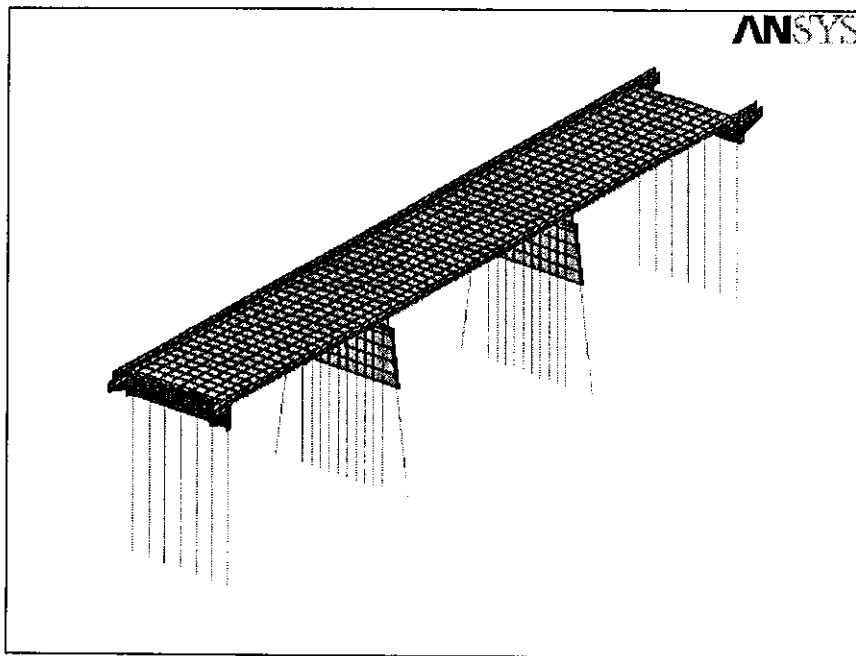
Finite-element models incorporating linear soil and material properties were developed for the Guthrie County Bridge and the Story County Bridge using the ANSYS [31] computer-software program. The Guthrie County Bridge, finite-element model contained 12,244 nodes and 7,762 elements. The Story County Bridge model contained 11,920 nodes and 6,630 elements. The finite-element models contained of shell, beam, spring, truss, and general matrix elements. Undeformed element plots of the finite-element models for the Guthrie County Bridge and Story County Bridge are shown in Figure 5.1. Portions of the finite-element model for the Guthrie County Bridge are shown in Figure 5.2.

Shell elements (ANSYS SHELL93 element) were used to model the RC deck, abutments, and piers. Both quadrilateral shell elements with four corner nodes and four mid-side nodes and triangular shell elements with three corner nodes and three mid-side nodes were used to form the analytical models for the bridges. Each node had three translational and three rotational degrees of freedom. The thickness of each shell element matched the thickness of the particular bridge member in the structure. The aspect ratios of the shell elements were generally less than 2:1. This ratio was less than the 5:1 maximum aspect ratio specified by the 1998 AASHTO LFRD Bridge Design Specifications [32].

PC girders, steel piles, and the Guthrie County Bridge guardrail were modeled using three-dimensional, beam elements (ANSYS BEAM44 element). Two

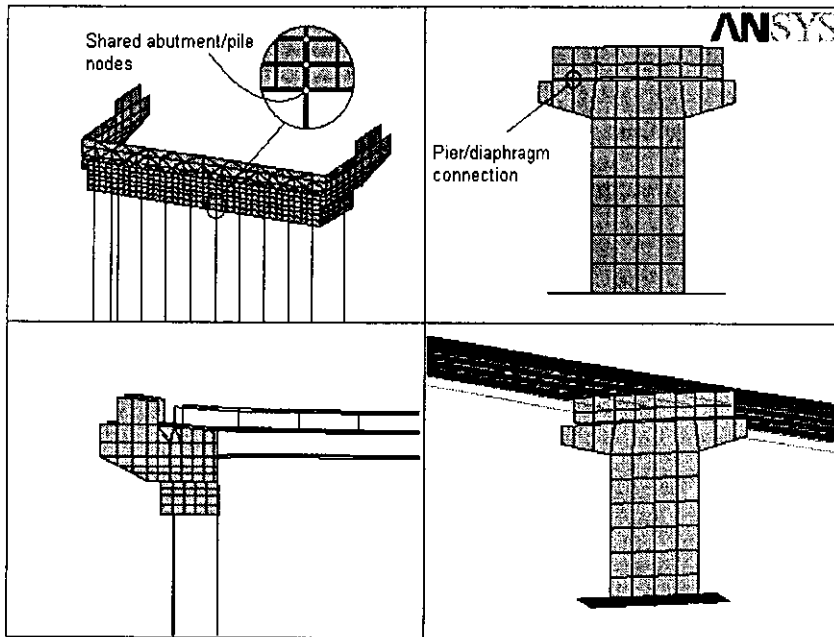


(a) Guthrie County Bridge

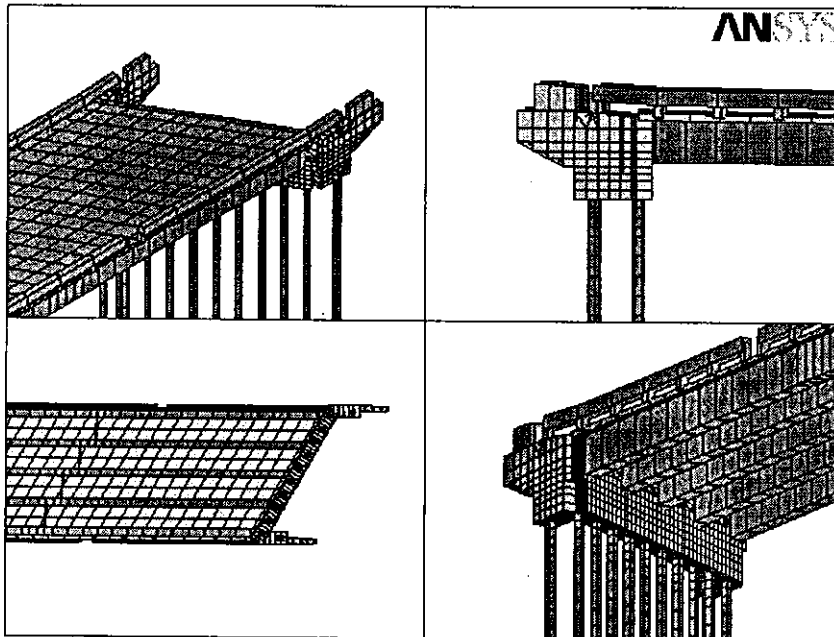


(b) Story County Bridge

Figure 5.1. ANSYS finite element bridge models



(a) Guthrie County Bridge, typical abutment and pier



(b) Guthrie County Bridge model showing elements with thickness

Figure 5.2. Components of the Guthrie County Bridge finite element model

nodes defined the beam element with a third node used to orient the cross-sectional axis. The two end nodes were located at the center of gravity of the beam member. Geometric beam properties including area, depth, and moments of inertia were assigned to the element.

Full-composite action was assumed between the slab and girders. Constraint equations (ANSYS CERIG command) were used to create rigid links that connected the vertically aligned nodes of the slab and girders. These constraint equations coupled all degrees of freedom (translation and rotation) between the slab and girder nodes.

A truss element (ANSYS LINK8 element) was used to model the steel intermediate diaphragms between the PC girders in the Guthrie County Bridge. A truss element is a uniaxial tension-compression element with three translational degrees of freedom at both of its nodes. The connection of the diaphragm to the web of the girder was assumed to be a pinned connection. Shell elements were used to model the RC intermediate diaphragms in the Story County Bridge.

Full-moment transfer was assumed between the piles and the RC abutment in which they are embedded. The abutment piles are embedded about 36 in. (910 mm) into the pile caps at both bridges. As shown in Figure 5.2(a), the beam nodes share the corner nodes of the shell elements at the location of the embedded pile, which creates a rigid connection between the elements. The piles in the Story County Bridge piers are embedded within the entire height of the piers.

The north pier at the Guthrie County Bridge is classified as a fixed pier. Between the girders of the fixed piers, a keyway is formed into the pier cap with the

concrete diaphragm bearing on expansion material placed on the bottom and along the sides of the keyway, as shown in Figure 5.3(a). The connection between the pier cap and the RC diaphragm is not perfectly fixed, since small relative longitudinal movements can occur by compressing the expansion pads on the sides of the keyways. A general matrix element (MATRIX27) is developed using structural analysis matrix methods [33] to model the connection of the concrete diaphragm and the pier cap on which the superstructure bears. The general stiffness element incorporates the translational and rotational stiffness of the connection and allows for small relative movements.

The south pier of the Guthrie County Bridge is an expansion pier with the PC girders bearing on 3.75 in. (95mm)-thick neoprene pads, as shown in Figure 5.3(b). A connection does not exist between the RC diaphragm and the pier cap. The low shear stiffness ($G = 0.10$ ksi or 0.69 MPa) of the thick neoprene pad provides minimal resistance to the translation of the superstructure over the piers, creating a connection similar to a roller support. Linear spring elements (COMBIN14) represented the vertical compression stiffness and the shear stiffness of the bearing pads that support the girders at the piers. Typical properties of neoprene pads were obtained from Lee [34].

The details of both diaphragm/pier connections at the Story County Bridge are the similar to the fixed pier at the Guthrie County Bridge. Because the relative movements measured at the fixed pier on the Guthrie County Bridge were very

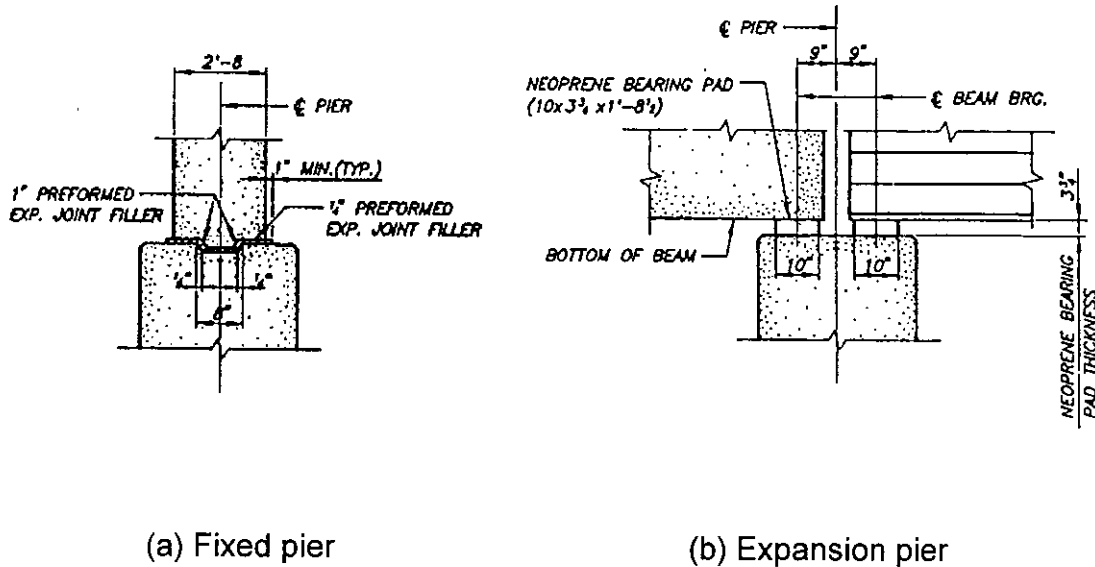


Figure 5.3. Typical pier/pier diaphragm connection details [35]

small, the relative movements at the piers of the Story County Bridge were neglected. The pier and pier cap elements had common nodes at the bearing point.

The pier footings for the Guthrie County Bridge are founded on shale. The normal foundation stiffness was assumed to be 100 ton/ft^3 (31400 kN/m^3) and the frictional stiffness is 50 ton/ft^3 (15700 kN/m^3), as recommended by Barkan [36].

A summary of the bridge elements and the material properties for the Guthrie County and Story County Bridges is given in Table 5.1. Material properties are based on the design plans for the respective bridges. Values of the α -coefficient are based on laboratory tests that were conducted by Ng [37] at Iowa State University.

Table 5.1. Properties of the modeled bridges

	GUTHRIE COUNTY BRIDGE	STORY COUNTY BRIDGE
CAST-IN-PLACE CONCRETE		
Compressive strength, f'_c (ksi)	3.5	3.5
Modulus of elasticity, E (ksi)	3400	3400
Shear modulus, G (ksi)	1420	1420
Poisson's ratio, μ	0.20	0.20
Dry coefficient of thermal expansion and contraction, α (in./in./°F)	5.8×10^{-6}	4.8×10^{-6}
Maximum coefficient of thermal expansion and contraction, α (in./in./°F)	6.4×10^{-6}	5.3×10^{-6}
PRESTRESSED CONCRETE		
Compressive strength, f'_c (ksi)	6.0	5.0
Modulus of elasticity, E (ksi)	4400	4000
Shear modulus, G (ksi)	1710	1680
Poisson's ratio, μ	0.20	0.20
Dry coefficient of thermal expansion and contraction, α (in./in./°F)	4.3×10^{-6}	4.3×10^{-6}
Maximum coefficient of thermal expansion and contraction, α (in./in./°F)	4.7×10^{-6}	4.7×10^{-6}
STEEL SECTIONS		
Coefficient of thermal expansion, α (in./in./°F)	6.5×10^{-6}	6.5×10^{-6}

5.2 Pile-soil model

The Winkler soil model [4] was used for the analysis of the soil/pile interaction, which assumes that the soil can be represented as a series of vertical and lateral springs along the length of the pile and an end bearing point spring. A discussion of the Winkler soil model is described by Greimann, et al., which is reproduced in Appendix C. Linear spring elements (ANSYS COMBIN14 element) were used to model the pile/soil interaction in the finite-element models.

The Guthrie County Bridge and Story County Bridge, finite-element models incorporated the linear, Winkler, pile, soil model based on the initial stiffness of the soil, k_n . Spring elements representing the two normal stiffnesses (normal to flange and normal to web), vertical skin friction stiffness, and the end bearing stiffness were applied at each pile element node.

Soil parameters were based on the soil-boring data that was presented in the construction plans for both of the bridges. Soil borings for the abutment locations at the Guthrie County Bridge are shown in Figure 5.4. Soil borings for the abutment and pier locations at the Story County Bridge are shown in Figure 5.5. Soil stiffness is calculated based on the equations presented in Tables C.1 through C.3 in Appendix C. The boring data was used to classify soil by type (clay or sand) and by standard penetration blow counts (N) to determine approximate soil parameters from Tables C.4 or C.5 in Appendix C. Effective soil unit weights were estimated by considering the moisture conditions at the bridge sites. At the Guthrie County Bridge, saturated soil conditions were encountered at the north abutment, and dry

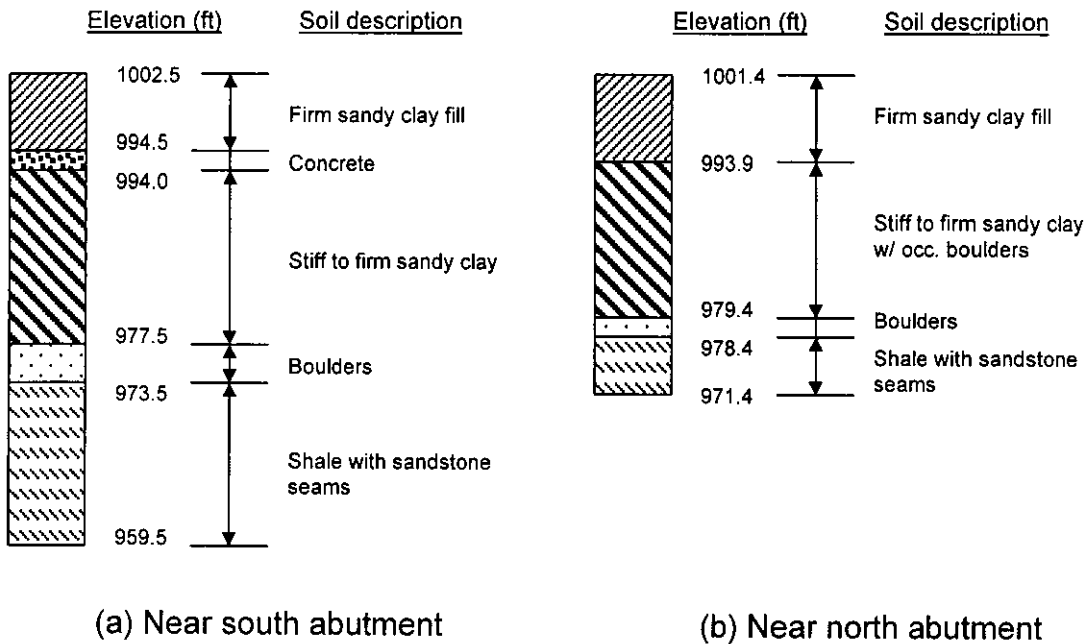
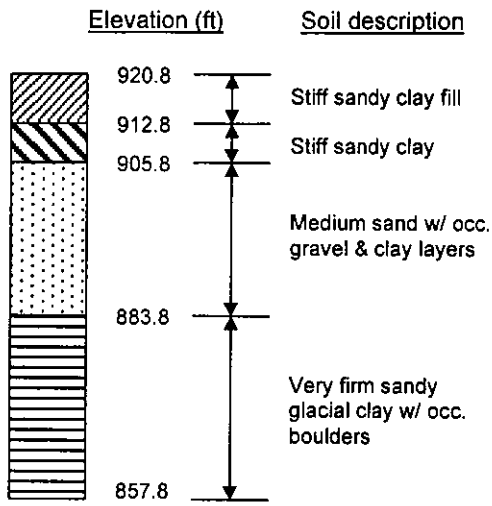


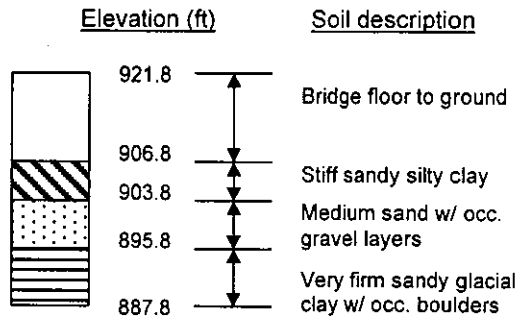
Figure 5.4. Soil borings at the Guthrie County Bridge (not to scale)

soil conditions were encountered at the south abutment. Soil in the berm adjacent to the abutments of the Story County Bridge was dry when first excavated for installing strain gages on the selected piles. Over the monitoring period, the soil near the north pile of the east abutment became saturated. Soil near the other monitored piles remained dry or became slightly damp. Soil for the Story County Bridge, finite-element model was assumed to be dry at all locations. A pile-soil stiffness distribution is given in Figure 5.6 for a pile in the south abutment at the Guthrie County Bridge, showing the lateral, soil-spring stiffness (normal to flange) at the node locations along the depth of a pile.

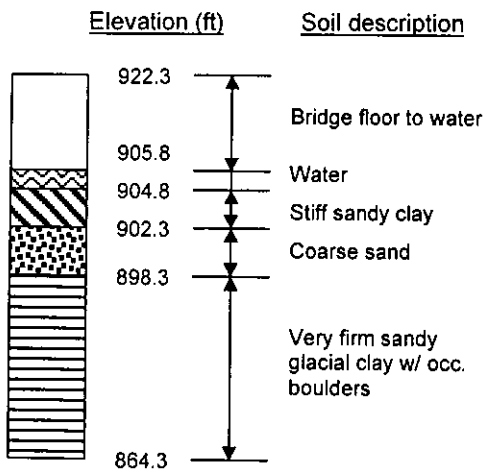
For the Guthrie County Bridge, the piles were driven through an 8-ft (2440 mm) deep, 16-in. (410 mm) prebored hole. A bentonite slurry filled the prebored



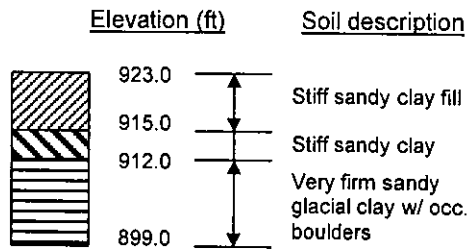
(a) Near west abutment



(b) Near west pier



(c) Near east pier



(d) Near east abutment

Figure 5.5. Soil borings at the Story County Bridge (not to scale)

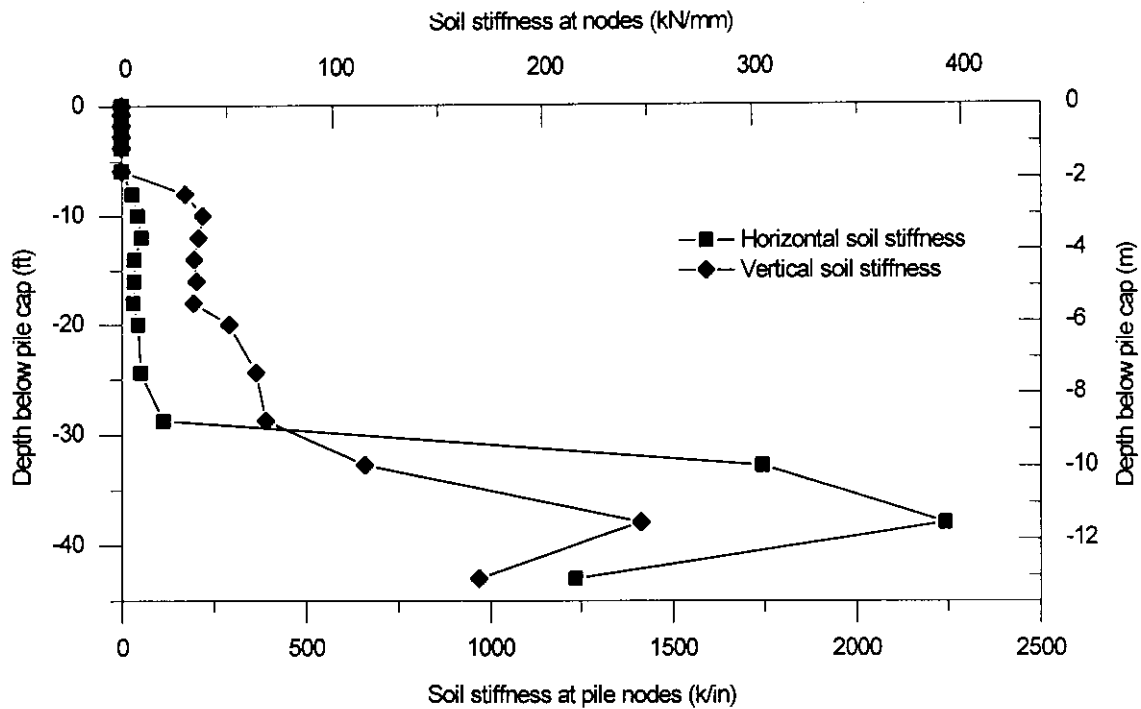


Figure 5.6. Pile soil stiffness distribution for the south center pile at the Guthrie County Bridge

holes. Bentonite slurry is a soft mixture with water being the majority of its composition [37]. During the excavation of the piles for installing the strain gages, the researchers noted that the bentonite had a consistency of a pliable, clay-type soil. The stiffness of the bentonite slurry was considered minimal; therefore, the lateral and vertical stiffness of this material was neglected in the Guthrie County Bridge, finite-element model.

The abutment piles at the Story County Bridge were driven in similar prebored holes that did not contain a bentonite slurry. An uncompacted loose sand was placed in the prebored holes. Loose sand properties were used for the region of the prebored holes for the Story County Bridge, finite-element model.

5.3 Abutment backfill model

Linear-spring elements (ANSYS COMBIN14 element) were also used to model the soil backfill behind the abutments. At each discrete point where the soil-interface conditions between the bridge structure and soil are modeled, one spring was oriented normal to the bridge member and two springs were oriented tangential to the bridge member surface, as shown in Figure 5.7. The tangential springs were orthogonal (horizontal and vertical) to each other to represent frictional forces induced by the soil interaction with the abutment surface.

Other researchers have presented design curves to describe the lateral soil pressure behind rigid retaining walls that is induced by wall movement towards the

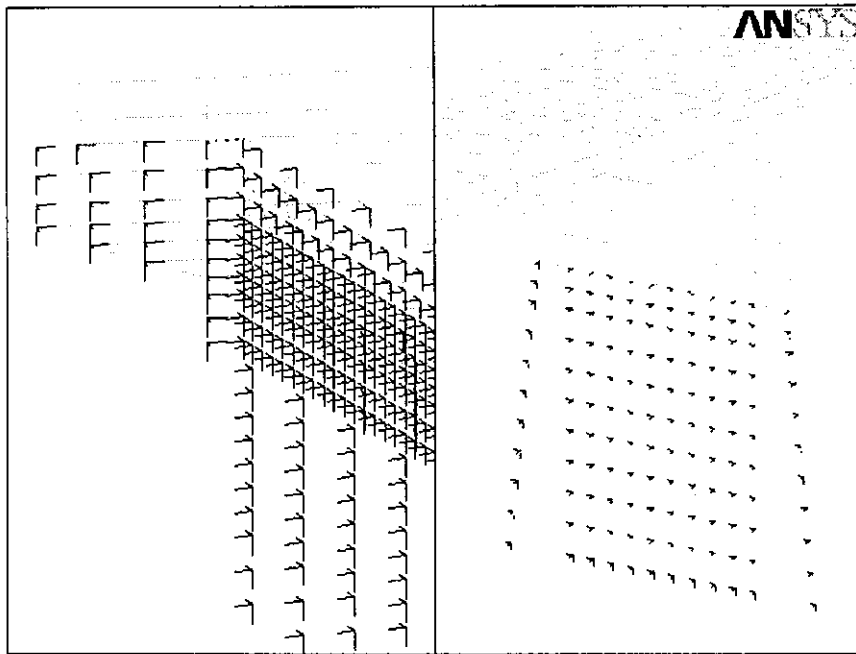


Figure 5.7. Typical soil springs on finite element models

backfill (passive movement) and away from the backfill (active movement) [14; 38-41]. Effective soil pressures induced by wall movements can be expressed in terms of an earth-pressure coefficient, k :

$$k = \sigma'_{horizontal} / \sigma'_{vertical} \quad (5.3)$$

where,

$\sigma'_{horizontal}$ = effective horizontal stress in the soil

$\sigma'_{vertical} = \gamma'z$ = effective vertical stress in the soil

γ' = effective unit weight of the soil

z = soil depth

The Rankine theory [42] provides a simple determination of the earth pressure coefficients neglecting wall friction. For a wall at rest, Rankine's coefficient of earth pressure at rest is:

$$k_o = 1 - \sin \phi \quad (5.4)$$

where, ϕ is the angle of internal friction of the soil. For a rigid wall pushed into a soil mass, Rankine's passive earth pressure coefficient is:

$$k_{passive} = \tan^2 (45^\circ + \phi / 2) \quad (5.5)$$

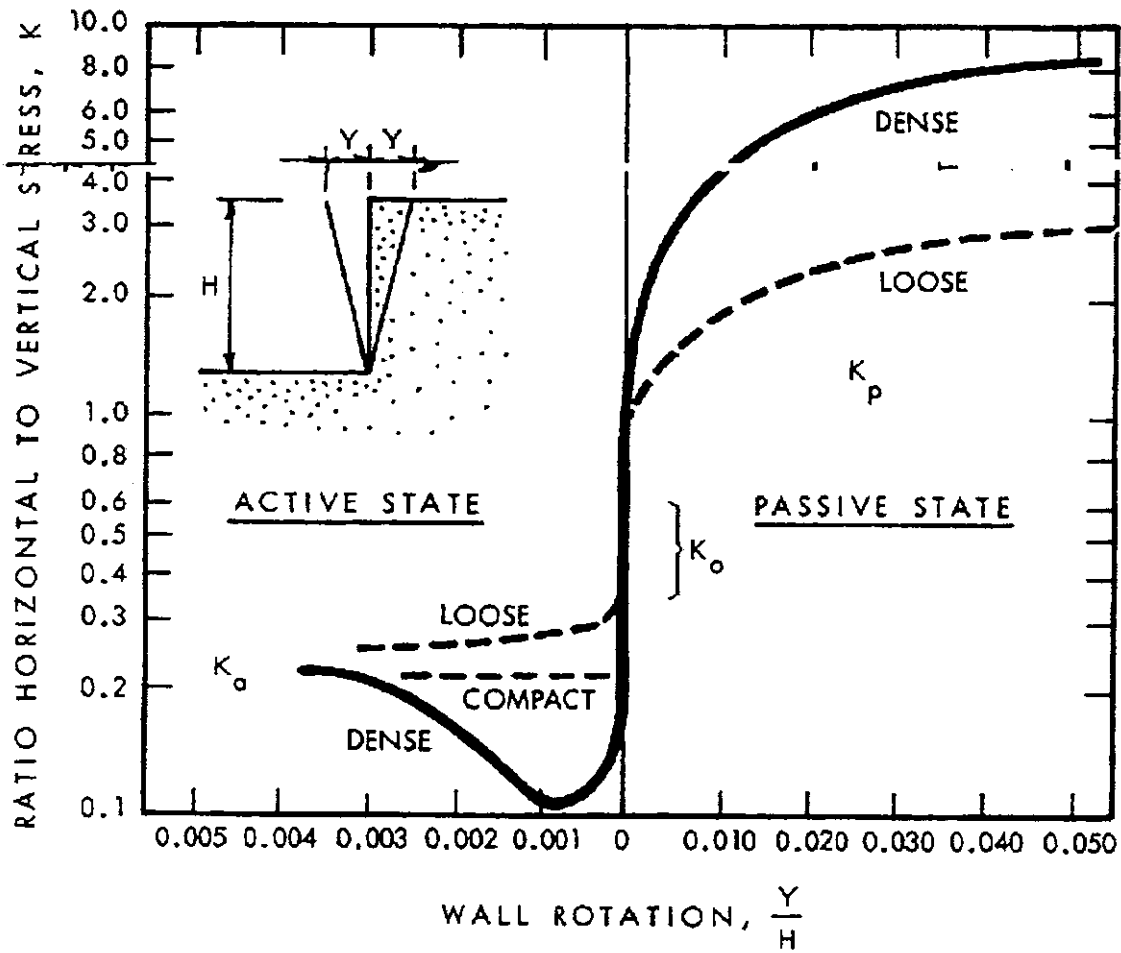
As a wall is moved away from the soil, Rankine's active earth pressure coefficient is:

$$k_{active} = \tan^2(45^\circ - \phi/2) \quad (5.6)$$

Design curves presented by the Canadian Foundation Engineering Manual [39], Husain and Bagnaroil [40], and Clough and Duncan [14] are shown in Figure 5.8. The Canadian Foundation Engineering Manual (1992) contains design curves similar to those proposed in NAVFAC DM-7 [41] that include wall friction effects. The National Cooperative Highway Research Program (NCHRP) [38] adopted design curves for cohesionless soil based on the work of Clough and Duncan's recommendations.

Research by Ting and Faraji [43] compared numerous design curves with experimental studies conducted for the pile-to-soil interaction. Ting and Faraji determined that the NCHRP design curve underestimates ultimate passive pressure and overestimates initial lateral stiffness for dense and medium dense sand. The Canadian Foundation Engineering Manual design curve more closely matches the experimental data for dense and medium sands. Both design curves provide an accurate representation of the experimental data for loose backfill.

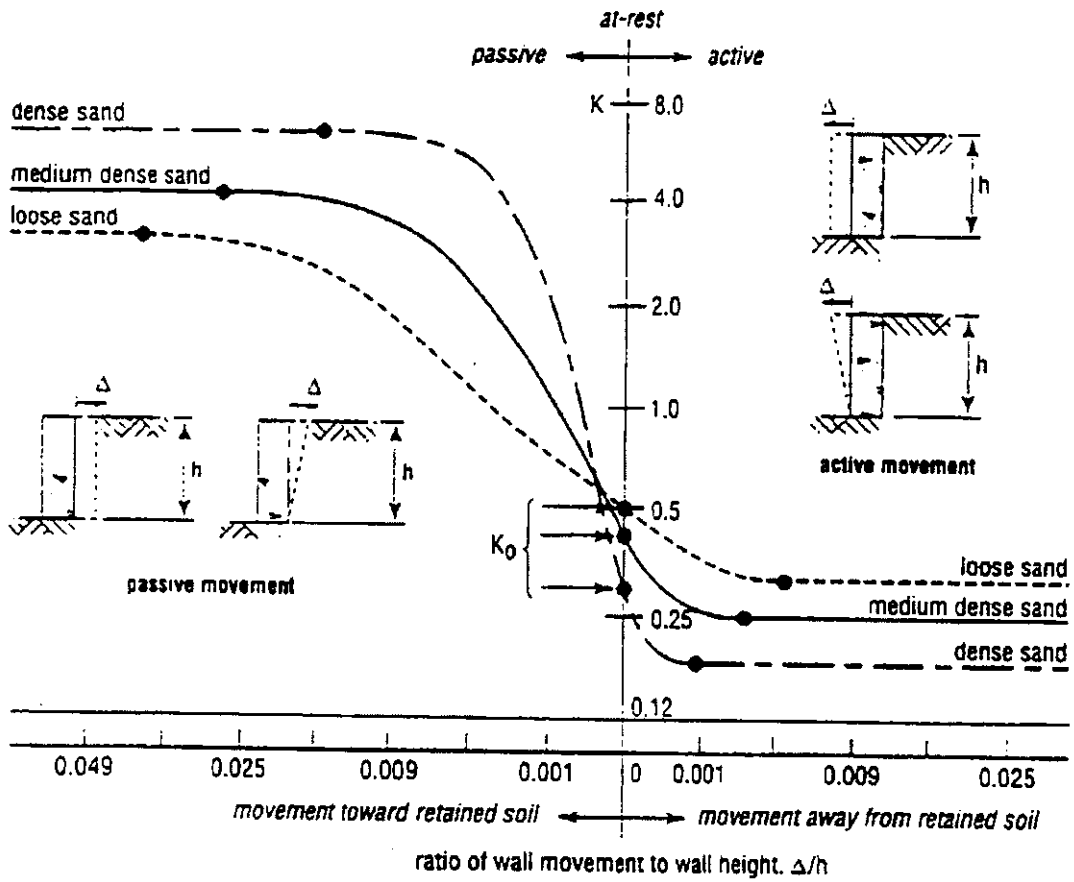
Ting and Faraji determined that the rotation of a wall about its base (top of wall displaces further into the soil than in a pure translational case) creates higher pressure in the top portion of the wall with slightly lower pressures at the bottom of the wall. Ting and Faraji stated that if a triangular soil pressure distribution is



(a) Canadian Foundation Engineering Manual [39]

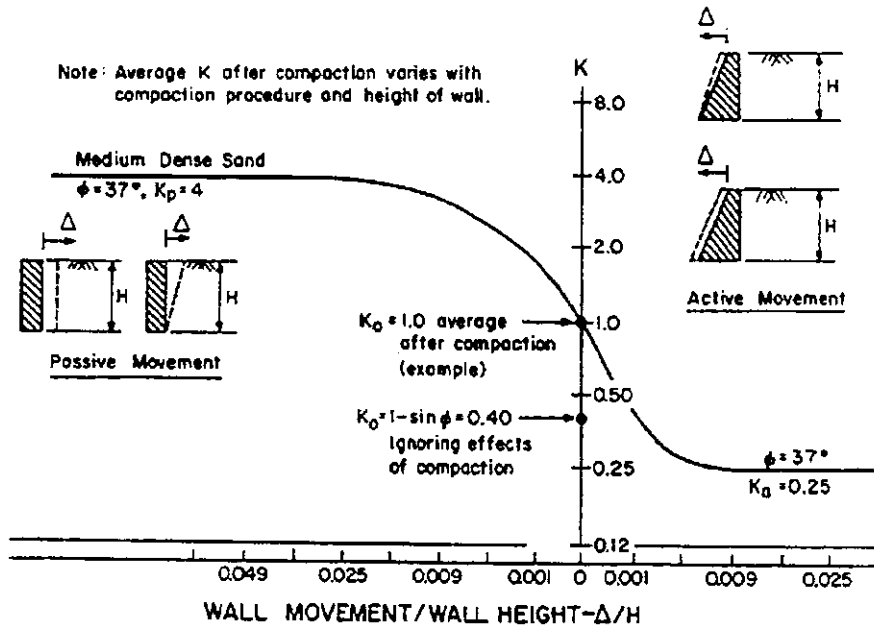
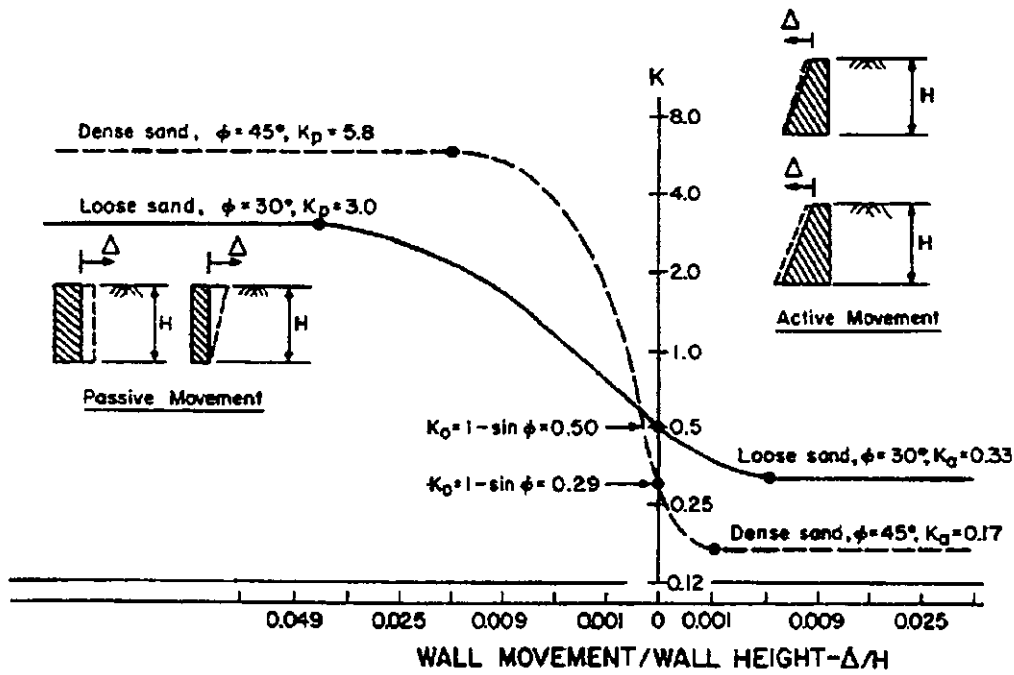
Figure 5.8. Wall backfill stiffness design curves

Various earth pressures



(b) Husain and Bagnaroil [40]

Figure 5.8. (continued)



(c) Clough and Duncan [14]

Figure 5.8. (continued)

distribution along the height of a wall will not create a significant error when determining the total soil pressure on the wall. Therefore, linear springs with a triangular stress distribution were used to approximate the force-deflection condition of the granular backfill.

Spring stiffness for the finite-element models were based on passive-soil stiffness to represent the effect of the abutment pushing into the backfill during bridge expansion. The initial slope of the passive, force-deflection curves presented in Figure 5.8 were used to represent the backfill stiffness behind the abutments in the finite-element models. The maximum passive force, $F_{passive}$, on an abutment finite element, with an area $A_{element}$, at a given depth is:

$$F_{passive} = (k_{passive} - k_o) \sigma'_{vertical} A_{element} \quad (5.7)$$

where, the effective vertical stress was determined at the depth below the surface of the element centroid. The total spring stiffness, K_{spring} , per wall element is:

$$K_{spring} = F_{passive} / \Delta_{passive} \quad (5.8)$$

in which, $\Delta_{passive}$ is the displacement required to reach the maximum passive-soil pressure. Nodal spring stiffnesses were computed by evenly distributing K_{spring} to each of the corner nodes of the abutment wall element.

The backfill soil behind the abutments is specified as a compacted granular soil. Loose, medium, and dense sand backfill properties are shown in Table 5.2. Approximate displacements required to reach active and passive-soil pressure conditions are shown in Table 5.3. The frictional stiffness of the abutment backfill was initially assumed to be one-half of the normal stiffness, as recommended by Barkan [36]. The frictional stiffness was adjusted if this initial value did not produce adequate transverse abutment displacement results. Both bridge finite-element models are calibrated by adjusting the backfill stiffness until the finite-element model displacements match the experimental displacements, as will be discussed in Chapters 6 and 7.

Table 5.2. Typical properties for cohesionless sands [43]

TYPE OF BACKFILL	ANGLE OF INTERNAL FRICTION, ϕ (degrees)	TYPICAL DRY UNIT WEIGHT, γ_{dry} (lb/ft ³)	TYPICAL SATURATED EFFECTIVE UNIT WEIGHT, γ'_{sat} (lb/ft ³)
Loose sand	30	90-125	55-65
Medium sand	35	110-130	60-70
Dense sand	40	110-140	65-80

Table 5.3. Approximate horizontal wall displacement to activate passive and active earth pressure [14]

TYPE OF BACKFILL	DISPL. TO REACH ACTIVE PRESSURE, Δ_{active}/H	DISPL. TO REACH PASSIVE PRESSURE, $\Delta_{passive}/H$
Loose sand	0.004	0.04
Medium-dense sand	0.002	0.02
Dense sand	0.001	0.01

Note: H = height of wall

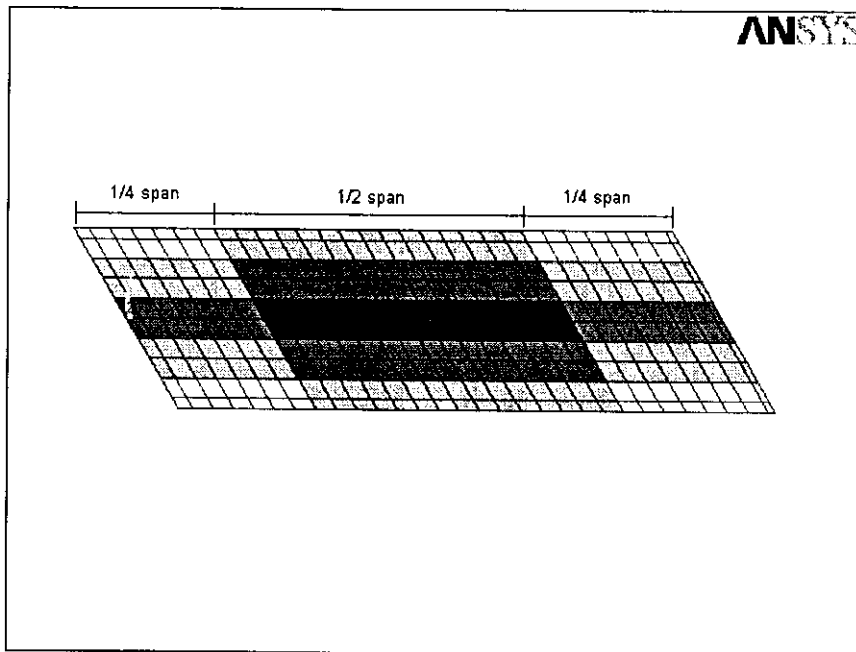
5.4 Applied temperature distribution

5.4.1 Spatial distribution

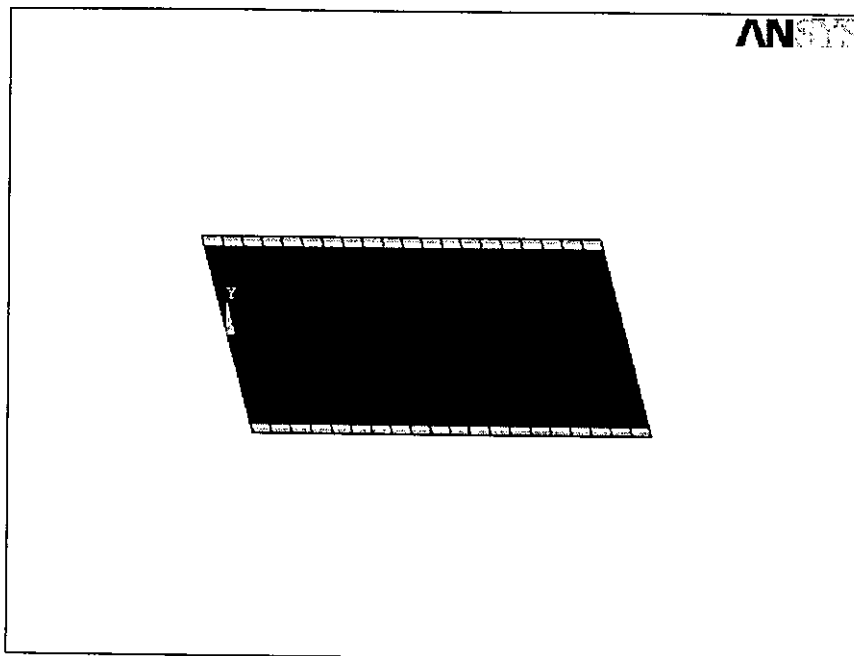
A primary emphasis of the project was to determine effects of thermal loads on abutment piles in integral-abutment bridges. Analysis of the experimental temperature data for the Guthrie County Bridge and Story County Bridge was described in Section 4.2. The experimental data were used to estimate longitudinal, transverse, and vertical temperature distributions that were applied to the finite element models for a given point in time.

For purposes of thermal loading, each span at the Guthrie County Bridge was divided into fifteen temperature regions, as shown in Figure 5.9(a). The temperature regions were selected based on the location of the thermocouples in the most intensely instrumented south span. The width of the bridge was divided into five regions corresponding to the five girders. Since thermocouples were not installed in the second and fourth PC girders, an average temperature distribution of the adjacent girders was used for these girders. The limited amount of thermocouples in the middle and north spans produced temperature readings that were similar to those at similar locations in the south span; therefore, the temperature distribution of these spans was assumed to be the same as that of the south span. Temperatures recorded by the thermocouples nearest to the abutment are also used for the locations nearest to the pier supports, since both of these locations are at regions of large thermal mass.

For a given point in time, a vertical temperature gradient through the slab thickness and girder depth was applied in each of the fifteen regions in the finite-



(a) Guthrie County Bridge



(b) Story County Bridge

Figure 5.9. Superstructure temperature regions

element model for the Guthrie County Bridge. The interpolated vertical temperature gradients were based on the experimental results that were described in Section 4.2.2. A bi-linear vertical temperature distribution was applied as a loading condition to the finite-element models of the bridges defined by three temperatures at specific points along the depth of the superstructure: top of slab, bottom of slab/top of girder, and bottom of girder.

A simpler temperature distribution was applied to the superstructure of the Story County Bridge, finite-element model. As discussed in Section 4.2.4, longitudinal temperature variations were not significant and were not incorporated into the applied temperature loading. The temperature distribution was relatively constant over the width of the Story County Bridge, except under the solid guardrail as shown in Figure 4.16. Figure 5.9(b) shows the applied slab temperature distribution in one span of the Story County Bridge.

A thermocouple was embedded in the abutment to estimate the temperature change of the exposed face of the abutment. The back face of the abutment was assumed to have a negligible change in temperature at a few feet below the surface. Temperatures for the portion of the piles exposed in the excavation were based on thermocouples located at the piles. Pier temperatures were estimated based on the average concrete temperature of the bridge.

5.4.2 Time variations

The range in the experimentally measured bridge member temperatures between the times of the coldest and hottest average bridge temperature was applied to the respective analytical bridge models. Bridge member strain

comparisons between the analytical models and the experimental data were made only when a given gage produced reliable data over at least one cold to hot temperature cycle. Many strain gages failed before a complete temperature cycle was achieved, resulting in incomplete temperature ranges of reliable data as discussed in Section 4.1.

6 ANALYTICAL STUDY AND INTERPRETATION OF EXPERIMENTAL RESULTS FOR THE GUTHRIE COUNTY BRIDGE

6.1 Bridge displacement

Thermal bridge length changes are investigated using the Guthrie County Bridge finite-element model. The magnitude of the thermal length change is a function of the bridge length, change in the bridge temperature, α -coefficient of the bridge members, and the soil restraining forces.

Magnitudes for the α -coefficients and other material properties for the Guthrie County Bridge are provided in Table 5.1. The applied temperature distribution on the bridge structure was discussed in Section 5.4 of this report. The temperature ranges applied to the analytical models were for a temperature rise from the coldest to the hottest day.

Lateral backfill stiffness behind the abutment is the major factor in restraining the longitudinal displacement of the abutments. The lateral soil stiffness adjacent to the piles affects the flexural-bending forces induced in the pile, but has a negligible effect on the longitudinal abutment displacement [43]. The abutment backfill material was only specified in the construction plans as a "compacted granular backfill". Compaction and moisture conditions were not prescribed, so that the in-situ properties of the backfill were not known. To study the bridge behavior, the finite-element model was calibrated by adjusting the soil properties until the abutment displacements approximately matched the corresponding experimental longitudinal and transverse abutment displacements.

The initial slope of the Clough and Duncan design curves (Figure 5.8(c)) was used to model the lateral stiffness of the abutment backfill. Only linear soil springs were used in the finite-element models. The non-dimensional initial slope, S , of the design curves for the lateral backfill stiffness is approximately:

$$S = \frac{(k_{\text{passive}} - k_o)}{\Delta/H} \quad (6.1)$$

where, Rankine's passive soil-pressure coefficient, k_{passive} , and the corresponding ratio of wall displacement to wall height, Δ/H , were chosen along the initial slope of the backfill stiffness design curve. Again, the reader is reminded that the model does not account for the nonlinear characteristics of the backfill. A summary of the approximate initial slopes for the three classifications of granular backfill is provided in Table 6.1.

The model calibration involved matching the analytical and experimental abutment displacement data for the time period with the largest average bridge temperature range. The applied temperatures corresponded to the temperature change from the time of the coldest average bridge temperature (January 5, 1999,

Table 6.1. Approximate initial slopes for lateral backfill stiffness based on the Clough and Duncan Design Curves in Figure 5.8(c)

TYPE OF BACKFILL	INITIAL SLOPE, S
Loose sand	130
Medium-dense sand	400
Dense sand	2000

4:00 a.m.) to the time of the hottest average bridge temperature (July 20, 1998, 8:00 p.m.). The maximum, experimental, average, bridge temperature range was 113°F (62.8°C).

6.1.1 Longitudinal abutment displacements and change in bridge length

The abutment backfill stiffness was adjusted until the analytical longitudinal abutment displacements at the mid-width of the north and south abutment and the south abutment transverse displacements were within an acceptable degree of accuracy. As discussed in Section 4.3.1, there was a significant difference in the magnitude of the longitudinal displacements of the north and south abutments at the Guthrie County Bridge. The longitudinal displacement of the north abutment was approximately twice that of the south abutment. Therefore, the lateral backfill stiffness of the south abutment must be greater than that of the north abutment. There was also a significant amount of water in the soil at the north abutment. The abutment backfill was considered saturated behind the north abutment and dry behind the south abutment.

If the dry condition for the α -coefficients of the concrete is applied to evaluate temperature effects on bridge length, the actual bridge length change will be underestimated. In reality, the α -coefficients of the concrete members is between that for the 100% dry and 100% saturated conditions. The Guthrie model used the maximum values for the α -coefficients of the concrete.

The analytical models of the Guthrie County Bridge that are based on the calibrated finite-element model are referred to as the Guthrie, Series-A models. (A second series of Guthrie County Bridge, finite-element models will be introduced

later in this chapter.) The analytical model, whose predicted abutment displacements closely matched the corresponding experimental displacements, is called the Guthrie, Series-A, Best-Soil model. For this model, the initial slope for the lateral stiffness relationship of the south abutment backfill, S_{south} , was equal to 520, which is slightly greater than the initial slope for a dry granular medium-dense soil as defined by the Clough and Duncan design curves (Figure 5.8(c)). The initial slope value of the north abutment backfill, S_{north} , was equal to 380 for a saturated granular soil, which is approximately equal to that for a medium-dense soil.

The analytical abutment displacements were compared with the experimental abutment displacements to determine if the soil was adequately represented in the calibrated finite-element model. The Guthrie, Series-A, Best-Soil model had displacement errors of less than 2% compared to the experimentally measured longitudinal displacements at the mid-width of the north and south abutments. The analytical transverse displacements were within 10% of the experimental measurements at the east and west corners of the south abutment.

To indicate sensitivity of the abutment displacements to the lateral soil stiffness, upper and lower-bound Guthrie, Series-A models were formulated by varying the abutment backfill stiffness and the stiffness of the soil adjacent to the piles. The upper and lower-bound models incorporated a fixed change in soil stiffness adjacent to the piles at both abutments and the stiffness of backfill behind the south abutment. The lateral stiffness of the backfill behind the north abutment was adjusted so that the experimental north-to-south longitudinal abutment

displacement ratio matched the ratio of the experimental differential abutment displacement.

Four finite-element bounding models with limits placed on the lateral stiffness of the soil behind the abutment and adjacent to the abutment piles were investigated: (1) lower-bound backfill/lower-bound pile-soil, (2) upper-bound backfill/upper-bound pile-soil, (3) upper-bound backfill/lower-bound pile-soil, and (4) lower-bound backfill/upper-bound pile-soil. A 50% change in the soil stiffness was used for the bounding models. The lower-bound backfill stiffness is approximately midway between the stiffness of the loose and medium-dense soils. The upper-bound backfill stiffness is approximately one-quarter of the way from the stiffness of the medium-dense to the stiffness of the dense backfill. A summary of the backfill stiffness and the change in bridge length for the Guthrie, Series-A models is provided in Table 6.2.

Table 6.2. Change in bridge length predicted by the Guthrie, Series-A models

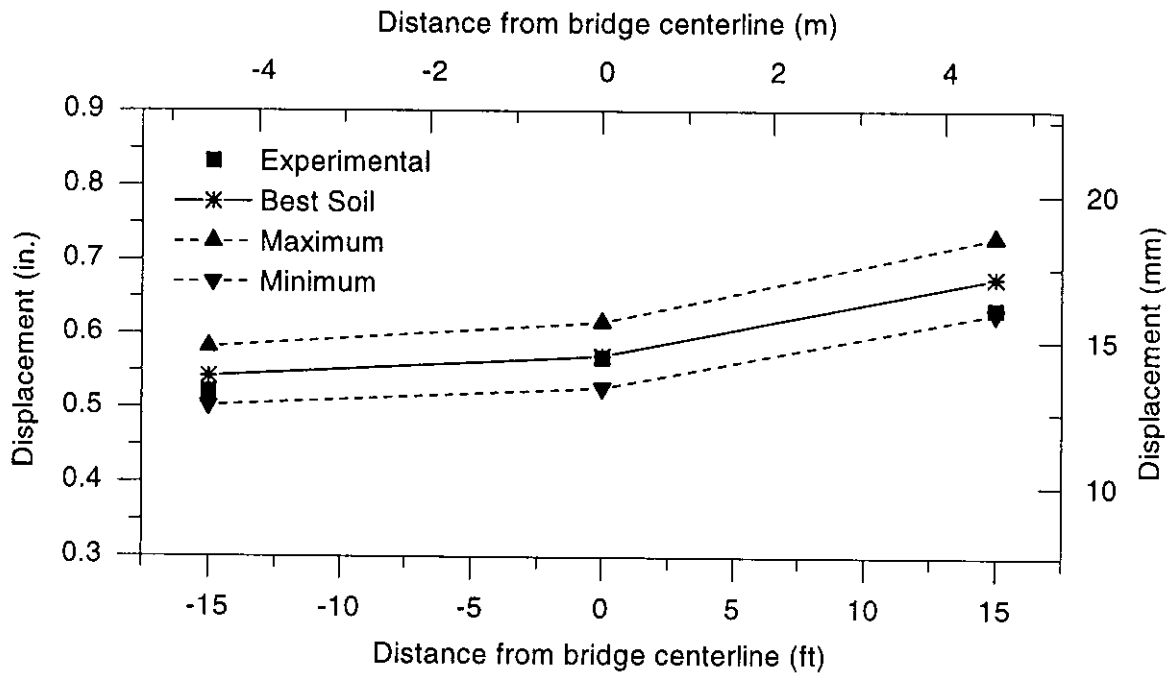
GUTHRIE, SERIES-A MODEL	S_{south}	S_{north}	CHANGE IN BRIDGE LENGTH (in.)	CHANGE FROM BEST-SOIL MODEL (%)
Best-Soil	520	380	1.772	----
Lower-bound backfill/lower-bound pile-soil	261	154	1.918	+8.2
Upper-bound backfill/upper-bound pile-soil	783	607	1.647	-7.1
Upper-bound backfill/lower-bound pile-soil	783	637	1.642	-7.3
Lower-bound backfill/upper-bound pile-soil	261	134	1.911	+7.8
Experimental	----	----	1.767	----

A comparison of the longitudinal abutment displacements across the width of the abutment is shown in Figure 6.1. Longitudinal displacements were experimentally measured at three locations across the width of the south abutment, but only at the mid-width location of the north abutment. The analytical predictions for the plan-view rotations of the south abutment occurred in the same direction as that measured in the field. The longitudinal abutment displacement was larger at the acute-angle corner than at the obtuse-angle corner of the bridge deck. The largest abutment displacement that was predicted by the four bound models is referred to as the maximum in Figure 6.1. The maximum displacement occurred under the loosest soil conditions (lower-bound backfill/lower-bound pile-soil). Conversely, the minimum abutment displacement shown in Figure 6.1 occurred under the stiffest soil conditions (upper-bound backfill/upper-bound pile-soil).

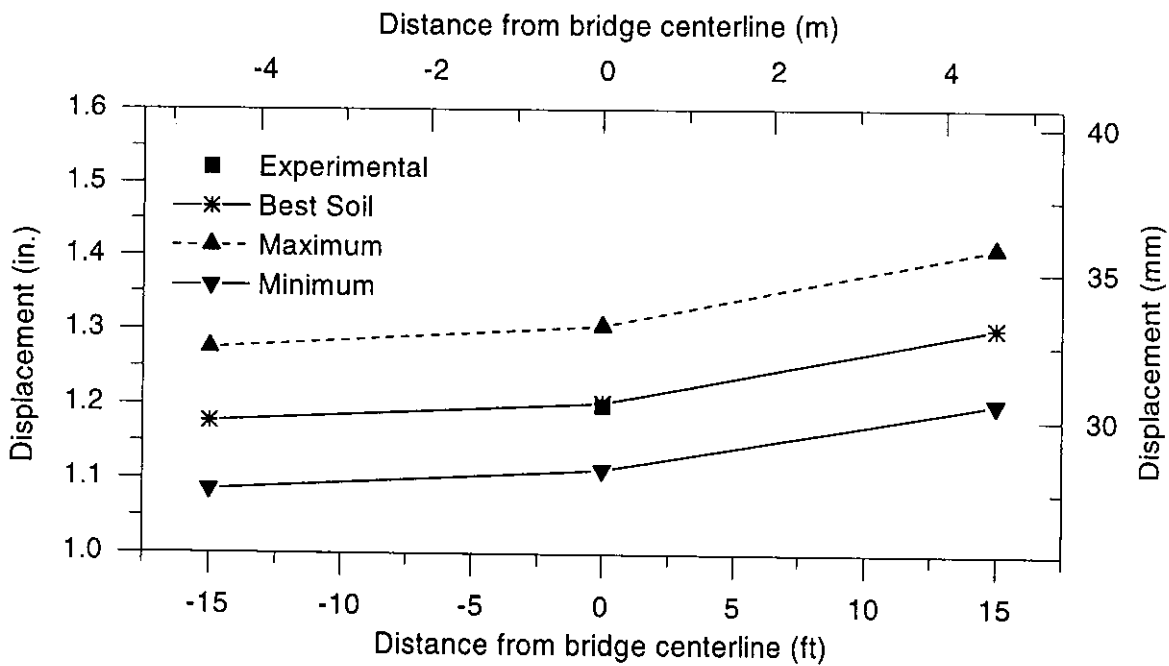
6.1.2 Transverse abutment displacement

Transverse abutment displacements occur in skew bridges due to the component of the passive-soil pressure that acts normal to the abutment backwall. The resulting force acts perpendicular to the longitudinal axis of the bridge and pushes the abutment in the direction of the acute-angle corner of the bridge deck. The thermal expansion and contraction of the abutment also causes transverse movements of an abutment. Thermal expansion of the abutment is additive with the transverse displacement at the acute-angle corner of the bridge deck.

The stiffness of the tangential soil-springs on the abutment back face was equal to a percentage of the normal backfill spring stiffness, which was adjusted to



(a) South abutment



(b) North abutment

Figure 6.1. Comparison of the longitudinal abutment displacements between those predicted by the Guthrie, Series-A models and the experimental measurements at the Guthrie County Bridge

match the experimental transverse displacements of the south abutment of the Guthrie County Bridge. The stiffness of the tangential springs was initially assumed to equal one-half of that for the normal backfill springs, as recommended by Barkan [36]. The transverse displacements of the south abutment were too high using this value for the tangential spring stiffness. A one-to-one ratio of tangential spring stiffness to the normal spring stiffness is used in the Guthrie, Series-A, Best-Soil model to match the experimental transverse abutment displacements.

The analytical and experimental ranges for south abutment transverse displacements between the coldest day (January 5, 1999) and hottest day (July 20, 1998) are shown in Figure 6.2. Transverse abutment displacements were not experimentally measured at the north abutment of the Guthrie County Bridge.

6.1.3 Abutment rotation in a vertical plane

Abutment rotation in a vertical plane parallel to the longitudinal axis of the bridge is caused by a moment produced by a resultant of the abutment backfill and pile restraining forces acting below the center of gravity of the superstructure, the temperature gradient existing through the depth of the superstructure, and the difference between the α -coefficients for the deck and girders. The experimental rotation of the south abutment of the Guthrie County Bridge was extremely small, with a range of approximately 0.080° (1400 microradians).

The Guthrie, Series-A, Best-Soil model overestimated the field-measured rotation of the south abutment by nearly a factor of two. Attempts to correct the predicted abutment rotations included: (1) applying a horizontal restraining force at the deck level to represent the force created by the bridge expansion against the

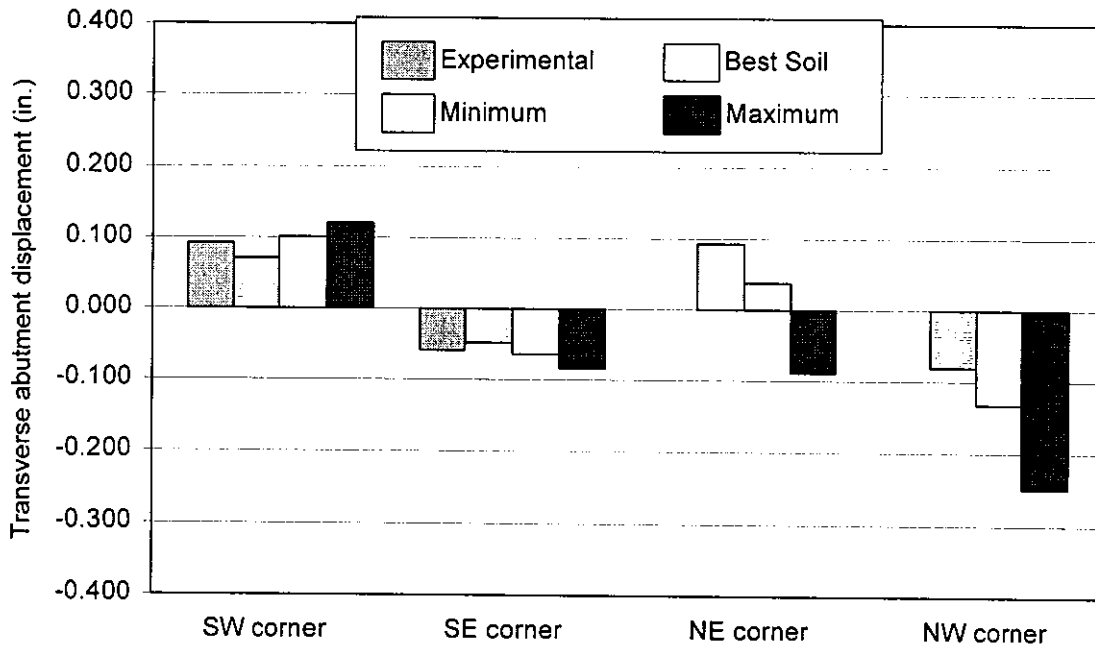


Figure 6.2. Comparison of the longitudinal abutment displacements between those predicted by the Guthrie, Series-A models and the experimental measurements at the Guthrie County Bridge (positive towards acute-angle corner of the bridge deck)

approach slab, (2) reducing the temperature gradient through the superstructure, (3) reducing the difference in the α -coefficient between the deck and girders, and (4) using different abutment backfill pressure profiles other than the assumed triangular distribution through the depth.

Forces representing the friction between the approach slab and the corbel located on the backside of the abutment had a negligible effect on the predicted abutment rotation. Reducing the temperature gradient or the difference in the α -coefficient between the girders and deck slightly reduced the rotation, but the

analytical abutment rotation still overestimated the experimental measurement.

Unreasonable abutment backfill pressure distributions, such as a reversed triangular distribution with the maximum pressure at the ground level reducing to zero pressure at the abutment base, did not correct the problem. Nonlinear abutment backfill pressures should be investigated in the future. The cause of the abutment rotation discrepancy could not be determined.

The predicted pile flexural-bending strains were affected by the overestimation of the abutment rotation. For the pile orientation used in the Guthrie County Bridge, the abutment rotation affects y-axis, flexural-bending strains induced in the pile. When a pile head translates in the longitudinal direction of the bridge, abutment rotation reduces the rotational restraint at the top of the pile and causes a reduction in the y-axis, flexural-bending strains for a pile. The predicted y-axis pile strains in the Guthrie, Series-A, Best-Soil model underestimated the experimental y-axis, flexural-bending strains.

Since the abutment rotates in a vertical plane, the abutment displacement in the longitudinal direction of the bridge varies with the depth of the abutment. When the bridge expands, the vertical abutment rotation caused the top of the bridge deck to displace further than the base of the abutment, as shown in Figure 6.3. Using small rotation theory and assuming that the abutment is a rigid body, the difference in the displacement between the top of the deck and the bottom of the abutment is equal to $h_{\text{abut}}\theta_{\text{abut}}$. Assuming a triangular backfill pressure distribution increasing with depth, the backfill pressures were minimal at the shallower depths behind the abutment. The magnitude of the thermal expansion of the bridge superstructure is

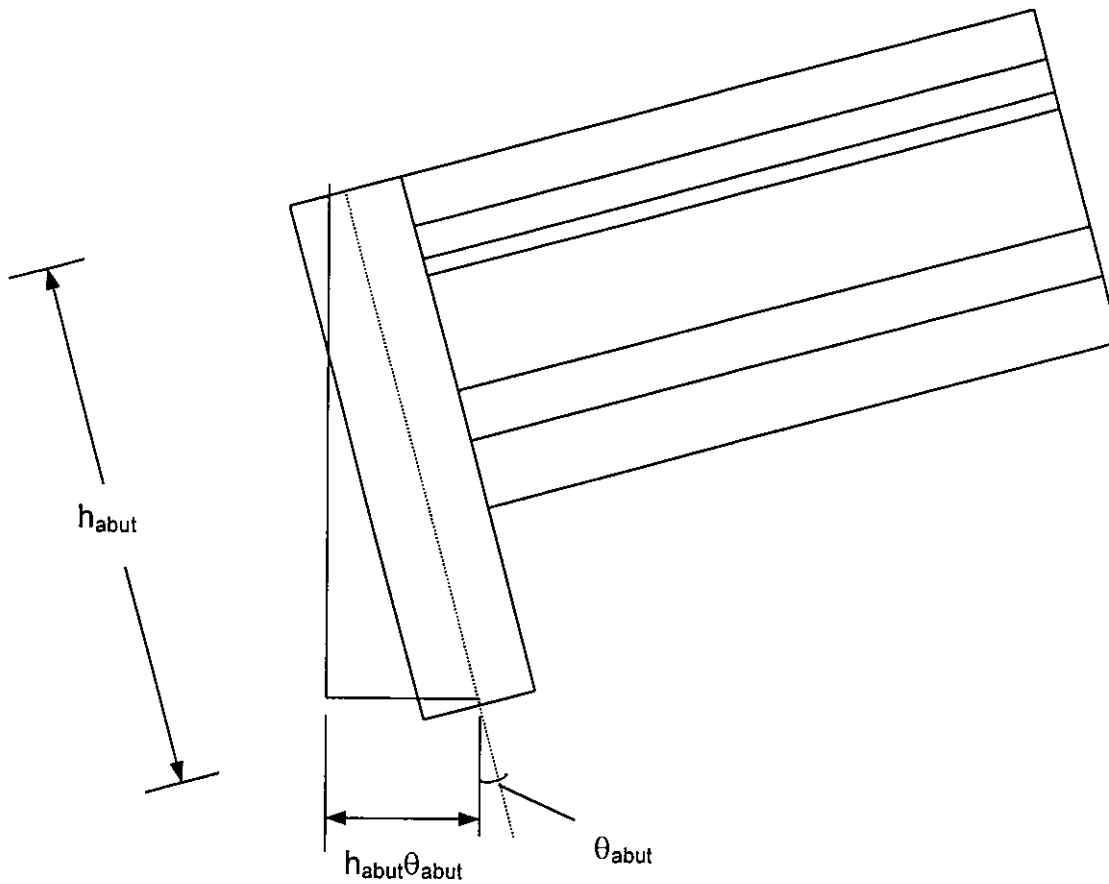


Figure 6.3. Rotation of an integral abutment

virtually unaffected by the low pressures at the top of the abutment. Other researchers state that the soil restraining forces have a minimal effect on the thermal bridge length changes [8,13]. The magnitude of the expansion of the bridge superstructure, and hence the longitudinal displacement at the top of the abutment, will be nearly the same regardless of abutment rotation. However, increasing the vertical rotation results in an increased $h_{abut}\theta_{abut}$ term, which results in a decreased longitudinal displacement at the bottom of the abutment.

To determine the consequences of the discrepancy between the predicted and measured abutment rotations, a second finite-element model was used in which the abutment rotation was adjusted to equal the experimental measurements. These finite-element models are referred to as the Guthrie, Series-B models. The previously described calibration method was used, except rotational constraints were applied to the element nodes for the south abutment nodes to cause the magnitude of the analytical abutment rotation to equal the experimental abutment rotations. Experimental abutment rotations were not available for the north abutment to study the rotations for this abutment. Since using the maximum thermal coefficient of expansion overestimates the abutment displacements, the Guthrie, Series-B models use the dry thermal coefficient of expansion values.

The Guthrie, Series-B models had a looser abutment backfill than that predicted for the Guthrie, Series-A models. The calibrated initial slope for the lateral stiffness relationship of the south abutment backfill, S_{south} , in the Guthrie, Series-B-Best-Soil model is 440, which is approximately equal to the initial slope of a dry, granular, medium-dense soil.

Upper and lower-bound soil-stiffness models were investigated using the Guthrie, Series-B models. Four bounding models as previously described (lower-bound backfill/lower-bound pile-soil, upper-bound backfill/upper-bound pile-soil, upper-bound backfill/lower-bound pile-soil, and lower-bound backfill/upper-bound pile-soil) were used to determine the minimum and maximum limits for the y-axis, flexural-bending strains of the south abutment piles. The x-axis, flexural-bending strains were only slightly affected by the abutment rotation. Therefore, these strains

were not investigated with these models. The changes in longitudinal abutment displacement for the Guthrie, Series-B models are shown in Table 6.3.

The abutment displaced further longitudinally at the acute-angle corner of the bridge deck than at the obtuse-angle corner of the bridge deck in the Guthrie, Series-B models, matching the trend of the experimentally measured abutment displacements.

Table 6.3. Change in bridge length predicted by the Guthrie, Series-B models

GUTHRIE, SERIES-B MODEL	S _{south}	S _{north}	CHANGE IN BRIDGE LENGTH (in.)	CHANGE FROM BEST-SOIL MODEL (%)
Best-Soil	435	284	1.772	----
Lower-bound backfill/lower-bound pile-soil	218	114	1.918	+8.2
Upper-bound backfill/upper-bound pile-soil	653	454	1.647	-7.1
Upper-bound backfill/lower-bound pile-soil	653	480	1.642	-7.3
Lower-bound backfill/upper-bound pile-soil	218	85	1.911	+7.8
Experimental	----	----	1.767	----

6.1.4 Relative displacements at the piers

Relative displacements in the longitudinal direction between the pier cap and a PC girder were measured at both piers of the Guthrie County Bridge. The range in the relative pier displacements was larger at the south pier, which is an expansion pier as shown in Figure 5.3(b). The experimental range for the relative pier displacements at the south pier between June 20, 1998 and January 5, 1999 was

0.040 in. (1.0 mm). For the south pier, the relative pier displacement from the Guthrie, Series-A, Best-Soil model was 0.023 in (0.6 mm). The upper and lower bounds for the relative pier displacement at the south pier were 0.033 in. (0.8 mm) and 0.011in. (0.3 mm), respectively. The models underestimate the experimental measurements.

The fixed-pier detail shown in Figure 5.3(a) for the north pier at the Guthrie County Bridge was not completely fixed regarding relative displacement between the pier diaphragm and the pier cap, since the keyway between these components is lined with a compressible expansion joint filler. Smaller relative displacements were measured at the north pier than at the south pier. An experimental range for the relative pier displacement of 0.027 in. (0.7 mm) was measured at the north pier between June 20, 1998 and January 5, 1999. The analytical prediction for the relative pier displacement was 0.014 in. (0.4 mm) at the north pier. The analytical models underestimate the relative pier movement at the north abutment, but the researchers considered the difference in the magnitude between the analytical and experimental to be too small to affect the predicted bridge behavior, such as the longitudinal abutment displacements.

6.1.5 Relative displacements at the abutment

The relative rotation was measured between the pile cap of the south abutment and a point on a pile that is 18 in. (460 mm) below the pile cap at the Guthrie County Bridge. The experimental range in relative pile rotation was approximately 0.100° (1700 microradians). As shown in Figure 6.4, the Guthrie,

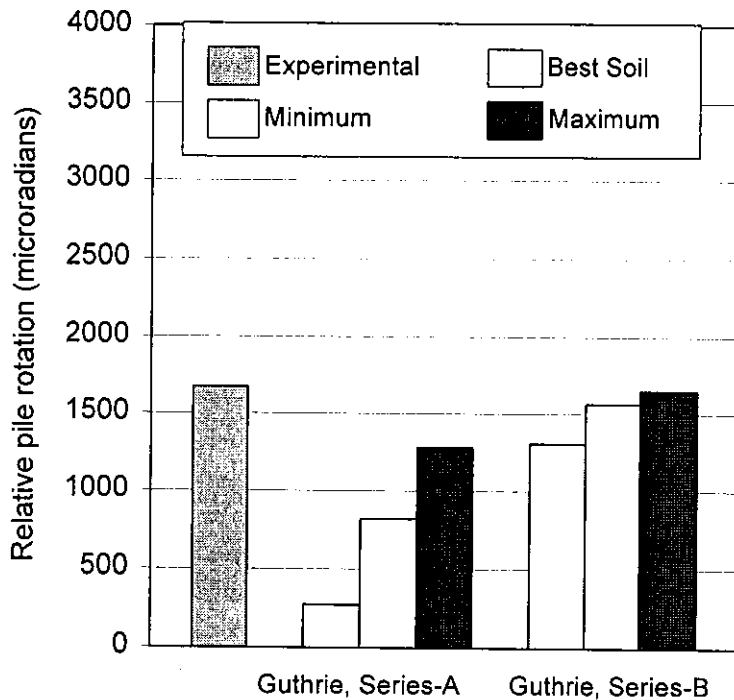


Figure 6.4. Comparison of predicted relative pile rotations with experimental measurements at the Guthrie County Bridge

Series-A models underestimated the relative pile rotation, which is attributed to the overestimated abutment rotation. Relative pile rotation results from the Guthrie, Series-B models are also shown in Figure 6.4. An elimination of the abutment rotation discrepancy results in a good correlation between the analytical and experimental relative pile rotation.

Relative displacements in the longitudinal direction of the bridge between the top and bottom flange of the center PC girder and the south abutment backwall were measured at the Guthrie County Bridge. The experimental results were extremely small compared to other displacement measurements obtained in this project, as previously shown in Figure 4.27. The analytical predictions for the relative rotation

between the PC girder at the location of the transducers and the abutment backwall were less than 0.0006° (10 microradians).

6.2 Pile strains

6.2.1 Pile flexural-bending strains

The abutment pile near the acute-angle corner of the bridge deck had the largest y-axis, flexural-bending strains compared to those in the other piles in the respective abutment, which corresponded to the largest longitudinal displacement across the width of the abutment. The largest x-axis, flexural-bending strains were predicted in the piles near the ends of the abutments, since the transverse abutment displacements were largest at these locations.

Pile strains were compared with the experimental data when reliable data was available over the time period for the maximum range of the average bridge temperature. The flexural-bending strain comparisons were made using the range of the experimental flexural-bending strains between the points in time of the maximum and minimum average bridge temperatures. A couple of piles had strain data that was reliable over a large range in the average bridge temperature, but did not have reliable data at the times of the maximum (July 20, 1998) and minimum (January 5, 1999) average bridge temperature. When continuous experimental flexural-bending strains were available for times corresponding to a range in the average bridge temperature of at least 100°F (56°C), they were also included in the pile strain study. The flexural-bending strains were minimally affected by small changes in average bridge temperature. This observation was especially true at the

south abutment where the abutment was nearly stationary for average bridge temperatures above 60°F (16°C). Table 6.4 shows the maximum average bridge temperatures range over which reliable pile flexural-bending strain data was available.

The x- and y-axis, flexural-bending strain ranges predicted by the Guthrie, Series-A models are shown in Figures 6.5 and 6.6. In these figures, the first letter in the pile notation refers to the abutment (S for south, N for north) where the pile is located. The second letter refers to the pile location in the abutment (W for west, C for near the mid-width, and E for east). Maximum flexural-bending strains were induced in the pile when the displacement of the pile head was large and when the soil adjacent to the pile was the stiffest, i.e. the lower-bound backfill/upper-bound pile-soil conditions. Minimum flexural-bending strains occurred in the pile when the pile head displacement is small and the soil adjacent to the pile was not as restraining, i.e. the upper-bound backfill/lower-bound pile-soil conditions.

The bridge construction plans show that the web of the abutment piles should be oriented parallel to the face of the abutment. However, due to a construction error, the near mid-width pile in the south abutment of the Guthrie County Bridge was orientated incorrectly. This pile was rotated approximately 25° clockwise from the correct orientation, as shown in Figure 6.7. This pile orientation induces essentially only y-axis, flexural-bending as a result of the longitudinal abutment displacement. The majority of the x-axis, flexural-bending in this pile was due to the transverse abutment displacement.

Table 6.4. Maximum average bridge temperature ranges over which reliable experimental pile strains were available at the Guthrie County Bridge

(a) X-axis pile flexural-bending

ABUTMENT	PILE	DEPTH BELOW PILE CAP (in.)	COLDEST AVERAGE BRIDGE TEMP. DATE	HOTTEST AVERAGE BRIDGE TEMP. DATE	AVERAGE BRIDGE TEMP. RANGE (°F)
South	West	9	1/5/99	7/20/98	113
South	West	33	N/A	N/A	N/A
South	Center	9	1/5/99	7/20/98	113
South	Center	33	3/12/98	6/27/98	100
South	East	9	N/A	N/A	N/A
South	East	33	N/A	N/A	N/A
North	West	9	1/5/99	7/20/98	113
North	West	33	3/12/98	7/20/98	103
North	Center	9	1/5/99	7/20/98	113
North	Center	33	N/A	N/A	N/A

(b) Y-axis pile flexural-bending

ABUTMENT	PILE	DEPTH BELOW PILE CAP (in.)	COLDEST AVERAGE BRIDGE TEMP. DATE	HOTTEST AVERAGE BRIDGE TEMP. DATE	AVERAGE BRIDGE TEMP. RANGE (°F)
South	West	9	N/A	N/A	N/A
South	West	33	N/A	N/A	N/A
South	Center	9	1/5/99	7/20/98	113
South	Center	33	N/A	N/A	N/A
South	East	9	N/A	N/A	N/A
South	East	33	N/A	N/A	N/A
North	West	9	N/A	N/A	N/A
North	West	33	1/5/99	7/20/98	113
North	Center	9	1/5/99	7/20/98	113
North	Center	33	N/A	N/A	N/A

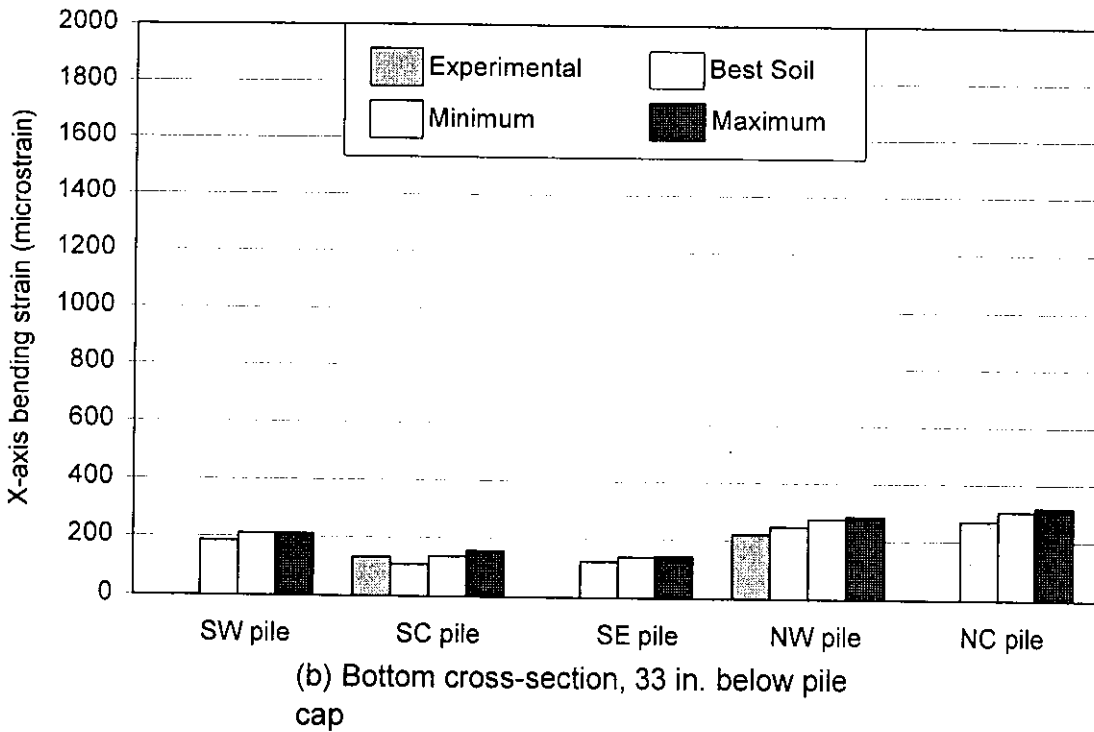
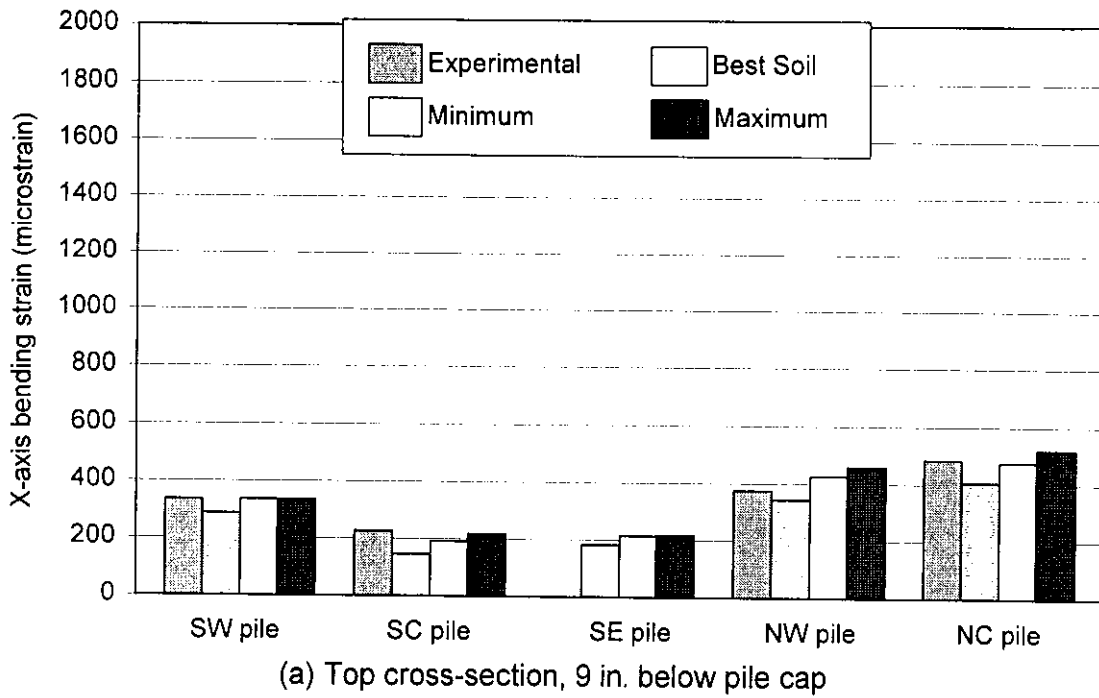
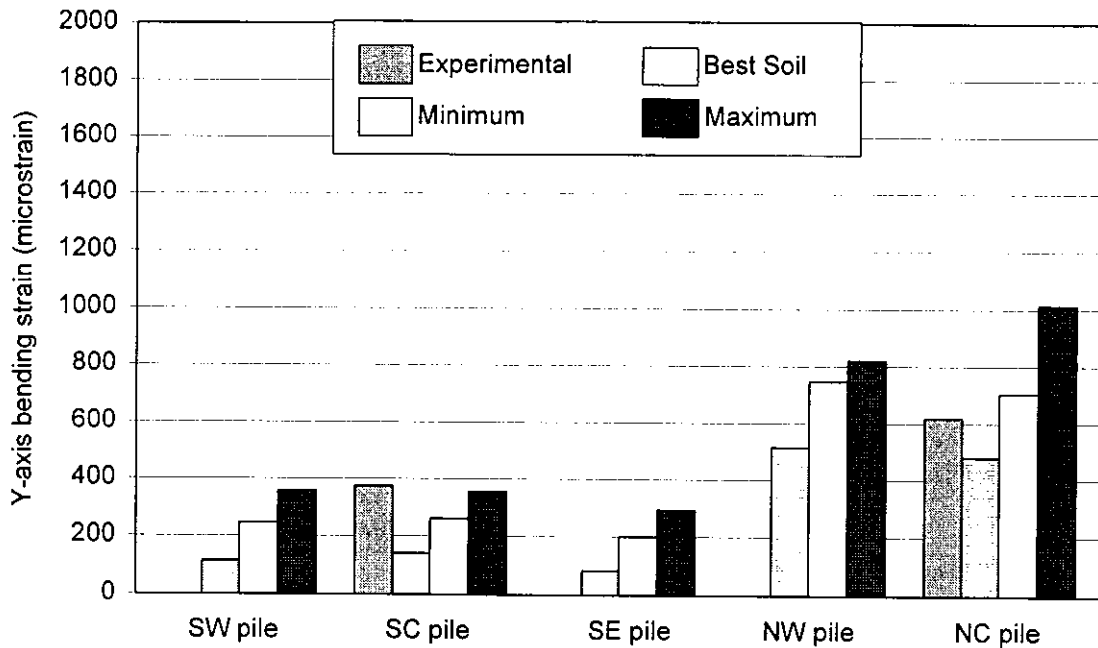
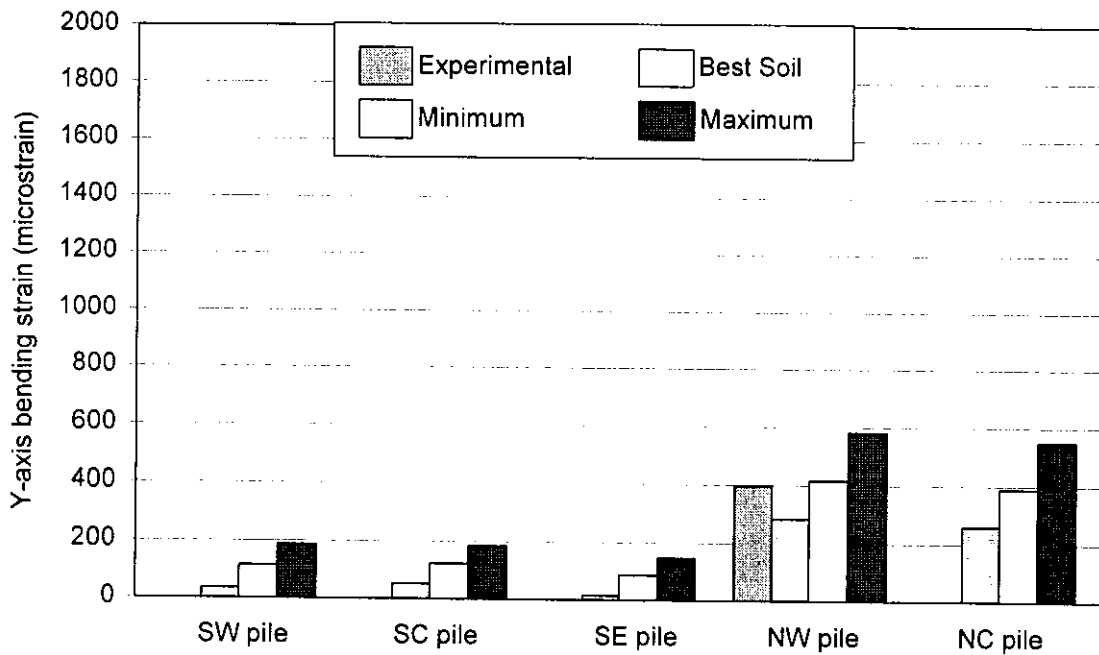


Figure 6.5. Comparison of the x-axis, flexural-bending strains predicted by the Guthrie, Series-A models and the experimental measurements



(a) Top cross-section, 9 in. below pile cap



(b) Bottom cross-section, 33 in. below pile cap

Figure 6.6. Comparison of the y-axis, flexural-bending strains predicted by the Guthrie, Series-A models and the experimental measurements

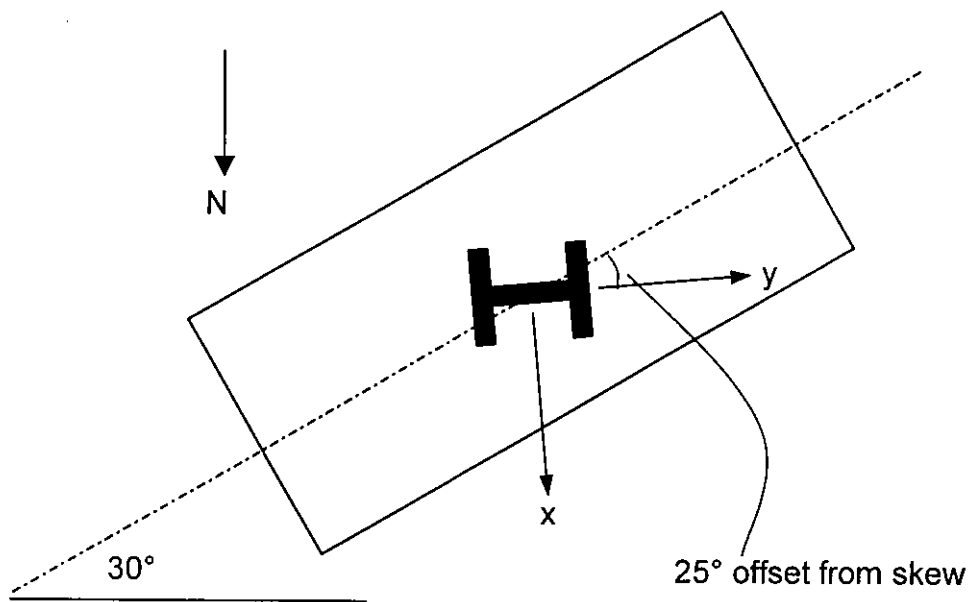


Figure 6.7. Orientation of the pile near the mid-width of the south abutment at the Guthrie County Bridge

Since the vertical rotation of the south abutment was overestimated in the Guthrie, Series-A models, the predicted y-axis, flexural-bending strains in the south abutment piles underestimated the experimental measurements. This error was expected since excess rotation of the abutment results in larger rotations at the pile head. The pile flexural-bending strains are decreased when the pile head rotates more freely than a fixed-pile head.

For the Guthrie, Series-A models, the y-axis, flexural-bending strains in the north abutment piles had a good correlation with the experimental measurements. This strain correlation may indicate that the predicted north abutment rotations did not exceed the actual rotations. This hypothesis cannot be confirmed certainly since vertical abutment rotation was not experimentally measured at this abutment.

The x-axis, flexural-bending strains from the Guthrie, Series-A models had a good correlation with the experimental x-axis, flexural-bending strains for the piles in both abutments.

The overestimation of the vertical rotation of the south abutment was corrected in the Guthrie, Series-B models. The y-axis, flexural-bending strains in the south abutment piles from the Guthrie, Series-B models are shown in Figure 6.8. Experimental y-axis, flexural-bending strain was only available at the top cross section of the pile near the mid-width of the south abutment. At this pile cross section, there is good correlation between the experimental and the Guthrie, Series-B y-axis, flexural-bending strains. Comparing the analytical results from Figure 6.6 and 6.8 shows the effect of the abutment rotation on the y-axis, flexural-bending strains in the piles. The overestimated abutment rotation caused a discrepancy in the y-axis, flexural-bending strain that ranged from 100 to 200 microstrains.

The analytical x- and y-axis, flexural-bending strains along the length of the west pile in the north abutment of the Guthrie County Bridge is shown in Figure 6.9. The flexural-bending strains in Figure 6.9 are the maximum flexural-bending strains in the pile cross section, which occurred at the flange tips. Data points for the experimental x-axis, flexural-bending strains extrapolated to the flange tips at 9 in. (230 mm) and 33 in. (840 mm) below the pile cap are included in Figure 6.9(a), which correspond to the plot of x-axis, flexural-bending strain versus time shown in Figure 4.29. The x-axis, flexural-bending strain for the lower cross section of this pile was only available for an average bridge temperature range of 103°F (57.2°C).

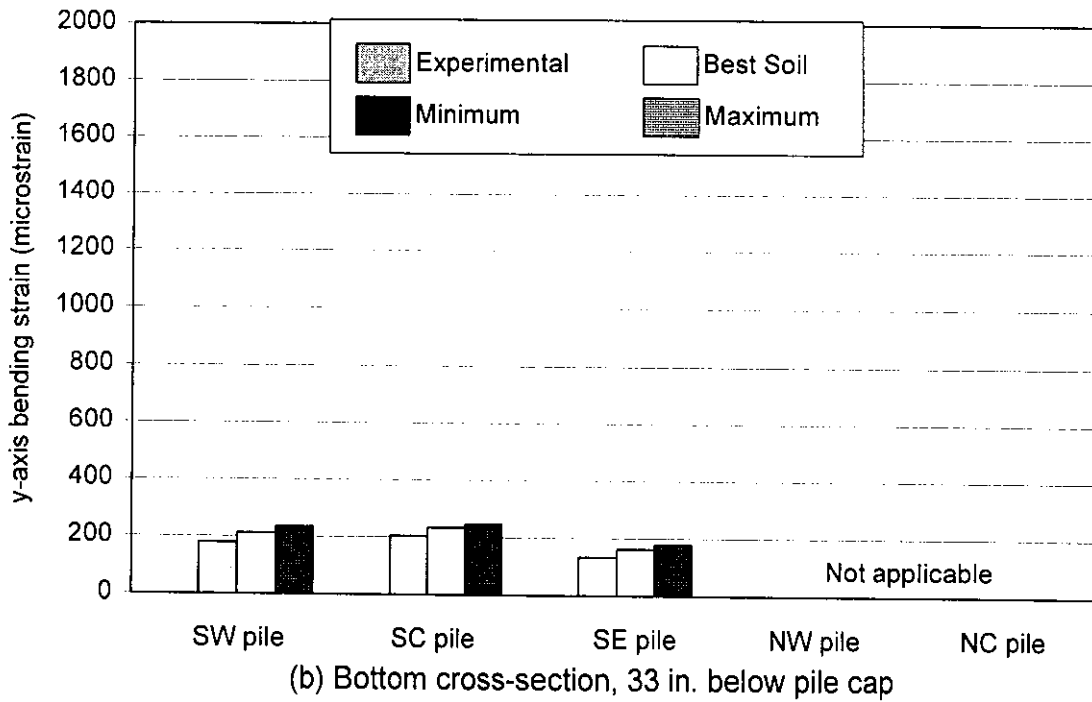
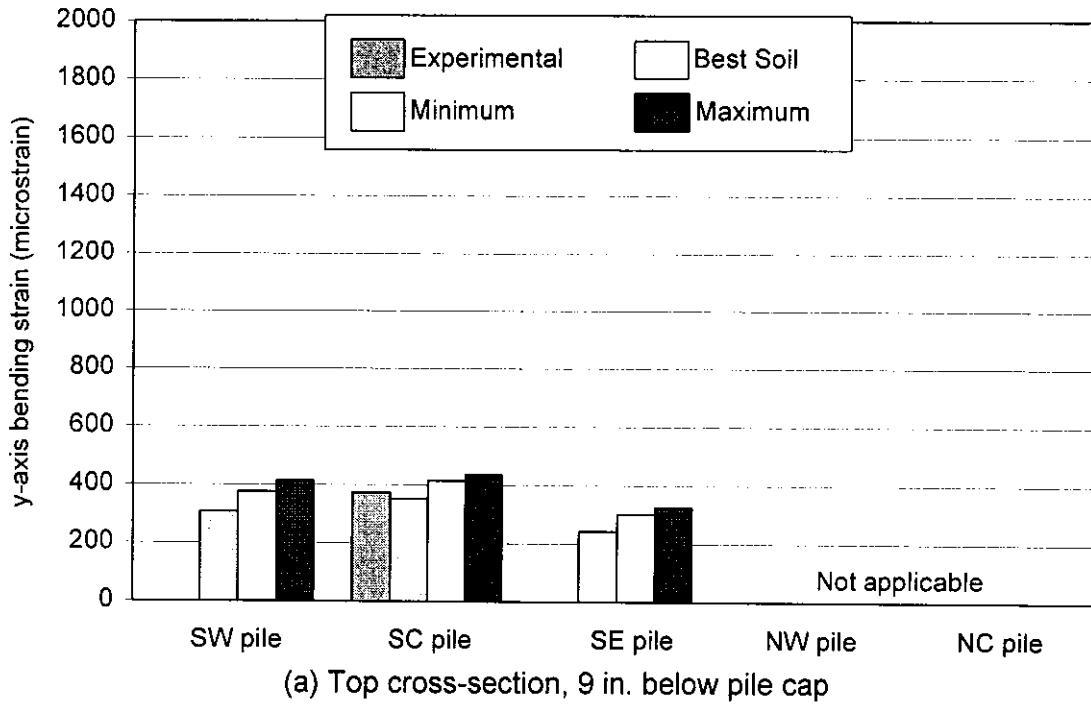


Figure 6.8. Comparison of the y-axis, flexural-bending strains predicted by the Guthrie, Series-B models and the experimental measurements

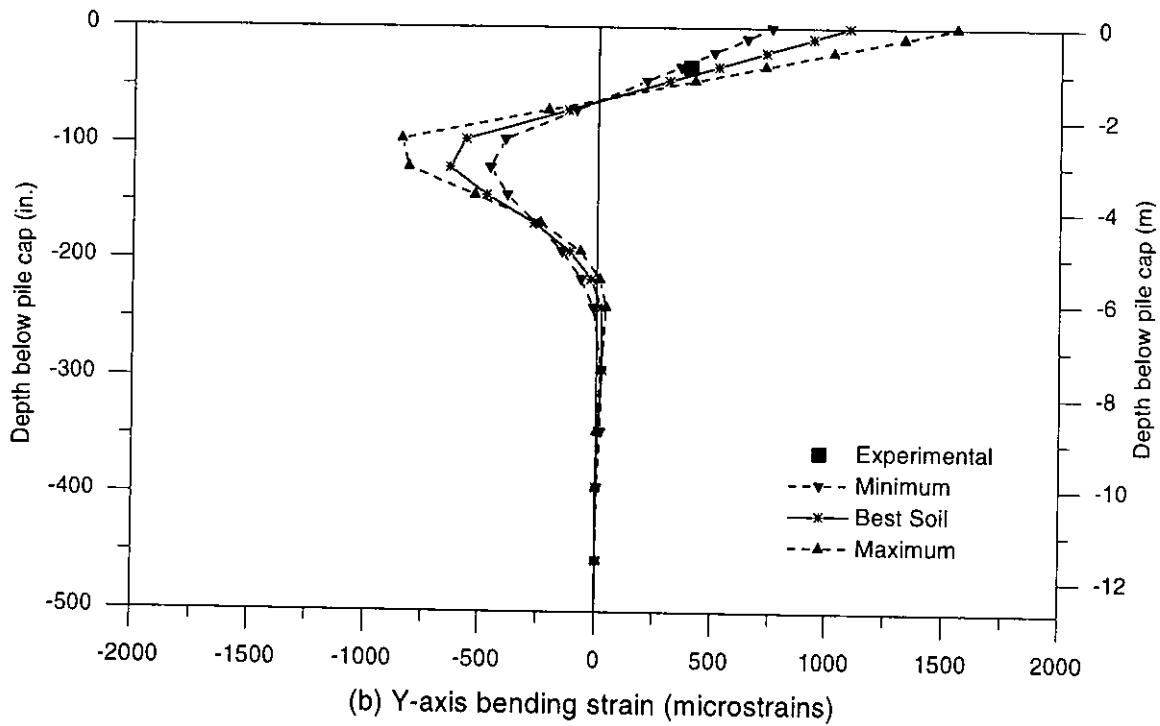
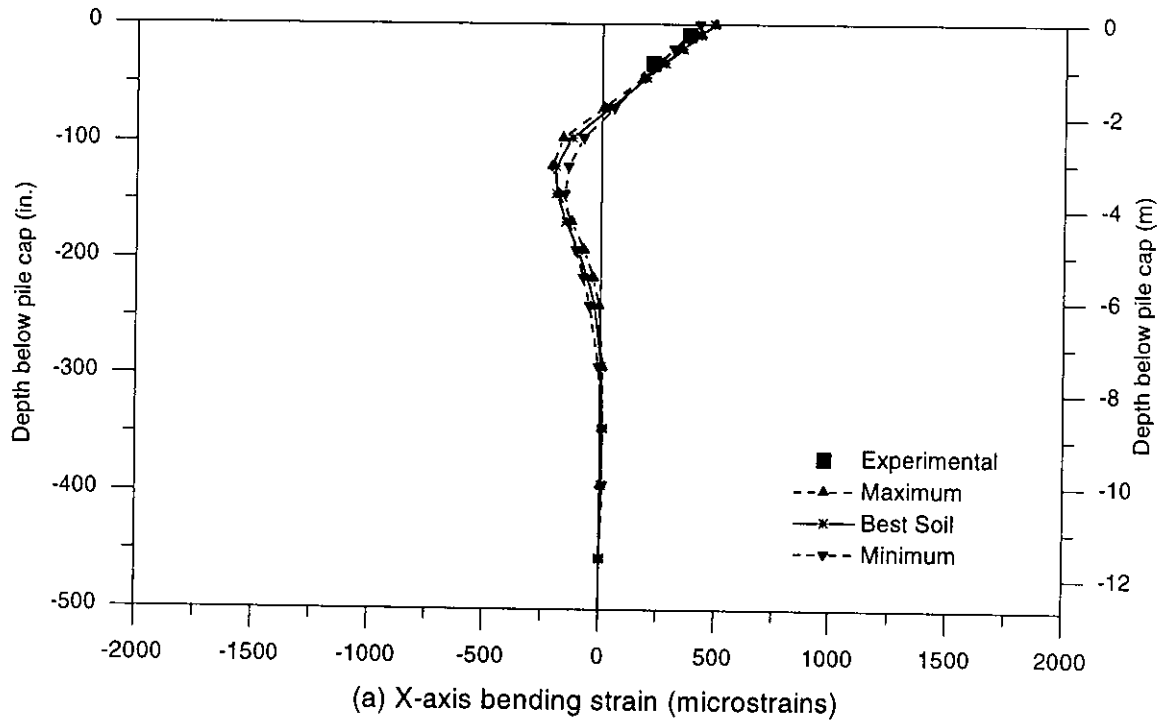
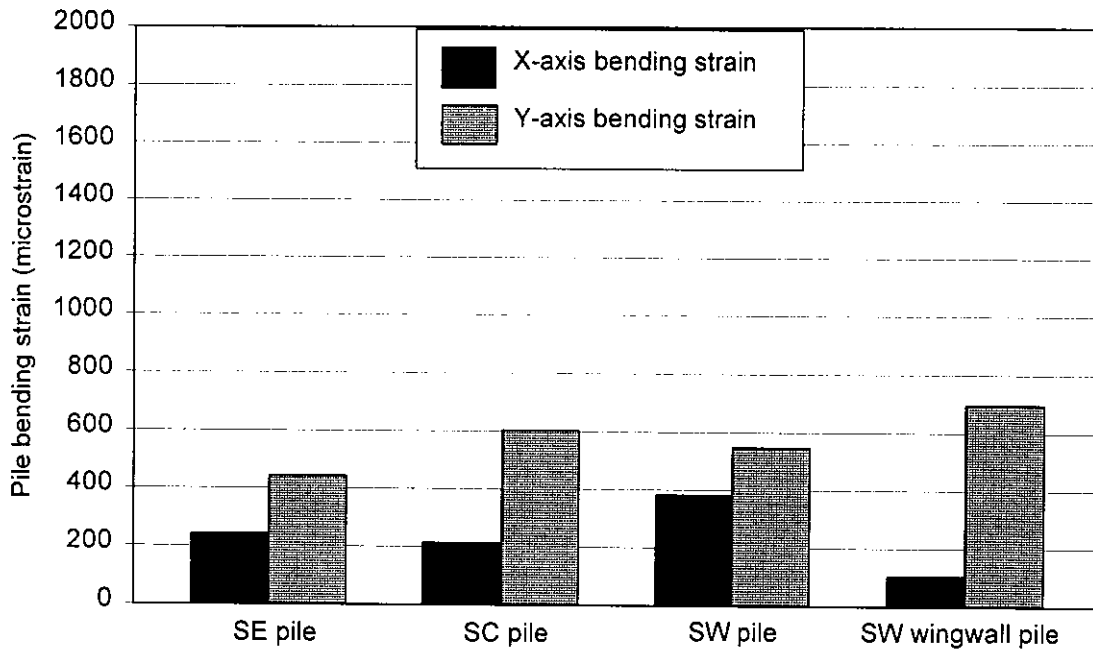


Figure 6.9. Strain variation along the length of the west pile in the north abutment at the Guthrie County Bridge (Guthrie, Series-A models)

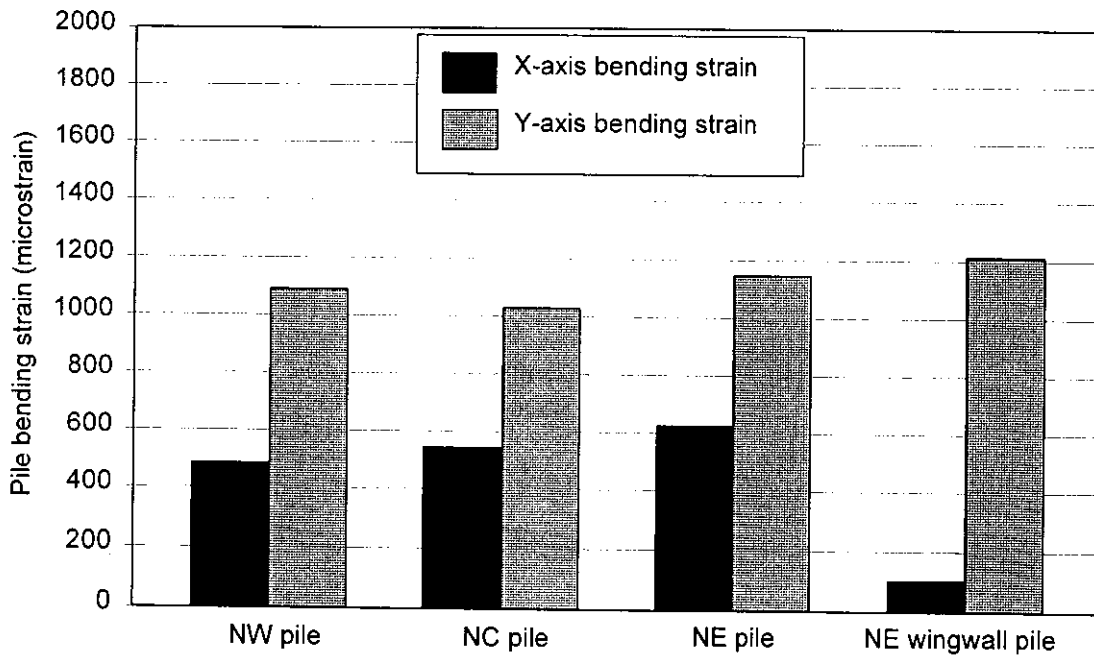
For the analytical models, the maximum, flexural-bending strains in the pile occurred at the pile cap, and an inflection point was located approximately 5 ft (1520 mm) below the bottom of the pile cap. The maximum, flexural-bending strains in the pile below the inflection point were approximately 60% of the maximum, flexural-bending strain at the bottom of the pile cap. The flexural bending strains were negligible in the lower portion of the pile length.

The maximum predicted x- and y-axis, flexural-bending strains at the flange tips for three piles across the width (east, near mid-width, and west) of each abutment and the pile in wingwalls at the acute-angle corner of the bridge deck are shown in Figure 6.10. The best estimate of the soil properties was used to predict the flexural-bending strains at the pile cap, i.e. the Guthrie, Series-A, Best-Soil model for all flexural-bending strains, except for the y-axis, flexural-bending of the piles in the south abutment which use the Guthrie, Series-B model.

Longitudinal abutment displacements were the greatest at the acute-angle corners of the bridge deck. Hence, the largest pile strains were in the abutment piles near the acute-angle corner of the bridge deck. As predicted by the Guthrie, Series-A, Best-Soil model, the combined, flexural-bending strain of the east pile at the pile cap in the north abutment of the Guthrie County Bridge was approximately 1800 microstrains. This predicted strain exceeded the yield strain for the A36 steel, which is equal to 1240 microstrains. At the pile cap, the west pile of the south abutment had an estimated combined, flexural-bending strain of about 750 microstrains. The predicted, combined, flexural-bending strain of the northeast



(a) South abutment



(b) North abutment

Figure 6.10. Maximum predicted flexural-bending strains for the abutment piles at the Guthrie County Bridge

wingwall pile at the pile cap was about 1300 microstrains, the majority of this strain was due to y-axis, flexural-bending of that pile.

6.2.2 Pile axial strains

Changes in the pile axial strains were a daily phenomenon. As previously shown in Figure 4.8(b), the pile axial strains did not have a seasonal correlation with the average bridge temperature or abutment displacement. Figure 6.11 shows the range in the pile axial strains for four piles in the north abutment. The maximum experimental axial strain range was about 95 microstrains for the pile near the mid-width of the north abutment of the Guthrie County Bridge. In the abutment wall, the axial strain predicted by the Guthrie, Series-A, Best-Soil model for the NC pile was a tension strain of approximately 110 microstrains. The experimental axial strain results at other pile cross sections in the Guthrie County Bridge were inconclusive and were not included in the comparison study.

Axial forces in the wingwall piles resist the vertical abutment rotation. The magnitude of the predicted axial strains in the NE wingwall pile was approximately five times larger than the predicted axial strains in the north abutment piles. Compressive axial strains are induced in the wingwall piles when the bridge expands. The axial strain for a typical wingwall pile is shown in Figure 6.11.

6.3 Girder strains

Strain gages were used to measure the strain gradient through the depth of the PC girders, as described in Section 4.4.2. The backfill passive-soil pressures and pile forces that act on the abutment backwall induce a moment in the bridge

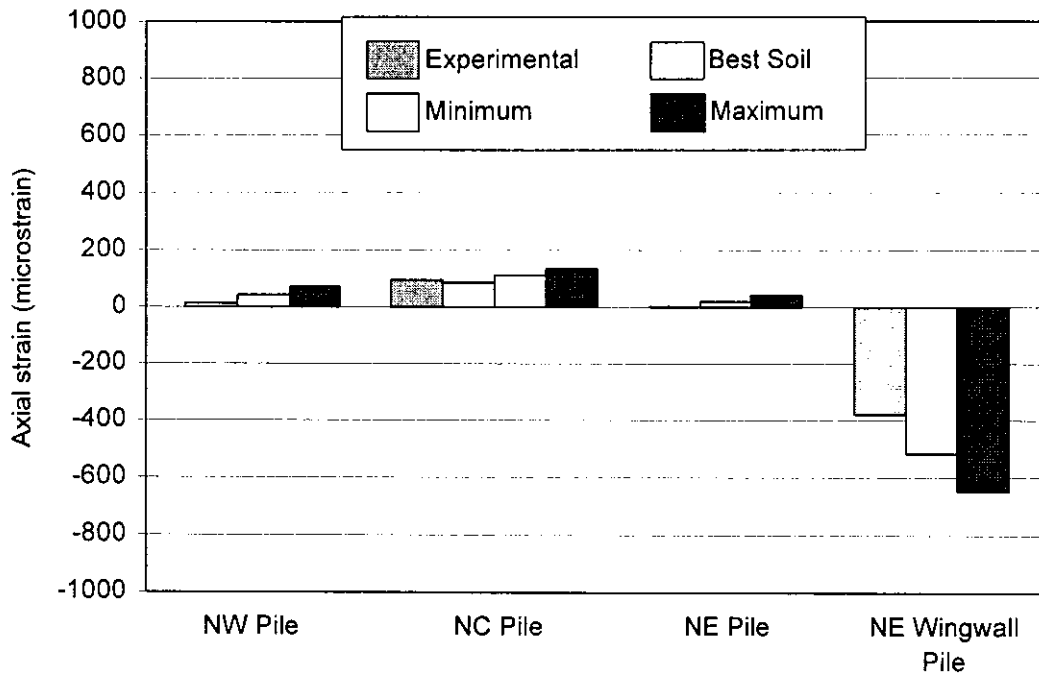


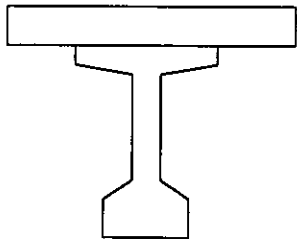
Figure 6.11. Predicted axial strains for the abutment piles at the Guthrie County Bridge

superstructure. If the bridge is assumed to be a continuous structure with three equal spans, the moment at the interior supports (piers) will be 20% of the applied moment at the end supports (abutments). The strain gradient in the girders near the abutment are noticeably larger than those recorded near the piers, as shown in Figure 4.32.

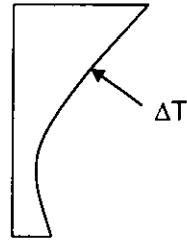
Internal restraining strains due to stress, $\Delta\epsilon_{\text{stress}}$, as given in Equation 3.3, were induced in the PC girders due to the difference between the unrestrained free temperature strains and the actual final strain profile through the depth of the superstructure [8]. The theoretical strain profiles through the depth are shown in Figure 6.12. The vertical temperature gradient and the unrestrained free

temperature strains, $\Delta\varepsilon_{temp}$, have a nonlinear distribution through the depth of the superstructure as shown in Figures 6.12(b) and 6.12(c). The vertical temperature gradient was assumed to be bilinear as discussed in Chapter 4. Also recall that the α -coefficient of the deck concrete was greater than that of the PC girders at the Guthrie County Bridge. The final strain profile was assumed to be linear according to the plane sections remain plane after bending assumption as shown in Figure 6.12(d). The shaded areas in Figure 6.12(e) indicate the internal restraint strains due to stress. Typically, compressive strains are expected in the deck while tensile strains are expected in the girders.

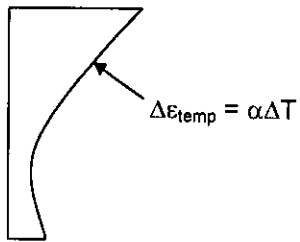
The girder strain gradient ranges from the Guthrie, Series-A models are shown in Figure 6.13. The absolute values of the strain gradients are presented in Figure 6.13. The strain ranges shown in Figure 6.13 are for total strains in the PC girders. The ranges of the strain gradient in the PC girders from the Guthrie, Series-A models were larger than the experimental PC girder strain gradients, which was attributed to the abutment rotation discrepancy described in Section 6.1.3. The PC girder strain gradients from the Guthrie, Series-B models shown in Figure 6.14 had a better correlation with the experimental data than the Guthrie, Series-A PC girder strain gradients. Since the vertical rotation was not measured at the north abutment, the Guthrie, Series-B model cannot be used for the prediction of girder strains near the north abutment.



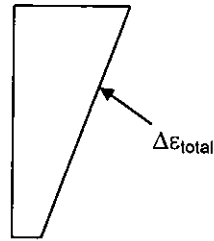
(a) Superstructure cross-section



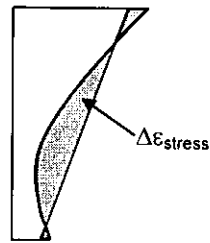
(b) Typical vertical temperature gradient



(c) Typical strain gradient due to temperature

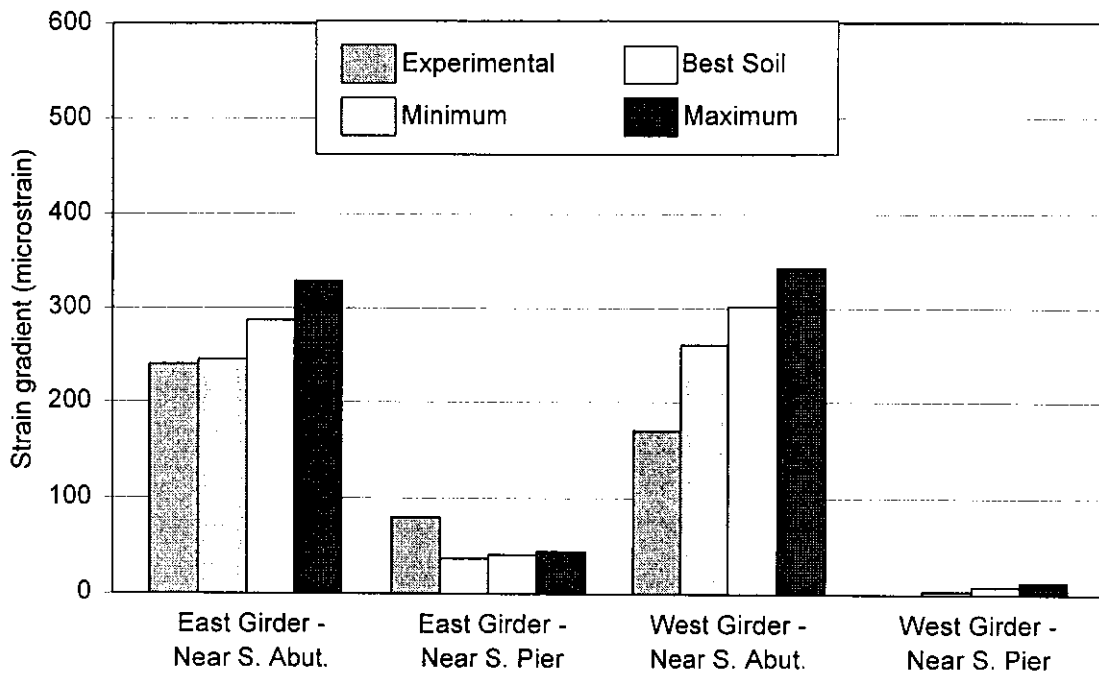


(d) Final total strain profile

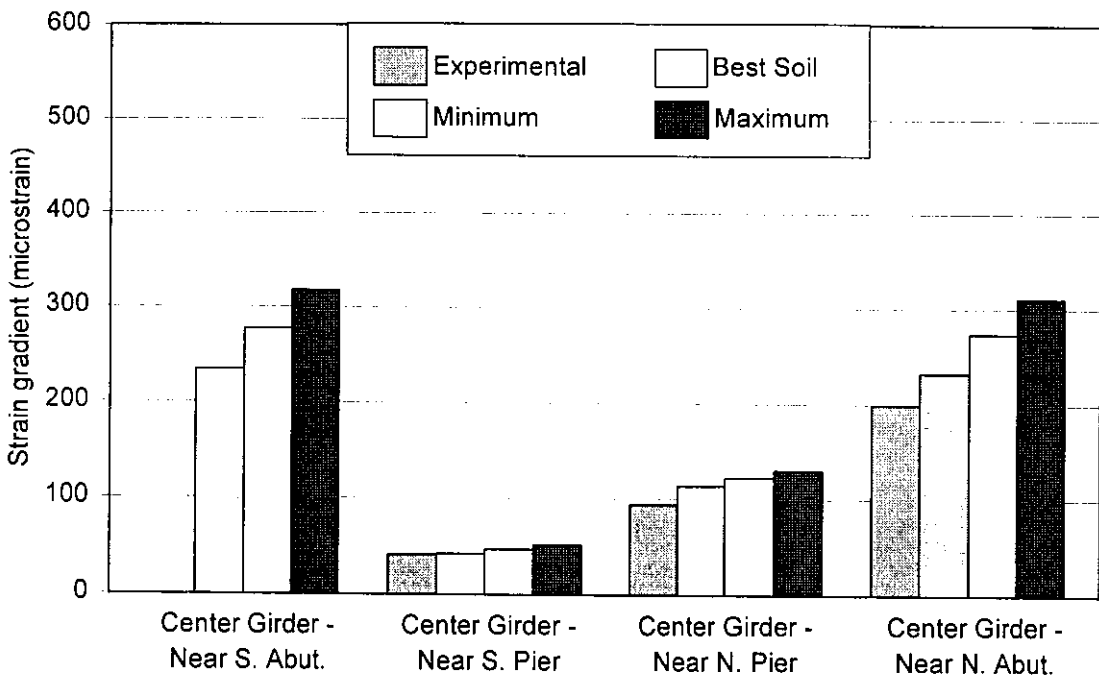


(e) Final strain profile showing the internal restrained strain due to stress

Figure 6.12. Strains through the depth of the bridge superstructure (adapted from [8])

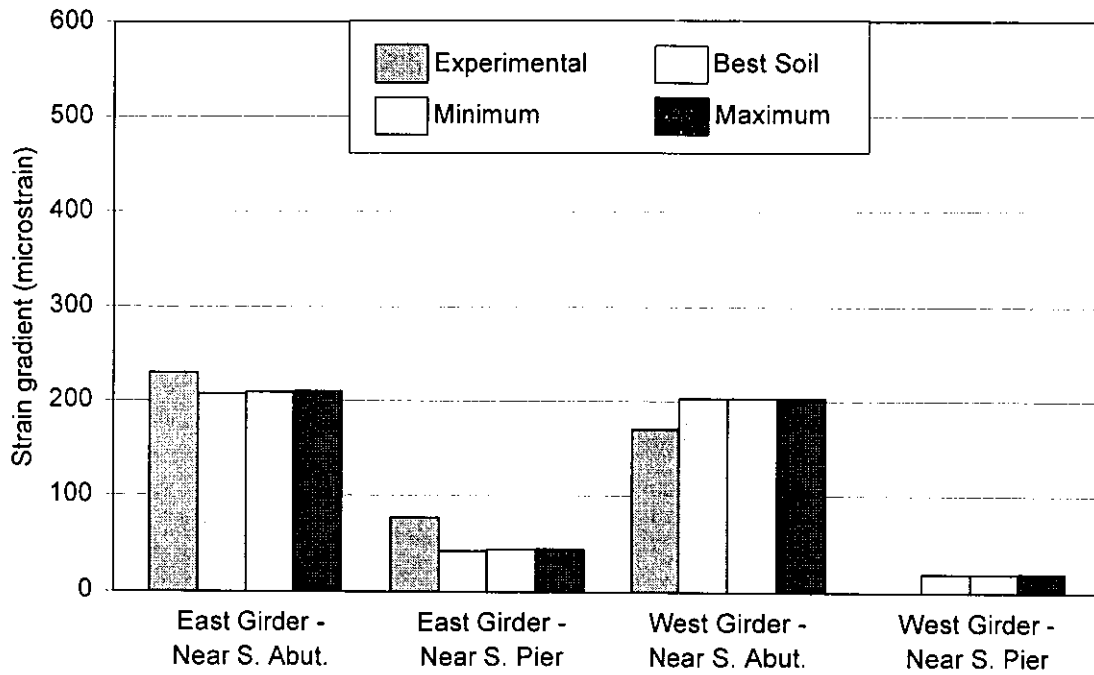


(a) East and west girder

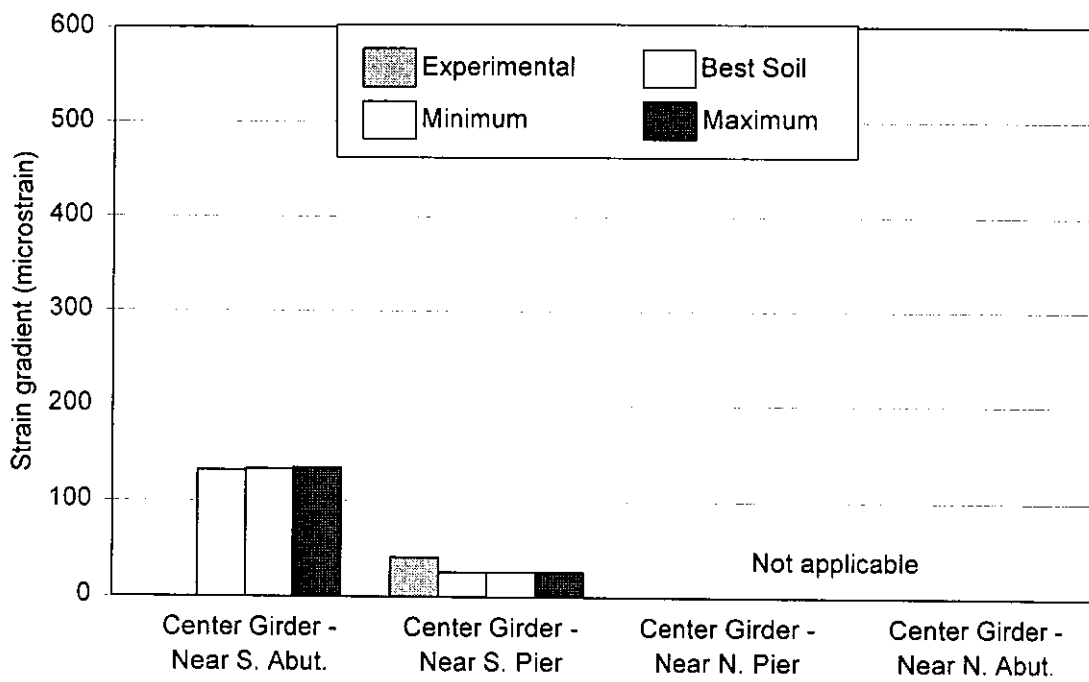


(b) Center girder

Figure 6.13. Comparison of the PC girder total-strain gradient predicted by the Guthrie, Series-A models and the experimental measurements



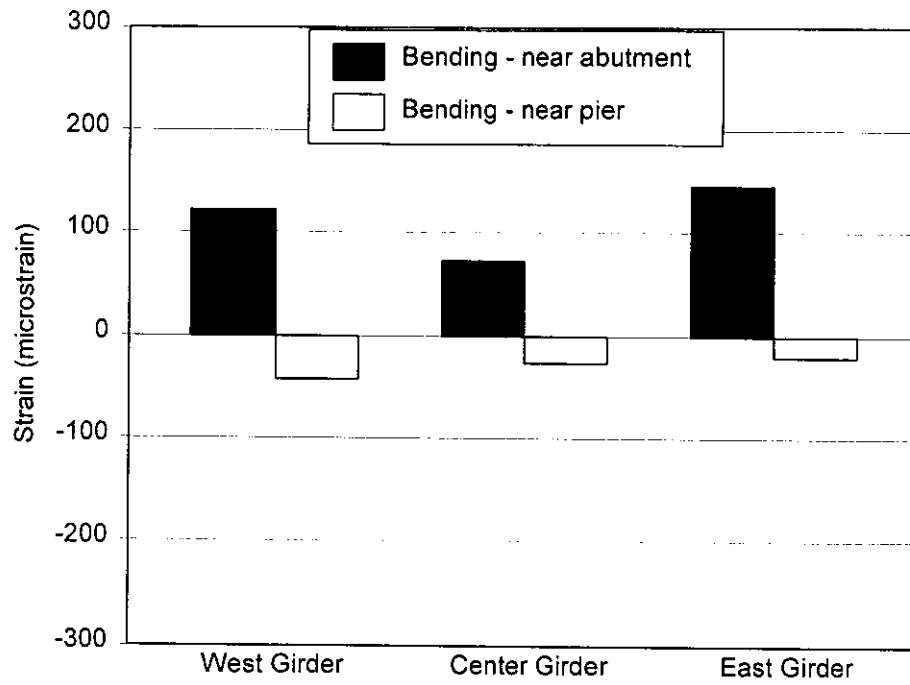
(a) East and west girder



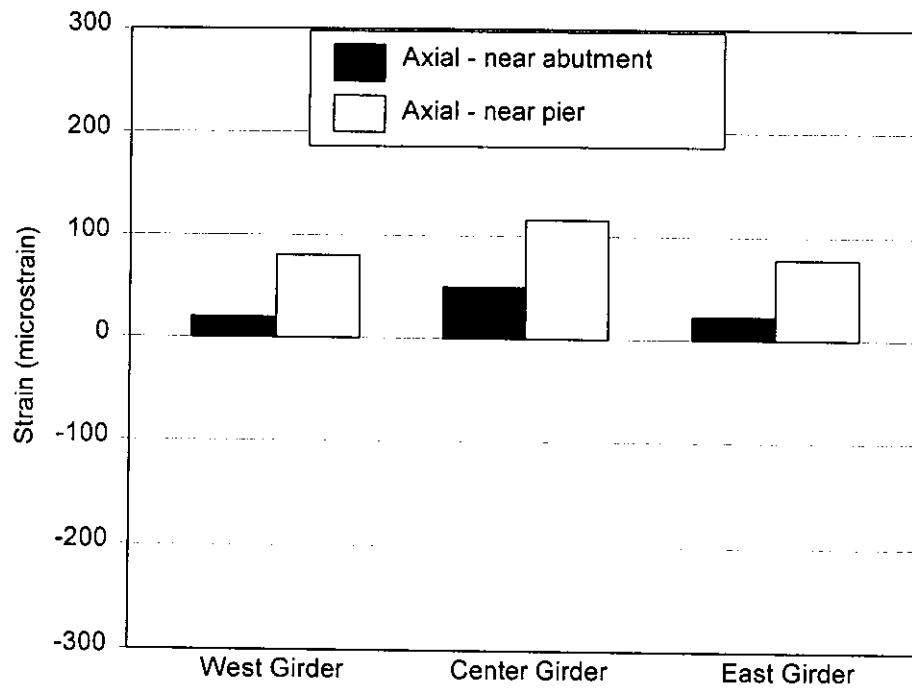
(b) Center girder

Figure 6.14. Comparison of the PC girder total-strain gradient predicted by the Guthrie, Series-B models and the experimental measurements

Predicted PC girder strains in the south span of the Guthrie County Bridge are provided in Figure 6.15, as predicted using the Guthrie, Series-B, Best-Soil model. The predicted strains shown in Figure 6.15 were due to stresses in the girder. The flexural-bending strains shown in Figure 6.15(a) are for the extreme top fiber of the girders. The maximum combined axial and flexural-bending strain in the top flange of the PC girder was approximately 170 microstrains in tension in the east girder near the south abutment of the Guthrie County Bridge. Using Hooke's Law with a modulus of elasticity for concrete as provided in Table 5.1, this strain is equivalent to a stress of about 0.750 ksi.



(a) X-axis bending strains



(b) Axial strains

Figure 6.15. Girder strains due to stress in the east span as predicted by the Guthrie, Series-B, Best-Soil model

7 ANALYTICAL STUDY AND INTERPRETATION OF EXPERIMENTAL RESULTS FOR THE STORY COUNTY BRIDGE

7.1 Bridge displacement

Thermal bridge length changes were investigated using the Story County Bridge finite-element model in the same manner as was performed for the Guthrie County Bridge finite-element models. The α -coefficients of the concrete members and other material properties of the Story County Bridge are provided in Table 5.1. The applied temperature distribution on the bridge structure was discussed in Section 5.4 of this report.

The Story County Bridge model calibration involved matching the analytical and experimental abutment displacements for the time period with the largest range in average bridge temperatures. At the time of this report, filtered experimental data from the Story County Bridge was available for all gages from August 1998 to July 1999. The applied temperatures corresponded to the temperature change from the time of the coldest average bridge temperature (January 5, 1999, 2:00 a.m.) to the time of the hottest average bridge temperature (July 5, 1999, 4:00 p.m.). The experimental average bridge temperature range was 110°F (61°C) between these times.

7.1.1 Longitudinal abutment displacements and change in bridge length

A smaller difference in the magnitude of the longitudinal displacements between the abutments was experimentally measured at the Story County Bridge than at the Guthrie County Bridge. The west abutment displaced approximately

25% further longitudinally than the east abutment at this bridge. Less water was encountered in the soil under the Story County Bridge abutments. The backfill was considered dry behind both abutments.

As was done with the Guthrie models, two series of finite-element models were used for the analysis of the Story County Bridge. The Story, Series-A models used the maximum α -coefficient since the dry α -coefficient underestimated the actual change in bridge length of the Story County Bridge. The Story, Series-B models, in which the abutment rotation was adjusted to match the experimental measurements, used the dry α -coefficient.

For the Story, Series-A, Best-Soil model, the initial slope of the east abutment backfill, S_{east} , was equal to 344, which is slightly less than the initial slope for the lateral stiffness relationship of a dry granular medium-dense soil as defined by the Clough and Duncan design curves (Figure 5.8(c)). The initial slope value of the west abutment backfill, S_{west} , was equal to 261 for a dry granular soil, which is halfway between that of a loose and medium-dense soil.

Acceptable limits on the abutment displacement errors were the same for the Story County Bridge and the Guthrie County Bridge finite-element models. The Story, Series-A, Best-Soil model had displacement errors of less than 2% compared to the experimentally measured longitudinal displacements at the mid-width of the east and west abutments. The transverse displacement was within 10% of the experimentally measured displacement at the south corner of the east abutment.

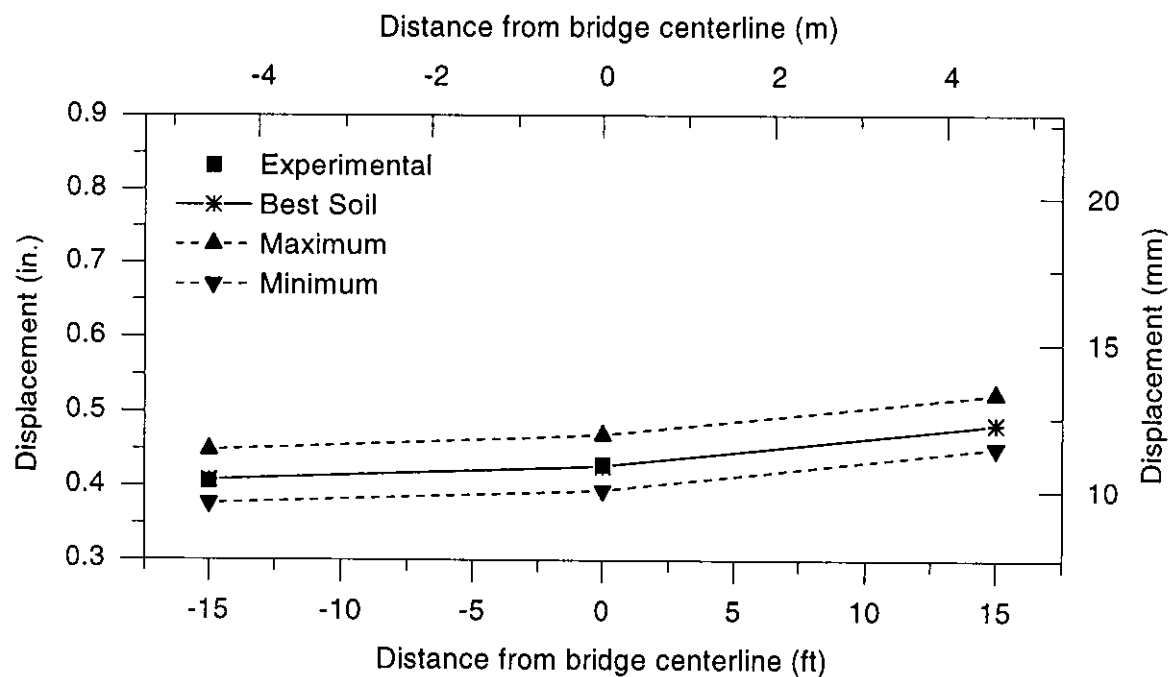
As discussed in Section 6.1.1, upper and lower-bound soil stiffness models were developed by varying the lateral stiffness of the abutment backfill and the soil

supporting the piles. The Story County Bridge bound models incorporated a fixed change in stiffness for the soil adjacent to the piles and the stiffness of the backfill at the both abutments. A summary of the backfill stiffness and the change in bridge length for the Story, Series-A finite-element models is shown in Table 7.1.

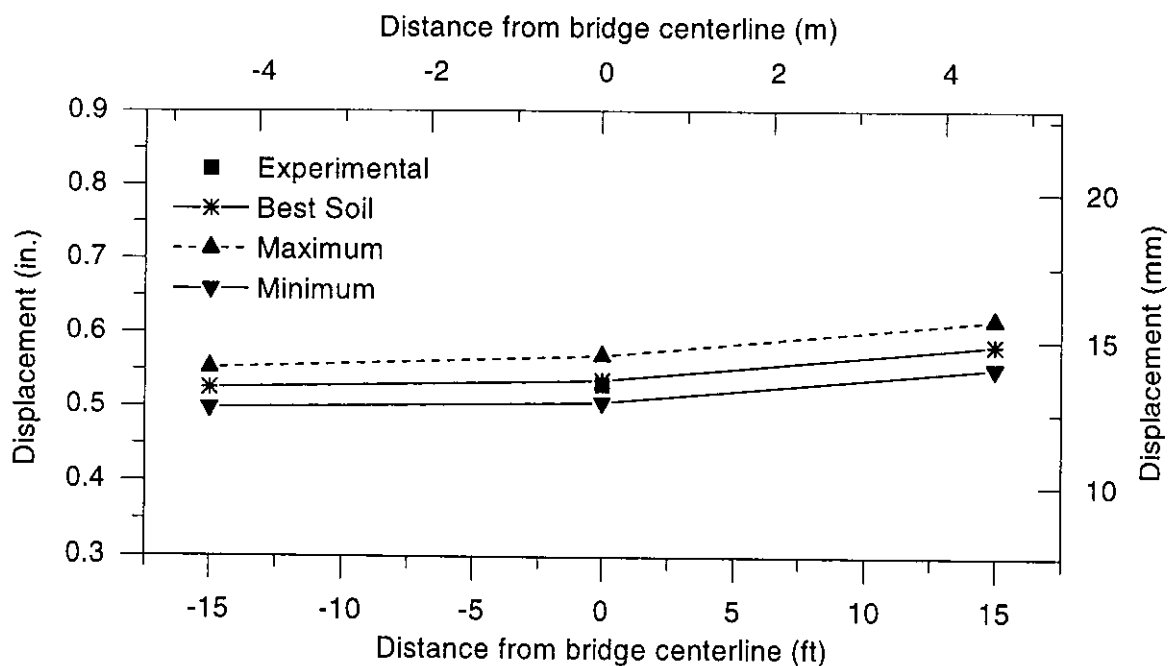
Longitudinal displacements were experimentally measured at three locations across the width of the east abutment, but only at the mid-width location of the west abutment. A comparison of the analytical and experimentally measured longitudinal abutment displacements across the width of the abutment is shown in Figure 7.1. The largest abutment displacement of the four bound models is referred to as the maximum in Figure 7.1. The maximum displacement occurred under the loosest soil conditions (lower-bound backfill/lower-bound pile-soil). Conversely, the minimum abutment displacement shown in Figure 7.1 occurred under the stiffest soil conditions (upper bound backfill/upper bound pile-soil). The abutment displaced

Table 7.1. Change in bridge length predicted by the Story, Series-A models

STORY, SERIES-A MODEL	S_{east}	S_{west}	CHANGE IN BRIDGE LENGTH (in.)	CHANGE FROM BEST-SOIL MODEL (%)
Best-Soil	344	261	0.964	----
Lower-bound backfill/lower-bound pile-soil	172	131	1.039	+7.8
Upper-bound backfill/upper-bound pile-soil	515	392	0.901	-6.5
Upper-bound backfill/lower-bound pile-soil	515	392	0.919	-4.7
Lower-bound backfill/upper-bound pile-soil	172	131	1.015	+5.3
Experimental	----	----	0.960	----



(a) East abutment



(b) West abutment

Figure 7.1. Comparison of the longitudinal abutment displacements between those predicted by the Story, Series-A models and the experimental measurements at the Story County Bridge

further longitudinally at the acute-angle edge of the bridge deck than at the obtuse-angle edge in the analytical models. Experimental measurements at the south corner of the east abutment were not reliable over the entire time period between January 5, 1999 and July 5, 1999, and are not included in Figure 7.1.

7.1.2 Transverse abutment displacement

At the east abutment of the Story County Bridge, experimentally measured transverse abutment displacements were only reliable at the acute-angle edge of the bridge deck. The transverse abutment displacement of the Story models was calibrated using this measurement. The transverse abutment displacement in the Story models was too large using Barkan's [36] recommendation for the transverse backfill stiffness, which was equal to one-half of the stiffness of the normal backfill springs. Barkan's recommendation for transverse backfill stiffness was also too low for the Guthrie County Bridge finite-element models. The ratio of the tangential spring stiffness to normal spring stiffness was 0.85 for the Story, Series-A, Best-Soil model.

A summary of the transverse abutment displacements is shown in Figure 7.2. The experimentally measured range of the transverse displacements at the south corner of the east abutment is also provided in Figure 7.2. Experimentally measured transverse abutment displacements were not reliable at the north corner of the east abutment, and were not monitored and both corners of the west abutment of the Story County Bridge.

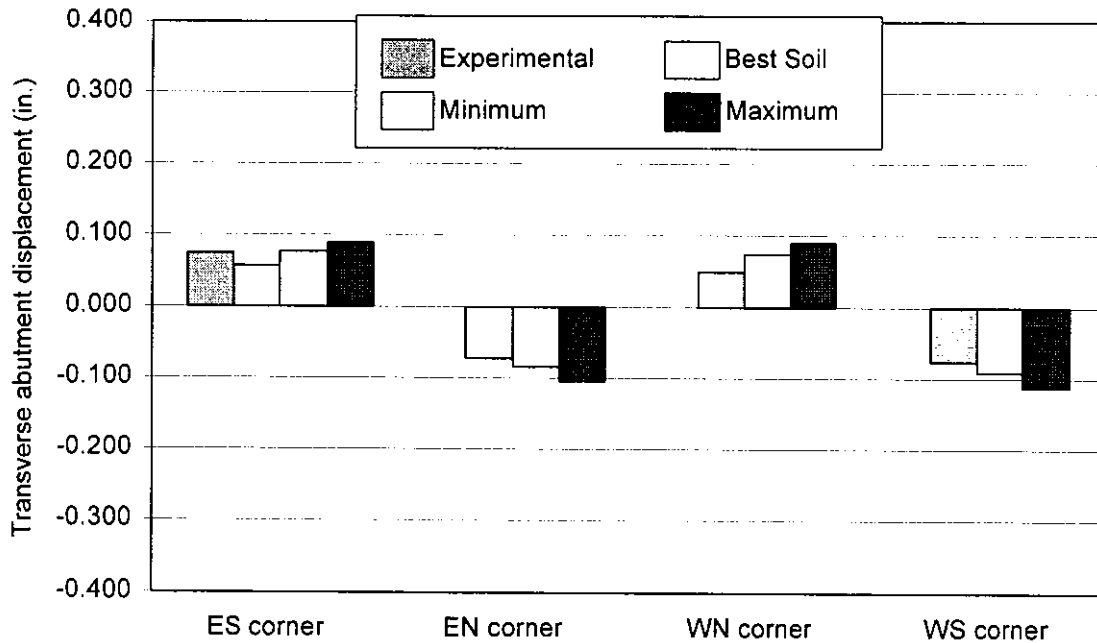


Figure 7.2. Comparison of the longitudinal abutment displacements between those predicted by the Story, Series-A models and the experimental measurements at the Story County Bridge (positive towards acute-angle edge of the bridge deck)

7.1.3 Abutment rotation in a vertical plane

The Story, Series-A, Best-Soil model overestimated the east abutment rotations in a vertical plane parallel to the longitudinal axis of the bridge by a factor of two, as was also encountered in the Guthrie, Series-A models. Again, the cause for the abutment rotation discrepancy was not determined. To determine the consequences of the discrepancy between the predicted and experimentally measured abutment rotations, the Story, Series-B models were developed. In these models, rotational constraints were applied to the element nodes for the east abutment to cause the magnitude of the analytical abutment rotations to equal the

experimental abutment rotations. The experimentally measured rotations of the east abutment of the Story County Bridge had a range of approximately 0.065° (1130 microradians). The west abutment rotations were not experimentally monitored.

The Story, Series-B models had a stiffer abutment backfill than the Story, Series-A models. The calibrated initial slope for the lateral stiffness relationship of the east abutment backfill, S_{east} , in the Story, Series-B, Best-Soil model was equal to 604, which is slightly greater than the initial slope of a dry granular medium-dense soil.

The four bounding models as previously described in Section 6.1.1 (lower-bound backfill/loose-bound pile-soil, upper-bound backfill/upper-bound pile-soil, upper-bound backfill/lower-bound pile-soil, and lower-bound backfill/upper-bound pile-soil) were used to determine the minimum and maximum limits for the y-axis, flexural-bending strain of the east abutment piles. The x-axis, flexural-bending was only slightly affected by the abutment rotation. Therefore, these strains were not investigated with these models. The changes in longitudinal abutment displacement for the Story, Series-B models are shown in Table 7.2.

7.1.4 Relative displacements at the piers

Fixed pier details, as shown in Figure 5.3(a), were specified for both piers at the Story County Bridge. As discussed in Section 5.1, the pier diaphragm and the pier cap elements shared nodes at the bearing point, negating relative translation at this location in the Story County Bridge finite-element models. The experimental measurements for the relative pier displacements are shown in Figure 4.25.

Table 7.2. Change in bridge length predicted by the Story, Series-B models

STORY, SERIES-B MODEL	S _{east}	S _{west}	CHANGE IN BRIDGE LENGTH (in.)	CHANGE FROM BEST-SOIL MODEL (%)
Best-Soil	604	480	0.968	----
Lower-bound backfill/lower-bound pile-soil	302	240	1.006	+3.9
Upper-bound backfill/upper-bound pile-soil	907	720	0.932	-3.7
Upper-bound backfill/lower-bound pile-soil	907	720	0.937	-3.2
Lower-bound backfill/upper-bound pile-soil	302	240	1.001	+3.4
Experimental	----	----	0.960	----

The experimentally measured relative pier displacement was less than 0.040 in. (1.0 mm) at both piers of the Story County Bridge.

7.1.5 Relative displacements at the abutment

The relative rotation was measured between the pile cap of the east abutment and a point on a pile that is 18 in. (460 mm) below the pile cap at the Story County Bridge. Referring back to Figure 4.26, the experimental range of relative pile rotations was approximately 0.168° (2930 microradians). As discussed in Section 4.3.5, the experimentally measured relative pile rotations were questionable. As shown in Figure 7.3, the predicted relative pile rotations from the Story, Series-A models underestimated the experimentally measured relative pile rotations. The predicted relative pile rotations from the Story, Series-B model were larger than the results of the Story, Series-A models, but still underestimated the experimental measurement. The Story County Bridge had larger relative pile rotations than predicted analytically and experimentally measured at the Guthrie County Bridge.

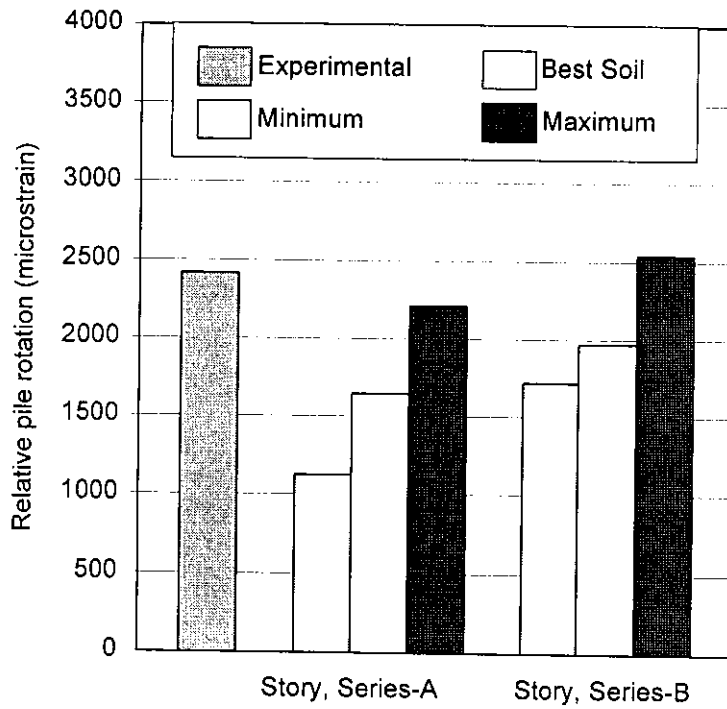


Figure 7.3. Comparison of predicted relative pile rotations and the experimental measurements at the Story County Bridge

This may be caused by the stiffer soil conditions along the upper portion of the pile at the Story County Bridge. The reader should recall that the pre-bored holes through which the piles were driven were filled with sand at the Story County Bridge, compared to a bentonite slurry that filled the pre-bored holes at the Guthrie County Bridge.

7.2 Pile strains

7.2.1 Pile flexural-bending strains

As described in Section 6.2, pile strains were compared with the experimental data when reliable data was available over the time span of the maximum range of

average bridge temperatures. The strain gages on the abutment piles at the Story County Bridge had a better rate of success than the strain gages on the abutment piles at the Guthrie County Bridge. Table 7.3 shows the maximum ranges of average bridge temperature over which reliable flexural-bending strain data was available for the abutment piles at the Story County Bridge.

The ranges of the x- and y-axis, flexural-bending strains for the abutment piles as predicted by the Story, Series-A were compared to the experimentally measured strains, as shown in Figures 7.4 and 7.5. In these figures, the first letter in the pile notation refers to the abutment (E for east, W for west) where the pile is located. The second letter refers to the pile location in the abutment (N for north, C for center, and S for south). As discussed in Section 6.2.1, the models that incorporated the lower-bound abutment backfill stiffness and the upper-bound stiffness for the soil supporting the piles predicted the maximum, flexural-bending strains. Conversely, the models that used the upper-bound abutment backfill stiffness and the lower-bound stiffness for the soil supporting the piles predicted the minimum, flexural-bending strains in the abutment piles.

The orientation of the abutment piles in the abutment pile cap was the same for both the Story County Bridge and Guthrie County Bridge, with the webs of the piles oriented parallel to the abutment face. The Story County Bridge has a 15° skew angle, which is smaller than the 30° skew angle at the Guthrie County Bridge. The ratio of y-axis to x-axis, flexural-bending strains in the abutment piles was larger at the Story County Bridge than at the Guthrie County Bridge because of the smaller skew angle.

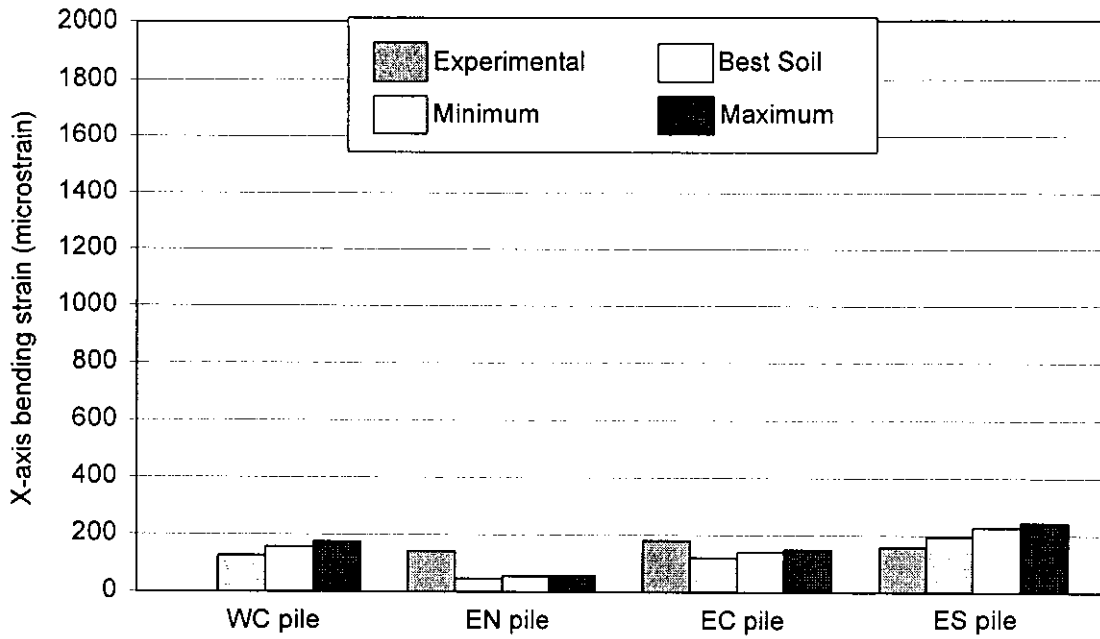
Table 7.3. Maximum average bridge temperature ranges for which reliable experimental pile strains were available at the Guthrie County Bridge

(a) X-axis pile flexural-bending

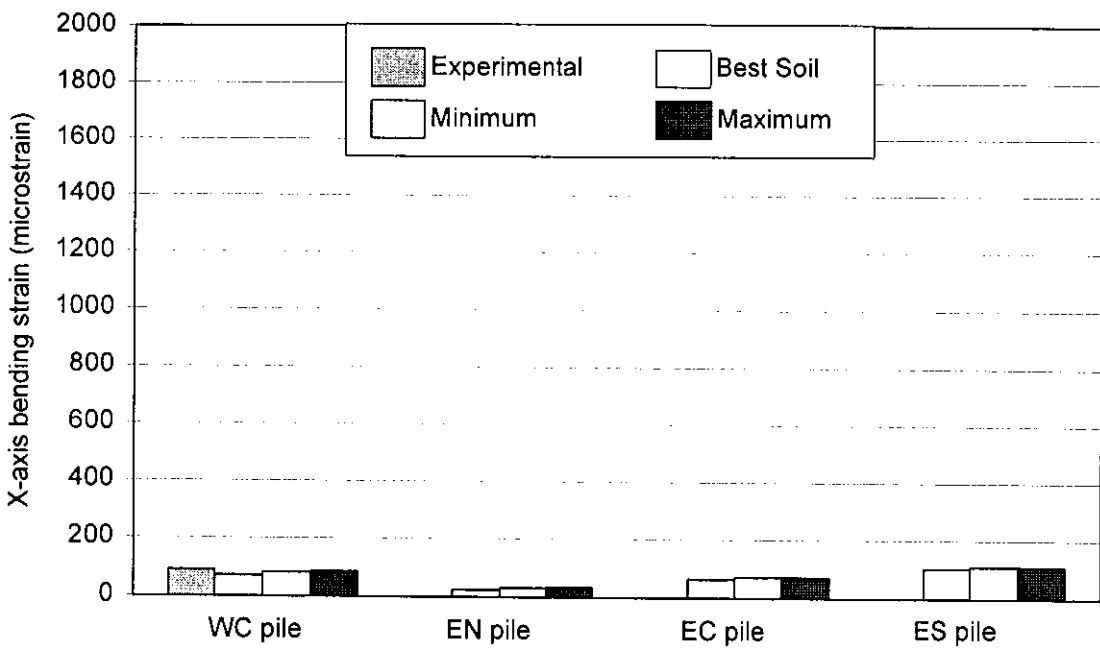
ABUTMENT	PILE	DEPTH BELOW PILE CAP (in.)	COLDEST AVERAGE BRIDGE TEMP. DATE	HOTTEST AVERAGE BRIDGE TEMP. DATE	AVERAGE BRIDGE TEMP. RANGE (°F)
West	Center	9	N/A	N/A	N/A
West	Center	33	1/5/99	8/20/99	108
East	North	9	1/5/99	7/5/99	110
East	North	33	1/5/99	7/5/99	110
East	Center	9	1/5/99	7/5/99	110
East	Center	33	N/A	N/A	N/A
East	South	9	1/5/99	7/5/99	110
East	South	33	1/5/99	8/20/99	108

(b) Y-axis pile flexural-bending

ABUTMENT	PILE	DEPTH BELOW PILE CAP (in.)	COLDEST AVERAGE BRIDGE TEMP. DATE	HOTTEST AVERAGE BRIDGE TEMP. DATE	AVERAGE BRIDGE TEMP. RANGE (°F)
West	Center	9	1/5/99	6/25/99	106
West	Center	33	1/5/99	7/5/99	110
East	North	9	1/5/99	7/5/99	110
East	North	33	1/5/99	7/5/99	110
East	Center	9	1/5/99	7/5/99	110
East	Center	33	1/5/99	7/5/99	110
East	South	9	1/5/99	7/5/99	110
East	South	33	N/A	N/A	N/A



(a) Top cross-section, 9 in. below pile cap



(b) Bottom cross-section, 33 in. below pile cap

Figure 7.4. Comparison of the x-axis, flexural-bending strains predicted by the Story, Series-A models and the experimental measurements

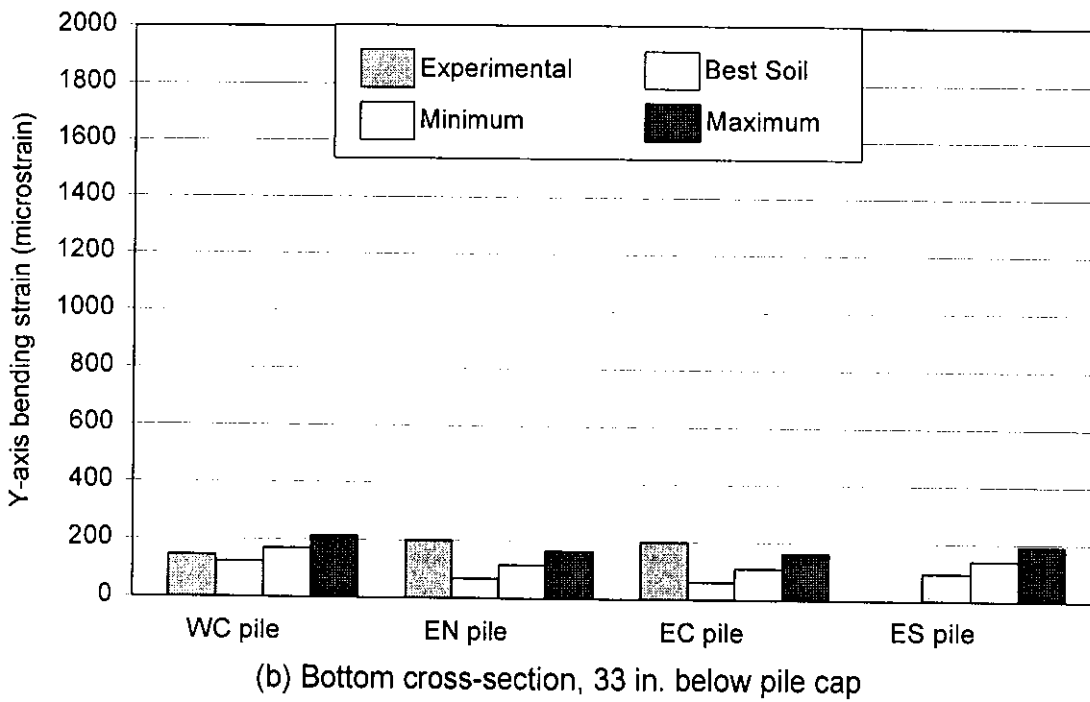
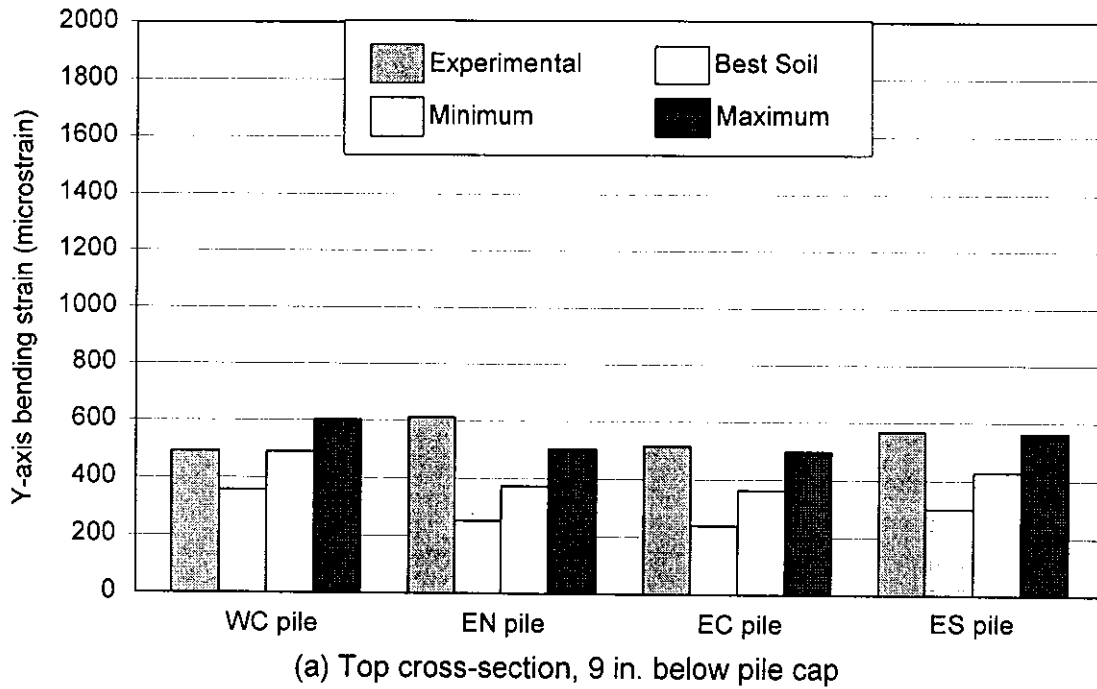


Figure 7.5. Comparison of the y-axis, flexural-bending strains predicted by the Story, Series-A models and the experimental measurements

The x-axis, flexural-bending strains predicted by the Story, Series-A models had a good correlation with the experimentally measured flexural-bending strains at the center and south piles in the east abutment. The predicted, x-axis, flexural-bending strains at the north pile of the east abutment underestimated the experimentally measured strains. The transducer that measured the transverse abutment displacements at this corner did not function properly. Therefore, the transverse displacement could not be calibrated in these finite-element models. The underestimated x-axis, flexural-bending strain predicted at this pile may indicate that the finite-element model may have underestimated the transverse displacement at the north corner of the east abutment.

As discussed in Section 6.2, the overestimation of the abutment rotations in a vertical plane parallel to the longitudinal axis of the bridge leads to an underestimation of the flexural-bending strains about the y-axis of the abutment piles. The abutment rotations were experimentally measured at the east abutment of the Story County Bridge. As shown in Figure 7.5, the y-axis, flexural-bending strains predicted by the Story, Series-A models underestimated the experimentally measured y-axis, flexural-bending strains for the piles at this abutment. The abutment rotations had a negligible effect on the x-axis, flexural-bending strains in the abutment piles.

The predicted y-axis bending strains at the center pile in the west abutment had a better correlation with the experimentally measured y-axis, flexural-bending strains. This may indicate that the west abutment rotation predicted by the Story, Series-A models had a good correlation with the actual rotation of this abutment.

This hypothesis cannot be confirmed since the abutment rotations were not measured at the west abutment of the Story County Bridge.

The overestimation of the vertical rotation of the south abutment was corrected in the Story, Series-B models. The y-axis, flexural-bending strains for the piles in the east abutment predicted by the Story, Series-B models are shown in Figure 7.6. These predicted strains had a better correlation with the experimentally measured y-axis, flexural-bending strains than did those predicted by the Story, Series-A models.

The variation of the flexural-bending strains along the length of the pile at the flange tips of the north pile in the east abutment is shown in Figure 7.7. The predicted minimum, maximum, and best-soil pile bending strains are shown in Figure 7.7. In Figure 7.7(b), the experimentally-measured, y-axis, flexural-bending strains were extrapolated to the flange tips. The maximum flexural-bending strains occurred at the pile cap. The inflection point for both the x- and y-axis, flexural-bending strains was located approximately 5 ft (1520 mm) below the pile cap. Flexural-bending strains were negligible in the lower portion of the pile length.

The maximum, predicted, flexural-bending strains that occurred at the flange tips for three piles along the width of each abutment at the Story County Bridge are shown in Figure 7.8. The best estimate of the soil properties was used to predict the flexural-bending strains in the abutment piles, i.e. the Story, Series-A, Best-Soil model for all flexural-bending strains except for the y-axis, flexural-bending strains for the piles in the south abutment. The Story, Series-B, Best-Soil model was used to predict the y-axis, flexural-bending strains for the piles in the south abutment.

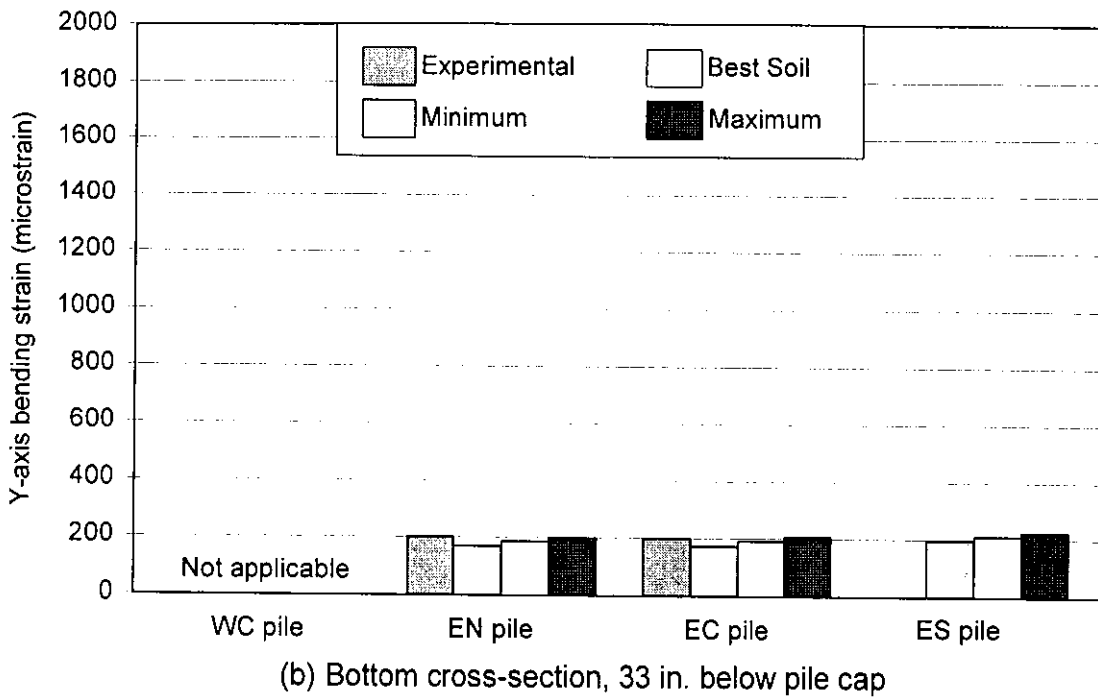
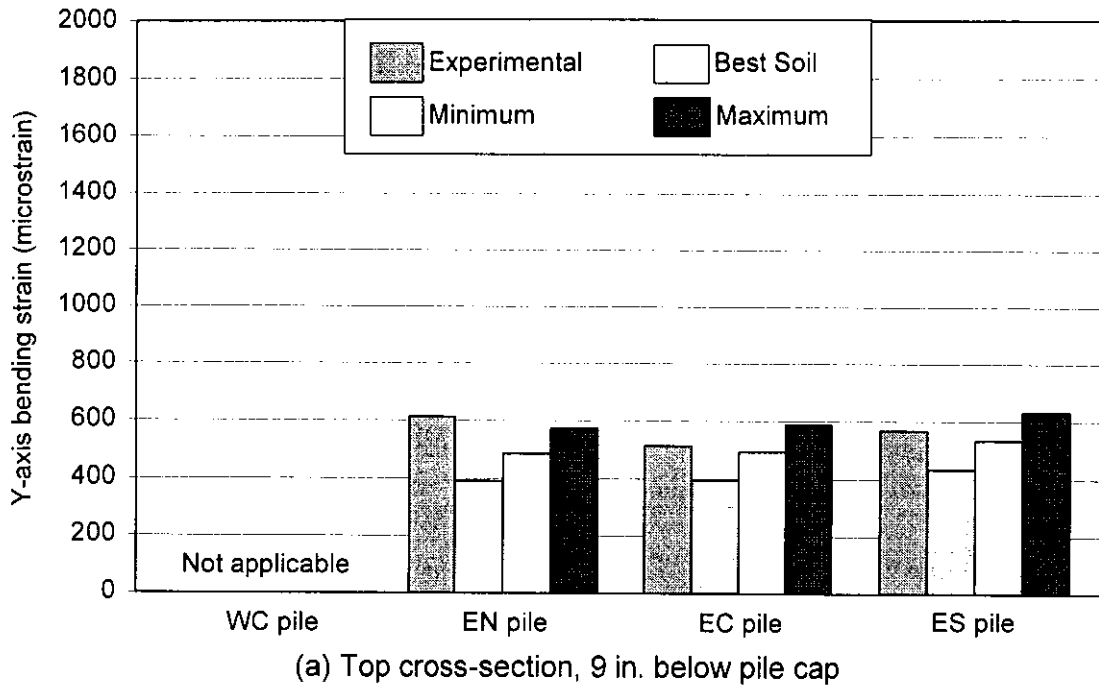


Figure 7.6. Comparison of the y-axis, flexural-bending strains predicted by the Story, Series-B models and the experimental measurements

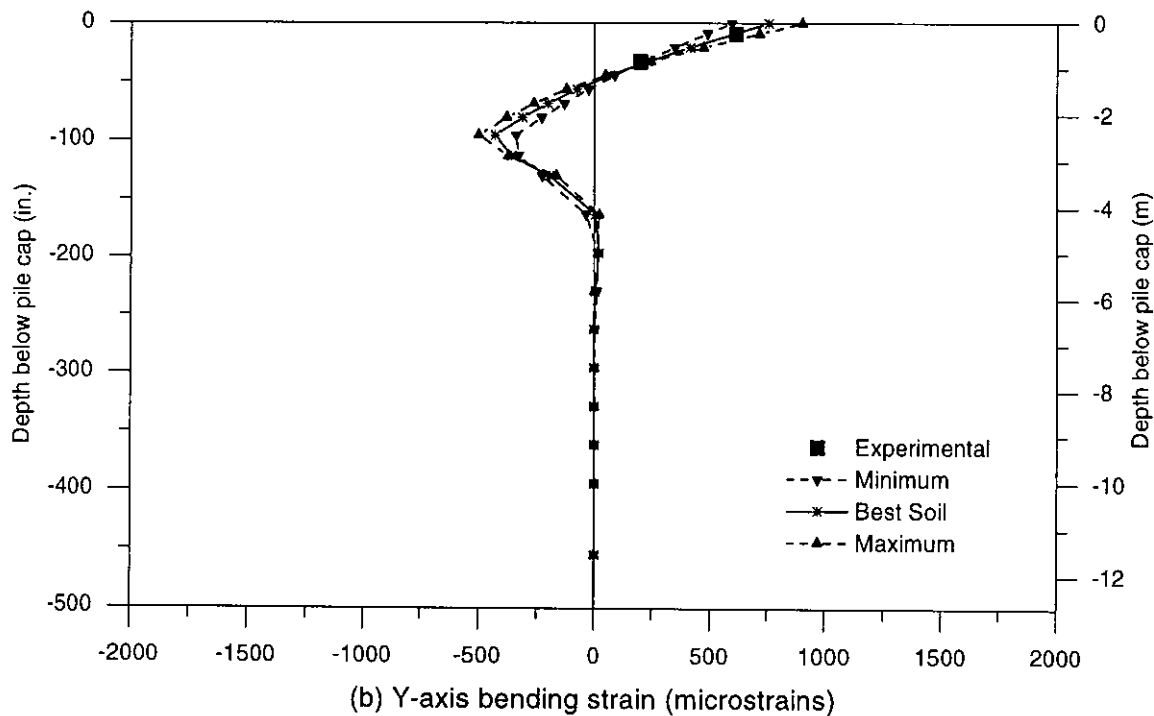
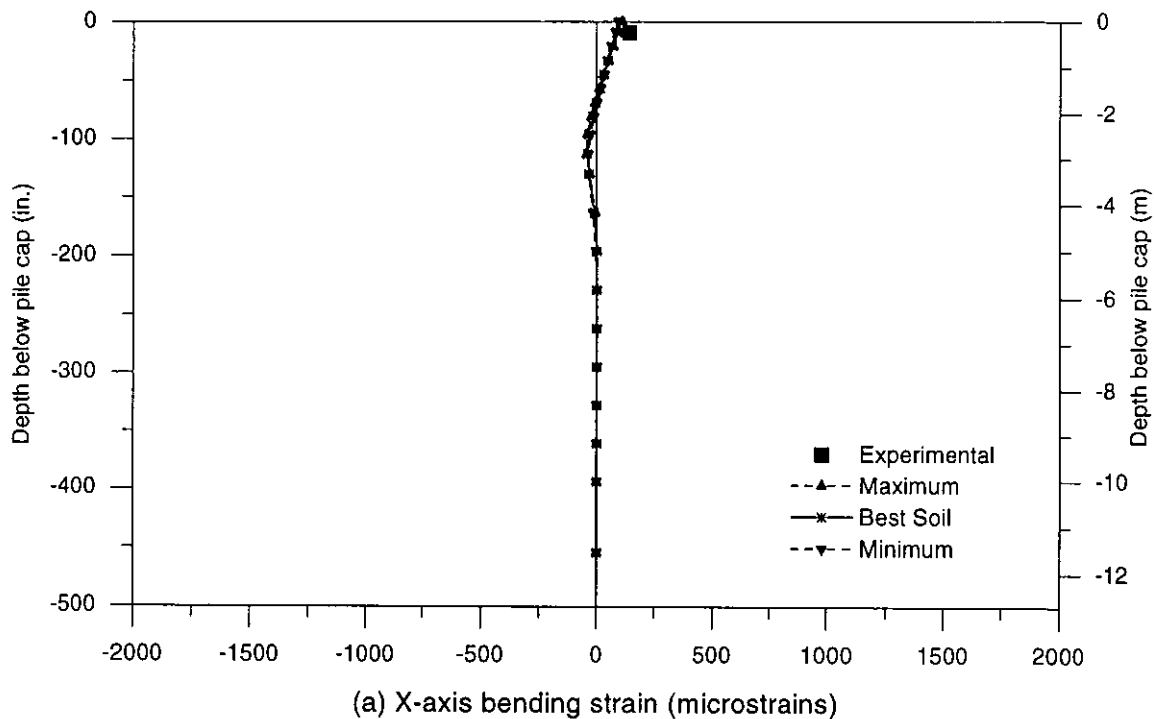
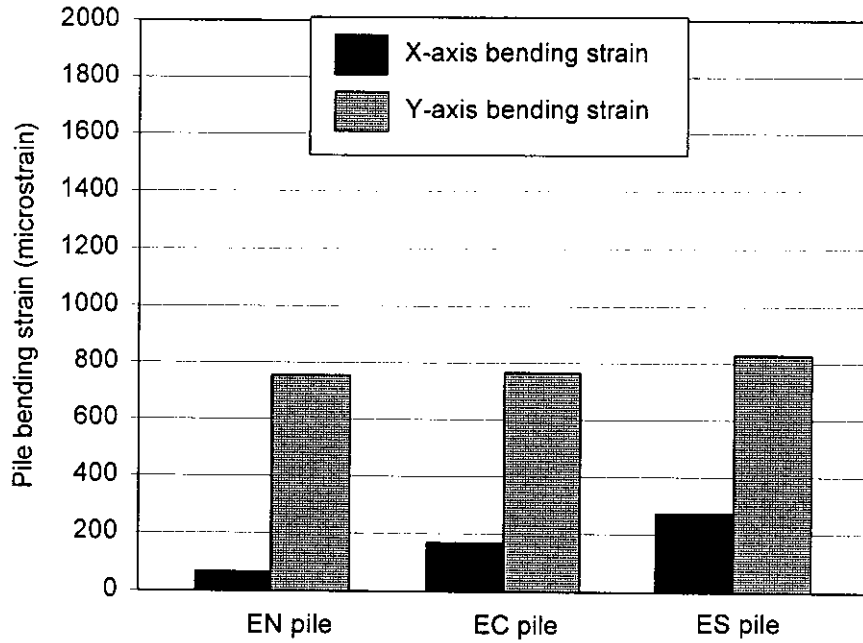
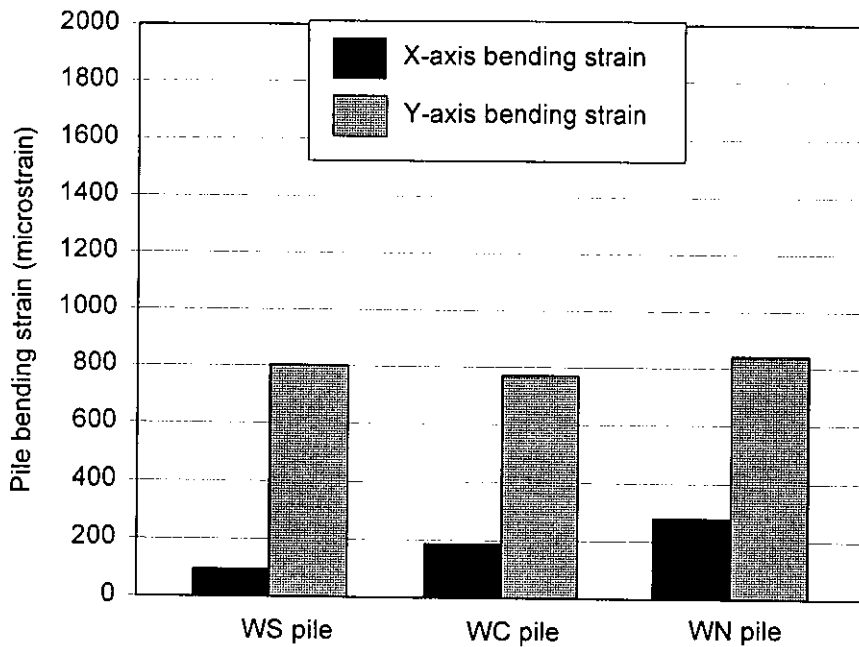


Figure 7.7. Strain variation with along the length of the north pile in the east abutment at the Story County Bridge (Story, Series-B models)



(a) East abutment



(b) West abutment

Figure 7.8. Maximum flexural-bending strains predicted for the abutment piles at the Story County Bridge

Since the difference between the longitudinal abutment displacements at the Story County Bridge was small, there was only a small difference between the flexural bending strains of the piles in the east and west abutments at the Story County Bridge. The maximum, combined, flexural-bending strain predicted in the south pile in the east abutment of the Story County Bridge was approximately 1100 microstrains. This predicted strain is only slightly less than the yield strain for A36 steel, which is about 1240 microstrains.

7.2.2 Pile axial strains

Axial strains that were predicted by the Story, Series-B models for three piles in the east abutment are shown in Figure 7.9. A compressive axial strain was predicted for the exterior abutment piles, while the interior pile had a negligible increase in axial strain. The maximum axial strain was located in the exterior pile in the east abutment at the acute-angle edge of the bridge deck, which was equal to a compressive strain of approximately 100 microstrains. Similar results were experimentally obtained by Lawver, French and Shield [13]. These researchers found that the axial strains in the exterior abutment piles decreased while the strain in an interior pile increased.

The experimentally measured axial strain for the piles at the Story County Bridge were questionable and were not compared with the analytical results shown in Figure 7.9. The dummy gage installed at the Story County Bridge produced strains that did not correlate with temperature after the first week of December 1998, and the results from this gage were considered unreliable after that time. Before this time, the experimentally measured axial strain ranges were generally less than 100

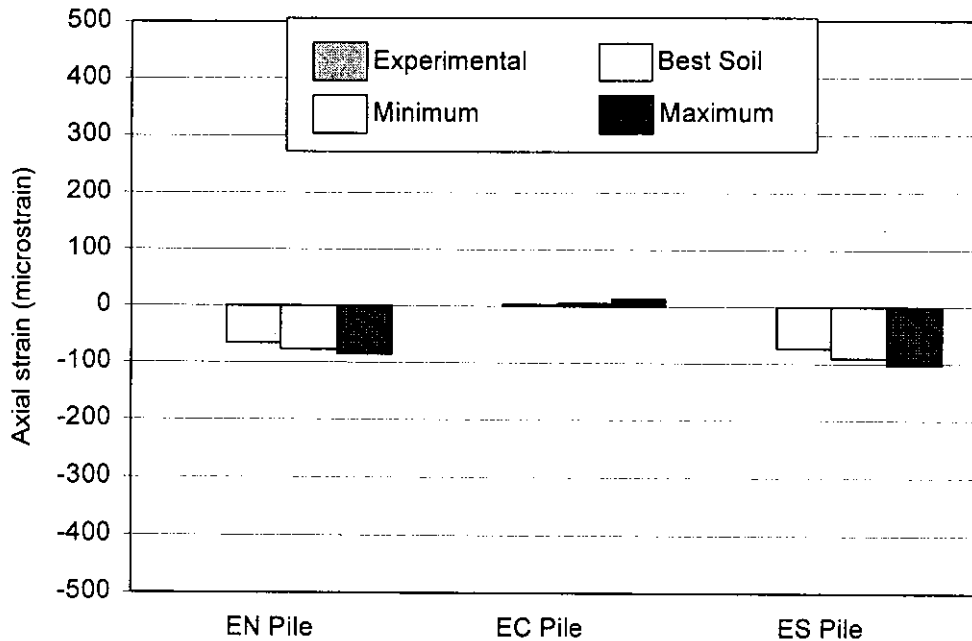


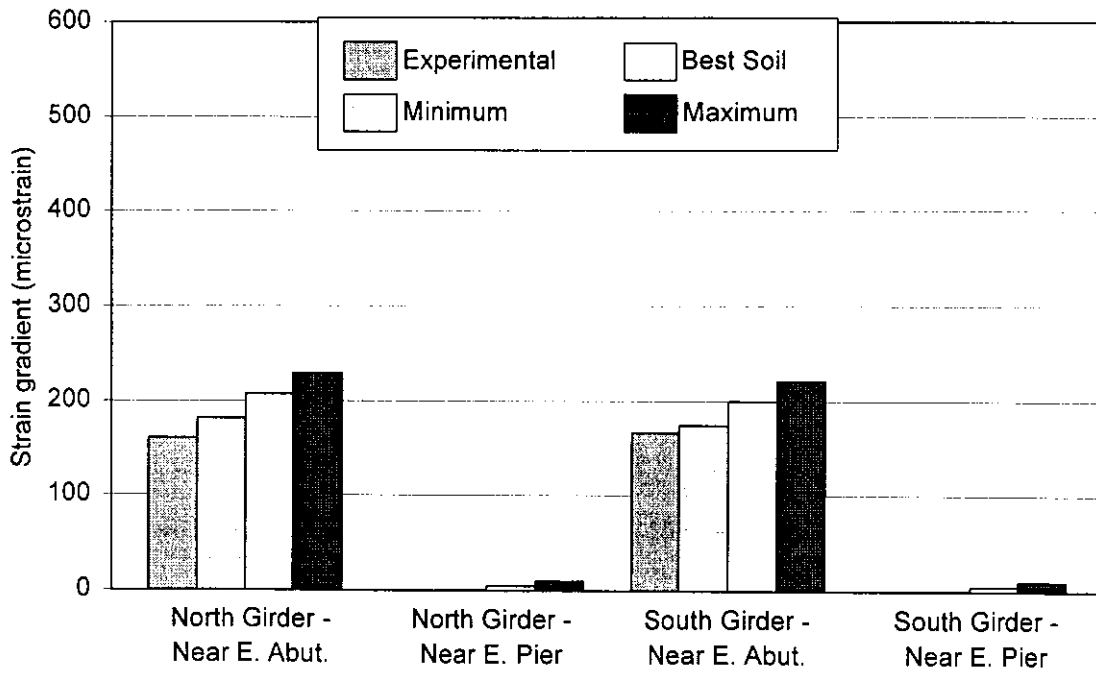
Figure 7.9. Predicted axial strains for the abutment piles at the Story County Bridge

microstrains. Daily variations of the pile axial strains were approximately 50 microstrains.

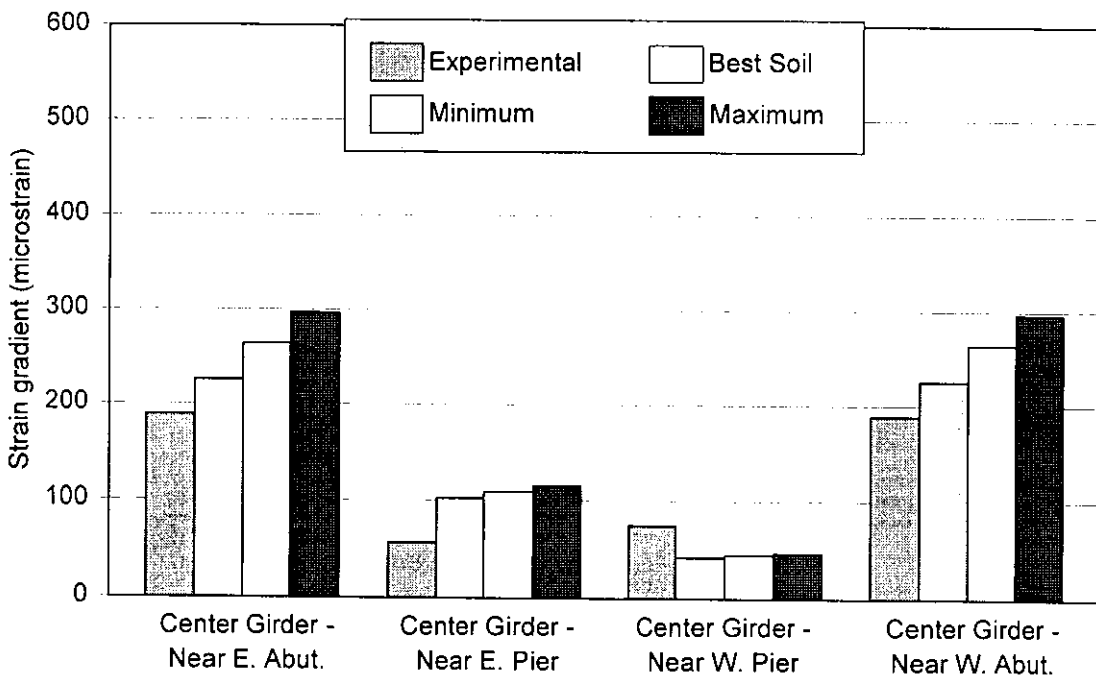
Unlike the Guthrie County Bridge, piles were not located under the abutment wingwalls at the Story County Bridge.

7.3 Girder strains

The analytically predicted and experimentally measured ranges for the PC girder total-strain gradients are shown in Figures 7.10 and 7.11. As was the case with the Guthrie, Series-A models, the Story, Series-A models overestimated the experimentally measured total-strain gradient in the PC girders. The strain gradient

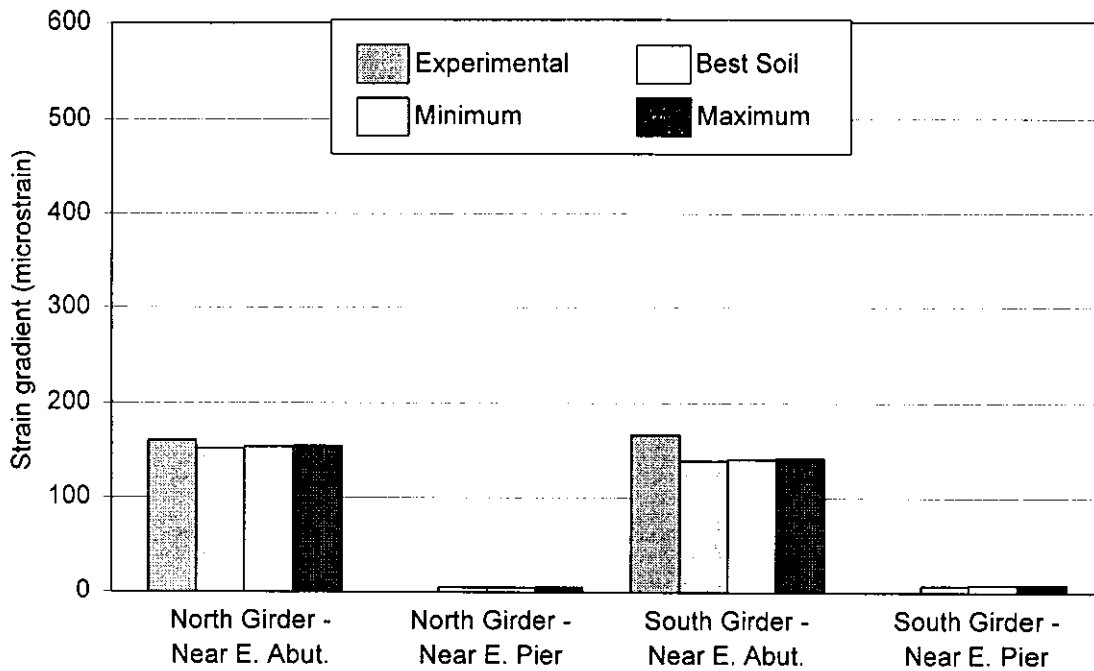


(a) North and South girder

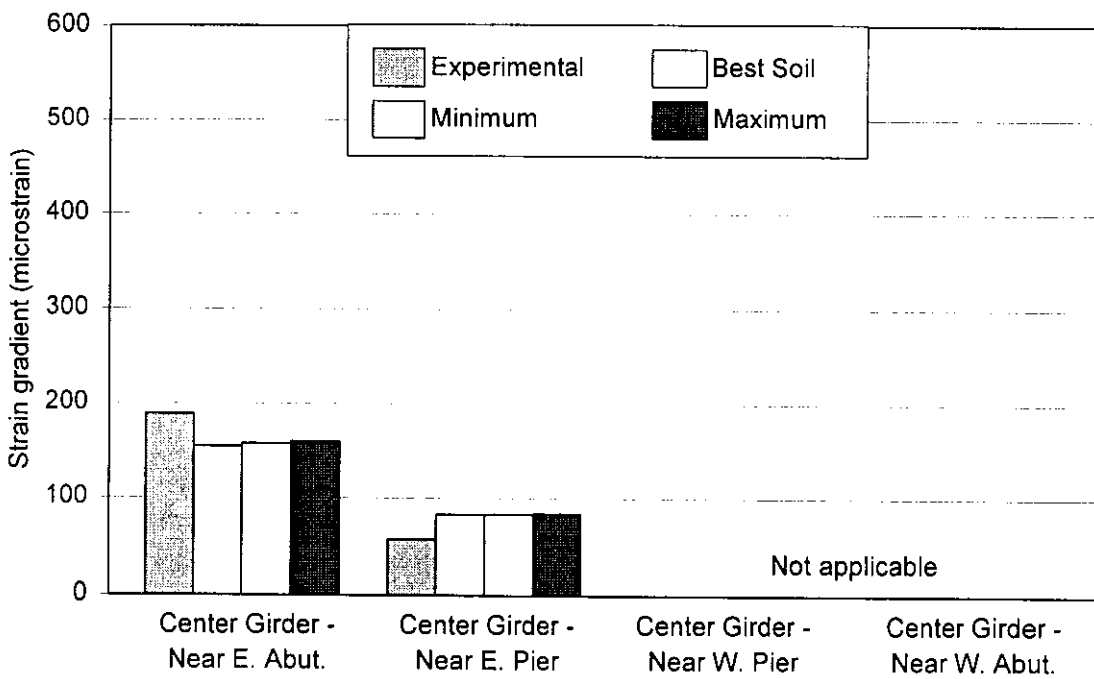


(b) Center girder

Figure 7.10. Comparison of the PC girder total-strain gradient predicted by the Story, Series-A models and the experimental measurements



(a) North and South girder

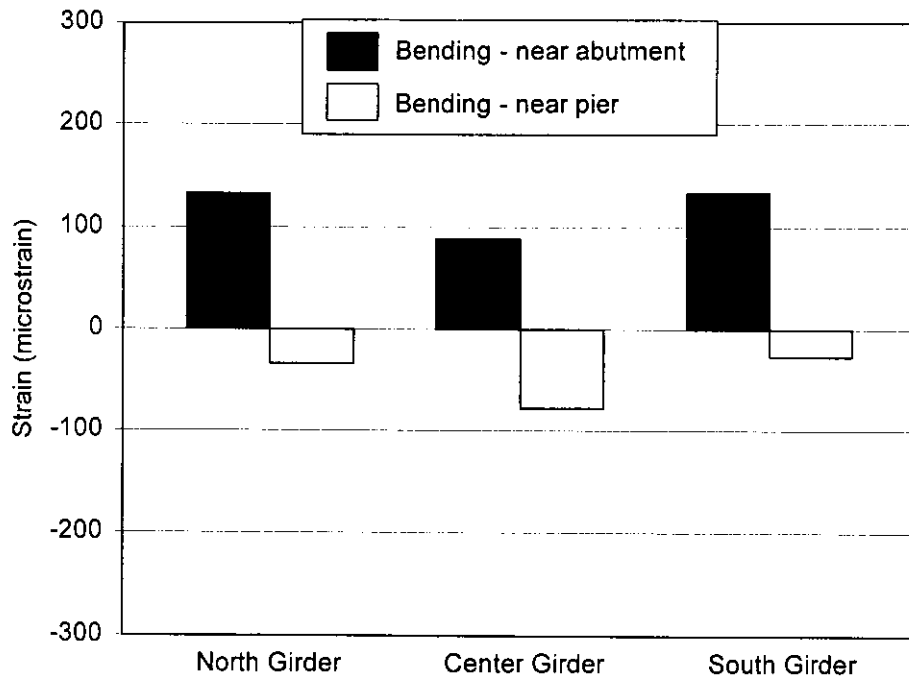


(b) Center girder

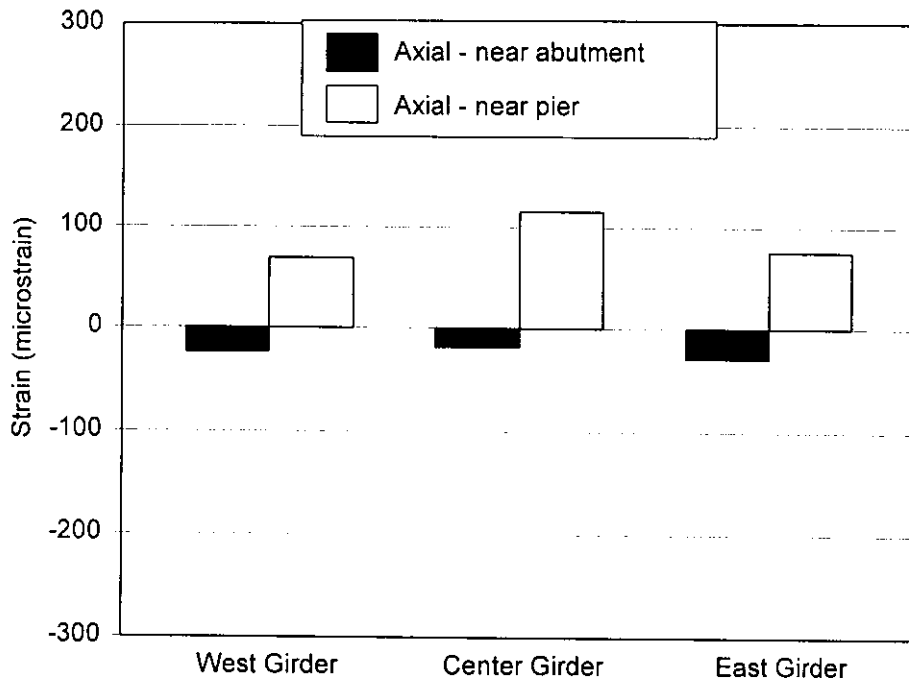
Figure 7.11. Comparison of the PC girder total-strain gradient predicted by the Story, Series-B models and the experimental measurements

in the PC girders is affected by the rotation of the abutment in a vertical plane parallel to the longitudinal axis of the bridge. Larger abutment rotations result in larger girder bending strain gradients. As shown in Figure 7.11, the total-strain gradient predicted by the Story, Series-B models had a better correlation with the experimentally measured total-strain gradients in the east span of the bridge than did those that were predicted Story, Series-A models. Since the abutment rotation was not experimentally measured at the west abutment, the abutment rotation could not be applied to this abutment and hence the Story, Series-B models could not be used to predict the girder strains in the west span.

Strains due to stress for the PC girders in the east span were predicted by the Story, Series-B models. The predicted girder strains due to stress are shown in Figure 7.12. The flexural-bending strains shown in Figure 7.12(a) are for the uppermost fiber in the top flange of the girders. In the Story finite-element models, the axial strains in the girder counteracted the bending strains at the top flange of the girders. The maximum combined strain due to stress predicted for the top flange was approximately 110 microstrains in tension, which is equivalent to a stress of about 0.450 ksi. The axial strains were additive with the flexural-bending strains at the bottom flange of the girder. The maximum combined strain due to stress predicted for the bottom flange was approximately 200 microstrain in compression, which is equivalent to a stress of about 0.800 ksi.



(a) X-axis bending strains



(b) Axial strains

Figure 7.12. Girder strains due to stress in the east span as predicted by the Story, Series-B, Best-Soil model

8 SUMMARY, CONCLUSIONS AND RECOMMENDATIONS

8.1 Summary

Two, in-service, skewed, integral abutment bridges subjected to thermal expansion and contraction were studied. The research program involved an experimental monitoring program and a finite-element analysis study for the integral-abutment bridges that were located in Guthrie and Story Counties in the State of Iowa. Field instrumentation included devices that measured bridge temperatures, displacements, and strains as the bridges experienced daily and seasonal changes in temperature. Presented in this thesis is the experimental data that was collected and analyzed for a period of 27 and 12 months at the Guthrie County Bridge and Story County Bridge, respectively. Finite-element models were created for each bridge using the ANSYS finite-element analysis program. The experimentally measured bridge temperatures were applied to the analytical bridge models. The soil stiffness behind the abutment and surrounding the piles was adjusted until the predicted abutment displacements matched the experimental abutment displacements. Analytically predicted pile and girder strains were compared with the experimental measurements to determine the validity of the finite-element models. These models were used to predict maximum pile and PC girder strains due to the thermal loading at the Guthrie and Story County Bridges.

8.2 Conclusions

The experimentally measured range in the average bridge temperatures was 113°F (63°C) and 114°F (63°C) for the Guthrie County Bridge and the Story County Bridge, respectively. Significant vertical temperature gradients were measured through the depth of the superstructure during the summer months. Slightly negative vertical temperature gradients were observed overnight during the winter months, i.e., the top of slab temperature was lower than the girder temperature.

Experimentally measured changes in bridge length correlated well with the change in average bridge temperature. Unsymmetrical longitudinal abutment displacements were measured at both bridge sites, with a significant difference observed at the Guthrie County Bridge. The range of the north abutment longitudinal displacement was twice as large as that measured at the south abutment. At the Story County Bridge, the west abutment displaced approximately 25% further than the east abutment over the 12-month measurement cycle. Plan-view rotation of the south abutment was noted at the Guthrie County Bridge. Both bridges, transverse abutment displacements were small compared to the longitudinal abutment displacements. The transverse movement of the south abutment at the Guthrie County Bridge was toward the obtuse-angle edge of the abutment. Small abutment rotations in a vertical plane were measured at both bridges. Also, small superstructure displacements over the pier caps were recorded at both bridges. Daily variations of the relative displacement of the superstructure over the pier caps were larger in the summer than in the winter.

Strain gages installed at the bridge sites indicated that the HP-shaped steel piles and the PC girders developed flexural-bending strains as a result of the daily and seasonal thermal movements of the bridges. Biaxial, flexural-bending strains were noted in the monitored abutment piles at each bridge. The magnitudes of the flexural-bending strains had a good correlation with the magnitudes of the abutment displacements. Combined, flexural-bending strains measured at 9 in. (230 mm) below the pile cap approached the yield strain of A36 steel. These strains combined with the axial strains induced by the dead load of the superstructure indicate that compression yielding has developed in a pile cross section. The strain gages installed on the PC girders indicated that the girder curvature was larger near the abutments than near the piers.

With the exception of the electrical-resistance strain gages installed on the abutment piles, the instrumentation used for the experimental field studies performed well. For the strain gages on the abutment piles, much of the strain gage wiring had been infiltrated with moisture that caused erroneous strain readings. The vibrating-wire strain gages installed on the PC girders at the Story County Bridge were very reliable over the duration of the experimental monitoring. The string-potentiometer, displacement transducers mounted on the post benchmarks provided an effective method for measuring abutment displacements for long-term studies.

Longitudinal displacements predicted by the finite-element models were successfully calibrated using the corresponding experimental displacement measurements. The lateral stiffness of the soil backfill behind the abutments was approximately equal to the lateral stiffness of a medium-dense, granular backfill as

defined by Clough and Duncan [14]. A good correlation was obtained between the analytically predicted and experimentally measured relative displacements at various locations on the bridges. However, the finite-element models overestimated the abutment rotation in the vertical plane parallel to the longitudinal direction of the bridge.

The finite-element predictions for the pile strains had a good correlation with the experimentally measured pile strains. The flexural-bending strains in the abutment piles were the largest at the pile cap, decreasing in magnitude along the pile length. Translation of the abutment created double-curvature bending in the piles. An inflection point in the elastic curve for the displaced pile was predicted to occur approximately 60 in. (1500 mm) below the bottom of the pile cap. At the Guthrie County Bridge, the predicted, combined, flexural-bending strains in one of the flanges of the piles at the abutment pile cap exceeded the minimum yield strain for A36 steel. The predicted, combined, flexural-bending strains in one of the flanges for each of the abutment piles at the Story County Bridge were approximately equal to the minimum yielding strain for A36 steel. When the axial strain induced by the dead load of the bridge is included in the total strain for the piles, a portion of the abutment pile cross-section yields in compression. Except for the wingwall piles in the Guthrie County Bridge, the axial strains in the abutment piles that were induced by the thermal movements of the abutments were small. However, significant axial compressive strains were predicted for the wingwall piles when thermal expansion occurred for this bridge.

A good correlation was achieved between the analytically predicted and experimentally derived strain gradients in the PC girders. The finite-element models were used to predict strains due to stresses in the PC girders. Larger flexural-bending strains occurred in the PC girders near the abutments than near the piers. The maximum concrete strain in the PC girders induced by the thermal bridge movements was approximately 200 microstrains.

8.3 Recommendations

For the Story County Bridge, the filtering and analysis of the experimental data needs to be completed for the monitoring period from July 1999 to April 2000. A final report containing the final experimental results will be presented to the Iowa Department of Transportation in the fall of 2000. A design model for integral abutment bridges with steel HP-shaped abutment piles and PC girders will be presented in that report.

Since only two bridges were instrumented, these results cannot be considered representative of all integral-abutment bridges of similar geometry. Further experimental studies can contribute to a better understanding of these types of bridges. Other integral-abutment bridges that could be investigated include bridges with: steel girders, different total length and span lengths, different skew angles, and abutments supported by PC piles. Strains induced in the piles supporting the abutment wingwalls should be experimentally monitored. Steps should be taken in future long-term monitoring projects to minimize gage loss. Moisture infiltration needs to be prevented at the location of the strain gages and at

any splices in the wiring for any instrumentation device. Additional information could be obtained through the use of soil pressure transducers to measure soil pressures acting on the abutment wall and on embedded piles. The use of these types of gages is limited, since they need to be installed before the backfill has been placed.

Future finite-element studies of integral-abutment bridges should focus on the soil interaction with the abutment wall and the abutment piles. More information about the in-situ backfill soil behind the abutment and the soil surrounding the piles should be obtained for future finite-element studies. Non-linear soil springs to model the lateral stiffness of the soil should be incorporated into finite-element models. A more in-depth analysis should be investigated regarding the abutment rotation in the vertical plane parallel to the longitudinal direction of the bridge. To determine the effect on the bridge displacements and induced strains in the bridge members, other parameters should be investigated, including: varying the bridge geometry, varying the α -coefficient of the concrete members, varying the thermal loading conditions, and incorporating steel girders instead of PC girders.

APPENDIX A - EXPERIMENTAL MONITORING PROGRAM

The following section details the experimental monitoring program used at the Guthrie County Bridge and the Story County Bridge, which is taken directly from Chapter 3 of the thesis written by Matt Thomas [26]. This excerpt is reproduced with the permission of Matt Thomas.

A.1 Overview

The primary objective of the research was to measure thermal movements of two bridge superstructures and strains in bridge elements due to restraints imposed by soil and structure indeterminacy. Two bridges were instrumented to measure the in-service displacements and stresses caused by thermal loading. The instrumentation installed at each bridge site consisted of displacement transducers and a tiltmeter to measure bridge movements, strain gages to measure strains, and thermocouples to measure temperature.

A.1.1 Bridge selection

The bridges selected for the field study needed to satisfy many criteria. The desirable characteristics for the bridges included:

- U-shaped integral abutment pile arrangement for one bridge
- Straight integral abutment pile arrangement for one bridge
- Prestressed concrete girders
- HP-shaped steel piling
- Long bridge length – for maximum abutment displacements

- High skew angle – for maximum transverse movements
- Low flooding potential – to minimize risk to electronic instrumentation
- Symmetry – less instrumentation required if behavior was symmetric
- Low traffic volume – to minimize disturbance of traffic during instrumentation installation and to minimize traffic effects on data readings
- Earth berm – for easier access to the abutment piles
- Reasonably close proximity to Iowa State University

The Iowa Department of Transportation database of bridges on the primary road system was searched and a letter was written to each of the 99 county engineering offices in Iowa requesting potential to identify all possible integral abutment bridges for the field study. Site visits were made to several potential bridges. The two selected bridges had the best combination of favorable attributes and satisfied the project requirements concerning the abutment pile configuration and PC girder construction.

A.1.2 Bridge descriptions

Both of the selected bridges were county bridges in central Iowa on the secondary roads system. The first bridge that was instrumented was located in Guthrie County, just south of the town of Panora on Route P28 and crossing the Middle Raccoon River. The second bridge that was instrumented for this project was located just northwest of Ames in Story County on Route E26 over Squaw Creek.

The Guthrie County Bridge is a three span, continuous, PC girder bridge with a right-ahead skew of 30° and total length of 318 ft (96.93 m). This bridge has a U-shaped abutment pile arrangement with a single row of 10 HP10x42 steel piles under the backwall and an HP10x42 pile under each wingwall. The piles under the backwall were oriented with their webs parallel to the abutment face. The wingwall piles were oriented with the webs perpendicular to the bridge longitudinal axis. The piles were to be driven to shale bedrock and to a depth of at least 45 ft at the south abutment and 40 ft at the north abutment. Prebored holes filled with a bentonite slurry were specified for the piles at this bridge. The two Tee-shaped piers are supported by a RC footing keyed into shale bedrock. At the south pier, the bridge superstructure rests on 3.75 in.-thick steel-reinforced neoprene pads. The partial-height pier diaphragm at this pier does not extend down to the top of the pier. At the north pier, the pier diaphragm was cast into a keyway that was lined with expansion joint filler. The superstructure is supported by thinner, 1 in.-thick, neoprene pads at this pier. A summary of the geometric characteristics of the Guthrie County Bridge is provided in Table A.1.

The Story County Bridge is a three span, 201 ft - 4 in. (61.36 m), continuous, PC girder bridge with a right-ahead skew of 15° . Each abutment is supported on a single row of seven HP10x42 steel piles, oriented with the webs parallel to the abutment face. The wingwalls are cantilevered straight back of the abutment backwall. The abutment piles were to be driven to bedrock or a minimum of 34

Table A.1. Characteristics of the instrumented bridges

	GUTHRIE COUNTY BRIDGE	STORY COUNTY BRIDGE
Total bridge length	318 ft. - 0 in. (96.9 m)	201 ft. - 4 in. (61.4 m)
Spans	105.75, 106.5, 105.75 ft. (32.2, 32.5, 32.2 m)	64.08, 73.17, 64.08 ft (19.5, 22.3, 19.5 m)
Skew	30°	15°
Abutment pile arrangement	U-shaped	Single row
# of piles per abutment	12	7
Bridge orientation	North-south	East-west
PC girders (number/type)	5 girders, Iowa D	5 girders, Iowa C
Pier type	Tee pier	Pedestal pier
Bridge width	30 ft. (9.1 m)	30 ft. (9.1 m)

tons/pile. The specified length of the abutment piles was 40 ft. Eight foot deep prebored holes filled with sand were provided for each abutment pile. The pedestal-type piers consisted of a single line of 12 HP10x42 steel piles encased by concrete. The bridge superstructure was supported at the piers by 1 in.-thick, neoprene pads. The full-depth pier diaphragms were cast into keyways in the pier cap that were lined with expansion joint filler. A summary of the geometric characteristics of the Story County Bridge is included in Table A.1.

A.1.3 Instrumentation packages

To quantify the displacements and stresses experienced by the bridges and their foundations due to thermal loads, instrumentation packages for long term field monitoring were developed. The instrumentation devices chosen for the project were selected to provide meaningful and useful information about the in-service

Table A.2. Summary of experimental results obtained

MEASUREMENT	GUTRIE COUNTY BRIDGE	STORY COUNTY BRIDGE
Longitudinal abutment displacements	Each abutment	Each abutment
Transverse abutment displacements	One abutment	One abutment
Strains in steel piling	Five piles	Four piles
PC girder strains	Eight locations	Six locations
Displacements of a pile relative to RC pile cap	One pile location	One pile location
Vertical temperature gradient through superstructure	12 locations	14 locations
Relative displacements of bridge superstructure over piers	Each pier	Each pier
Concrete strains in pile cap	One abutment	One abutment

behavior of the integral abutment structure. Table A.2 lists the effects that were measured for each bridge.

To measure bridge movements, string-type displacement transducers and a tiltmeter were used at each bridge site. Several displacement transducers were mounted on benchmark posts that were installed to measure absolute abutment displacements. Displacement transducers were also mounted on the bridge structures to record differential displacements between bridge elements. Weldable, electrical-resistance strain gages were applied to the steel, HP-shaped abutment piles at each bridge to measure bending strains in the piles. Electrical-resistance and vibrating-wire strain gages were mounted on several PC bridge girders to measure axial and bending strains. These strain gages were also applied to the bridge superstructure to measure the concrete temperature. These measurements

were used to establish an average bridge temperature and the temperature distributions in the bridge. A data acquisition system for each bridge remotely and automatically recorded data for each instrumentation device at selected time intervals. Table A.3 shows the number of each type of instrument installed at each bridge site.

The instrumentation devices are described more thoroughly in Sections A.2 through A.4. To individually identify all of the instruments installed at each bridge, each instrument was assigned an acronym-based code name. The first part of the code refers to the instrument type and the remaining letters or numbers indicate the location of the instrument on the bridge or the type of measurement. For example, the name SP-ENL described the **S**tring **P**otentiometer installed at the **E**ast abutment under the **N**orth girder measuring **L**ongitudinal displacements.

Table A.3. Number of instrumentation devices installed for field monitoring

INSTRUMENT TYPE	NUMBER OF INSTRUMENTS INSTALLED AT THE:	
	Guthrie County Bridge	Story County Bridge
Displacement transducers	16	11
Tiltmeters	1	1
Strain gages on piles	40	31
Strain gages on PC girders	16	12
Strain gages on pile cap	5	4
Thermocouples	43	46
Total	121	105

A.2 Displacement transducers

At each bridge, longitudinal displacements (translations parallel to the longitudinal axis of the bridge) of one abutment were measured at three locations across the width of the backwall. Also, transverse displacements (translations perpendicular to the longitudinal axis of the bridge) of this abutment were measured at the ends of the backwall. Longitudinal displacements of the other abutment at each bridge were measured at the mid-width of the bridge. Displacement transducers were mounted on each bridge structure to record differential displacements between a pile and the pile cap of one abutment and between the center PC girder and the pier caps. Additional transducers were installed at the Guthrie County Bridge to measure differential displacement between center PC girder and the abutment backwall. A tiltmeter was mounted at the center of pile cap of one abutment of each bridge to measure rotations of the pile cap in the vertical plane parallel to the longitudinal axis of the bridge.

A.2.1 Guthrie County Bridge

Bridge movements at the Guthrie County Bridge were measured with sixteen, string-potentiometer, displacement transducers and a tiltmeter. Table A.4 lists the transducers and Fig. A.1 shows the location of these transducers for the Guthrie County Bridge. Nine of these transducers (SP-SW-LT, SP-SW-LB, SP-SC-LT, SP-SC-LB, SP-SE-LT, SP-SE-LB, SP-NC-L, SP-SW-T, and SP-SE-T) were used to measure absolute displacements of the abutments. These transducers were mounted on benchmark posts that were installed about 10 ft from the bridge abutments. To verify the stability of one of the benchmark posts, a displacement

Table A.4. Transducers at the Guthrie County Bridge

INSTRUMENT CODE	LOCATION	MEASUREMENT
SP-SW-LB	South abutment at West end	Longitudinal movement at Bottom of pile cap
SP-SC-LT	South abutment at Center of width	Longitudinal movement at Top of pile cap
SP-SC-LB	South abutment at Center of width	Longitudinal movement at Bottom of pile cap
SP-SE-LB	South abutment at East end	Longitudinal movement at Bottom of pile cap
SP-NC-L	North abutment at Center of width	Longitudinal movement of pile cap
SP-SW-T	South abutment at West edge	Transverse movement of pile cap
SP-SE-T	South abutment at East edge	Transverse movement of pile cap
SP-SC-LV	South abutment near Center of width	Relative Longitudinal displacement between benchmark posts for Verification
SP-SC-RGT	South abutment at Center girder	Relative displacement between abutment backwall and Girder Top flange
SP-SC-RGB	South abutment at Center girder	Relative displacement between abutment backwall and Girder Bottom flange
SP-SC-RPB	South abutment at Center of width	Relative displacement between Pile cap Back and pile
SP-SC-RPF	South abutment at Center of width	Relative displacement between Pile cap Front and pile
SP-SP-RPL	South Pier	Relative movement of superstructure over south Pier along Longitudinal axis
SP-NP-RPL	North Pier	Relative movement of superstructure over north Pier along Longitudinal axis
TM-SC-LR	South abutment at Center of width	Longitudinal Rotation of the south abutment pile cap

transducer (SP-SC-LV) was installed to measure any differential longitudinal movement between two posts. The remaining six displacement transducers (SP-SC-RGT, SP-SC-RGB, SP-SC-RPB, SP-SC-RPF, SP-SP-RPL, SP-NP-RPL) were mounted on the bridge structure to record differential displacements between bridge elements. The tiltmeter (TM-SC-LR) was mounted at the center of the south abutment pile cap to measure rotations in the vertical plane parallel to the longitudinal axis of the bridge.

Abutment rotations were also measured using the pairs of post-mounted displacement transducers measuring absolute longitudinal displacements of the top and bottom of the pile cap. Two of these displacement transducers (SP-SE-LT and

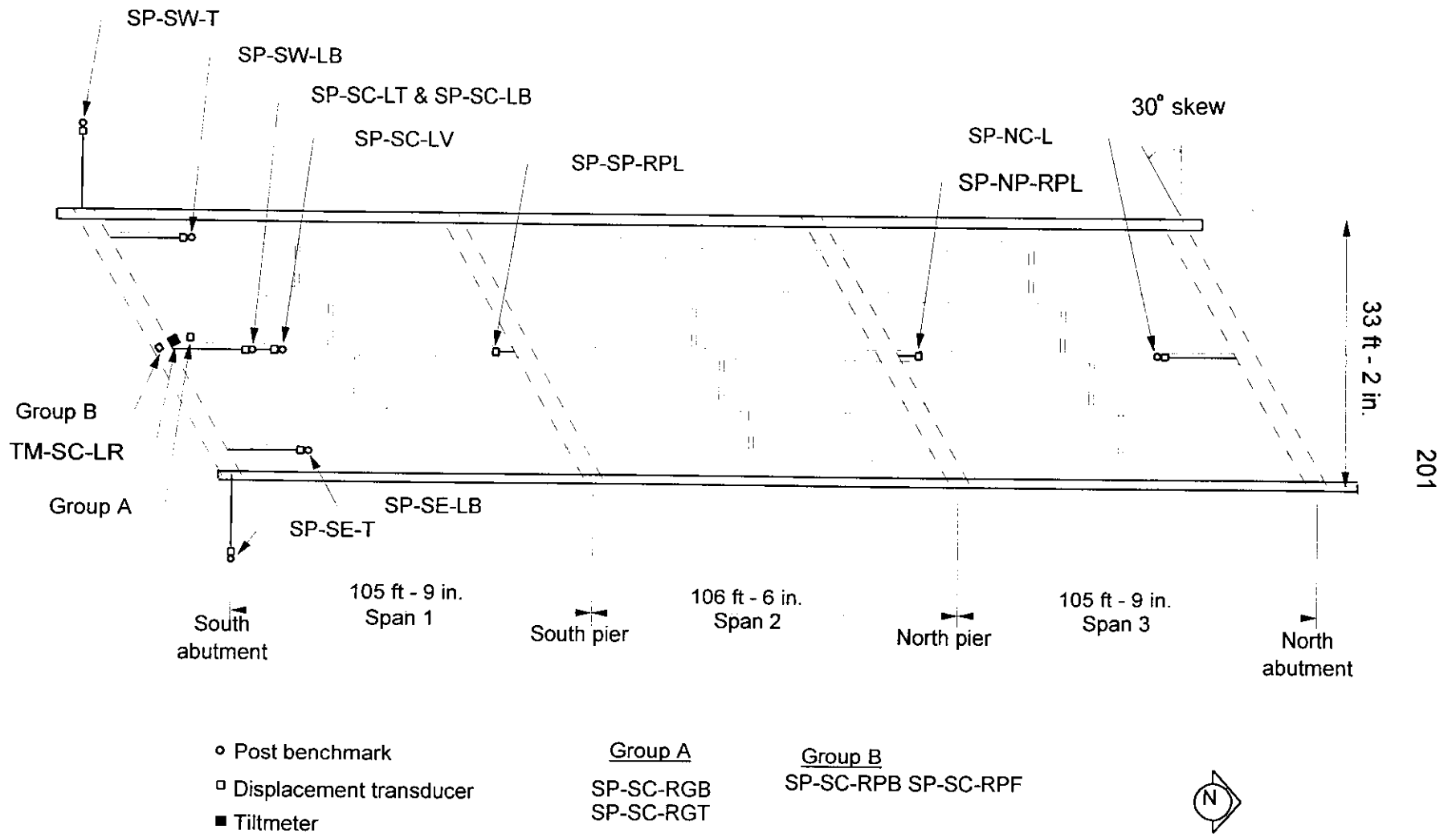


Figure A.1. Displacement transducer locations at the Guthrie County Bridge (not to scale)

SP-SW-LT) were removed in July 1999, because of concerns about the validity of this method for determining the abutment rotations. To compare the abutment rotation measurements obtained with the tiltmeter, the pair of displacement transducers at the midwidth of the south abutment (SP-SC-LT and SP-SC-LB) were monitored for the duration of the experimental program.

A.2.2 Story County Bridge

Eleven, string-potentiometer, displacement transducers and a tiltmeter were installed at the Story County Bridge to measure bridge displacements. Table A.5 lists the transducers and Figure A.2 shows the location of the transducers for the Story County Bridge. Six of these displacement transducers (SP-EN-L, SP-EC-L, SP-ES-L, SP-WC-L, SP-EN-T, and SP-ES-T) were used to measure displacements of the abutments. These transducers were mounted on benchmark posts that were

Table A.5. Transducers at the Story County Bridge

INSTRUMENT CODE	LOCATION	MEASUREMENT
SP-EN-L	East abutment, North end	Longitudinal movement of pile cap
SP-EC-L	East abutment, Center	Longitudinal movement of pile cap
SP-ES-L	East abutment, East end	Longitudinal movement of pile cap
SP-WC-L	West abutment, Center	Longitudinal movement of pile cap
SP-EN-T	East abutment, North edge	Transverse movement of pile cap
SP-ES-T	East abutment, South edge	Transverse movement of pile cap
SP-EC-LV	East abutment, Center	Relative Longitudinal displacement between benchmark posts for Verification
SP-EC-RPB	East abutment, Center	Relative displacement between Pile cap Back and pile
SP-EC-RPF	East abutment, Center	Relative displacement between Pile cap Front and pile
SP-EP-RPL	East Pier	Relative movement of superstructure over east Pier along Longitudinal axis
SP-WP-RPL	West Pier	Relative movement of superstructure over west Pier along Longitudinal axis
TM-EC-LR	East abutment, Center	Longitudinal Rotation of the pile cap

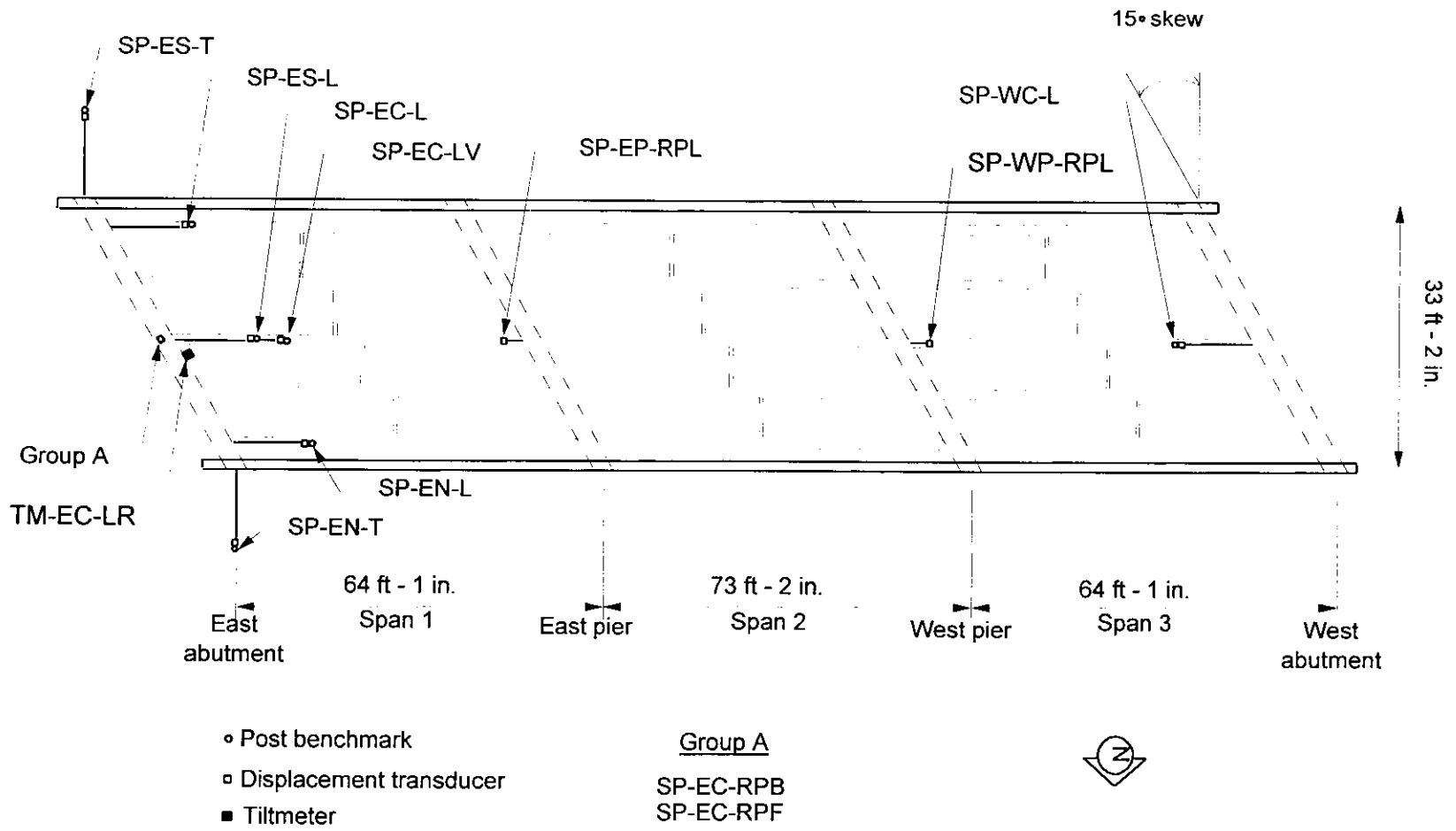


Figure A.2. Displacement transducer locations at the Story County Bridge (not to scale)

installed near the bridge abutments. To verify the stability of one of the benchmark posts, a displacement transducer (SP-EC-LV) was installed to measure any differential movement between two adjacent posts. The remaining four displacement transducers (SP-EC-RPB, SP-EC-RPF, SP-EP-RPL, SP-WP-RPL) were mounted on the bridge structure to record differential displacements between bridge elements. The tiltmeter (TM-EC-LR) was mounted at the center of the east abutment pile cap to measure rotations in the vertical plane parallel to the longitudinal axis of the bridge.

A.2.3 Transducers mounted on benchmarks

Each post-mounted transducer was firmly bolted to a benchmark post and its sensor cable was linked to a bridge abutment with a steel wire. As a bridge abutment moved relative to a benchmark post, the displacement was measured by the transducer sensor wire moving into and out of the transducer.

For the longitudinal displacement measurements at the south abutment of the Guthrie County Bridge, the transducer wires for SP-SW-LT, SP-SC-LT, and SP-SE-LT were attached to the abutment at approximately 3 in. from the top of the pile cap. The wires for SP-SW-LB, SP-SC-LB, and SP-SE-LB were attached at approximately 3 in. above the bottom of the pile cap. The vertical distance between the transducer wires allowed for the determination of pile cap rotations in a plane parallel to the longitudinal axis of the bridge. The wires for the displacement transducers measuring transverse displacements of the south abutment and longitudinal displacements of the north abutment at the Guthrie County Bridge were attached at

the mid-height of the pile cap. At the Story County Bridge, all of the abutment displacement measurements were made at the mid-height of the pile cap.

For each bridge site, the benchmark posts consisted of a steel pipe supported by a concrete foundation. Fig. A.3 shows a typical longitudinal cross section near an abutment. The top of the concrete foundation for a benchmark post was 3 to 4 ft below grade. The steel posts were surrounded by a 12-in. diameter, corrugated plastic pipe that was filled with batt insulation to prevent the soil backfill from contacting the steel posts and to insulate the post footing. To protect the transducers and extension wires from vandalism and weather, the post-mounted transducers were enclosed by wood housings.

The steel posts that held the transducers that measured transverse movements of the south abutment of the Guthrie County Bridge were installed by first drilling with a truck-mounted auger a 16-in. diameter hole to a depth of about 10 ft. Then, concrete for these post foundations was cast in the hole to a depth of about 5 ft below grade and the steel post was placed in the fresh concrete. These posts were also isolated from the surrounding soil by the technique previously described.

To check the stability of one of the benchmark posts that supported a transducer that measured longitudinal bridge movements, an additional post was installed approximately 4 ft from the post located under the center girder near the south abutment at the Guthrie County Bridge. A transducer was bolted to this additional post and the transducer string was attached to the post under the center girder. At the Story County Bridge, a similar installation was used under the center

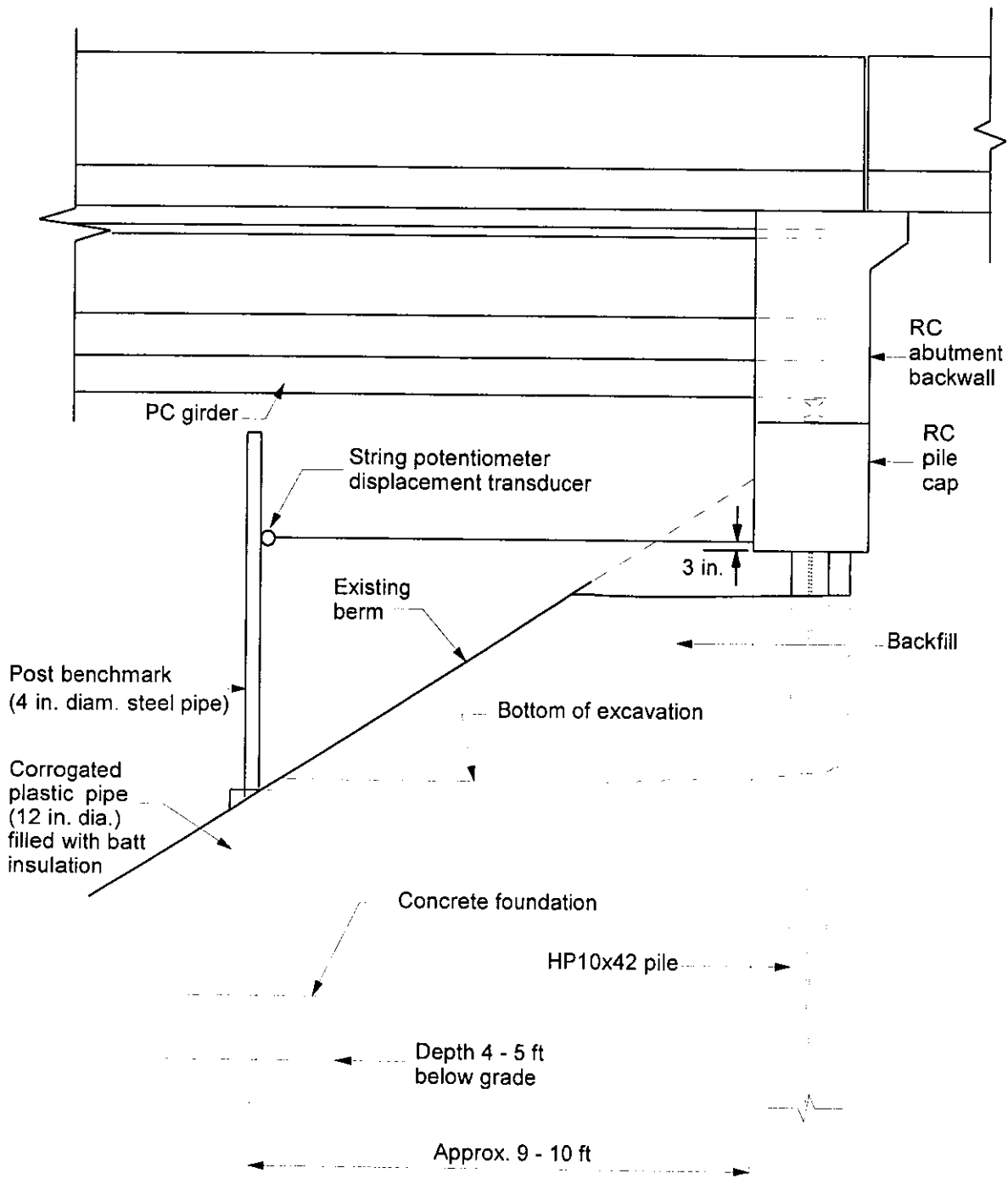


Figure A.3. Typical benchmark post installation (not to scale)

girder near the east abutment. Any differential displacement recorded by these transducers after correcting for the temperature-induced wire length change between the two posts would indicate some instability in one or both of the benchmark posts and transducer assemblies.

A.2.4 Transducers mounted to bridge

Relative longitudinal movements between the bridge superstructure and each pier were measured with displacement transducers that were mounted to the undersides of the center girders as shown in Figure A.4. When possible, a transducer wire was directly attached to the pier cap concrete using an eyehook and a concrete screw. However, at the south pier of the Guthrie County Bridge, the displacement transducer wire was hooked to a steel plate that had been glued and

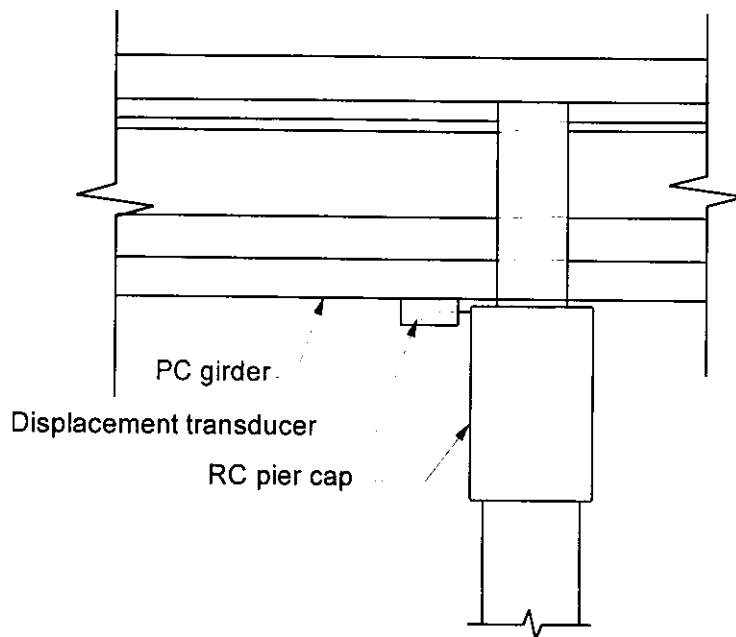


Figure A.4. Typical displacement transducer installation for the relative displacement measurements between the center girder and a pier cap

screwed to the vertical face of the pier cap. The 3.75 in.-thick, neoprene bearing pads below the PC girders at this pier created a gap between the bottom of the girder and the top of the pier cap. The steel plate served as an extension of the vertical face of the pier cap.

At the Guthrie County Bridge, differential displacements of the superstructure over the north pier were initially expected to be negligible; therefore, a displacement transducer was not initially installed at this pier. The bridge plans showed a full-depth pier diaphragm that was keyed into the pier cap. The drawings indicated that the north pier was a "fixed" pier, while the south pier was an "expansion" pier. However, longitudinal displacements at the north abutment were found to be larger than the longitudinal displacements at the south abutment. A displacement transducer (SP-NP-RPL) measuring any relative superstructure movement over the north pier of the Guthrie County Bridge was added on July 17, 1998.

At the Guthrie County Bridge, displacement transducers were installed on the top and bottom flanges of the center girder near the south abutment to measure relative movements of the PC girder with respect to the abutment backwall as shown in Fig. A.5. Each transducer was attached to the inside of a steel box and each box was attached to wood 2x6's that had been glued and screwed to the vertical face of one of the girder flanges. Relative displacements between a PC girder and a RC abutment backwall were not measured at the Story County Bridge.

At each bridge, two displacement transducers that were clamped to a pile measured relative vertical displacements between an abutment pile cap and a pile as shown in Fig. A.6. At the Guthrie County Bridge, the transducers were mounted

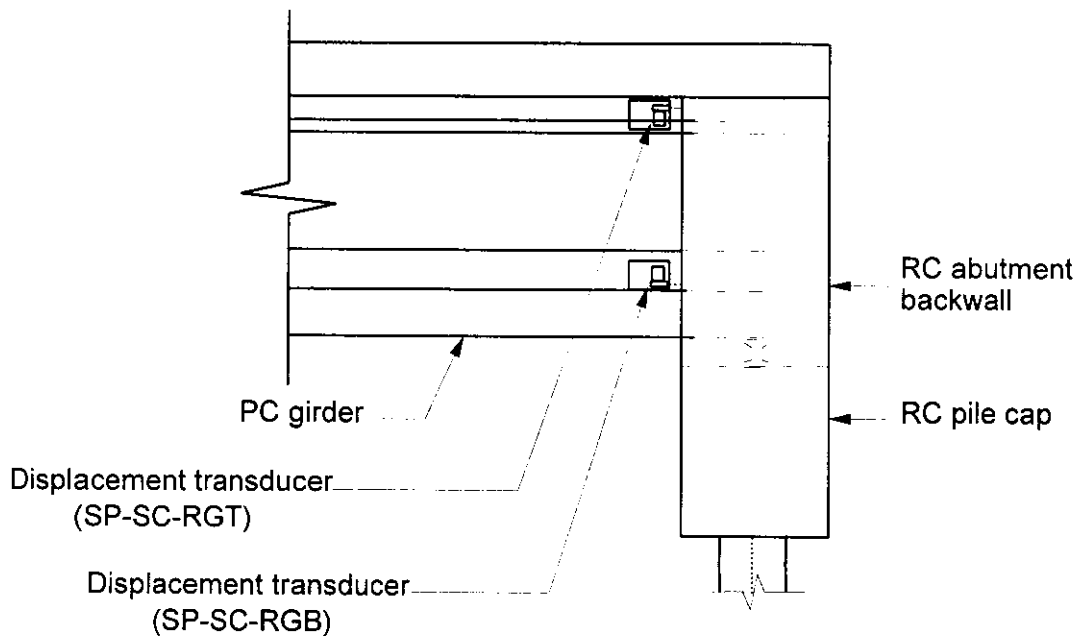


Figure A.5. Displacement transducer installation for the relative displacement measurements between the abutment backwall and a PC girder

to a pile near the mid-width of the south abutment. At the Story County Bridge, these transducers were mounted to the center pile under the east abutment. The horizontal separation between the two transducers allowed for the determination of the relative rotation between the pile and the pile cap in the vertical plane parallel to the longitudinal axis of the bridge.

A.3 Strain gages

Several types of strain gages were used to monitor strains in selected members of each bridge. Weldable, electrical-resistance, strain gages were applied to several steel HP-shaped abutment piles at each bridge. At the Guthrie County Bridge, bondable, electrical-resistance strain gages were applied to the flanges of selected PC girders and to the exposed face of an abutment pile cap. At the Story

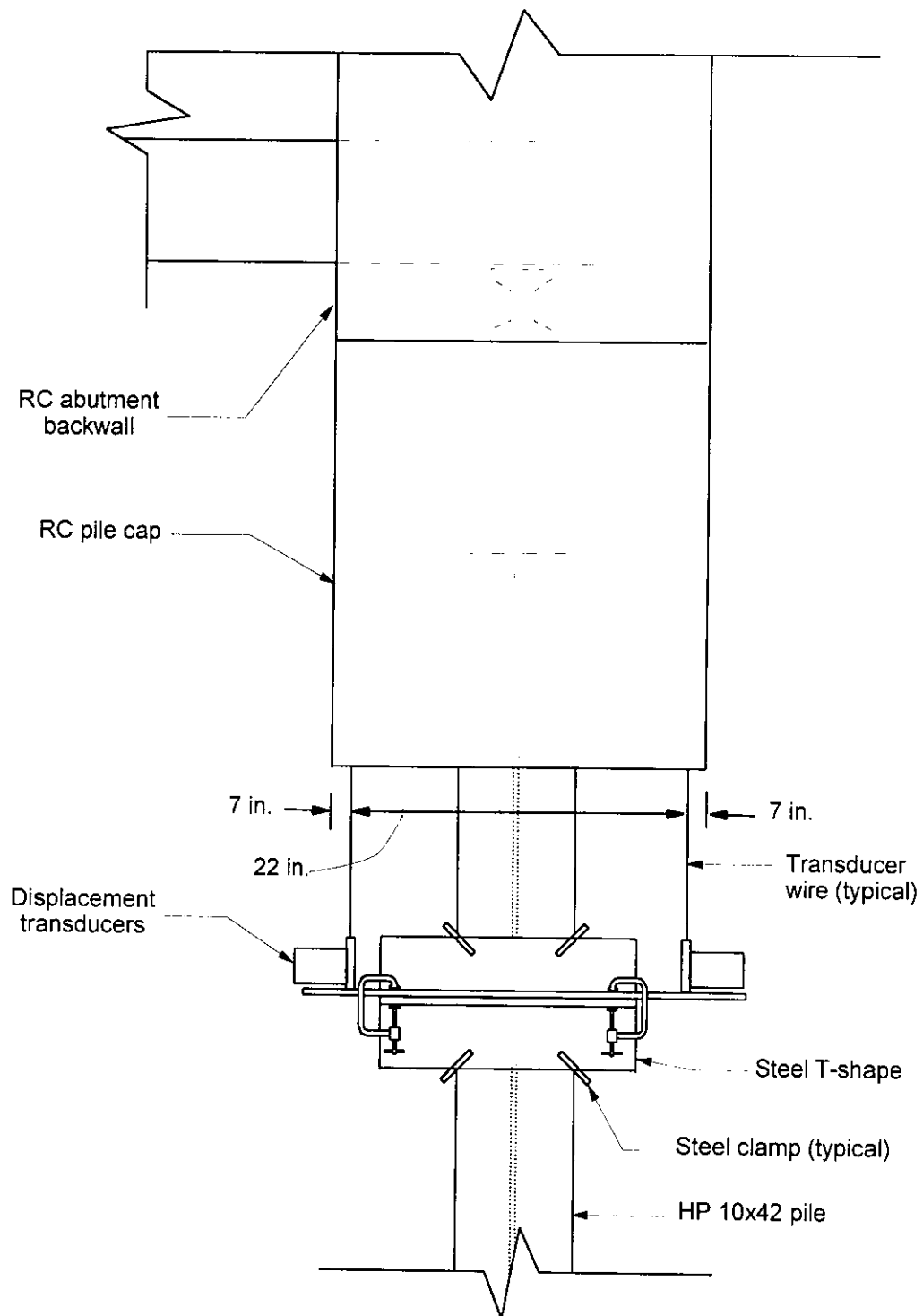


Figure A.6. Displacement transducer installation for the relative displacement measurements between the abutment pile cap and a HP10x42 steel pile

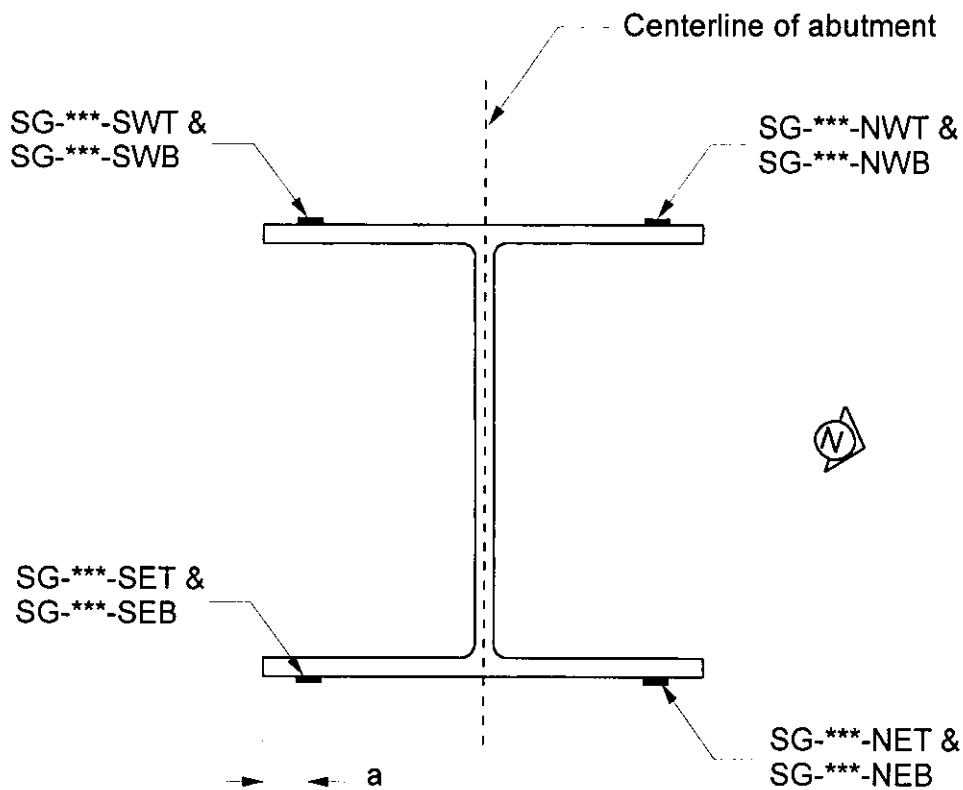
County Bridge, vibrating-wire, strain gages were used to measure strains in PC girders and in a pile cap.

Each abutment pile that was instrumented had a total of eight strain gages applied to the outside faces of the flanges near the flange tips as shown in Figure A.7. An arrangement of four strain gages was used at two cross sections that were located at 9 in. and 33 in. below the bottom of the pile cap. If four longitudinal pile strains are known at a pile cross section the x and y-axis bending, axial, and torsional strains can be evaluated at the monitored cross section. Strain gages were used at two pile cross sections to permit the determination of the moment gradient along the pile length.

The strain gages that were applied to selected PC girders were located at 5 ft from the face of support at each end of the girders. These gages were positioned at the mid-height of the top and bottom flanges. If the longitudinal girder strains are known at two points on a girder cross section the axial and bending strains can be calculated at those two points. The strain gages that were applied to the pile caps were mounted in a single line at the mid-height of the pile cap and at a spacing equal to one-half of the pile spacing. The gages were used to determine if there was significant horizontally bending deformation in the pile cap due to expansion of the bridge superstructure.

A.3.1 Guthrie County Bridge

Five abutment piles were instrumented with strain gages at the Guthrie County Bridge as shown in Figure A.8. At the south abutment, the two exterior piles and a pile near the mid-width of the abutment pile cap were monitored. At the north

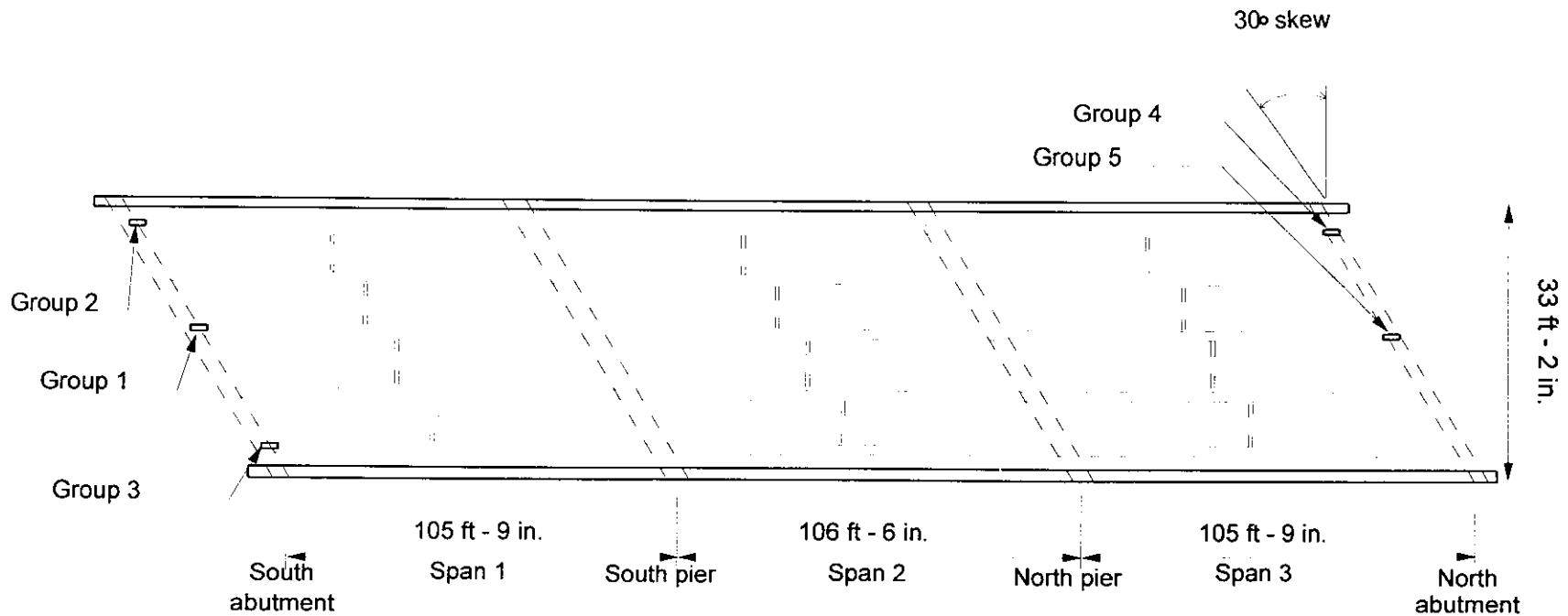


a: 1 in. typical (all monitored piles at both bridges), except 1/2 in. at NW pile at the Guthrie County Bridge

Figure A.7. Strain gage locations on a HP10x42 steel pile (two cross-sections)

abutment, a pile near the mid-width of the abutment and the west exterior pile were instrumented. Table A.6 lists the instrumentation code and description of the acronym used for the strain gages installed on the abutment piles at the Guthrie County Bridge.

Twenty-one bondable, electrical-resistance, strain gages were applied to the Guthrie County Bridge as shown in Fig. A.9 to measure strain in concrete elements. Table A.7 lists the locations of these gages. Sixteen of these gages were bonded to



<u>Group 1</u>	<u>Group 2</u>	<u>Group 3</u>	<u>Group 4</u>	<u>Group 5</u>
SG-SCP-SWT	SG-SWP-SWT	SG-SEP-SWT	SG-NWP-SWT	SG-NCP-SWT
SG-SCP-NWT	SG-SWP-NWT	SG-SEP-NWT	SG-NWP-NWT	SG-NCP-NWT
SG-SCP-SET	SG-SWP-SET	SG-SEP-SET	SG-NWP-SET	SG-NCP-SET
SG-SCP-NET	SG-SWP-NET	SG-SEP-NET	SG-NWP-NET	SG-NCP-NET
SG-SCP-SWB	SG-SWP-SWB	SG-SEP-SWB	SG-NWP-SWB	SG-NCP-SWB
SG-SCP-NWB	SG-SWP-NWB	SG-SEP-NWB	SG-NWP-NWB	SG-NCP-NWB
SG-SCP-SEB	SG-SWP-SEB	SG-SEP-SEB	SG-NWP-SEB	SG-NCP-SEB
SG-SCP-NEB	SG-SWP-NEB	SG-SEP-NEB	SG-NWP-NEB	SG-NCP-NEB



Figure A.8. Pile strain gage locations at the Guthrie County Bridge (not to scale)

Table A.6. Abutment pile strain gages at the Guthrie County Bridge

INSTRUMENT CODE	MEMBER	GAGE LOCATION
SG-SWP-SWT	South abutment, West Pile	South West flange corner, Top cross section
SG-SWP-NWT	South abutment, West Pile	North West flange corner, Top cross section
SG-SWP-SET	South abutment, West Pile	South East flange corner, Top cross section
SG-SWP-NET	South abutment, West Pile	North East flange corner, Top cross section
SG-SWP-SWB	South abutment, West Pile	South West flange corner, Bottom cross section
SG-SWP-NWB	South abutment, West Pile	North West flange corner, Bottom cross section
SG-SWP-SEB	South abutment, West Pile	South East flange corner, Bottom cross section
SG-SWP-NEB	South abutment, West Pile	North East flange corner, Bottom cross section
SG-SCP-SWT	South abutment, Center Pile	South West flange corner, Top cross section
SG-SCP-NWT	South abutment, Center Pile	North West flange corner, Top cross section
SG-SCP-SET	South abutment, Center Pile	South East flange corner, Top cross section
SG-SCP-NET	South abutment, Center Pile	North East flange corner, Top cross section
SG-SCP-SWB	South abutment, Center Pile	South West flange corner, Bottom cross section
SG-SCP-NWB	South abutment, Center Pile	North West flange corner, Bottom cross section
SG-SCP-SEB	South abutment, Center Pile	South East flange corner, Bottom cross section
SG-SCP-NEB	South abutment, Center Pile	North East flange corner, Bottom cross section
SG-SEP-SWT	South abutment, East Pile	South West flange corner, Top cross section
SG-SEP-NWT	South abutment, East Pile	North West flange corner, Top cross section
SG-SEP-SET	South abutment, East Pile	South East flange corner, Top cross section
SG-SEP-NET	South abutment, East Pile	North East flange corner, Top cross section
SG-SEP-SWB	South abutment, East Pile	South West flange corner, Bottom cross section
SG-SEP-NWB	South abutment, East Pile	North West flange corner, Bottom cross section
SG-SEP-SEB	South abutment, East Pile	South East flange corner, Bottom cross section
SG-SEP-NEB	South abutment, East Pile	North East flange corner, Bottom cross section
SG-NCP-SWT	North abutment, Center Pile	South West flange corner, Top cross section
SG-NCP-NWT	North abutment, Center Pile	North West flange corner, Top cross section
SG-NCP-SET	North abutment, Center Pile	South East flange corner, Top cross section
SG-NCP-NET	North abutment, Center Pile	North East flange corner, Top cross section
SG-NCP-SWB	North abutment, Center Pile	South West flange corner, Bottom cross section
SG-NCP-NWB	North abutment, Center Pile	North West flange corner, Bottom cross section
SG-NCP-SEB	North abutment, Center Pile	South East flange corner, Bottom cross section
SG-NCP-NEB	North abutment, Center Pile	North East flange corner, Bottom cross section
SG-NWP-SWT	North abutment, West Pile	South West flange corner, Top cross section
SG-NWP-NWT	North abutment, West Pile	North West flange corner, Top cross section
SG-NWP-SET	North abutment, West Pile	South East flange corner, Top cross section
SG-NWP-NET	North abutment, West Pile	North East flange corner, Top cross section
SG-NWP-SWB	North abutment, West Pile	South West flange corner, Bottom cross section
SG-NWP-NWB	North abutment, West Pile	North West flange corner, Bottom cross section
SG-NWP-SEB	North abutment, West Pile	South East flange corner, Bottom cross section
SG-NWP-NEB	North abutment, West Pile	North East flange corner, Bottom cross section

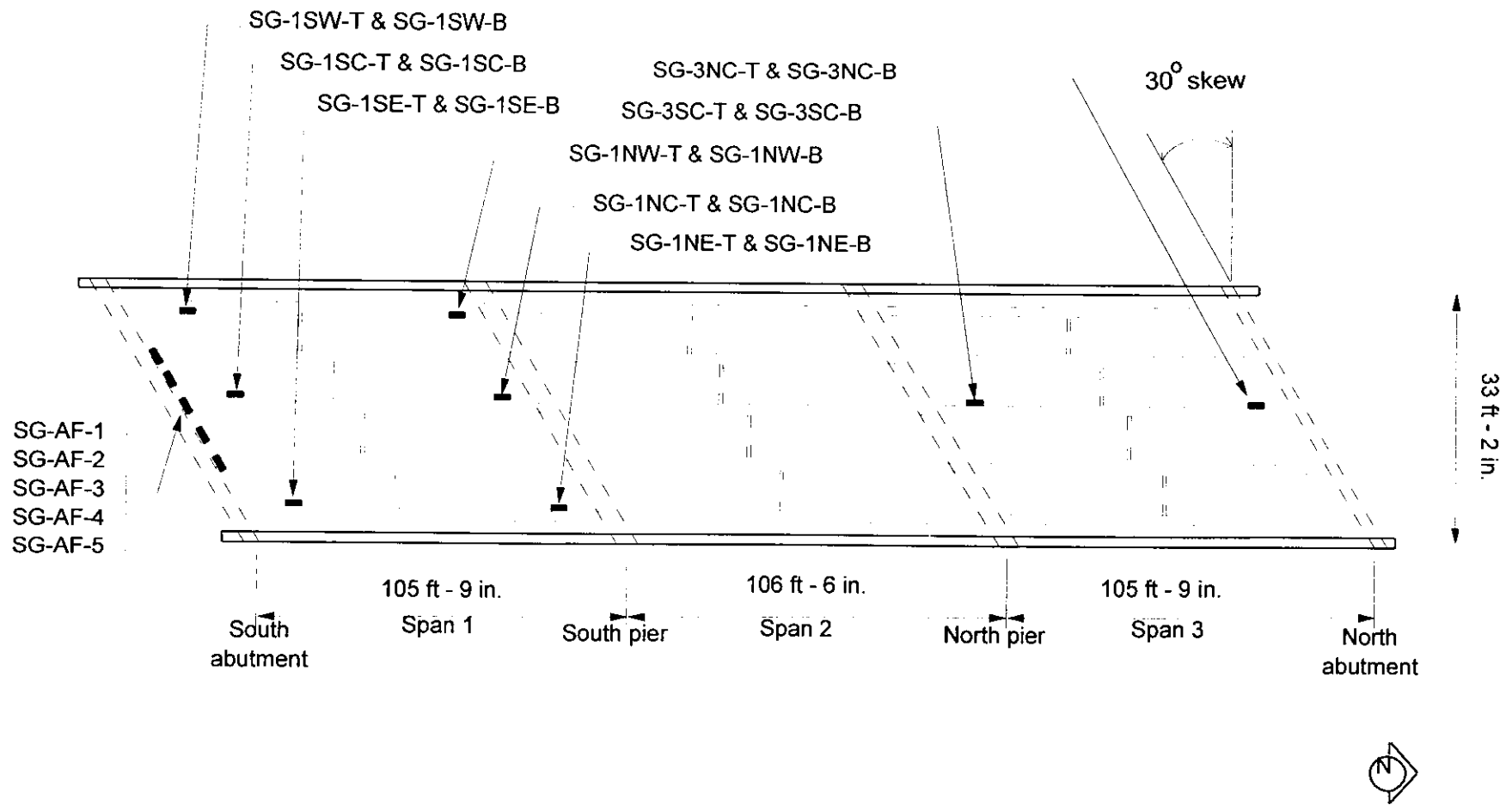


Figure A.9. PC girder and RC pile cap strain gage locations at the Guthrie County Bridge (not to scale)

Table A.7. PC girder and RC pile cap strain gages at the Guthrie County Bridge

INSTRUMENT CODE	GAGE LOCATION
SG-1SW-T	1 st Span, South end of the West girder, Top flange
SG-1SW-B	1 st Span, South end of the West girder, Bottom flange
SG-1SC-T	1 st Span, South end of the Center girder, Top flange
SG-1SC-B	1 st Span, South end of the Center girder, Bottom flange
SG-1SE-T	1 st Span, South end of the East girder, Top flange
SG-1SE-B	1 st Span, South end of the East girder, Bottom flange
SG-1NW-T	1 st Span, North end of the West girder, Top flange
SG-1NW-B	1 st Span, North end of the West girder, Bottom flange
SG-1NC-T	1 st Span, North end of the Center girder, Top flange
SG-1NC-B	1 st Span, North end of the Center girder, Bottom flange
SG-1NE-T	1 st Span, North end of the East girder, Top flange
SG-1NE-B	1 st Span, North end of the East girder, Bottom flange
SG-3NC-T	3 rd Span, North end of the Center girder, Top flange
SG-3NC-B	3 rd Span, North end of the Center girder, Bottom flange
SG-3SC-T	3 rd Span, South end of the Center girder, Top flange
SG-3SC-B	3 rd Span, South end of the Center girder, Bottom flange
SG-AF-1	South Abutment pile cap Face position #1
SG-AF-2	South Abutment pile cap Face position #2
SG-AF-3	South Abutment pile cap Face position #3
SG-AF-4	South Abutment pile cap Face position #4
SG-AF-5	South Abutment pile cap Face position #5

four PC girders. The remaining five strain gages were bonded to the north face of the south abutment pile cap.

A.3.2 Story County Bridge

Four abutment piles were instrumented with strain gages at the Story County Bridge as shown in Fig. A.10 and listed in Table A.8. At the east abutment, the two exterior piles and the center pile were monitored. At the west abutment, the center pile was instrumented. Each pile had eight strain gages whose locations were as described for the piles at the Guthrie County Bridge. However, to permit the use of a dummy strain gage to correct measured strains for changes in the temperature of the data acquisition system, a strain gage at the bottom cross section of the south pile in the east abutment was not installed. At the Story County Bridge twelve,

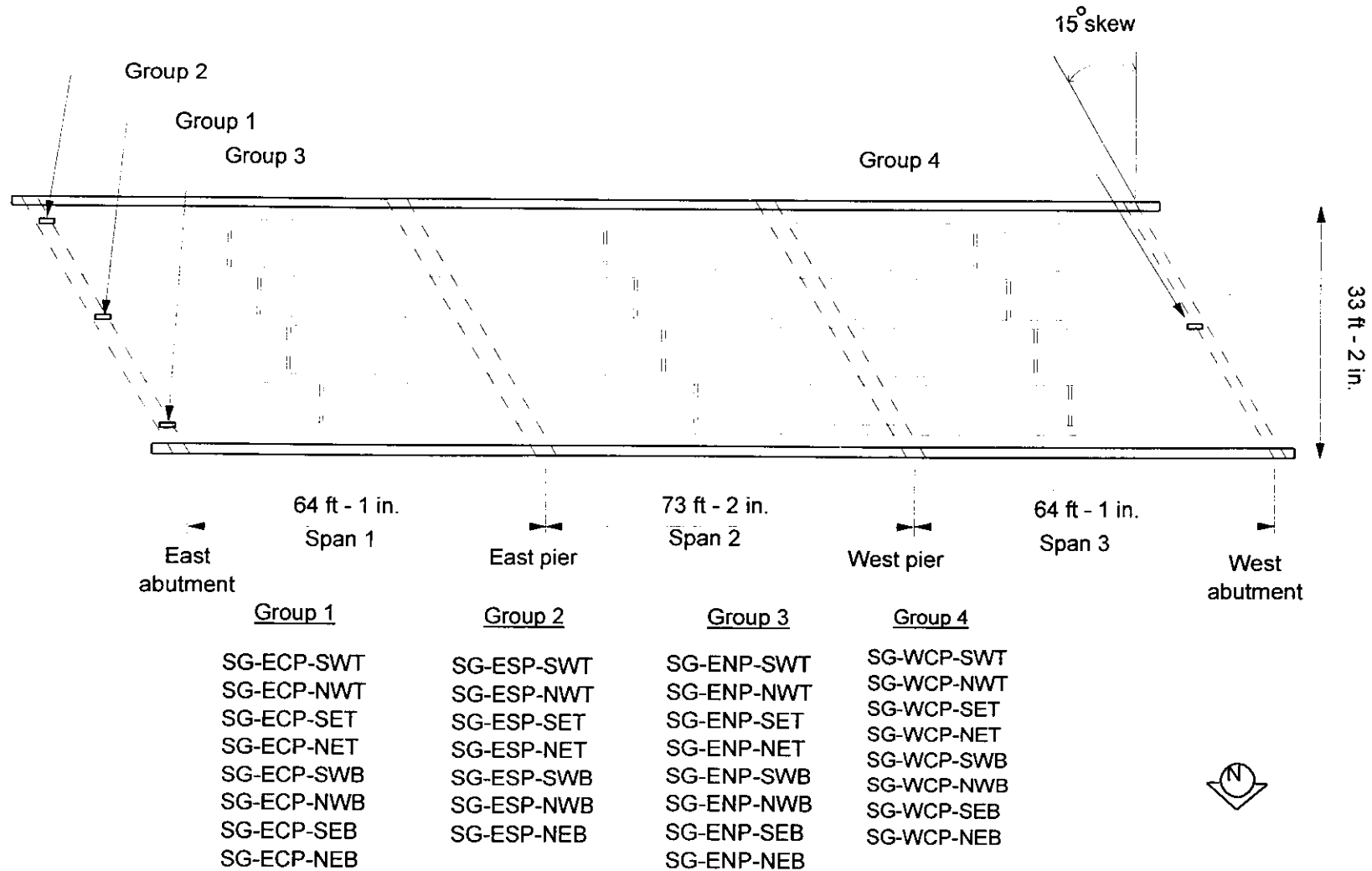


Figure A.10. Pile strain gage locations at the Story County Bridge (not to scale)

Table A.8. Abutment pile strain gages at the Story County Bridge

INSTRUMENT CODE	MEMBER	GAGE LOCATION
SG-ENP-SWT	East abutment, North Pile	South West flange corner, Top cross section
SG-ENP-NWT	East abutment, North Pile	North West flange corner, Top cross section
SG-ENP-SET	East abutment, North Pile	South East flange corner, Top cross section
SG-ENP-NET	East abutment, North Pile	North East flange corner, Top cross section
SG-ENP-SWB	East abutment, North Pile	South West flange corner, Bottom cross section
SG-ENP-NWB	East abutment, North Pile	North West flange corner, Bottom cross section
SG-ENP-SEB	East abutment, North Pile	South East flange corner, Bottom cross section
SG-ENP-NEB	East abutment, North Pile	North East flange corner, Bottom cross section
SG-ECP-SWT	East abutment, Center Pile	South West flange corner, Top cross section
SG-ECP-NWT	East abutment, Center Pile	North West flange corner, Top cross section
SG-ECP-SET	East abutment, Center Pile	South East flange corner, Top cross section
SG-ECP-NET	East abutment, Center Pile	North East flange corner, Top cross section
SG-ECP-SWB	East abutment, Center Pile	South West flange corner, Bottom cross section
SG-ECP-NWB	East abutment, Center Pile	North West flange corner, Bottom cross section
SG-ECP-SEB	East abutment, Center Pile	South East flange corner, Bottom cross section
SG-ECP-NEB	East abutment, Center Pile	North East flange corner, Bottom cross section
SG-ESP-SWT	East abutment, South Pile	South West flange corner, Top cross section
SG-ESP-NWT	East abutment, South Pile	North West flange corner, Top cross section
SG-ESP-SET	East abutment, South Pile	South East flange corner, Top cross section
SG-ESP-NET	East abutment, South Pile	North East flange corner, Top cross section
SG-ESP-SWB	East abutment, South Pile	South West flange corner, Bottom cross section
SG-ESP-NWB	East abutment, South Pile	North West flange corner, Bottom cross section
SG-ESP-NEB	East abutment, South Pile	North East flange corner, Bottom cross section
SG-WCP-SWT	West abutment, Center Pile	South West flange corner, Top cross section
SG-WCP-NWT	West abutment, Center Pile	North West flange corner, Top cross section
SG-WCP-SET	West abutment, Center Pile	South East flange corner, Top cross section
SG-WCP-NET	West abutment, Center Pile	North East flange corner, Top cross section
SG-WCP-SWB	West abutment, Center Pile	South West flange corner, Bottom cross section
SG-WCP-NWB	West abutment, Center Pile	North West flange corner, Bottom cross section
SG-WCP-SEB	West abutment, Center Pile	South East flange corner, Bottom cross section
SG-WCP-NEB	West abutment, Center Pile	North East flange corner, Bottom cross section

Table A.9. PC girder and RC pile cap strain gages at the Story County Bridge

INSTRUMENT CODE	GAGE LOCATION
SG-1EN-T	1st Span, East side, North girder, Top flange
SG-1EN-B	1st Span, East side, North girder, Bottom flange
SG-1EC-T	1st Span, East side, Center girder, Top flange
SG-1EC-B	1st Span, East side, Center girder, Bottom flange
SG-1ES-T	1st Span, East side, South girder, Top flange
SG-1ES-B	1st Span, East side, South girder, Bottom flange
SG-1WC-T	1st Span, West side, Center girder, Top flange
SG-1WC-B	1st Span, West side, Center girder, Bottom flange
SG-3WC-T	3rd span, West side, Center girder, Top flange
SG-3WC-B	3rd span, West side, Center girder, Bottom flange
SG-3EC-T	3rd span, East side, Center girder, Top flange
SG-3EC-B	3rd span, East side, Center girder, Bottom flange
SG-AF-1	East Abutment Face No. 1
SG-AF-2	East Abutment Face No. 2
SG-AF-3	East Abutment Face No. 3
SG-AF-4	East Abutment Face No. 4

vibrating-wire strain gages were applied to four PC girders and four vibrating-wire strain gages were applied to the west face of the east abutment pile cap. Table A.9 lists the location and Figure A.11 shows the location of these 16 gages.

A.3.3 Strain gage installation procedure

To provide access to the strain gage locations on the outside face of the pile flanges the top portions of the selected piles were exposed. The excavation procedure consisted of removing the berm rubble in front of a pile and digging down through the berm soil to expose the pile flanges for a depth of about 42 in. At the gage locations the pile was cleared of soil and an electric grinder was used to expose clean bare steel. These surfaces were then sanded to provide a flat, smooth surface onto which the gage was welded.

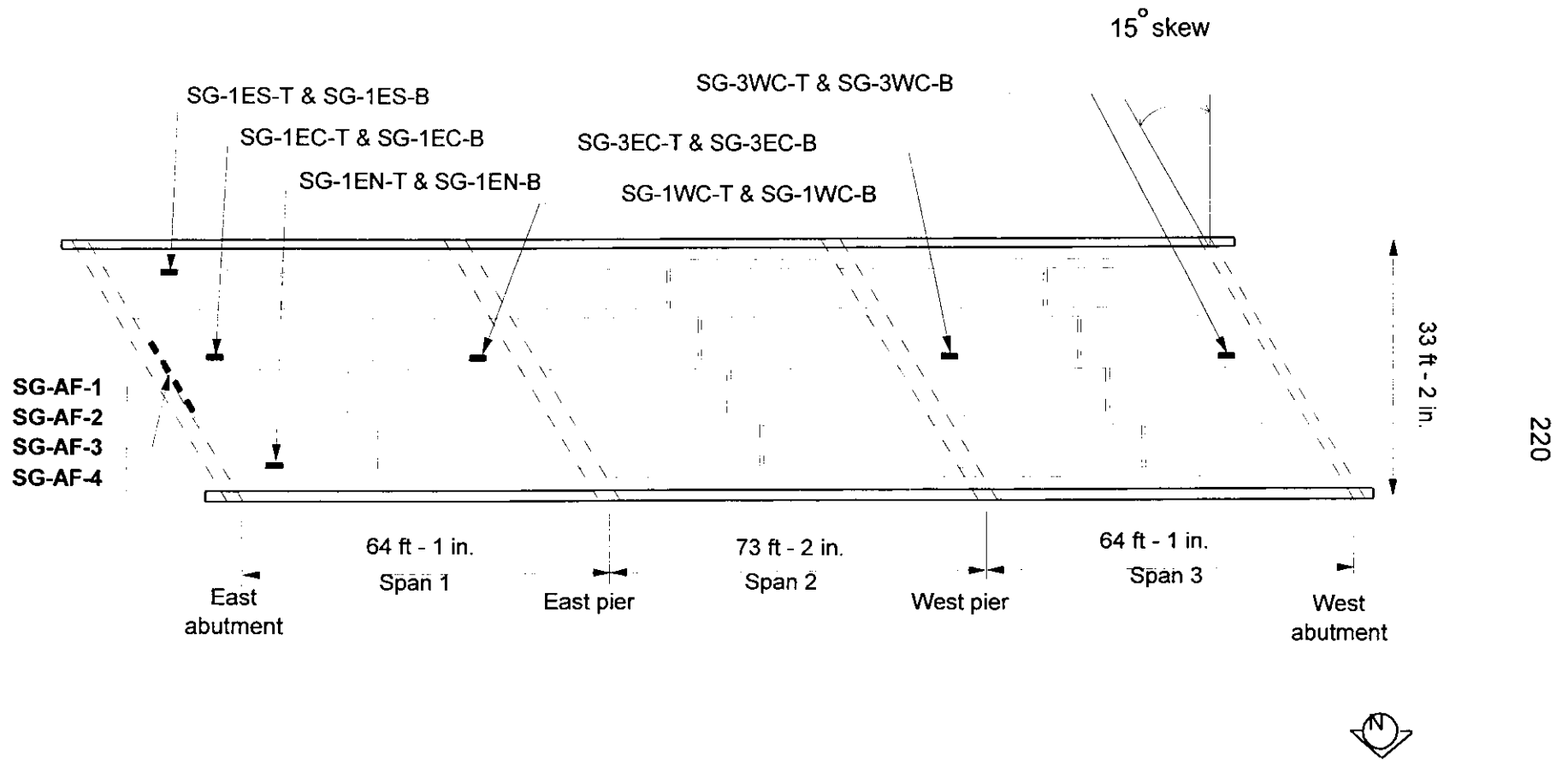


Figure A.11. PC girder and RC pile cap strain gage locations at the Story County Bridge (not to scale)

Each weldable, electrical-resistance gage (Hitec model HBW-35-125-6-3VH-SS) consisted of a strain gage that had been bonded to a thin metal tab by the manufacturer. This metal tab for each gage was attached to the steel pile with a series of closely spaced, small tack welds. To strengthen the connection between a metal tab and a pile surface, Superglue was applied around the edges of the tab. At the Guthrie County Bridge, these gages were protected from moisture penetration by applying silicone caulk over the gages. At the Story County Bridge, asphalt cement was used to protect the pile gages.

The bondable, electrical-resistance strain gages that were applied to the PC girders and the RC pile cap at the Guthrie County Bridge were bonded to the concrete surfaces with epoxies (AE-10 and Mbond 300) from Measurements Group, Inc. Several of the gages were installed at temperatures too cold to use the AE-10 epoxy. These gages were bonded to the concrete with a faster setting epoxy Mbond 300. This epoxy can cure at lower temperatures, but it has a low peel strength. Gages that were bonded with Mbond 300 could be easily peeled away from the epoxy.

The concrete surfaces at the strain gage locations were cleaned and prepared as directed in the gage application instructions provided by the manufacturer of the strain gage epoxies. The epoxy was mixed and spread onto the concrete surface. The gages were positioned on the epoxy bed and held in place with a bracket designed to apply pressure to the gage while the epoxy set. After the epoxy had set, the gage was covered with a strip of butyl rubber to keep moisture away from the gage and epoxy. Several gages had to be re-bonded to the concrete

after they became loose during the application of the weatherproofing protection. The gages that peeled-off were re-bonded to the concrete with the AE-10 epoxy and heat was applied to properly cure the epoxy. The strain gage at the 1SCB location on the Guthrie County Bridge was accidentally peeled-off when removing a clamping bracket in July of 1998. This gage was not re-bonded to the concrete.

A vibrating-wire strain gage consists of a taut wire stretched between two anchor blocks. Changes in strain in the specimen are indicated by the change of the natural frequency of this taut wire. Each vibrating-wire gage installed at the Story County Bridge was attached to the PC girders or the RC abutment pile cap by firmly clamping the gage anchor blocks into the two mounting blocks that had been bonded to the concrete surfaces using a high-modulus epoxy cement. To protect the gage installation, a one-half cylindrical section of 4 in.-diameter PVC pipe was placed over the gage. The pipe covering was glued to concrete surface.

The electrically-shielded extension wires that connected the strain gages to the data acquisition system were soldered to the wire leads of the gages in the field. The connections were protected against moisture infiltration by using shrink tubing around each of the three conductor wires and also around the entire extension wire.

A.4 Thermocouples

To measure the temperature of the concrete and to establish temperature gradients in each of the instrumented bridges, thermocouples were installed along the length, across the width, and through the depth of the bridge superstructures. Thermocouples were embedded in the RC deck slab and PC girders at several

locations by drilling a hole in the concrete member and grouting a thermocouple into the hole. Deck slab temperatures were measured at 4 in. from the bottom of the slab and girder temperatures were measured at a depth of about $\frac{3}{4}$ in. into the member.

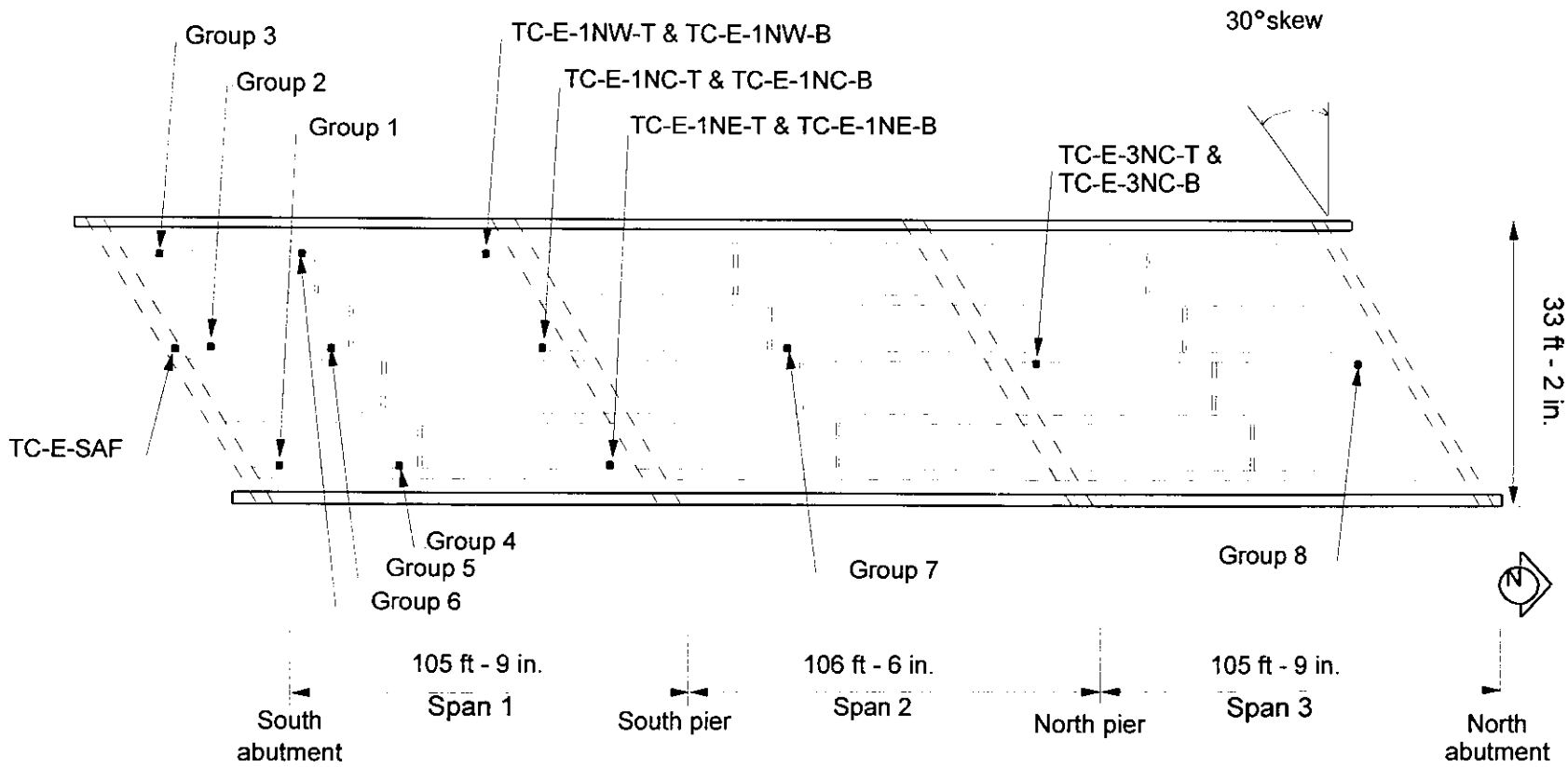
Thermocouples were also used to measure the air temperature near the displacement transducer wires so that temperature corrections could be made to the raw displacement data. These thermocouples were suspended in the air near the mid-length of the transducer wires and did not provide information about the bridge temperatures. Only the thermocouples that were used to measure bridge temperatures are described in Sections A.4.1 and A.4.2. The "E" in the instrument code indicates that the thermocouple was Embedded into the concrete bridge structure.

A.4.1 Guthrie County Bridge

A total of 41 thermocouples, listed in Table A.10, were installed at the Guthrie County Bridge as shown in Figure A.12. Most of the thermocouples were installed in the south span (Span 1) of this bridge. In this span, temperatures were measured in both of the exterior and center PC girders near the south abutment, at the midspan, and near the south pier. The remaining thermocouples in the bridge superstructure were embedded in the slab and in the center girder at the midspan of the center span (Span 2) and at both ends of the west span (Span 3). At each PC girder cross section where temperatures of the concrete were measured, thermocouples were embedded into the top and bottom flanges of the girders. At several of these locations, deck slab and PC girder web temperatures were also measured. An

Table A.10. Thermocouple locations at the Guthrie County Bridge

INSTRUMENT CODE	MEMBER	LOCATION
TC-E-SAF	South Abutment pile cap Face	Mid-height
TC-E-1SE-S	1st Span, South end of the East girder	Slab
TC-E-1SE-T	1st Span, South end of the East girder	Top flange
TC-E-1SE-W	1st Span, South end of the East girder	Web
TC-E-1SE-B	1st Span, South end of the East girder	Bottom flange
TC-E-1SC-S	1st Span, South end of the Center girder	Slab
TC-E-1SC-T	1st Span, South end of the Center girder	Top flange
TC-E-1SC-W	1st Span, South end of the Center girder	Web
TC-E-1SC-B	1st Span, South end of the Center girder	Bottom flange
TC-E-1SW-S	1st Span, South end of the West girder	Slab
TC-E-1SW-T	1st Span, South end of the West girder	Top flange
TC-E-1SW-W	1st Span, South end of the West girder	Web
TC-E-1SW-B	1st Span, South end of the West girder	Bottom flange
TC-E-1MSE-S	1st span, MidSpan, East girder	Slab
TC-E-1MSE-T	1st span, MidSpan, East girder	Top flange
TC-E-1MSE-W	1st span, MidSpan, East girder	Web
TC-E-1MSE-B	1st span, MidSpan, East girder	Bottom flange
TC-E-1MSC-S	1st span, MidSpan, Center girder	Slab
TC-E-1MSC-T	1st span, MidSpan, Center girder	Top flange
TC-E-1MSC-W	1st span, MidSpan, Center girder	Web
TC-E-1MSC-B	1st span, MidSpan, Center girder	Bottom flange
TC-E-1MSW-S	1st span, MidSpan, West girder	Slab
TC-E-1MSW-T	1st span, MidSpan, West girder	Top flange
TC-E-1MSW-W	1st span, MidSpan, West girder	Web
TC-E-1MSW-B	1st span, MidSpan, West girder	Bottom flange
TC-E-1NE-T	1st Span, North end of the East girder	Top flange
TC-E-1NE-B	1st Span, North end of the East girder	Bottom flange
TC-E-1NC-T	1st Span, North end of the Center girder	Top flange
TC-E-1NC-B	1st Span, North end of the Center girder	Bottom flange
TC-E-1NW-T	1st Span, North end of the West girder	Top flange
TC-E-1NW-B	1st Span, North end of the West girder	Bottom flange
TC-E-2MSC-S	2nd span, MidSpan, Center girder	Slab
TC-E-2MSC-T	2nd span, MidSpan, Center girder	Top flange
TC-E-2MSC-W	2nd span, MidSpan, Center girder	Web
TC-E-2MSC-B	2nd span, MidSpan, Center girder	Bottom flange
TC-E-3SC-T	3rd Span, South end of the Center girder	Top flange
TC-E-3SC-B	3rd Span, South end of the Center girder	Bottom flange
TC-E-3NC-S	3rd Span, North end of the Center girder	Slab
TC-E-3NC-T	3rd Span, North end of the Center girder	Top flange
TC-E-3NC-W	3rd Span, North end of the Center girder	Web
TC-E-3NC-B	3rd Span, North end of the Center girder	Bottom flange



Group 1	Group 2	Group 3	Group 4	Group 5	Group 6	Group 7	Group 8
TC-E-1SE-S	TC-E-1SC-S	TC-E-1SW-S	TC-E-1MSE-S	TC-E-1MSC-S	TC-E-1MSW-S	TC-E-2MSC-S	TC-E-3NC-S
TC-E-1SE-T	TC-E-1SC-T	TC-E-1SW-T	TC-E-1MSE-T	TC-E-1MSC-T	TC-E-1MSW-T	TC-E-2MSC-T	TC-E-3NC-T
TC-E-1SE-W	TC-E-1SC-W	TC-E-1SW-W	TC-E-1MSE-W	TC-E-1MSC-W	TC-E-1MSW-W	TC-E-2MSC-W	TC-E-3NC-W
TC-E-1SE-B	TC-E-1SC-B	TC-E-1SW-B	TC-E-1MSE-B	TC-E-1MSC-B	TC-E-1MSW-B	TC-E-2MSC-B	TC-E-3NC-B

Figure A.12. Thermocouple locations at the Guthrie County Bridge (not to scale)

additional thermocouple was installed in the north face of the south abutment pile cap near the mid-width of the abutment.

A.4.2 Story County Bridge

The thermocouple locations at the Story County Bridge were similar to those at the Guthrie County Bridge as shown in Fig. A.13. Most of the thermocouples were placed in the east span. There were some changes made to the thermocouple installation once the Guthrie County Bridge instrumentation was complete. To obtain a more complete transverse temperature distribution, more thermocouples were embedded in the deck slab at the midspan of the east span at the Story County Bridge than were used in the south span at the Guthrie County Bridge. These additional thermocouples were placed in the slab near the PC girders and midway between the girders. Table A.11 lists the 46 thermocouples that were installed in the superstructure of the Story County Bridge.

A.5 Data acquisition procedure

Data acquisition was accomplished using Campbell Scientific, Inc. dataloggers and peripherals. A CR10X datalogger at each bridge provided the excitation voltage for the instrumentation and recorded the instrumentation output. The data were initially stored in the CR10X's memory until the data was downloaded to a laptop computer. Multiplexers (Model AM416) were used to increase the number of instrumentation devices that the CR10X could accommodate.

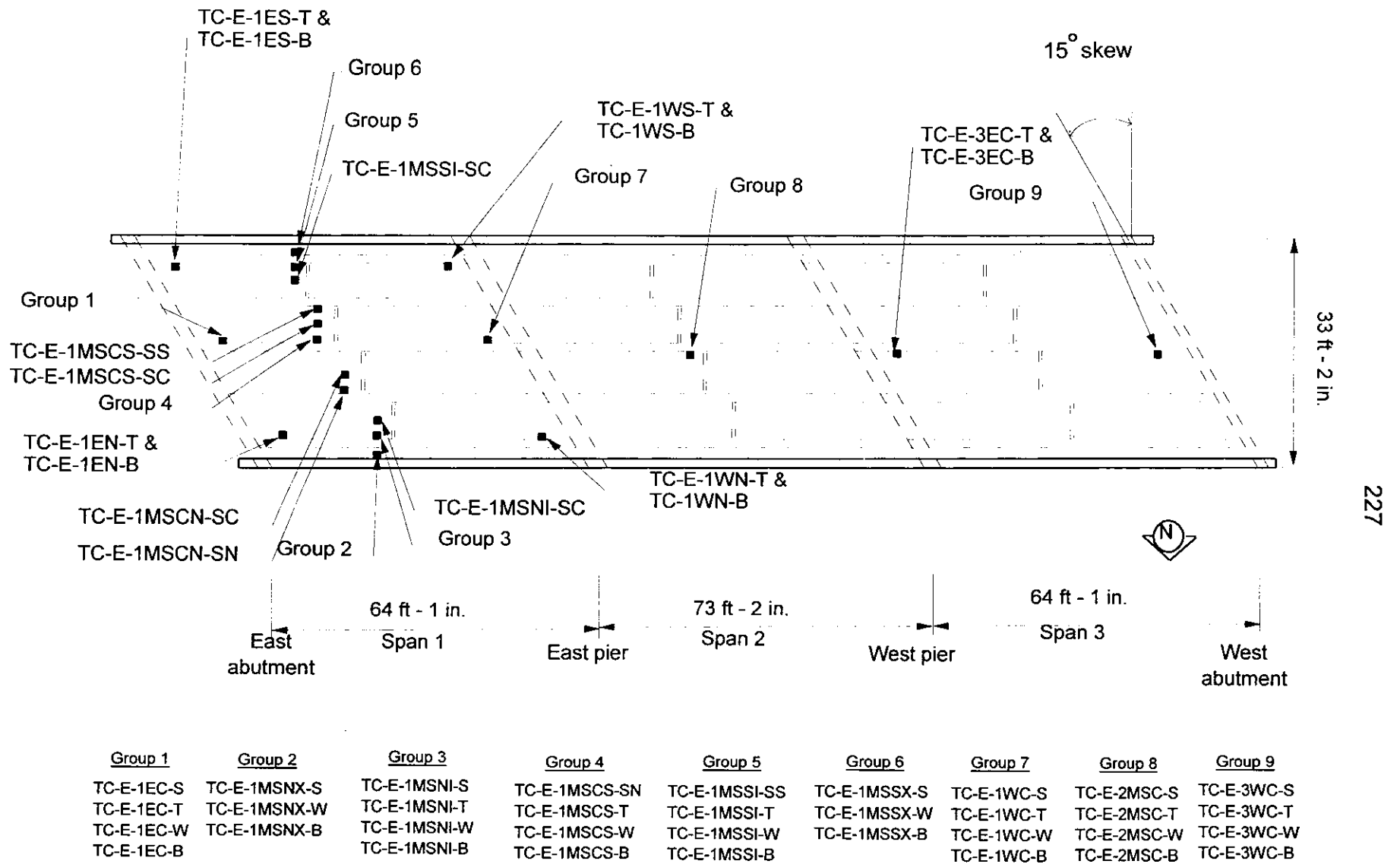


Figure A.13. Thermocouple locations at the Story County Bridge (not to scale)

Table A.11. Thermocouples installed at the Story County Bridge

INSTRUMENT CODE	MEMBER	LOCATION
TC-E-1EN-T	1st span, East end of North girder	Top flange
TC-E-1EN-B	1st span, East end of North girder	Bottom flange
TC-E-1EC-S	1st span, East end of Center girder	Slab
TC-E-1EC-T	1st span, East end of Center girder	Top flange
TC-E-1EC-W	1st span, East end of Center girder	Web
TC-E-1EC-B	1st span, East end of Center girder	Bottom flange
TC-E-1ES-T	1st span, East end of South girder	Top flange
TC-E-1ES-B	1st span, East end of South girder	Bottom flange
TC-E-1MSNX-S	1st span, MidSpan, North girder, Exterior side	Slab
TC-E-1MSNX-W	1st span, MidSpan, North girder, Exterior side	Web
TC-E-1MSNX-B	1st span, MidSpan, North girder, Exterior side	Bottom flange
TC-E-1MSNI-SN	1st span, MidSpan, North girder, Interior side	in Slab span, North side
TC-E-1MSNI-SC	1st span, MidSpan, North girder, Interior side	in Slab span, Center
TC-E-1MSNI-T	1st span, MidSpan, North girder, Interior side	Top flange
TC-E-1MSNI-W	1st span, MidSpan, North girder, Interior side	Web
TC-E-1MSNI-B	1st span, MidSpan, North girder, Interior side	Bottom flange
TC-E-1MSCN-SN	1st span, MidSpan, Center girder, North side	in Slab span, North side
TC-E-1MSCN-SC	1st span, MidSpan, Center girder, North side	in Slab span, Center
TC-E-1MSCS-SN	1st span, MidSpan, Center girder, South side	in Slab span, North side
TC-E-1MSCS-SC	1st span, MidSpan, Center girder, South side	in Slab span, Center
TC-E-1MSCS-SS	1st span, MidSpan, Center girder, South side	in Slab span, South side
TC-E-1MSCS-T	1st span, MidSpan, Center girder, South side	Top flange
TC-E-1MSCS-W	1st span, MidSpan, Center girder, South side	Web
TC-E-1MSCS-B	1st span, MidSpan, Center girder, South side	Bottom flange
TC-E-1MSSI-SC	1st span, MidSpan, South girder, Interior side	in Slab span, Center
TC-E-1MSSI-SS	1st span, MidSpan, South girder, Interior side	in Slab span, South
TC-E-1MSSI-T	1st span, MidSpan, South girder, Interior side	Top flange
TC-E-1MSSI-W	1st span, MidSpan, South girder, Interior side	Web
TC-E-1MSSI-B	1st span, MidSpan, South girder, Interior side	Bottom flange
TC-E-1MSSX-S	1st span, MidSpan, South girder, Exterior side	Slab
TC-E-1MSSX-W	1st span, MidSpan, South girder, Exterior side	Web
TC-E-1MSSX-B	1st span, MidSpan, South girder, Exterior side	Bottom flange
TC-E-1WC-S	1st span, West end of Center girder	Slab
TC-E-1WC-T	1st span, West end of Center girder	Top flange
TC-E-1WC-W	1st span, West end of Center girder	Web
TC-E-1WC-B	1st span, West end of Center girder	Bottom flange
TC-E-2MSC-S	2nd span, MidSpan, Center girder	Slab
TC-E-2MSC-T	2nd span, MidSpan, Center girder	Slab
TC-E-2MSC-W	2nd span, MidSpan, Center girder	Web
TC-E-2MSC-B	2nd span, MidSpan, Center girder	Bottom flange
TC-E-3WC-S	3rd span, West end of Center girder	Slab
TC-E-3WC-T	3rd span, West end of Center girder	Top flange
TC-E-3WC-W	3rd span, West end of Center girder	Web
TC-E-3WC-B	3rd span, West end of Center girder	Bottom flange
TC-E-3EC-T	3rd span, East end of Center girder	Top flange
TC-E-3EC-B	3rd span, East end of Center girder	Bottom flange

A.5.1 Data acquisition equipment

At the Guthrie County Bridge the CR10X datalogger and six multiplexers were bolted into two, large (18 in. by 24 in. by 6 in.), steel, electrical boxes. These boxes were attached to the bottom surface of the deck slab about 20 feet from the south abutment near the center girder. Another multiplexer was located at the north end of the bridge. This multiplexer was bolted into a smaller (6 in. by 8 in. by 4 in.) electrical box that was attached to the south face of the north abutment.

A datalogger and seven multiplexers were used at the Story County Bridge. These units were bolted into two, large, electrical boxes that were attached to the west face of the east abutment backwall between two PC girders. All of the electrical wires from the instrumentation devices converged at this location, where they were connected to the data acquisition system.

Additional Campbell Scientific data acquisition equipment used at the bridge sites included two units that recorded strain in the electrical-resistance and vibrating-wire strain gages. At the Guthrie County and the Story County Bridges, a Terminal Input Module, TIM (Model 4FWB350) was used to measure strain changes in the electrical-resistance strain gages installed on the bridges. All of the electrical-resistance strain gages at each bridge were multiplexed through one TIM unit. To provide excitation and measure strain changes in the vibrating-wire strain gages installed at the Story County Bridge, a Vibrating Wire Sensor Interface (Model AVW1) was used.

To communicate with the datalogger at the Guthrie County Bridge from an office in the Town Engineering Building on the Iowa State University campus, a

Campbell Scientific modem (Model COM 200) was used. The modem was connected to a phone jack that was installed at the bridge site. Using the modem, recorded instrumentation data was transferred from the CR10X datalogger to the laptop computer on the ISU campus. Data collected at the Story County Bridge was directly downloaded to a laptop computer by directly connecting the computer to the CR10X datalogger at the bridge site.

A.5.2 Data acquisition interval and initial data reduction

Diurnal (daily) temperature variations occur quickly compared to the seasonal temperature variations. To establish the diurnal temperature variation, measurements were frequently recorded. For the Guthrie County Bridge, all instrumentation readings were recorded at 20-minute intervals between December 17, 1997 and May 15, 1998. After May 15, 1998 the data collection frequency was changed to every 30 minutes to reduce to volume of data that needed to be stored and analyzed, yet maintain sufficient sensitivity to record changes in the bridge response due to diurnal temperature variations. Since data acquisition began in the middle of July 1998 at the Story County Bridge, the instrumentation measurements were recorded at 30-minute intervals.

Each time data were collected, the datalogger recorded each instrumentation measurement six times. To minimize strain and displacement measurement errors due to the possibility that highway traffic may have been on the bridge when the instrumentation measurements were made, the raw data were "filtered" to eliminate outlier values. Rather than computing a simple average of the six recorded data values for each instrumentation device, an algorithm was developed and applied to

discard any questionable data. The algorithm used two criteria for determining an allowable range of data values. For the first criterion, an outlier data point was defined as a value that was more than one standard deviation away from the mean value of the six data points. For a normal distribution in the data values, this meant that, on average, 32% of the measured values would be discarded. The second criterion was based on the median of the six measured values. If the standard deviation of a data set was small and the first criterion would throw out good data, the data values were not thrown out unless it was more than a fixed amount away from the median value. The limits of acceptable deviations from the median value were different for each instrument type. The allowable deviations were: 0.0015 in. for displacement transducers, 7.5 microstrains for strain gages, and 0.2° C for thermocouples. These values were based on the expected repeatability of the instrumentation measurements. After the filtering algorithm had discarded the questionable data a mean value of the remaining data values for each instrumentation device was calculated and used as the representative instrumentation reading for that particular time.

With a 30-minute data collection interval, the volume of data was too large to analyze and plot efficiently. To facilitate the analysis of the data, the volume of data was reduced by deleting three of every four filtered data points. All of the data files were stored on a computer hard drive and on several floppy (Zip brand) disks.

APPENDIX B –ADDITIONAL ANALYSIS OF THE EXPERIMENTAL RESULTS

The following section provides supplementary discussion of the experimental results from the Guthrie County Bridge and Story County Bridge. This section comprises of excerpts from Chapter 4 of the thesis written by Matt Thomas [26], and is reproduced with the permission the author. The experimental data presented in this chapter is for the time period beginning at the start of the project through January 1999.

The subheading numbering in this appendix corresponds to the subheading numbering in Chapter 4 of this thesis. In other words, Section B.2.2 corresponds to Section 4.2.2. The section headings in this appendix correspond to the headings in this thesis, not to original numbering in Chapter 4 of the thesis written by Matt Thomas.

B.2 Bridge temperatures

B.2.1 Average concrete temperature

The maximum average bridge temperatures were warmer than the air temperatures measured by a thermocouple placed under each bridge. The temperature recorded by the National Weather Service (NWS) for Des Moines (located within 30 miles of the bridge) on July 20, 1998 was 98°F (37°C). In this case, the air temperature reported by the NWS was close to the maximum average bridge temperature.

B.2.2 Vertical temperature gradients

Vertical temperature distributions in each bridge superstructure were measured by thermocouples installed in each bridge's deck slab and in selected PC girders. Significant temperature gradients were measured through the depth of each bridge superstructure. Vertical thermal gradients are a concern because they can create secondary moments in continuous bridge structures and cause longitudinal stresses to develop in the cross section. The largest positive thermal gradients occurred at the times of the maximum average bridge temperatures.

Vertical temperature distributions were found to be bilinear by Girton, et al. [7]. His research showed that for a PC girder bridge there was a moderate vertical thermal gradient through the depth of the girders and a steep vertical thermal gradient in the slab. Since the temperature of the deck slabs of the Guthrie and Story County Bridges were made only at one depth in the slab, bilinear temperature distributions could not be verified. Several temperature measurements through the depth of the slab would have been necessary to be able to characterize the vertical temperature gradients.

Using temperature measurements made in the top flange, web, and bottom flange of the PC girders, a linear, best-fit thermal gradient for the girder was computed for each instrumented cross section. Extrapolating the girder temperature gradient, a temperature at the bottom of the slab was calculated. The thermal gradient in the slab was found by assuming that a bilinear temperature distribution existed through the superstructure depth as shown by Girton. The extrapolated temperature at the bottom of the slab and the measured temperature at the mid-

thickness of the deck slab established the linear thermal gradient in the deck. The temperature at the top of the deck slab was determined by a linear extrapolation of the slab thermal gradient.

The temperatures measured at each depth (top flange, web, and bottom flange) in the PC girders were averaged and an average, linear, best-fit thermal gradient for the girders was determined for these average temperatures. An average temperature at the bottom of the slab was computed by extrapolating the average temperature gradient in the girders. Also, an average slab thermal gradient was determined for each bridge using the extrapolated temperature of the bottom of the slab and the temperature at the mid-depth of the slab.

The magnitude of the slope of the thermal gradient varies seasonally as well as daily. The magnitude of the maximum vertical temperature gradient is much larger in the summer due to increased exposure of the bridge to solar radiation. Negative temperature gradients through the depth of the superstructure occur more frequently in the winter months, but do not have nearly as large a magnitude as the positive thermal gradients in the summer.

B.2.3 Transverse temperature gradients

The Story County Bridge had a large number of thermocouples in the slab to measure temperature variations across the width of the bridge. Temperature measurements made in the slab at the midspan of the east span did not indicate a horizontal temperature gradient. However, a significant temperature variation was noted at the edges of the Story County Bridge. The temperatures measured in the slab sections at the edges of the bridge that were beneath the continuous, Jersey-

type, concrete barriers were significantly cooler than the rest of the slab at the time of the maximum average bridge temperature. The concrete barriers shade the slab areas beneath them and provide additional thermal mass at that location. At the time of the minimum average bridge temperature on January 5, 1999, the slab temperatures were warmer at the edges of the bridge. No thermocouples were installed in the concrete barriers at either bridge site.

Variations in the measured slab temperature across the bridge width did exist away from the bridge edges, but these small variations may have been due to differences in the vertical positions of the thermocouples in the slab. The steep vertical temperature gradient in the slab at the maximum temperature can create apparent transverse temperature variations if the slab thermocouples were not all installed at exactly the same depth.

B.2.4 Longitudinal temperature gradients

Temperature measurements were made at six locations along the longitudinal axis of each bridge. The temperatures measured in the PC girders and the slab along the centerline of each bridge were compared. Differences in the measured temperatures along the bridge length did not appear significant. To show a longitudinal temperature variation, temperature information for more locations along the length of the bridge would be necessary. Previous analytical work has shown that longitudinal temperature variations are neither significant, nor consequential.

B.2.5 Pile temperatures

The temperatures of several piles were measured near the bottom of the pile cap at each bridge. The changes in pile temperature were not as extreme as the

changes in the superstructure temperatures. Only the top several inches of the piles were exposed to open air. The temperature of the piles likely varies along the length of the pile and the measured temperatures represent only the temperature of the top portion of the piles.

B.3 Bridge displacements

B.3.1 Longitudinal abutment displacements and change in bridge length

Absolute longitudinal displacements parallel to the bridge longitudinal axis were measured with displacement transducers mounted to benchmark posts. These displacement measurements provided information concerning the change in length of the bridges and the rigid body motion of one abutment in a horizontal plane.

The change in the bridge length was found by summing the longitudinal abutment displacements measured at the mid-width of the abutment pile cap at each end of the bridge. The recorded range of the change in bridge length during a complete yearly cycle [December 1997 through January 1999] was about 1.75 inches (45 mm) for the Guthrie County Bridge. At the Story County Bridge, the displacements measured at the west abutment became erratic during September 1998, due to a problem with the data acquisition program. A change in bridge length was not calculated until the middle of October 1998, so the change in bridge length was not monitored during the full summer-to-winter contraction period. The bridge will be monitored through the summer of 1999 to obtain data for a full yearly cycle.

The displacement data has indicated a good correlation between the recorded change in bridge length and the change in temperature. The extent to

which the change in bridge length is related to the change in temperature can be indicated by plotting the change in bridge length versus the change in average bridge temperature. Since the average bridge temperature is not a perfect indicator of the influence of temperature on the longitudinal expansion and contraction of the bridge superstructure, this analysis is made to only show a general trend in the bridge displacement results.

Nonlinearity of the longitudinal abutment displacements at the Guthrie County Bridge was observed. The south abutment experienced a decreased rate of displacement in the longitudinal direction as the average bridge temperature increased. The north abutment experienced an increase in longitudinal displacement rate when the south abutment was undergoing less displacement. The net effect produced a change in the bridge length that was approximately linear with respect to changes in temperature. This nonlinearity of abutment displacement response to increasing bridge temperature could be due to an increase in the backfill stiffness behind the south abutment as the abutment expands. A decrease in backfill stiffness behind the north abutment is not the likely cause, as soil pressures tend to increase in response to additional displacement. Factors affecting backfill stiffness include: backfill slope, backfill compaction, and moisture content of the backfill.

B.3.2 Abutment rotation in a horizontal plane

(No supplemental commentary)

B.3.3 Abutment rotation in a vertical plane

Pairs of displacement transducers and a tiltmeter were used to measure the rotation of an abutment pile cap in a vertical plane parallel to the longitudinal axis of the bridge. The rotation measurements obtained with each method at the Guthrie County Bridge were compared. At the Story County Bridge, only a tiltmeter was used to measure rotations of the east abutment pile cap. Those rotations were in a vertical plane that was parallel to the longitudinal axis of the bridge.

The initial method of measuring abutment rotations at the Guthrie County Bridge used the difference in two longitudinal abutment displacement readings that were made with displacement transducers at the top and bottom of the pile cap. The difference in the two displacement readings divided by the vertical separation between the two transducers indicated the rotation of the abutment in radians. This method of measuring abutment rotations was called into question when the relative movement between two benchmark posts was significant compared to the magnitudes of the differences in the two displacement transducer measurements. If the posts were moving, the accuracy of such a small difference in longitudinal displacements was very uncertain. To reliably measure abutment rotations, a temperature-compensated tiltmeter was installed at the Guthrie County Bridge. Two transducers that measured the longitudinal abutment displacement at the top of the pile cap at the east and west ends of the south abutment pile cap were removed at the time of the tiltmeter installation. The transducer pair at the center of the south abutment pile cap was kept to determine whether previous rotation measurements were valid.

The correlation between the results obtained by each of the two methods was very good. The researchers concluded that the two independent methods of obtaining rotation measurements were both correct and that the rotation measurements indicated by the pairs of post-mounted displacement transducers were valid.

The daily variation in the pile cap rotation appears to be greater during the summer months. This may be due to a greater daily range in average bridge temperatures or due to higher vertical thermal gradients that can occur during the summer months.

A vertical temperature gradient would tend to arch the concrete superstructure upward. Unless the abutment was held rigidly, rotation of the abutment about a horizontal axis would occur. Rotation of the abutment may be also due to restraints on the abutment applied by the piles and the backfill soil. As the abutment translates longitudinally, forces are activated in the soil backfill and the steel piles. The shear force at the top of the pile is below the centroid of the bridge superstructure. The eccentricity of this shear force produces a moment at the end of the bridge. Similarly, if the resultant of the backfill soil pressure is below the centroid of the superstructure, an additional negative moment is applied to the end of the bridge. The evaluation of the significance of the contribution that these effects have on abutment rotations is beyond the scope of this experimental program and can be more easily accomplished with analytical methods.

B.3.4 Transverse abutment displacements

Two post-mounted transducers measured the transverse displacement of an abutment at each end of the pile cap at each bridge. Two displacement measurements were necessary because the change in position of the abutment ends is a combination of two effects: the temperature-dependant volumetric expansion of the pile cap concrete and the rigid body translation of the abutment due to the longitudinal expansion of a skewed bridge. Skewed bridges may translate laterally because soil pressure exerted on the back of the abutment has a component of force perpendicular to the longitudinal axis of the bridge.

To determine the magnitudes of the transverse abutment expansion and translation, it was assumed that the transverse thermal expansion of the pile cap was uniform across the width. The change in the abutment width was then the sum of the recorded displacements measured at each end of the pile cap. If each post-mounted transducer recorded displacements away from the benchmark posts, the pile cap changed dimension by the sum of those two measured displacements. The translation of the centroid of the pile cap can be estimated by dividing the difference in the measured displacements by two. This relationship can be illustrated easily if the measured displacement at one end of the pile cap is 2 in. and the displacement at the other end is zero. The translation of the center of mass of the abutment is then 1 in.

B.3.5 Relative displacements

Differential displacements between an abutment pile and the RC pile cap were measured at each bridge site. The relative rotation could be determined using

two displacement measurements separated by a distance. The relative rotation (in microradians) was calculated by dividing the difference between the measured relative vertical displacements at the front and the back of the pile cap by the horizontal separation of the displacement measurements. This relative rotation measurement was not the relative rotation between the top of the pile and the pile cap; but rather, it was the relative rotation between the pile cap and the point on the pile at which the transducers were attached. Since the bracket, to which the transducers were clamped, was clamped to the pile at a distance of about 18 inches down from the bottom of the pile cap, the measured relative rotation may be due to flexural curvature in the pile.

B.4 Bridge member strains

B.4.1 Pile strains

As integral abutment bridges expand and contract, the tops of the abutment piles move with the abutment. If the abutment pile cap and the bridge superstructure restrain rotation of the pile top about a horizontal axis, a moment develops in the top of the pile. The strain induced in the steel piling by the abutment displacements was measured by electrical-resistance strain gages that were welded to the pile flanges. The measured pile strains indicated that biaxial bending of the pile occurred and that a moment gradient developed along the length of the pile. Normal torsional warping strains measured in the piles at each bridge were found to be very small.

At both bridges, higher magnitudes of bending strains in the abutment piles were measured at 9 in. (230 mm) than at 33 in. (840 mm) below the pile cap. The bending strains measured at the two cross sections have a similar cyclic trend. The range in the y-axis bending at the upper and lower cross sections [at a pile in the Guthrie County Bridge] was about 700 and 400 microstrain, respectively. The difference in measured y-axis bending strains indicates that there is a moment gradient along the length of the pile. If there was negligible soil pressure contacting the pile between the instrumented cross sections, the moment gradient in the pile should be linear. The piles at the Guthrie County Bridge were in predrilled holes, surrounded with a bentonite slurry. This highly plastic soil has a low stiffness and will not exert much force on the pile between the instrumented cross sections. Using the measured bending strains in the pile, the bending strain at the bottom of the pile cap can be determined by linear extrapolation.

At the Story County Bridge, the magnitude of the bending strains at the bottom cross section were also lower than the bending strains recorded at the cross section near the pile cap. The difference between the y-axis bending strains at the two cross sections in the piles at the Story County Bridge was greater than the difference in y-axis bending strain recorded in one pile at the Guthrie County Bridge. The difference in the y-axis bending strains of the piles at the two bridges may be due to differences in the lateral restraint on the pile offered by the soil surrounding the piles or due to different magnitudes of abutment rotation and displacement. The predrilled holes for the piles at the Story County Bridge were filled with sand. When the abutment piles were exposed by excavating the berm soil, the sand around the

top of the pile sloughed away from the pile. Therefore, there was no lateral restraint between the monitored cross sections and a linear extrapolation of the strain gage readings was possible.

B.4.2 Girder strains

The abutment rotation may be due to eccentric pile shear and backfill pressure restraint on the abutment displacement. These eccentric forces would tend to create a moment on the bridge superstructure at the abutment. For a continuous structure with three equal spans and constant flexural rigidity, the moment carried over to the other end of the first span would be just over one-quarter of the moment applied to the end. The girder likely experiences less bending deformation at the pier because the moment applied at the abutment is not completely carried over to the pier.

APPENDIX C – PILE-TO-SOIL INTERACTION

The following section details the pile-to-soil interaction theory used for the Guthrie County Bridge and Story County Bridge, finite-element models. This is taken directly from Chapter 2 of the report written by Greimann, Abendroth, Johnson, and Ebner [4]. This excerpt is reproduced with the permission of Greimann and Abendroth:

The Winkler soil model [44,45] was used for the analysis of the soil/pile interaction. The model assumes that the soil can be represented as a series of vertical and lateral springs along the length of the pile and an end bearing point spring, as shown in Figure C.1. The model assumes that there is no interaction between the different soil springs as the pile is displaced.

The soil characteristics of each of the three types of springs can be described by soil resistance versus displacement curves: (1) p-y curves, which describe the relationship between the lateral soil pressure (horizontal force per unit length of pile) and the corresponding lateral pile displacement: (2) f-z curves, which describe the relationship between skin friction (vertical force per unit length of pile) and the relative vertical displacement between the pile and the soil: and (3) q-z curves, which describe the relationship between the bearing stress (vertical force on effective pile tip area) at the pile tip and the pile tip settlement. All three types of curves assume the soil behavior to be nonlinear. Again, the Winkler model assumes

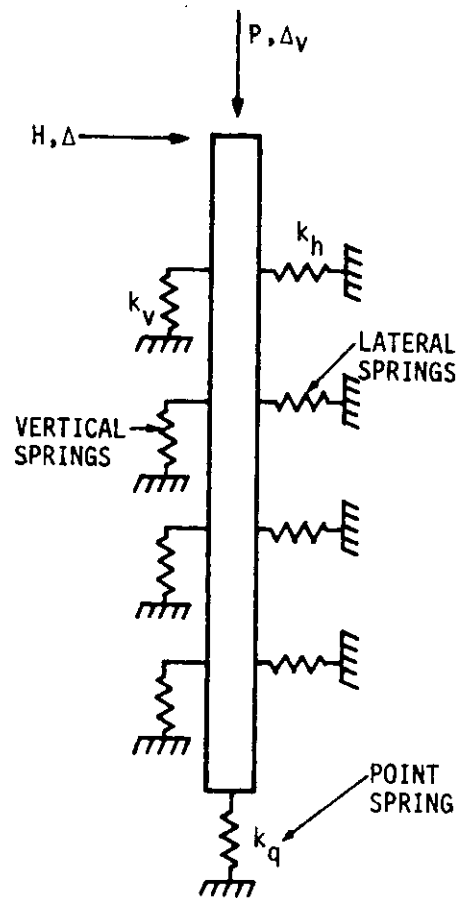


Figure C.1. Winkler soil model

that these springs are uncoupled, that is, that motion at one spring does not affect another.

Nonlinear soil pile interaction models are presented by a number of researchers [46-54]. The modified Ramberg-Osgood model [55] was used to approximate the p - y , f - z , and q - z soil resistance and displacement curves to model the nonlinear pile-to-soil interaction:

$$p = \frac{k_h y}{\left[1 + \left| \frac{y}{y_u} \right|^n \right]^{\frac{1}{n}}} \quad (\text{C.1})$$

$$y_u = \frac{p_u}{k_h} \quad (\text{C.2})$$

in which,

k_h = initial soil stiffness

p = generalized soil resistance

p_u = ultimate soil resistance

n = shape parameter for the modified Ramberg-Osgood curve

y = generalized displacement

Figure C.2 and Equation C.1 show the modified Ramberg-Osgood curve for a typical p - y curve. Similar equations for a typical f - z curve (with f_{\max} , the maximum shear stress developed between the pile and soil, and k_v , the initial vertical stiffness) or a typical q - z curve (with q_{\max} , the maximum bearing stress at the pile tip, and k_q , the initial point stiffness) were used. Figure C.3 shows the effect of the shape parameter, n , on the soil resistance and displacement behavior. The constants required in Equation C.1 were empirically determined from basic soil properties as

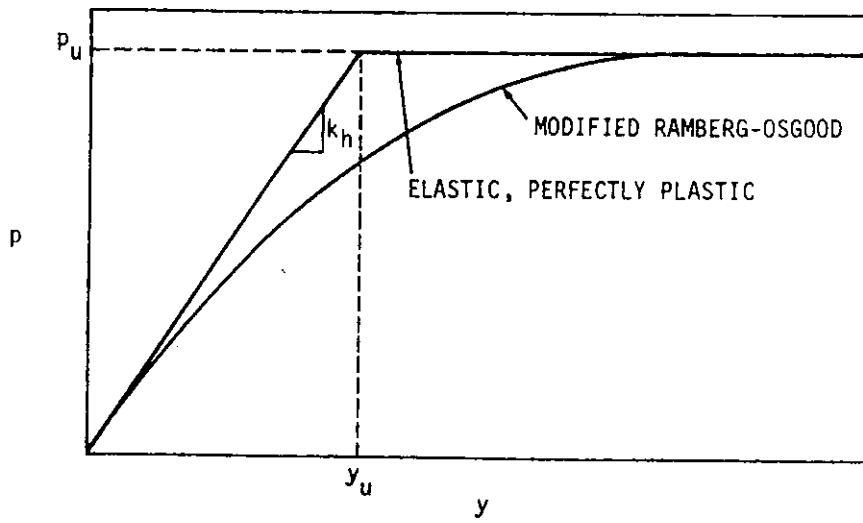


Figure C.2. Typical p-y curve

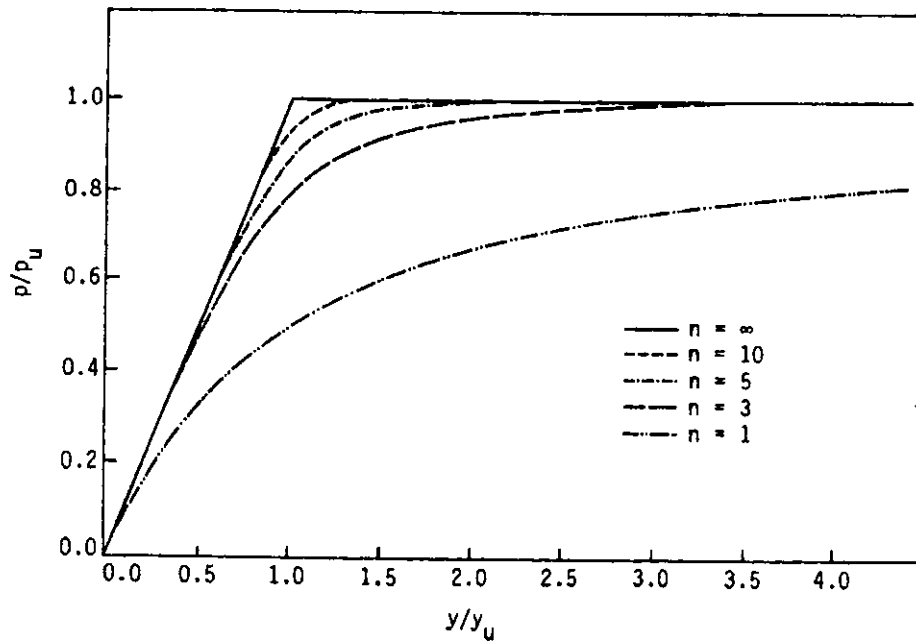


Figure C.3.

presented in Tables C.1, C.2, and C.3 [20,45, 56-58]. Typical values are listed for clay and sand in Tables C.4 and C.5, respectively for an HP10 x 42 steel pile.

For practical purposes, k_h is often assumed to be constant or to vary linearly with depth. Uncertainty in estimating soil behavior from standard tests will usually be consistent with the errors introduced by the use of such a simple soil modulus versus depth function [51]. For the parameters presented in Tables C.1 through C.5, the subgrade-reaction modules for clay soils are assumed to be constant within a soil layer and to vary linearly for granular soils.

Table C.1. Parameters for p-y curve

CASE	n	p_u (use lesser value)	k_h
Soft clay and stiff clay	1.0	$p_u = 9c_u B$	
		$p_u = \left[3 + \frac{\gamma'}{c_u} x + \frac{0.5}{B} x \right] c_u B$	$\frac{p_u}{y_{50}}$
Very stiff clay	2.0	$p_u = 9c_u B$	
		$p_u = \left[3 + \frac{\gamma'}{c_u} x + \frac{2.0}{B} x \right] c_u B$	$\frac{p_u}{2y_{50}}$
Sand	3.0	$p_u = \gamma' x [B(k_p - k_a) + x k_p \tan \alpha \tan \beta$ $+ x k_o \tan \beta (\tan \phi - \tan \alpha)]$	
		$p_u = \gamma' x k_p^3 + 2k_p^2 k_o \tan \phi - k_a B$	$\frac{J \gamma' x}{1.35}$

ϵ_{50}	Axial strain at one-half peak stress difference from triaxial test; or use 0.02 for soft clay, 0.01 for stiff clay, or 0.005 for very stiff clay.
c_u	Cohesion from an unconsolidated, undrained test
B	Pile width
γ'	Effective unit soil weight
x	Depth from soil surface
ϕ	Angle of internal friction
k_p	$= \tan^2(45^\circ + \phi/2)$
k_a	$= \tan^2(45^\circ - \phi/2)$
k_o	$= 1 - \sin \phi$
α	$= \phi/2$ for dense or medium sand, $\phi/3$ for loose sand
β	$= 45^\circ + \phi/2$
J	$= 200$ for loose sand, 600 for medium sand, 1500 for dense sand
y_{50}	Displacement at one-half ultimate soil reaction: $2.5B\epsilon_{50}$ for soft and stiff clay, $2.0B\epsilon_{50}$ for very stiff clay.

Table C.2. Parameters for f-z curve

CASE	n	f_{max}		k_v
		H PILES	OTHERS	
Clay	1.0	The least of: $2(d + b_f)c_u$ $2(d + 2b_f)c_a$ $2(dc_u + b_fc_a)$	The lesser of c_u or c_a times pile perimeter	$\frac{10f_{max}}{z_c}$
Sand	2.0	$0.02N[2(d + 2b_f)]$ (klf)	$0.04N$ times pile perimeter (klf)	$\frac{10f_{max}}{z_c}$

c_u Undrained cohesion of the clay soil, approximately $97N + 114$ (psf)
 c_a Adhesion between soil and pile, αc_u (psf). See Figure C.4 for α .
 N Average standard penetration blow count
 x Depth from soil surface
 z_c Displacement at maximum force: 0.4 in. for sand, 0.25 in. for clay
 d, b_f Depth and flange width, respectively, of H shape

Table C.3. Parameters for q-z curve

CASE	N	f_{max}	K_v
Clay	1.0	$9c_u$	$\frac{10q_{max}}{z_c}$
Sand	1.0	$8N_{corr}$ (ksf)	$\frac{10q_{max}}{z_c}$

N_{corr} Corrected standard penetration test blow count at depth of pile tip; equal to N if $N \leq 15$ or $15 + 0.5(N - 15)$ if $N > 15$.

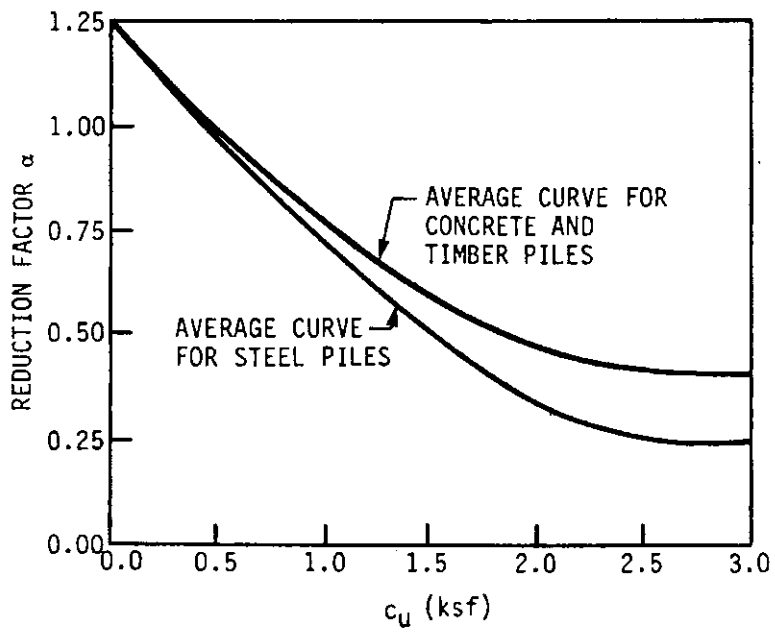


Figure C.4. Reduction factor for a pile in clay

Table C.4. Soil properties and curve parameters for an HP10x42 pile in clay

	SOFT	STIFF	VERY STIFF
SOIL PROPERTIES:			
Blow Count, N	3	15	40
Saturated effective unit weight, γ' (pcf)	50	60	65
Dry unit weight, γ (pcf)	90-110	115-135	120-140
Undrained cohesion, c_u (psf)	400	1600	5000
p-y CURVE PARAMETERS:			
n	1.0	1.0	1.0
Saturated conditions p_u (klf) (use lesser value)	3.0 or $1.0 + 0.24x$	12 or $3.9 + 0.85x$	37 or $12.5 + 10.1x$
Saturated conditions k_h (ksf) (use lesser value)	72 or $24 + 5.8x$	580 or $190 + 41x$	2200 or $750 + 610x$
f-z CURVE PARAMETERS:			
n	1.0	1.0	1.0
Saturated conditions f_{max} (klf) (use lesser value)	1.3	3.6	6.2
Saturated conditions k_v (ksf) (use lesser value)	620	1700	2960
q-z CURVE PARAMETERS:			
n	1.0	1.0	1.0
Saturated conditions q_{max} (ksf) (use lesser value)	3.6	14	45
Saturated conditions k_q (kcf) (use lesser value)	1700	6700	21000

Table C.5. Soil properties and curve parameters for an HP10x42 pile in sand

	LOOSE	MEDIUM	DENSE
SOIL PROPERTIES:			
Blow Count, N	5	15	30
Saturated effective unit weight, γ' (pcf)	55	60	65
Dry unit weight, γ (pcf)	90-125	110-130	110-140
Angle of friction, ϕ	30°	35°	40°
p-y CURVE PARAMETERS:			
n	3.0	3.0	3.0
Saturated conditions p_u (klf) (use lesser value)	$0.070x^2 + 0.12x$ for $x \leq 20\text{ft}$	$0.15x^2 + 0.17x$ for $x \leq 18\text{ft}$	$0.26x^2 + 0.24x$ for $x \leq 22\text{ft}$
	$1.5x$ for $x > 20\text{ft}$	$2.9x$ for $x > 18\text{ft}$	$5.9x$ for $x > 22\text{ft}$
Saturated conditions k_h (ksf) (use lesser value)	$8.0x$	$27x$	$72x$
f-z CURVE PARAMETERS:			
n	1.0	1.0	1.0
Saturated conditions f_{\max} (klf) (use lesser value)	0.5	1.5	3.0
Saturated conditions k_v (ksf) (use lesser value)	150	450	900
q-z CURVE PARAMETERS:			
n	1.0	1.0	1.0
Saturated conditions q_{\max} (ksf) (use lesser value)	40	120	180
Saturated conditions k_q (kcf) (use lesser value)	12000	36000	55000

REFERENCES

1. Burke, M.P., Jr., "Integral Bridges: Attributes and Limitations," Paper No. 930104 Presented at Transportation Research Board 72nd Annual Meeting, Washington D.C., 1993.
2. Wasserman, E.P., and Walker, J.H., "Integral Abutments for Continuous Steel Bridges," Tennessee Department of Transportation, 1993.
3. Russell, H.G., and Gerken, L.J., "Jointless Bridges – The Knowns and the Unknowns," Concrete International, Vol. 16, No. 4, 1994.
4. Greimann, L.F., Abendroth, R.E., Johnson, D.E., and Ebner, P.B., "Pile Design and Tests for Integral Abutment Bridges," Final Report to the Highway Division, Iowa Department of Transportation, Iowa DOT Project HR-273, 1987.
5. Kennedy, J. B., and Soliman M. H., "Temperature Distribution in Composite bridges," ASCE Journal of Structural Engineering, American Society of Civil Engineers, Vol. 113, No. 3, 1987.
6. Branco, F. A., and Mendes, P.A., "Thermal Actions for Concrete Bridge Design," ASCE Journal of Structural Engineering, American Society of Civil Engineers, Vol. 119, No. 8, 1993.
7. Girton, D.D., Hawkinson, T.R., and Greimann, L.F., "Validation of Design Recommendations for Integral Abutment Piles," Final Report to the Highway Division, Iowa Department of Transportation, Iowa DOT Project HR-292, 1989.
8. Oesterle, R. G., Tabatabai, H., Lawson, T.J., Refai, T.M., Volz, J.S., and Scanlon, A., "Jointless and Integral Abutment Bridges – Draft Summary Report," Construction Technology Laboratories, Skokie, Illinois, 1999.
9. Kunin, J., and Alampalli, S., "Integral Abutment Bridges: Current Practice in the United States and Canada," New York State Department of Transportation, Special Report 132, 1999.
10. Wolde-Tinsae, A.M., Greimann, L.F., and Johnson, B.V., "Performance of Integral Bridge Abutments," International Associations for Bridge and Structural Engineering, IABSE Proceedings P-58/83, 1983.
11. Hoppe, E.J., Gomez, J.P., "Field Study of an Integral Backwall Bridge", Final Report: Virginia Transportation Research Council Project 97-R7, 1996.

12. AASHTO LRFD Bridge Design Specifications, 1st Edition, American Association of State Highway and Transportation Officials, Washington, D.C., 1994.
13. Lawver, A., French, C., and Shield, C.K., "Field Performance of an Integral Abutment Bridge," Paper presented at the Transportation Research Board 79th Annual Meeting, Washington, D.C., 2000.
14. Clough, G.W., and Duncan, J.M., "Earth Pressures" Foundation Engineering Handbook, 2nd Edition, edited by H.Y. Fung, Van Nostrand Reinhold, New York, 1991.
15. Lehane, B.M., Keogh, D.L., and O'Brien, E.J., "Simplified Elastic Model for Restraining Effects of Backfill Soil on Integral Bridges," Computers and Structures, Vol. 73, 1999.
16. Ting, J.M., and Faraji, S., "Streamlined Analysis and Design of Integral Abutment Bridges," Department of Civil and Environmental Engineering, University of Massachusetts Lowell, Technical Report, 1998.
17. "GTSTRUDL User's Manual," GTICES Systems Laboratory, Georgia Institute of Technology, Atlanta, Georgia, Vol. 1, Revision M, 1991.
18. O'Neill, M.W., and Murchison, J.M., "An Evaluation of p-y Relationships in Sands," University of Houston, Report GT-DF02-83 to the American Petroleum Institute, 1983.
19. Amde, A.M. (formerly Wolde-Tinsae, A.M.), Chini, S.A., and Mafi, M., "Model Study of H-Piles Subjected to Combined Loading," Geotechnical and Geological Engineering, Vol. 15, No. 4, 1997.
20. Wolde-Tinsae, A.M., Greimann, L.F., and Yang, P.S., "Nonlinear Pile Behavior in Integral Abutment Bridges," Final Report to the Highway Division, Iowa Department of Transportation, Iowa DOT Project HR-227, 1982.
21. Desai, C.S., and Wu, T.H., "A General Function for Stress-Strain Curves," Proceedings 2nd International Conference on Numerical Methods in Geomechanics, 1976.
22. Kamel, M.R., Benak, J.V., Tadros, M.K., and Jamshidi, M., "Prestressed Concrete Piles in Jointless Bridges," PCI Journal, Vol. 41, No. 2, 1996.
23. ACI Committee 209, "Prediction of Creep, Shrinkage, and Temperature Effects in Concrete Structures," ACI 209R-92, Detroit, Michigan, 1992.

24. Emanuel, J.H., and Hulseay, J.L., "Prediction of the Thermal Coefficient of Expansion of Concrete," Journal of American Concrete Institute, Vol. 74, No. 4, 1977.
25. Springman, S.M., Norrish, A.R.M., and Ng, C.W.W., "Cyclic Loading of Sand Behind Integral Bridge Abutments," Transportation Research Laboratory, TRL Report 146, United Kingdom, 1996.
26. Thomas, M.E., "Field Study of Integral Abutment Bridges," M.S. Thesis, Iowa State University, 1999.
27. Kirkpatrick, C., "Instrumentation for Field Testing of Integral Abutment Bridges," Creative Component Project, Iowa State University, 1997.
28. Measurements Group, Inc., "Temperature-Induced Apparent Strain and Gage Factor Variation in Strain Gages," Technical Note TN-504, Raleigh, North Carolina, 1983.
29. Dally, J., and Riley, B., Experimental Stress Analysis, 3rd Edition, McGraw-Hill, Inc., New York, 1991.
30. Girton, D.D., Hawkinson, T.R., and Greimann, L.F., "Validation of Design Recommendations for Integral Abutment Piles," ASCE Journal of Structural Engineering, American Society of Civil Engineers, Vol. 117, No. 7, 1991.
31. "ANSYS User's Manual," Revision 5.0, Swanson Analysis Systems, Inc., Houston, Texas, 1992.
32. AASHTO LRFD Bridge Design Specifications, 2nd Edition, American Association of State Highway and Transportation Officials, Washington, D.C., 1998.
33. Weaver, W. Jr., and Gere, J.M., Matrix Analysis of Framed Structures, 3rd Edition, Van Nostrand Reinhold, 1990.
34. Lee, D.J., Bridge Bearings and Expansion Joints, 2nd Edition, E & FN Spon, United Kingdom, 1994.
35. Standard Specifications for the Iowa Department of Transportation, Highway Division, Series of 1984, Iowa Department of Transportation, Ames, Iowa, 1984.
36. Barkan, D.D., Dynamics of Bases and Foundations, McGraw-Hill, New York, 1962.

37. Filz, G.M., Boyer, R.D., and Davidson, R.R., "Bentonite-Water Slurry Rheology and Cutoff Wall Trench Stability," Geotechnical Special Publication, ASCE, No. 71, 1997.
38. "Manuals for the Design of Bridge Foundations," Barker, R.M., Duncan, J.M., Rojiani, K.B., Ooi, P.S.K., Tan, C.K., and Kim, S.G. editors, National Cooperative Highway Research Program Report 343, Transportation Research Board, 1991.
39. "Canadian Foundation Engineering Manual," 3rd Edition, Canadian Geotechnical Society, Toronto, Canada, 1992.
40. Husain, I., and Bagnaroil, D., "Integral Abutment Bridge" Report SO-96-01, Structures Office, Ontario Ministry of Transportation, Ontario, Canada, 1996.
41. "Design Manual - Soil Mechanics, Foundations and Earth Structures." NAVFAC DM-7, Department of the Navy, Naval Facilities Engineering Command, Alexandria, Virginia, 1971.
42. Clayton, C.R.I., Milititsky, J., and Woods, R.I., Earth Pressure and Earth-Retaining Structures, Blackie Academic and Professional, Glasgow, 1993.
43. Winklehorn, H.F., and Fang, H.Y., editors, Foundation Engineering Handbook, Van Nostrand Reinhold Co., New York, 1975.
44. Flemming, W.G., Weltman, A.J., Randolph, M.F., and Elson, W.K., Piling Engineering, Halsted Press, New York, 1985.
45. Poulos, H.G., and Davis, E.H., Pile Foundation Analysis and Design, John Wiley and Sons, Inc., New York, 1980.
46. Duncan, J.M., and Chang, C.-Y., "Nonlinear Analysis of Stress and Strain in Soils," Proceedings Paper 7513, Journal of Soil Mechanics and Foundation Engineering Division, ASCE, Vol. 96, 1970.
47. Finn, W.D., Lee, K.W., and Martin, G.R., "An Effective Stress Model for Liquefaction," Proceedings Paper 13008, Journal of the Geotechnical Engineering Division, ASCE, Vol. 103, 1977.
48. Martin, P.P., "Nonlinear Methods for Dynamic Analysis of Ground Response," Ph.D. Thesis, University of California at Berkeley, 1975.
49. Streeter, V.L., Wylie, E.B., and Richard, F.E. Jr., "Soil Motions Computations by Characteristic Methods," Proceedings Paper 10410, Journal of the Geotechnical Engineering Division, ASCE, Vol. 100, 1974.

50. Pyke, R., "Nonlinear Soil Models for Irregular Cyclic Loadings," Proceedings Paper 14642, Journal of the Geotechnical Engineering Division, ASCE, Vol. 105, 1977.
51. Matlock, H., and Reese, L.C., "Generalized Solutions for Laterally Loaded Piles," Journals of the Soil Mechanics and Foundation Division, ASCE, Vol. 86, 1960.
52. Parker, F. Jr., Reese, L.C., "Experimental and Analytical Study of Behavior of Single Piles in Sand Under Lateral and Axial Loading," Research Report No. 117-2, Center for Highway Research, University of Texas, Austin, Texas, 1979
53. O'Neill, M.W., and Murchison, J.M., "An Evaluation of p-y Relationships in Sands," University of Houston Research Report GT-DF02-83 to the American Petroleum Institute, Houston, Texas, 1983.
54. Ting, J.M., Kauffman, C.R., and Lovicsek, M. "Centrifuge Static and Dynamic Lateral Pile Behaviour," Canadian Geotechnical Journal, Vol. 24, 1987.
55. Desai, C.S., and Wu, T.H., "A General Function for Stress-Strain Curves," Proceedings of the 2nd International Conference on Numerical Methods in Geomechanics 1, 1976
56. Davisson, M.T., "Lateral Load Capacity of Piles," Transportation Research Record, Vol. 333, 1970.
57. Ha, N.B., and O'Neill, M.W. "Field Study of Pile Group Action (Appendix A)." Final Report, Federal Highway Administration, Washington, D.C., 1981.
58. Highway Structures Design Handbook. Vol. 1. Pittsburgh, Pennsylvania, United States Steel Corporation, 1965.

ACKNOWLEDGMENTS

The work described in this thesis was sponsored by the Iowa Department of Transportation. The offices of the Guthrie and Story County Engineers also deserve recognition for their assistance over the duration of the project.

A special thanks goes to Dr. Lowell Greimann and Dr. Robert Abendroth for their close guidance throughout all stages of the research project and in preparation of this thesis. I would also like to thank Dr. Les Schmerr for serving on my Program of Study Committee and Dr. Fouad Fanous for his assistance with the finite element portion of the project.

Finally, I would like to thank the following graduate students that also worked on this project: Matt Thomas, Kuok-hung Lim, and Wei Chei Ng.